A ROBUST ROTORCRAFT FLIGHT CONTROL SYSTEM DESIGN METHODOLOGY UTILIZING QUANTITATIVE FEEDBACK THEORY

by

PETER JAMES GORDER

B. S. (University of California, Davis) 1986

M.S. (University of California, Davis) 1988

DISSERTATION

Submitted in partial satisfaction of the requirements for the degree of

DOCTOR OF PHILOSOPHY

in

MECHANICAL ENGINEERING

in the

OFFICE OF GRADUATE STUDIES

of the

UNIVERSITY OF CALIFORNIA

DAVIS

Approved:

Committee in Charge

1993

ABSTRACT

Rotorcraft flight control systems present design challenges which often exceed those associated with fixed-wing aircraft. First, large variations in the response characteristics of the rotorcraft result from the wide range of airspeeds of typical operation (hover to over 100 kts). Second, the assumption of vehicle rigidity often employed in the design of fixed-wing flight control systems is rarely justified in rotorcraft where rotor degrees of freedom can have a significant impact on the system performance and stability. This research was intended to develop a methodology for the design of robust rotorcraft flight control systems. Quantitative Feedback Theory (QFT) was chosen as the basis for the investigation. Quantitative Feedback Theory is a technique which accounts for variability in the dynamic response of the controlled element in the design robust control systems. It was developed to address a Multiple-Input-Single-Output (MISO) design problem, and utilizes two degrees of freedom to satisfy the design criteria. Two techniques were examined for extending the QFT MISO technique to the design of a Multiple-Input-Multiple-Output (MIMO) flight control system (FCS) for a UH-60 Black Hawk Helicopter. In the first, a set of MISO systems, mathematically equivalent to the MIMO system, was determined. QFT was applied to each member of the set simultaneously. In the second, the same set of equivalent MISO systems were analyzed sequentially, with closed loop response information from each loop utilized in subsequent MISO designs. The results of each technique were compared, and the advantages of the second, termed Sequential Loop Closure, were clearly evident.

ACKNOWLEDGEMENTS

This work was supported by the Flight Dynamics and Controls Branch at NASA, Ames Research Center, Moffett Field, California. The author would like to specifically thank Mark Tischler, the contract monitor, Mark Takahashi, and Ed Aiken, the branch manager, for their support and guidance. A special thanks to Ronald A. Hess, PhD, of the Department of Mechanical, Aeronautical, and Materials Engineering Department at the University of California, Davis, for his assistance throughout the project. Thanks also are due to my parents, Dr. James L. and Paula P. Gorder, whose continuing guidance and support are much appreciated. Last, but certainly not least, thanks to the two most important ladies in my life: my wife, Diane, without whose support and encouragement this project would not have been possible, and my daughter, Kayla, born during this project, who is both a constant source of joy and a continuing reminder of what is really important.

TABLE OF CONTENTS

LIST OF FIGURES

LIST OF TABLES

CHAPTER 1

INTRODUCTION

Rotorcraft flight control systems present design challenges which often exceed those associated with fixed-wing aircraft. First, large variations in the response characteristics of the rotorcraft result from the wide range of airspeeds of typical operation (hover to over 100 kts). Second, the assumption of vehicle rigidity often employed in the design of fixed-wing flight control systems is rarely justified in rotorcraft where rotor degrees of freedom can have a significant impact of the system performance and stability.

The issue of rotor dynamics is magnified when one realizes that the performance requirements of modern rotorcraft necessitate high response-bandwidth, full-authority flight control systems (FCS). Here, high response-bandwidth refers to the ability of the FCS to produce a desired pilot-input/vehicle-output response type (e.g., attitude command/attitude hold) over a broad frequency range. While seeking to maximize response feedback bandwidth, the designer is also interested in minimizing feedback bandwidth. As shown in Fig. 1.1, response bandwidth refers to that associated with y/y_c, while feedback bandwidth is that associated with y/y_f. In addition to the limitations imposed by rotor degrees of freedom, the rotorcraft flight control system designer must also consider the effects of sensor and actuator dynamics, digital control law

implementation, and non-linear aerodynamic effects [1,2].

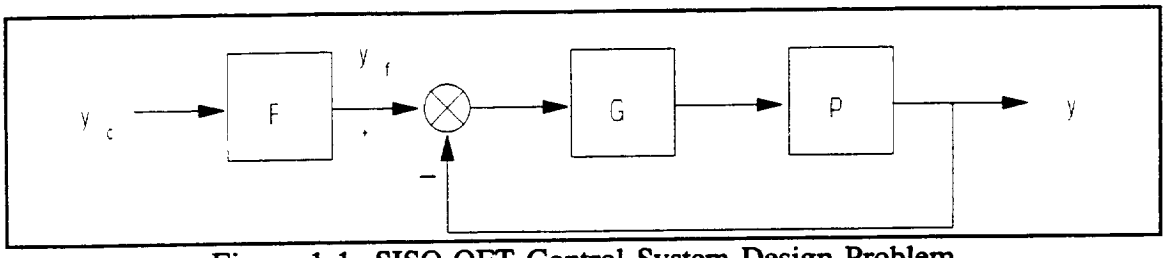

Figure 1.1 SISO QFT Control System Design Problem

The research proposed herein will attempt to meet these challenges by applying Quantitative Feedback Theory (QFT) to the design of a rotorcraft flight control system. QFT is a technique for designing robust control systems [3,4,5]. It is a frequency domain design technique in which uncertainty in the dynamic characteristics of the controlled element is represented as either variations in the coefficients of the control input to response transfer functions or as variations in the magnitude and phase of the frequency response of the transfer functions with frequency. Tracking or command-following performance bounds are also considered, defined as acceptable upper and lower limits of the magnitude of the closed loop system frequency response.

Consider the Single-Input/Single-Output (SISO) control system design depicted in Fig. 1.1, where $P \in \mathcal{P}$, and $\mathcal{P}$ is the set of all possible variations in the controlled element, y is the output, y_c is the command, and F and G are the two degrees of freedom (DOF) utilized in the QFT design process. First, the controller G is defined such that the variation in the closed loop frequency response due to the uncertainty in the dynamic characteristics of the controlled element are within the variations defined across

frequency by the bounds just described. Next, the precompensator F is defined such that the closed-loop frequency response, $y/y_c(j\omega)$, actually lies within the bounds just described given the uncertainty in the controlled element.

Disturbance rejection may also be considered, as shown in Figs. 1.2 and 1.3. In either of these cases, the only difference in the design procedure is that the controller G

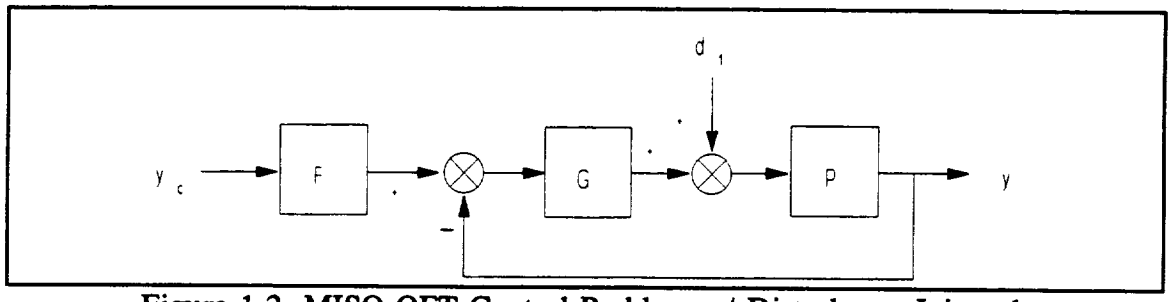

Figure 1.2 MISO QFT Control Problem w/ Disturbance Injected Before Controlled Element

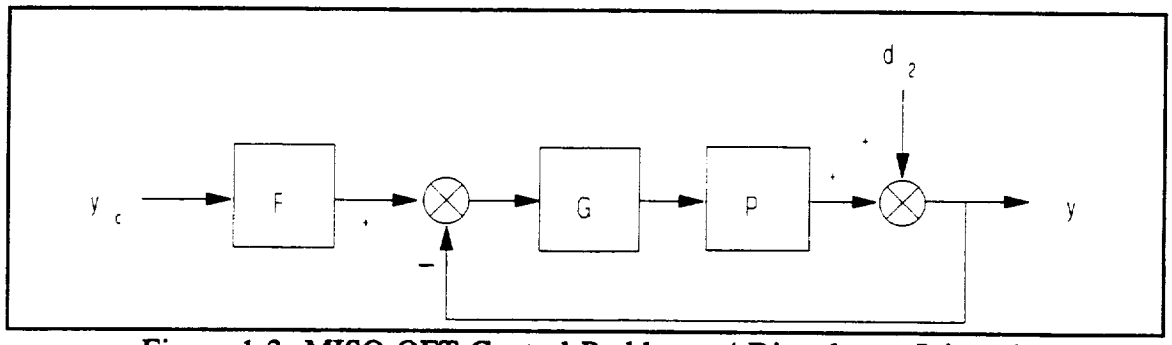

Figure 1.3 MISO QFT Control Problem w/ Disturbance Injected After Controlled Element

must be selected to satisfy both the disturbance rejection and tracking performance specifications for every $P \in P$. This is referred to as a Multi-Input/Single-Output (MISO) system in the literature.

Pilots control rotorcraft through three cockpit controllers, one of which combines two axes of control authority. A rotorcraft flight control system must, therefore, be a multiple-input-multiple-output (MIMO) control system, as opposed to the MISO control systems described above. The "collective" controller, changes the magnitude of the rotor thrust by "collectively" changing the pitch of the main rotor blades. Positive deflection of this controller, denoted δ_c, increases the magnitude of the thrust vector by "collectively" changing the pitch of the rotor blades. The pedals effect the yawing moment on the rotorcraft by a similar change in the tail-rotor collective pitch. Right pedal increases yaw rate, positive toward the right. This control input is denoted δ_p. The cyclic controller, generally a center stick, is a two axis controller used to control the longitudinal and lateral axes. Rearward or rightward deflection of the cyclic, inputs denoted δ_b and δ_a, respectively, induce pitching or rolling moments on the airframe by "cyclically" changing the pitch of the main rotor blades. With a full-authority FCS, a break is made in the physical connection between the cockpit controllers and the main and tail rotor systems. The cockpit control inputs are fed to a flight control computer to determine appropriate inputs to the main and tail rotor systems.

Extension of the QFT design technique to MIMO control system design problems has been shown to be equivalent to the simultaneous application of the QFT design technique to a number of MISO design problems [6,7,8]. It is this application of the QFT design technique which is necessary in order to design a full authority FCS for a

rotorcraft, where four (4) control inputs exist. In this case, the QFT design technique will have to be applied simultaneously to sixteen (16) MISO systems.

CHAPTER 2

BACKGROUND

Reference [1] provides an overview of the state of the art of high bandwidth rotorcraft flight control system design. Problems associated with high bandwidth FCS's, such as biodynamic interactions, rotor lead-lag dynamics, and the phase lags introduced by the rotor flapping response are discussed in some detail. The overall control system bandwidth is shown to be limited by the high frequency dynamics of the rotor, actuators, and sensors. These high frequency characteristics must obviously be taken into account in the design of high bandwidth flight control systems. As an example, the full-authority digital flight control system design for the Advanced Digital Optical/Control System program (ADOCS) was dominated by these high frequency dynamics [9].

Model-following flight control systems have been shown to be desirable because they reduce the problems of high gain feedback by employing feed-forward control [10]. A simple SISO example of a model-following system is presented in Fig.4, where P' is a model of the plant, P, and H is designed to obtain the desired closed loop dynamics. It is possible to approximate the high frequency dynamic effects of rotor, hydraulic, and sensor systems by adding time delays to a six (6) degree of freedom mathematical model, i.e., one assuming a rigid vehicle. To create a model-following FCS, however, the mathematical model must be inverted, and these time delays become non-causal time

advances. This non-causal information is obviously unavailable in real-time, and so the time delays are ignored for the inversion process. For low bandwidth operation of the model-following FCS, this is acceptable, but if the bandwidth of the ignored dynamics approaches the bandwidth of the required operation, large errors are inevitable. Indeed, it has been shown that an autopilot devised for a flight control system designed without regard to the rotor degrees of freedom can produce an unstable closed-loop response [11]. Thus, accurate mathematical models of the rotorcraft are required in the design of high bandwidth-model following flight control systems.

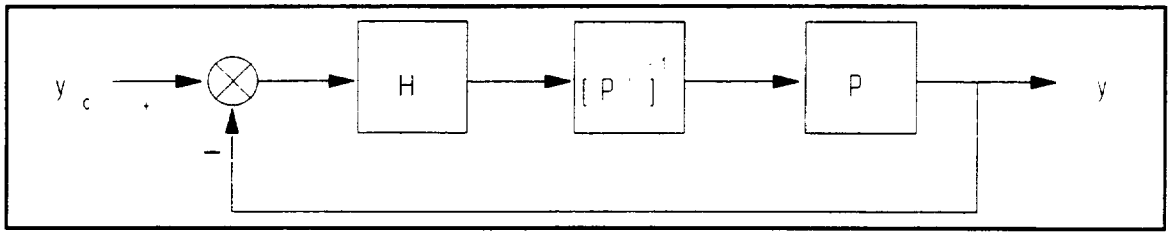

Figure 1.4 SISO Model Following Control Problem

The modeling problem may be reduced in its severity by including additional degrees of freedom in the original mathematical model. This obviates the inclusion of effective time delays, resulting in a more accurate inverted mathematical model-following implementation [15]. The problem of this approach, however, is in the identification of the higher order system dynamics.

A means of obviating the explicit inclusion of high frequency system dynamics in the generation of high response-bandwidth flight control systems is to design a FCS robust enough to accommodate the exclusion of high frequency effects, themselves. In

this case, the high frequency dynamics are treated as uncertainties in the low order rotorcraft model and the control system is designed to perform within specifications as long as the effect of the high frequency dynamics on the overall rotorcraft dynamics is within specified limits. One method of robust controller design is known as the H^∞ optimal design method [12,13]. H^∞ is a frequency domain technique amenable to integration with handling qualities specifications based on frequency domain criteria. The H^∞ norm of a given transfer function, intrinsic to this technique, is defined as the maximum of its largest singular value over all frequencies. The norm naturally characterizes the uncertainty in the system because the singular values provide information in terms of guaranteed bounds on performance. The H^∞ norm is used to place an upper bound on the closed-loop transfer function which can be minimized to create the optimal design.

Lower normed FCS designs are also possible. For example, an H^2 design was discussed in Ref.[14]. There, the control system was designed using a complete non-linear helicopter model linearized about a design point. When the FCS resulting from this exercise was tested in a simulator which used the same model as that used in the design, pilot evaluations were satisfactory. However, when the same FCS was implemented on a variable stability helicopter [15], pilot evaluations were unsatisfactory. This discrepancy was assumed to be due to differences between the dynamics of the model and the actual rotorcraft. Regardless, it was stated that a correction for the FCS was not readily apparent.

Eigenstructure assignment methods provide another alternative for rotorcraft flight control system design [16,17]. Here, the robustness is measured by the maximum singular value of the return matrix. These design techniques do not explicitly account for specified uncertainty in the assumed rotorcraft model. Eigenstructure assignment has also been combined with reduced-order modeling of rotorcraft [18]. The reduced-order model proved adequate in Ref. [20] since high bandwidth control was not a priority in this research.

FCS design techniques have also been proposed to eliminate specific vibratory modes in the rotor system. One such approach is referred to as High Harmonic Control (HHC) [19]. The basic notion behind HHC is to control the rotor blades at harmonics of the rotor rotational frequency so that unsteady airloads are cancelled.

Another FCS design approach aimed at reducing rotor-induced vibration is Individual Blade Control (IBC) [20]. As opposed to HHC in which feedback measurements are based upon body-fixed sensors (e.g., rotor mast forces and moments), IBC employs sensors in the rotating coordinate frame (e.g., rotor blade mounted accelerometers). The controller for IBC can most easily be designed using state variable feedback since this approach can easily handle the interacting rigid and elastic degrees of freedom present in any rotor system, as well as the periodically time-varying parameters [21]. To use this technique, it is generally necessary to feed back all of the state variables in the system, some of which may not be measurable. Estimates of

unattainable state variables must be determined using an observer. An observer is essentially a dynamic model which takes inputs and known state variables and provides estimates of the unknown state variables. Reference [22] presents a possible observer design which provides robustness in the closed-loop control system. Speculation is also made that the described design methodology may have additional benefit in the determination of more accurate rotor mathematical models to aid the control design process.

HHC and IBC can be accurately described as techniques for improving the performance of the main rotor as a force and moment producer, rather than as an overall FCS design technique. The sensor and modelling requirements of these two approaches can obviously be demanding. In the FCS design which is the subject of this research, it is assumed that the sensing requirements are limited to those associated with rigid body motion, hence the HHC and IBC approaches will not be discussed.

Uncertainty which is attributable to variation in vehicle characteristics with airspeed is often circumvented in practice by designing FCS's for specific flight conditions (i.e., point designs) and then developing algorithms which provide a smooth transition from one flight condition to another. These are so-called "gain-scheduled" systems [23], the name arising from the fact that the FCS gains are scheduled to the dominant flight condition parameter which for the rotorcraft is typically airspeed. The problem here, of course, is that a certain amount of design complexity is involved, not

only in implementing multiple designs, but in providing the appropriate scheduling algorithm.

The shortcomings of the FCS design approaches briefly described in the preceding led to the investigation of QFT for designing a robust rotorcraft FCS. As opposed to the model-following approach, specified uncertainty in the vehicle dynamics is not a handicap, but rather is an intrinsic part of the design procedure. As opposed to the H^{∞} approach, where one is constrained to a single scaler optimization variable (the H^{∞} norm), the QFT technique allows the designer considerable freedom in loop shaping to meet a variety of design constraints. As opposed to the eigenstructure approach, which is not a robust design technique, *per se*, the QFT approach guarantees performance and stability with specified uncertainty. As opposed to IBC and HHC approaches, the QFT approach is an output feedback technique, using measurements associated with rigid body motion. Finally, as opposed to gain-scheduled approaches, the variation in vehicle characteristics which accompany different flight conditions is used to define the uncertainty which is part and parcel of the QFT approach leading to the design of a single controller and prefilter for all flight conditions.

CHAPTER 3

HELICOPTER AERODYNAMICS AND CONTROL

3.1 Introduction

The purpose of this chapter is to provide the reader with a basic understanding of helicopter aerodynamics and control. For more detailed information, the reader is referred to [24, 25, 26, 27, 28].

This chapter is organized into three main sections in addition to this introduction. In the first of these, the basic aerodynamics of the helicopter will be discussed. Next, the rotorcraft mechanical control system will be presented. In the final section, the UH-60 mathematical model utilized in this study will be introduced. The reader familiar with rotorcraft fundamentals may proceed directly to Section 3.4.

3.2 Basic Helicopter Aerodynamics

This section is organized into two (2) subsections, hover and vertical flight and forward flight. Both momentum theory and blade element theory will be used to describe the aerodynamic effects experienced by the helicopter.

3.2.1 Hover and Vertical Flight

The main rotor of the helicopter generates thrust by forcing a column of air downwards through the plane of the rotor. A relationship between the thrust and the

velocity imparted on the air can be determined using Newtonian principles, namely conservation of mass, momentum, and energy. This approach is referred to as momentum theory for helicopters.

The rotor is considered an 'actuator disc,' across which a large pressure increase occurs. The column of air, larger above and tapering below, is the only air effected by the motion of the rotor in hovering flight. It increases velocity from zero far above the rotor to v_i at the disc, and continues to increase to v_∞ far below the rotor. As the air is drawn into the rotor from above, the pressure falls. There is then a sudden increase in pressure at the disc, and the pressure falls off to atmospheric below the disc. Conservation of mass dictates that the velocity change is continuous through the disc. This process is indicated in Fig. 3.1.

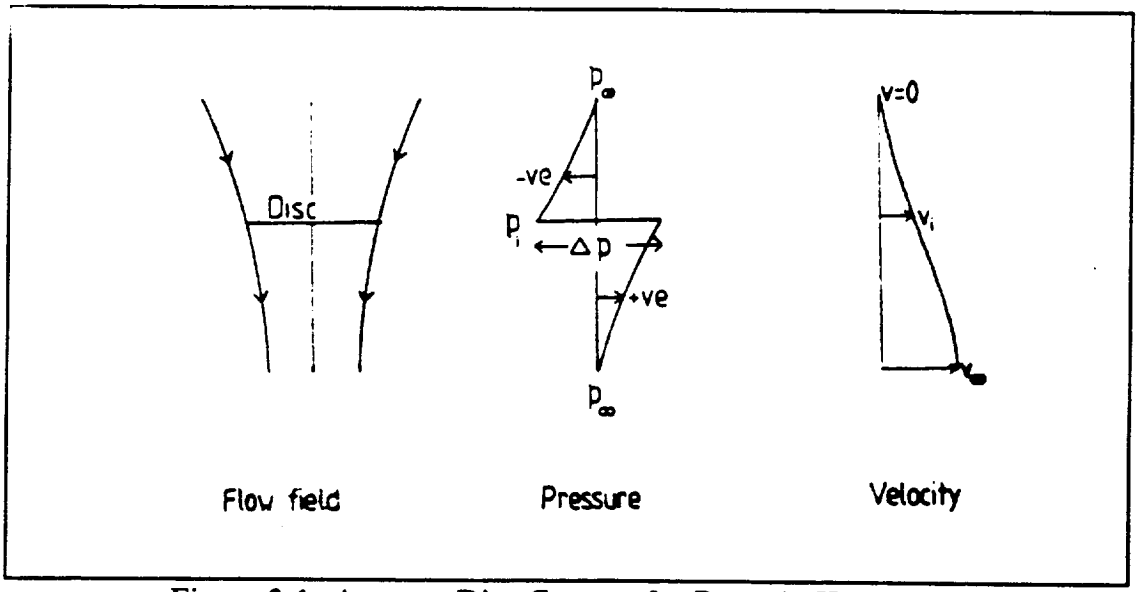

Figure 3.1 Actuator Disc Concept for Rotor in Hover [24]

Bernoulli's equation for the conservation of energy may be applied separately

above and below the disc. Above the disc, we see that the inflow equation is

$$p_\infty = p_i + \frac{1}{2}\rho v_i^2 \tag{3.1}$$

while the outflow equation for the conservation of energy is

$$p_i + \Delta p + \frac{1}{2}\rho v_i^2 = p_\infty + \frac{1}{2}\rho v_\infty^2 \tag{3.2}$$

where v_i is known as the induced velocity, ρ is the density of the air and p is pressure. The assumption of incompressible flow is made. These two equations indicate that the change in pressure across the disc may be written as

$$\Delta p = \frac{1}{2}\rho v_\infty^2 \tag{3.3}$$

By conservation of momentum, the thrust, T, generated by the rotor is equal to the overall rate of increase of the axial momentum of the air, or

$$T = \rho A v_i v_\infty \tag{3.4}$$

where A is the area of the disc so that $\rho A v_i$ is the mass flow through the disc. Since the change in pressure across the disc is the thrust per unit area, we may write

$$\Delta p = \frac{T}{A} = \rho v_i v_\infty \tag{3.5}$$

From Eqns. 3.3 and 3.5 we see that

$$v_\infty = 2v_i \tag{3.6}$$

and, if the thrust is known (equal to the weight in steady hovering flight),

$$v_i = \sqrt{\frac{T}{2\rho A}} = \sqrt{\frac{w}{2\rho}} \tag{3.7}$$

where $w = T/A$ is the "disc loading." Figure 3.2 illustrates the relationship between disc loading and downwash velocity, v_∞, with several helicopters indicated.

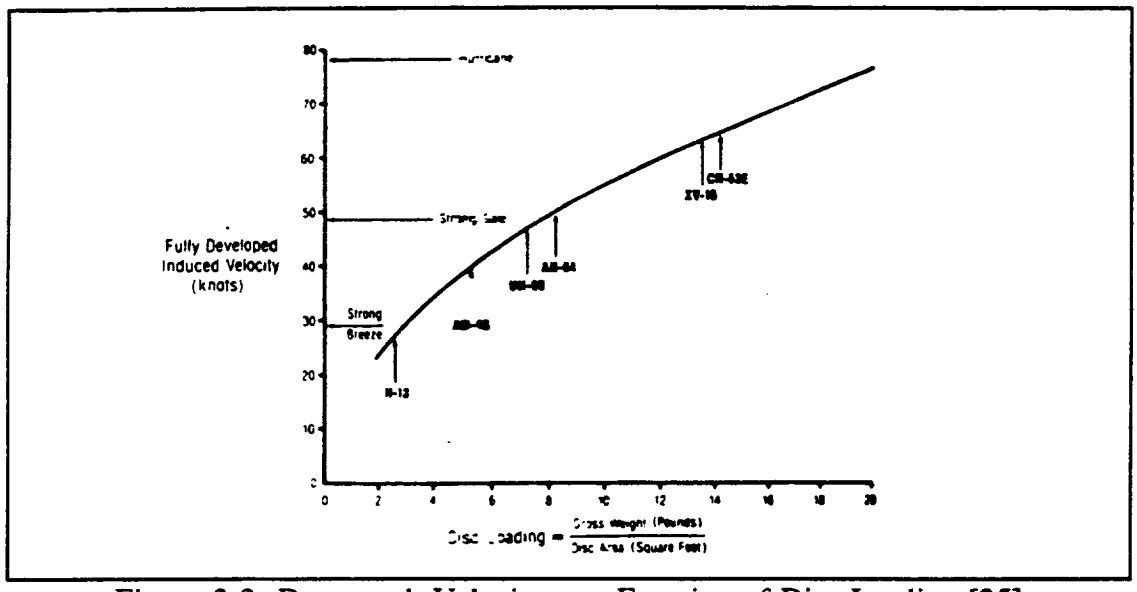

Figure 3.2 Downwash Velocity as a Function of Disc Loading [25]

Momentum theory may also be applied to the case of a vertical climb. In this case, the air is accelerated not from zero, as with hover, but from V_c, the vertical velocity of the helicopter. Now, we may rewrite Eqns. 3.1 and 3.2 as

$$p_\infty + \frac{1}{2}\rho V_c^2 = p_i + \frac{1}{2}\rho(V_c + v_i)^2 \tag{3.8}$$

$$p_i + \Delta p + \frac{1}{2}\rho(V_c + v_i)^2 = p_\infty + \frac{1}{2}\rho(V_c + v_\infty)^2 \tag{3.9}$$

It can be shown that the relationship between the hover induced velocity, v_{ih}, and the

induced velocity in Eqns. 3.8 and 3.9 is:

$$\frac{v_i}{v_{i_h}} = -\frac{V_c}{2v_{i_h}} + \sqrt{\left(\frac{V_c}{2v_{i_h}}\right)^2 + 1} \tag{3.10}$$

indicating that the induced velocity decreases asymptotically to zero as V_c increases. The power consumption may be written as

$$P_i = T(V_c + v_i) \tag{3.11}$$

which leads to the realization that for low rates of climb, the power over and above the power required for hover is only half the climb work, TV_c. In other words, a helicopter, taking advantage of the greater flow of air through the rotor, can ascend vertically with only half the additional power that would be required of an elevator raising the same mass at the same rate [25].

The same equations hold for vertical descent as long as the descent is slow. When the descent rate approaches the hover induced velocity, the flow becomes more complex, with air flowing in both directions through the rotor. This is referred to as a "vortex ring" state, and the magnitude and direction of the rotor thrust fluctuates dramatically in this condition. Once the descent rate reaches approximately twice the hover induced velocity, a condition known as autorotation occurs. At this point, no power is required to spin the rotor and generate thrust, since $V_c + v_i \approx 0$. What this means is that in the event of engine failure, the descent of the helicopter may be controlled by the free-spinning rotor which acts in much the same way as a parachute.

Momentum theory provides a good means for investigating the basics of how a rotorcraft hovers, but to really get an accurate model of the hovering helicopter, one must look to see what actually is happening at the blade of the rotor. The method used to investigate this is known as blade element theory. The principal behind blade element theory is to treat a blade element, shown in Fig. 3.3, as an airfoil and applying standard airfoil theory to determine the lift and drag contributions of that element. These contributions are then integrated over the entire rotor to determine aerodynamic characteristics of the helicopter. Figure 3.4 shows the flow conditions of a blade section during hover or vertical flight. The blade is assumed rigid for this analysis and, although the rotor blades are in general flexible, this is a valid assumption since the outward centrifugal force on the rotor tends to keep the rotor rigid.

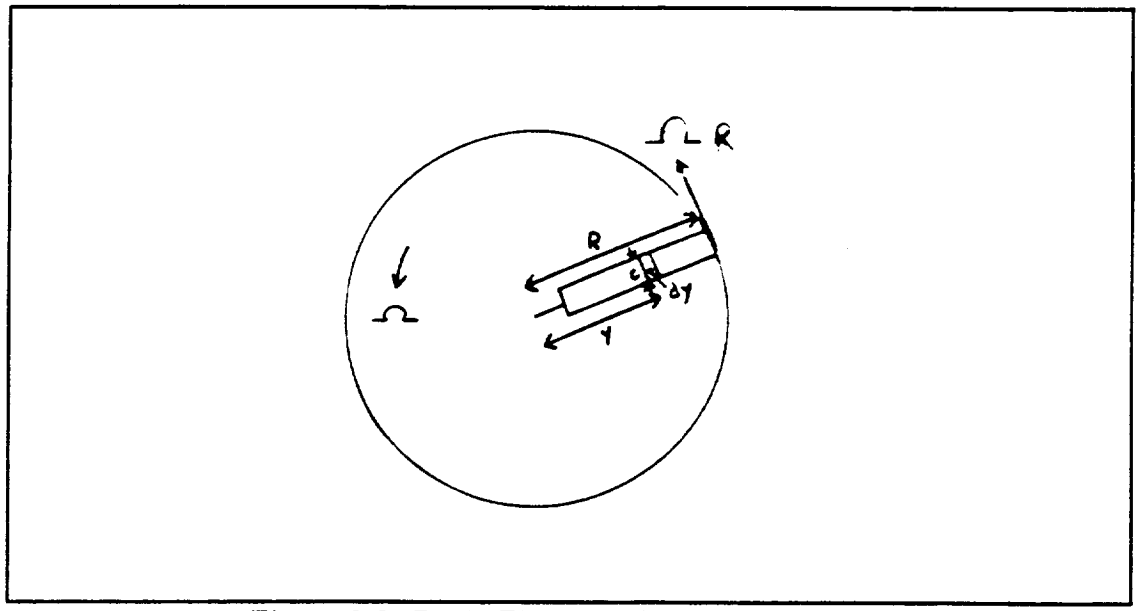

Figure 3.3 Blade Element Viewed from Above [24]

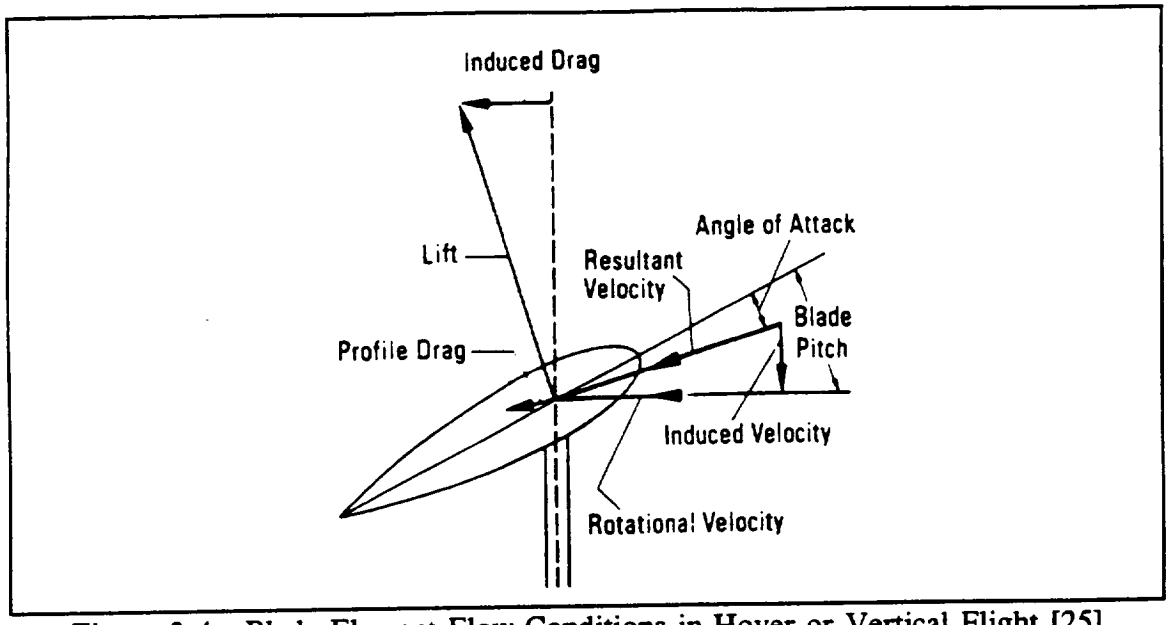

Figure 3.4 Blade Element Flow Conditions in Hover or Vertical Flight [25]

In airfoil theory, lift and drag are dependent upon the angle of attack of the airfoil. Typical plots of these relationships are presented in Fig. 3.5. Note that the helicopter engine must overcome the drag in order to spin the rotor, so that the most efficient operating condition for the helicopter is at the highest lift to drag ratio. The incremental lift and drag forces on a blade element may be written as

$$dD = \frac{1}{2}\rho U^2 c\, dy\, C_D \tag{3.12}$$

$$dL = \frac{1}{2}\rho U^2 c\, dy\, C_L \tag{3.13}$$

where C_L and C_D are the lift and drag coefficients, respectively, and the velocity, U, is expressed as follows.

$$U=\left[(v_i+V_c)^2+(\Omega y)^2\right]^{1/2} \tag{3.14}$$

Note that the incremental lift and drag forces on the blade element depend upon that elements' distance from the hub, with greater forces experienced near the tip of the blade. To account for this non-uniform distribution of forces, most helicopter blades have a negative twist, decreasing the angle of attack and, consequently, the lift and drag coefficients in Eqns. 3.11 and 3.12, towards the tip of the blade. This tends to more evenly distribute the lift and drag along the blade.

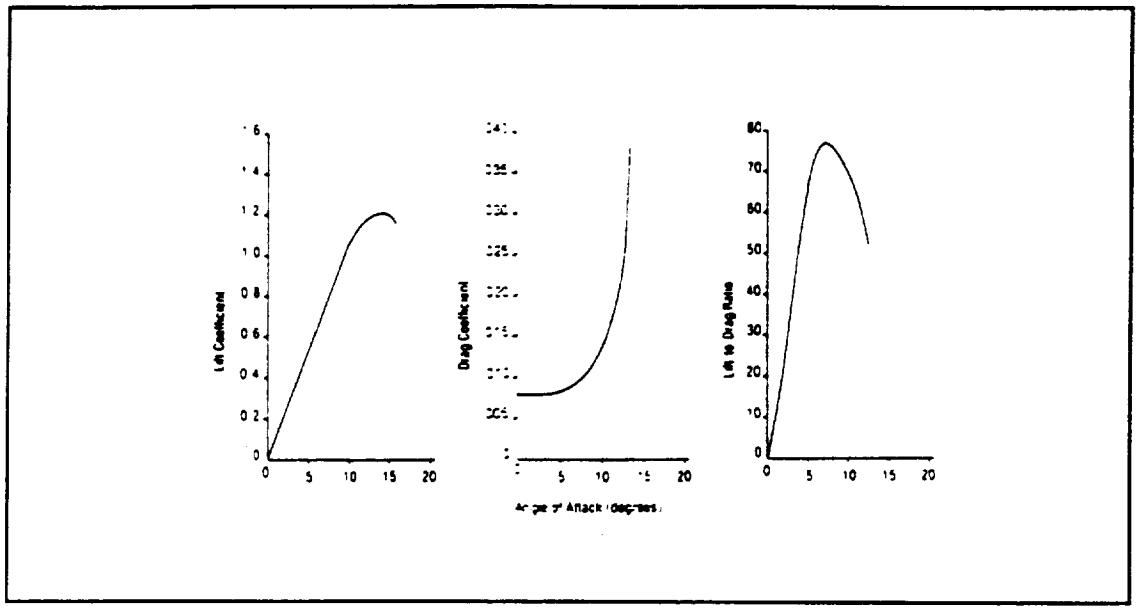

Figure 3.5 Typical Airfoil Aerodynamic Characteristics [25]

As with other disciplines, it is useful to establish dimensionless quantities. Consider the following:

$$r=\frac{y}{R} \tag{3.15}$$

$$\frac{U}{\Omega R}=\frac{\Omega y}{\Omega R}=r \tag{3.16}$$

$$dC_T=\frac{dT}{\rho A(\Omega R)^2} \tag{3.17}$$

$$dC_Q=\frac{dQ}{\rho A(\Omega R)^2 R} \tag{3.18}$$

$$\lambda=\frac{(V_c+v_i)}{\Omega R}=r\phi \tag{3.19}$$

where dQ is the incremental blade torque, dT is the incremental thrust, and λ is the inflow factor. Assuming small angles, such that $dT \approx dL$, and from Eqns. 3.11 and 3.16, we obtain the following expression for the incremental thrust coefficient.

$$dC_T=\frac{1}{2}\sigma C_L r^2 dr \tag{3.20}$$

where σ is the solidity factor of the rotor which, for a constant blade chord, c, and for N blades in the rotor, is given by

$$\sigma=\frac{NcR}{A} \tag{3.21}$$

The angle of attack, α, may be referenced to the zero lift line of the airfoil section. This implies that the blade pitch angle, θ, is also referenced to the zero lift line of the airfoil section. Also, as can be seen in Fig. 3.5, the lift coefficient is linear with respect to α for a significant range of α, or

$$C_L = a\alpha = a(\theta - \phi) \tag{3.22}$$

To determine the total thrust coefficient, in this case, the following integration is required.

$$C_T = \frac{1}{2}\sigma a \int_0^1 (\theta r^2 - \lambda r) dr \tag{3.23}$$

In the momentum theory portion of this discussion, the assumption was made that the inflow velocity was constant over the actuator disc. This assumption translates in Eqn. 3.22 to a constant λ. It is not necessary in this case to make this assumption. Indeed, as will be discussed in the following chapter, the dynamic helicopter model used for this research allows for non-uniform inflow velocities and, consequently, variable λ.

3.2.2 Forward Flight

The mathematical analysis for the aerodynamics of a helicopter in forward flight is very similar to that presented for hover and vertical flight. Several complications are presented, however. In level forward flight, the rotating blade is edgewise to the airstream. This is unnatural for a propelling operation of the rotor. Complications are introduced because the velocity of the airstream over the rotor blades varies over the cycle of the blade rotation. Mechanical devices have been devised which take care of the cyclic loading of the rotor system, but these in turn add to the complexity of the aerodynamics.

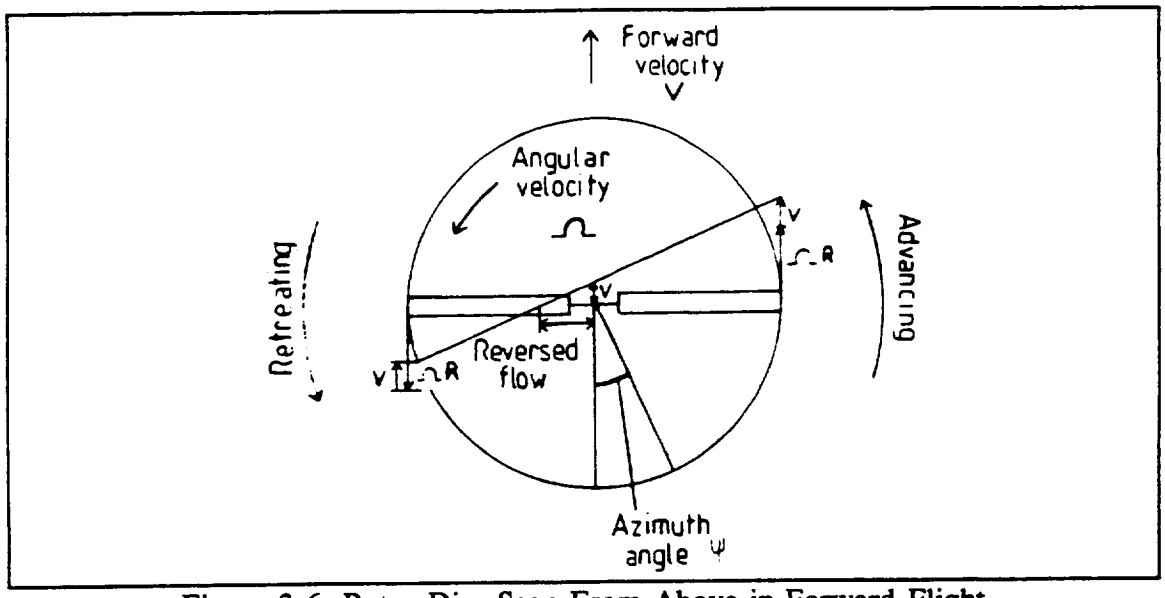

Figure 3.6 Rotor Disc Seen From Above in Forward Flight

Figure 3.6 depicts a top view of the rotor system travelling edgewise to the airstream. This figure demonstrates the variance on the airstream velocity over the rotor blade as the blade rotates. The airstream velocity over the blade is faster as the blade "advances" on the right hand side of the figure than as the blade "retreats" on the left hand side due to the velocity component attributable to the forward velocity, V. The conventional direction of blade rotation adopted by all Western countries is counter-clockwise, with the rotor speed denoted Ω. A quantity known as the advance ratio is defined by the ratio

$$\mu = \frac{V}{\Omega R}$$

where R is the radius of the rotor disc, and provides an indication of the effect of the forward flight on the velocity seen by the rotor blades. Under normal operating conditions, the advance ratio varies between 0 and 0.5.

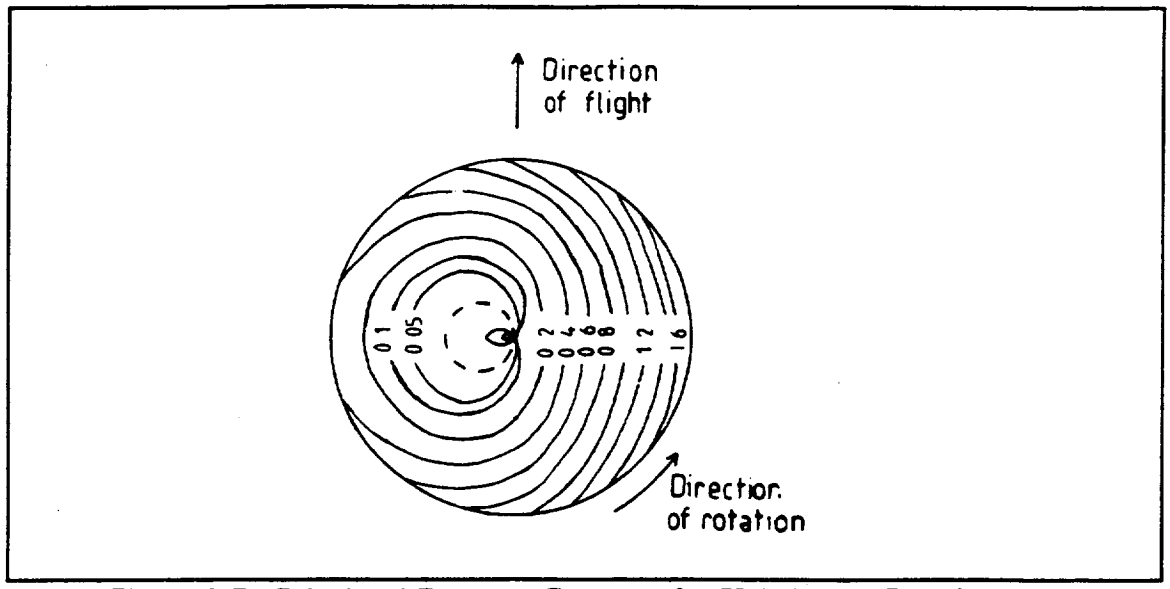

Figure 3.7 Calculated Pressure Contours for Unbalanced Rotation [24]

If the blade rotates with a constant angle of incidence, the lift generated on the advancing side of the rotor disc will be much larger than that generated on the retreating side. Figure 3.7 shows the pressure distribution over the rotor disc with μ=0.3. In this example, about four fifths of the total lift is produced on the advancing side of the rotor disc. Consequences of this unbalanced loading would be two-fold: 1) it would produce large oscillatory bending moments on the rotor blades; and 2) it would produce a large rolling moment on the airframe. These problems would make the helicopter unflyable.

To address the unbalanced loading induced by forward flight, flapping hinges were introduced by Juan de la Cierva circa 1923. The blade is freely hinged as closely as possible to the root (center of rotation) to allow it to "flap" up and down as it rotates. This hinge relieves the bending moments on the rotor blades experienced at the rotor blade root. Also, as the blade experiences an increased velocity on the advancing side,

the increased lift causes the blade to rise, which in turn decreases the incidence of the blade, reducing the lift and allowing the blade to fall again. The reverse is experienced on the retreating side. The net result is an evening out of the pressure distribution laterally on the rotor disc, reducing the roll moment imparted on the vehicle. The resulting pressure distribution is shown in Fig. 3.8.

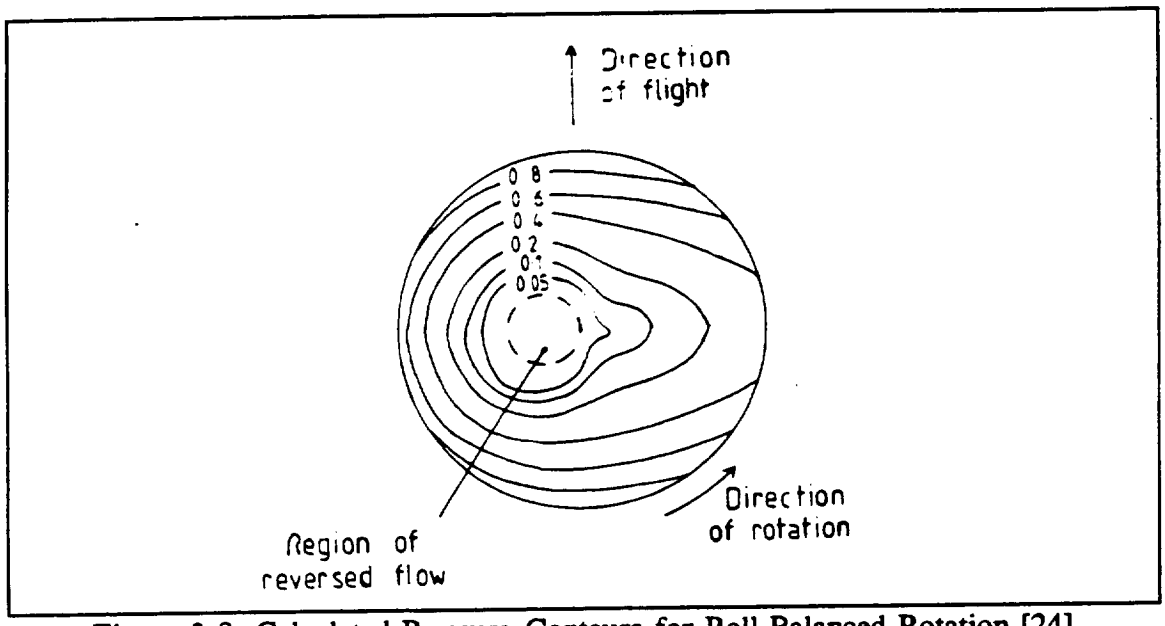

Figure 3.8 Calculated Pressure Contours for Roll-Balanced Rotation [24]

The flapping motion of the blade as it rotates induces Coriolis moments in the plane of the disc. To relieve these moments, a second hinge, called a lead-lag hinge, may be included in the rotor system. This hinge allows the blade to advance and retreat relative to the hub as it travels through a complete rotation.

3.3 Basic Helicopter Control System

An additional hinge or bearing situated axially on each blade is included which

allows pilot controller inputs to effect the pitch of the blade. It is this control mechanism on both the main and tail rotors that allows the pilot to control the rotorcraft. Figure 3.9 depicts a sample articulated rotor containing the three hinges described above.

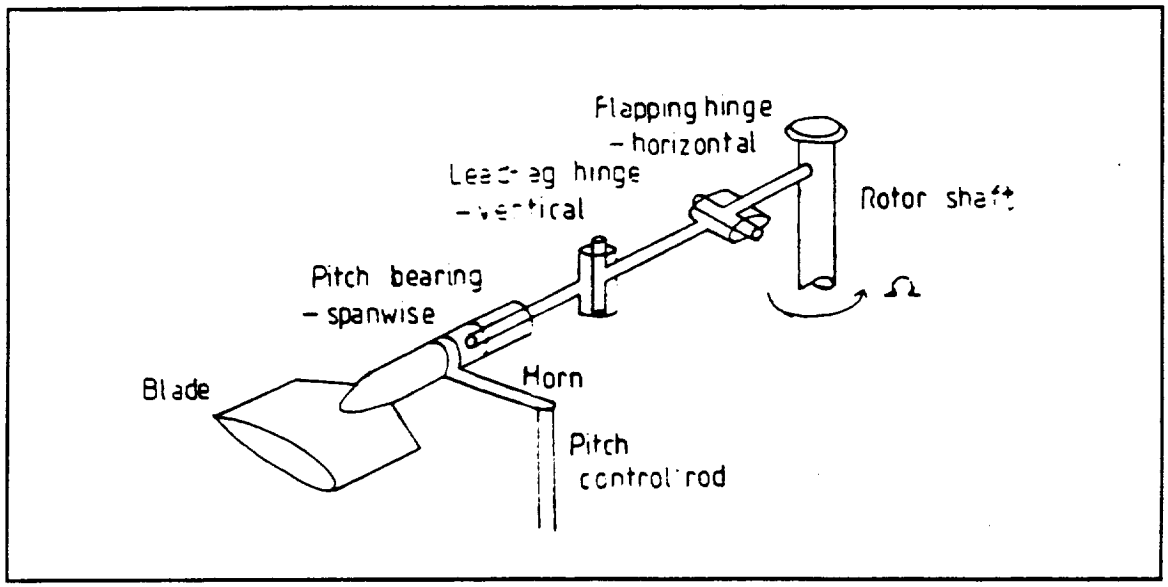

Figure 3.9 Principals of Articulated Rotor [24]

A swash plate, consisting of a rotating plate and a parallel non-rotating plate, is situated around the rotor shaft below the connection point of the rotor blades. The pitch control rods for each of the blades are connected to the rotating swash plate. The pilot controls the vertical motion of the swash plate using the collective controller. This changes the blade pitch evenly throughout a rotation, effecting the magnitude of the rotor thrust vector. The swash plate may also be tilted, through the use of the cyclic controller. Tilting the swashplate longitudinally and/or laterally effects the blade pitch cyclically, causing a moment on the rotorcraft in roughly the direction of the swash plate tilt. As the rotorcraft rotates in response to this imposed moment, the direction of the

thrust vector is changed. Ultimately, therefore, the pilot can control the direction of flight by utilizing the cyclic controller to tilt the swash plate. The pedals are to the tail rotor what the collective is to the main rotor. Changing the magnitude of the thrust vector for the tail rotor causes a yawing moment about the rotorcraft's vertical body axis. This control arrangement is illustrated in Fig. 3.10.

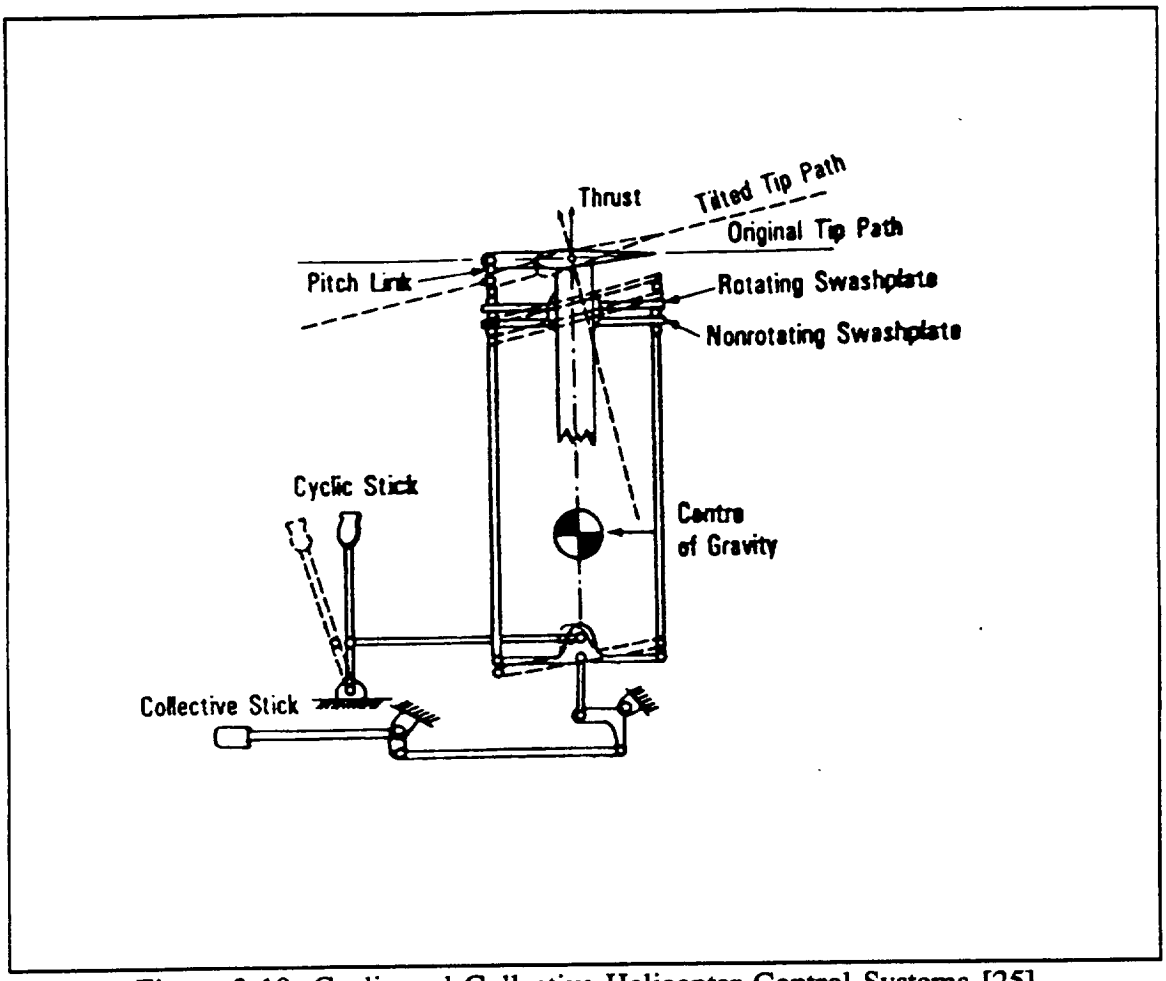

Figure 3.10 Cyclic and Collective Helicopter Control Systems [25]

3.4 The UH-60 Rotorcraft Mathematical Model

The preceding sections discussed the aerodynamic forces and moments produced

by a rotor, the fundamental degrees of freedom of the rotor, and finally, the mechanical means by which the aerodynamic forces and moments can be modulated to control the vehicle. The derivation of the vehicle equations of motion is obviously quite complex and will not be presented here. However, Appendix A shows the 28 state linear vehicle model for the UH-60A Black Hawk rotorcraft shown in Fig. 3.11. The model is presented for each of six (6) flight conditions to be utilized in the FCS design process. The linear models were obtained from a general non-linear 28^{th} order rotorcraft model which may be tailored to represent a variety of rotorcraft [29].

As has been indicated in Chapter 2, the complexity of the mathematical model to be used in the FCS design is of singular importance. Low-order rigid body models of rotorcraft are satisfactory for the design of low response-bandwidth FCS's, but the limitations on the validity of such models at higher frequencies compromises their utility for the design of high response-bandwidth systems.

The model of Appendix A includes the flapping and lead-lag dynamics of the rotor and the dynamics of the rotor inflow. One addition to the vehicle model of Ref. [6] was an actuator for each of the controls. Each actuator was modelled as a second order system with a natural frequency of 30 rad/sec and a damping ratio of 0.7 [30].

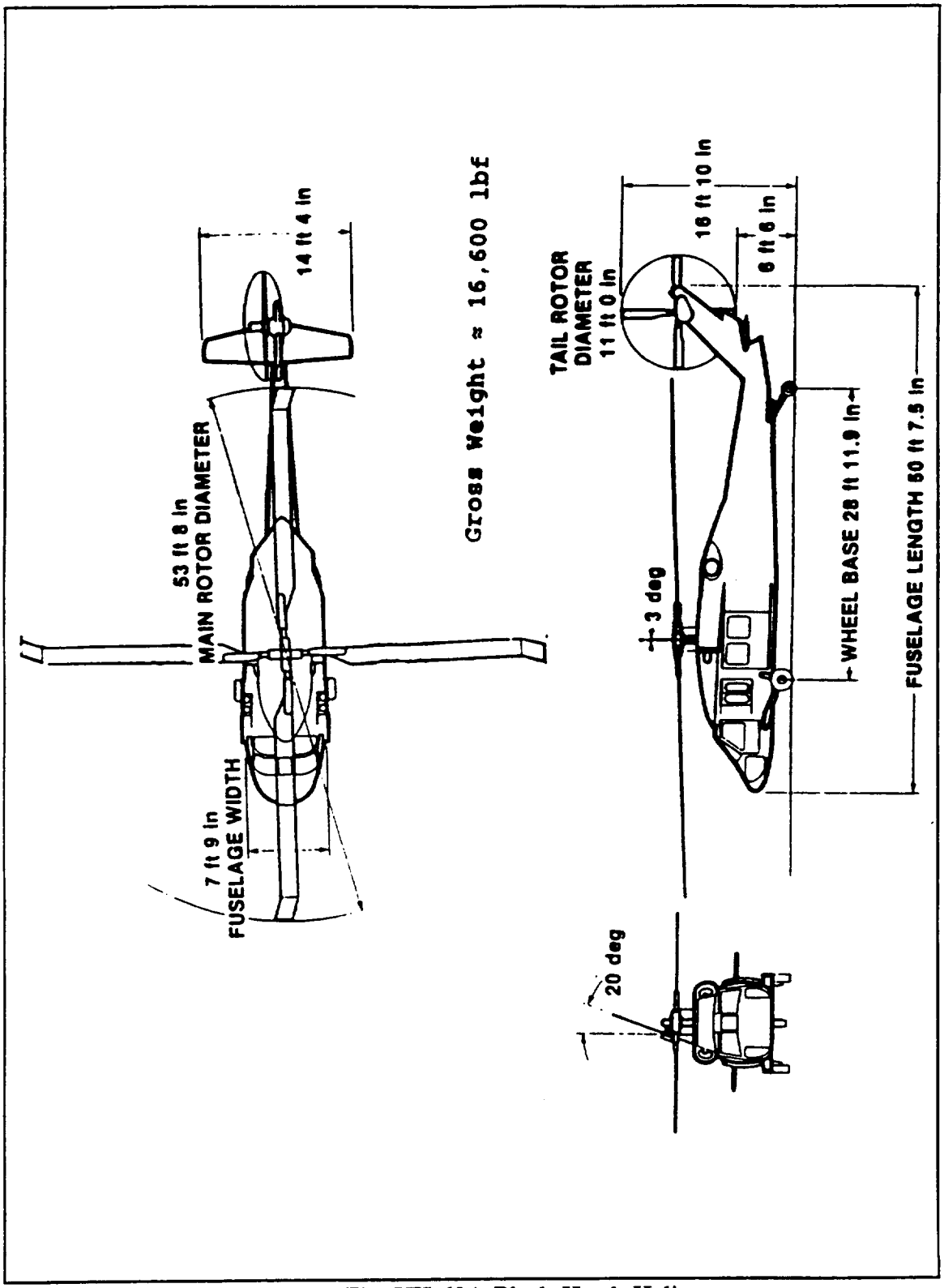

Figure 3.11 The UH-60A Black Hawk Helicopter

CHAPTER 4

FLIGHT CONTROL SYSTEM DESIGN

4.1 Introduction

As the crux of this research, this chapter will present a more detailed description of the QFT design approach. First, a more detailed description of Quantitative Feedback Theory and its extension to a MIMO design problem will be presented. The next two sections will present a detailed account of the QFT design specifications, and the final two sections will present the design effort and the results. For purposes of exposition, the QFT design will have as its goal the specification of continuous (as opposed to discrete) compensators and prefilters.

4.2 Quantitative Feedback Theory

As briefly discussed in Chapter 1, Quantitative Feedback Theory is a technique for designing robust control systems which include uncertainty or variation in the plant dynamic model to yield adequate performance as specified by the performance boundaries. It was developed to address a Multiple-Input-Single-Output (MISO) design problem such as that depicted in Fig. 4.1, a reprise of Fig. 1.2.

In order to employ this control system design technique, several elements are required in the problem definition. First, the plant, defined as that which is to be

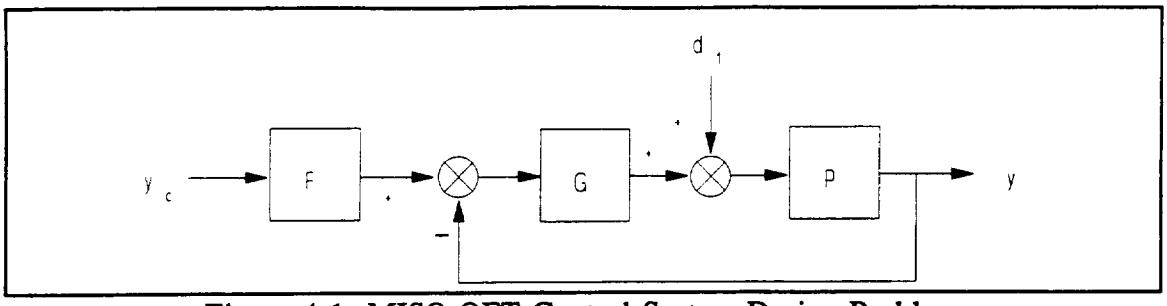

Figure 4.1 MISO QFT Control System Design Problem

controlled and labeled P in Fig. 4.1, must be an element of a known set of possible plant dynamic models, *P*. In other words, the plant dynamic model is not precisely known but limits as to its dynamic responses are known. For example, if the plant consists of a robotic armature which is moving a variety of loads to a precise location, the exact dynamic model of the plant is unknown due to the uncertainty of the load at any given time. The range of dynamic responses are known for the plant, however, if the limits on the load sizes are known.

The second requisite element of the problem definition is the specification of acceptable performance. Unlike some design techniques which attempt to achieve a specific response type, QFT acknowledges the fact that due to the variation of the plant dynamic models, some variation will occur in the response as well. It is desirable, therefore, to ensure that some level of performance will be achieved over the entire set of possible plant dynamic models. Returning to the robotic armature example, let us assume that the arm is placing its loads on a conveyor belt. Further, there is a wall behind the belt which limits the overshoot of the armature. Performance specifications define acceptable performance that the system should exhibit for the entire range of load

sizes. For example, performance specifications in this case could be a tolerance on the placement position, a maximum time to placement of the load, a maximum translational velocity of the end effector, and a maximum overshoot of the end effector. This set of specifications may be expressed in terms of two bounding transfer functions, T_U and T_L, where T_U exhibits the maximum translational velocity, the maximum overshoot, and the farthest load placement, and T_L exhibits the maximum time to placement and the nearest load placement.

The design objectives given these specifications are three-fold. The first and most basic is known as stability robustness. That is, the closed loop system must be stable for any of the possible plant dynamic models. This requirement is quantified by the following two inequalities.

$$|1 + GP| > S_1, \qquad P \in P \tag{4.1}$$

$$\left|\frac{GP}{1 + GP}\right| < S_2, \qquad P \in P \tag{4.2}$$

where S_1 limits the closest approach of the loop transmission, GP, to the $-1+0j$ point, and S_2 limits the peak magnitude of the closed loop system thereby guaranteeing a minimum damping ratio for the closed loop system.

The second design objective is to ensure performance robustness, meaning that for any of the possible plant dynamic models, the performance of the closed loop system will be acceptable as defined by the performance specifications. Although no

mathematical justification is presented here, it is the premise of QFT that if the frequency response of a given transfer function lies between T_U and T_L its time response will be acceptable. In other words, the design objective is to ensure that the closed loop frequency response of the system remains between T_U and T_L for all possible plant dynamic models, or

$$T_L \leq \frac{FGP}{1+GP} \leq T_U, \qquad P \in P \tag{4.3}$$

in order to ensure performance robustness.

Disturbance robustness is another of the design objectives. For this, an upper limit of the frequency response of the closed loop system due to disturbance inputs is defined. The design objective here is to ensure that the closed loop frequency response of the system due to disturbance inputs remains below the disturbance boundary, T_D, for all possible plant dynamic models, or

$$\frac{P}{1+GP} \leq T_D, \qquad P \in P \tag{4.4}$$

in order to ensure disturbance robustness.

These design objectives are addressed in a two step process. In the first step, the feedback compensator, G, is designed to meet the following design objectives.

1. Stability Robustness (Eqns. 4.1 and 4.2)
2. Disturbance Robustness (Eqn. 4.4)

3. Performance variation requirements.

The last of these design objectives is a subset of the performance robustness objective. Simply put, the objective of this part of the design process is to ensure that the variation in the closed loop performance due to the range of possible plant dynamic models will be less than the difference between the upper and lower performance boundaries, or

$$\Delta\left|\frac{GP}{1+GP}\right| \leq |T_U| - |T_L| \tag{4.5}$$

Although ideally the inequalities of Eqns. 4.1, 4.2, 4.4, and 4.5 should be satisfied for a continuous spectrum of all frequencies, it is not possible to accomplish this. Instead, QFT employs a graphical technique to design the feedback compensator in compliance with these inequalities for a finite set of design frequencies. The designer should select this set to encompass a broad range of frequencies about the projected crossover frequency (the frequency at which the magnitude of the loop transmission $GP(j\omega)$ equals 0 db).

To begin the first step of the QFT design process, the Bode magnitude and phase of each of the set of possible plant dynamic models is determined for each of the design frequencies. When these magnitudes and phases are plotted on a Nichols chart for a particular design frequency as in Fig. 4.2, a bounding area may be drawn. This bounding area, known in the QFT lexicon as a template, defines the variation of the frequency response at that frequency due to the range of plant dynamic models. One

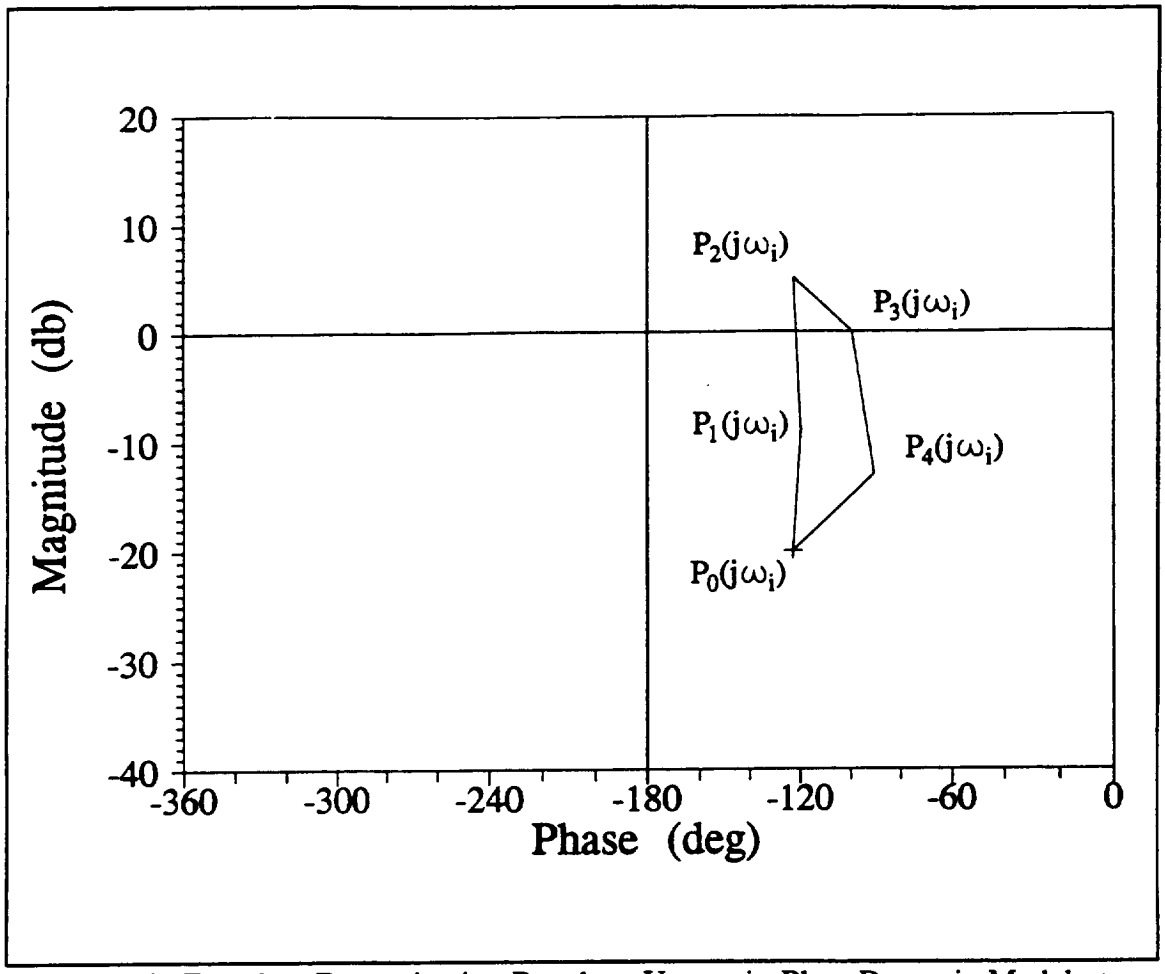

Figure 4.2 Template Determination Based on Uncertain Plant Dynamic Model at ω_i

plant dynamic model is selected arbitrarily as the "nominal plant," hereafter denoted P_0, and the corresponding point on the template is identified.

It might be helpful at this point to introduce some key points about Nichols charts, the feedback compensator design environment for QFT. The Nichols chart is a plot of open loop magnitude on the ordinate and open loop phase, generally ranging from -360° to 0°, on the abscissa. On these charts lines indicating constant closed loop magnitude

may be drawn. These lines are called M-circles. One characteristic of M-circles is that at higher open loop magnitude (higher on the Nichols chart), the spacing between the M-circles increases. This implies that for the same variation in open loop magnitude, the variation in closed loop magnitude will be less at higher absolute open loop magnitudes. QFT utilizes this fact to address the design objectives by defining on the Nichols chart boundaries for each design frequency above which the known open loop variation due to the set of possible plant dynamic models will result in an acceptable level of closed loop variation as stipulated by the difference between T_U and T_L (Eqn. 4.5). The template for a given design frequency is moved vertically at a given open loop phase until it fits between two M-circles whose difference is equal to the difference between T_U and T_L. A mark is made on the Nichols chart at the location of the nominal plant mark on the template. With this process continuing for different open loop phases, one can envision that a line may be drawn connecting these marks for a given design frequency template from one side of the Nichols chart to the other. A similar approach is taken in the generation of boundaries on the Nichols chart which guarantee the satisfaction of the inequalities of Eqns. 4.1, 4.2, and 4.4. The most conservative of these boundary definitions (i.e., highest on the Nichols chart) for a given design frequency becomes the design boundary for that frequency. Figure 4.3 depicts a Nichols chart with several design boundaries, denoted $B(j\omega_i)$ in the figure, in place.

Once these boundaries are defined, the feedback compensator is designed such that the nominal loop transmission, $L_0 = GP_0$, lies above and to the right of each of the

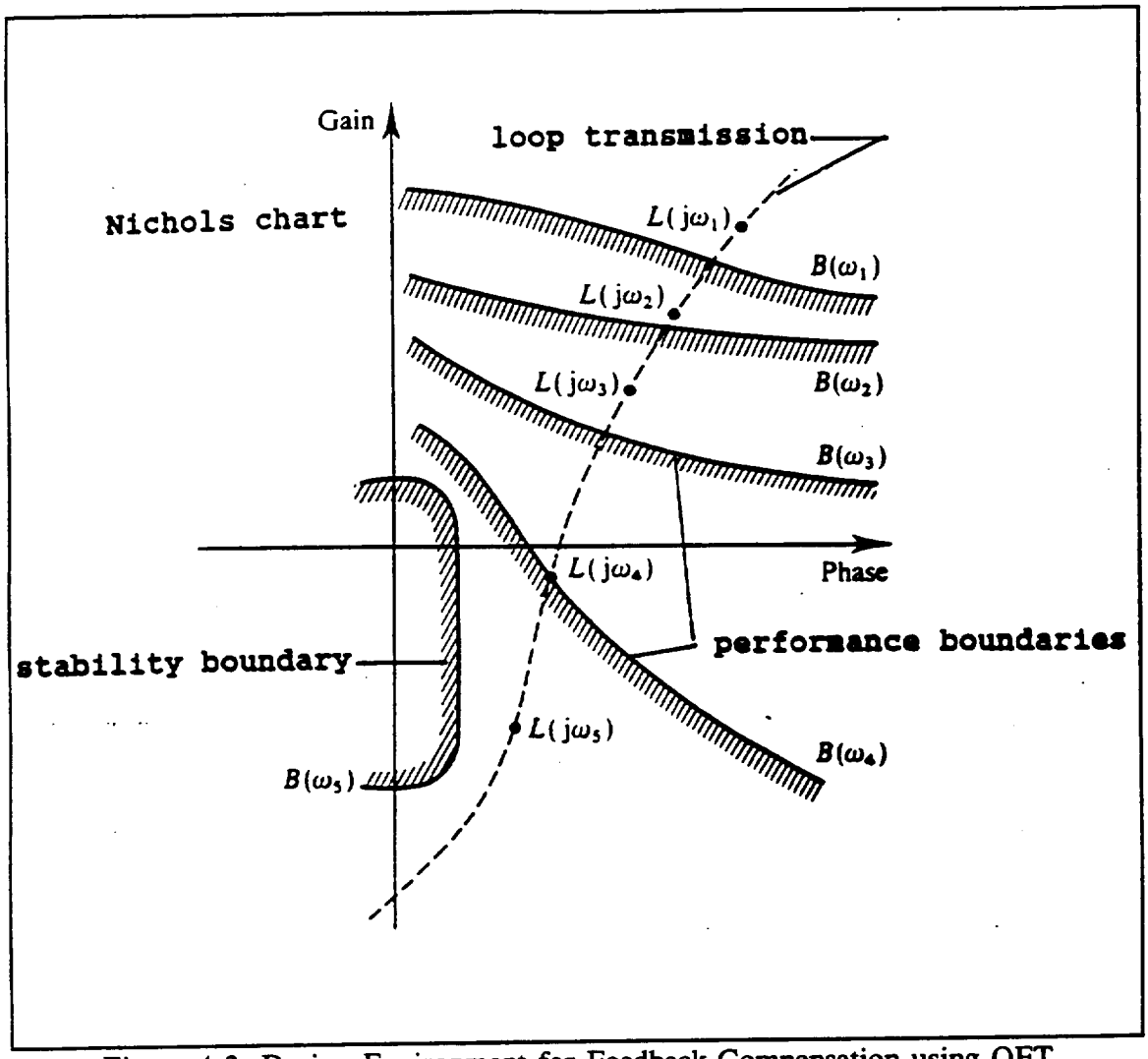

Figure 4.3 Design Environment for Feedback Compensation using QFT

boundaries at the associated frequencies. If such a feedback compensator can be attained, Quantitative Feedback Theory states that the design objectives of this first step of the design process will be satisfied.

With the feedback compensator designed, the second step of the design process

is to address the last of the design objectives, performance robustness. This objective is expressed in the inequality of Eqn. 4.3. The prefilter, F, is designed to satisfy this design objective. For each design frequency, the closed loop magnitude is determined for each of the possible plant dynamic models. The prefilter is designed using a plot of Bode magnitude versus frequency to ensure that at each of the design frequencies, Eqn. 4.3 is satisfied.

To employ QFT to a MIMO problem one must first determine the equivalent set of MISO design problems which fully represent the MIMO design problem. The following is a derivation of such a set of design equations, each of which is equivalent to a MISO design equation, which fully describes the MIMO system. This decomposition of the MIMO design problem into MISO design equations is depicted graphically in Fig. 4.4.

The top half of Fig. 4.4 depicts a MIMO QFT design problem. In this case, the input and output vectors, $\underline{y}$ and $\underline{u}$, are of length n, and $\underline{P}$, $\underline{G}$, and $\underline{F}$ are square matrices of transfer functions with dimensions n x n. A transform is selected as

$$\underline{c} = \underline{P}\underline{G}(\underline{F}\underline{u} - \underline{c}) \tag{4.6}$$

so that

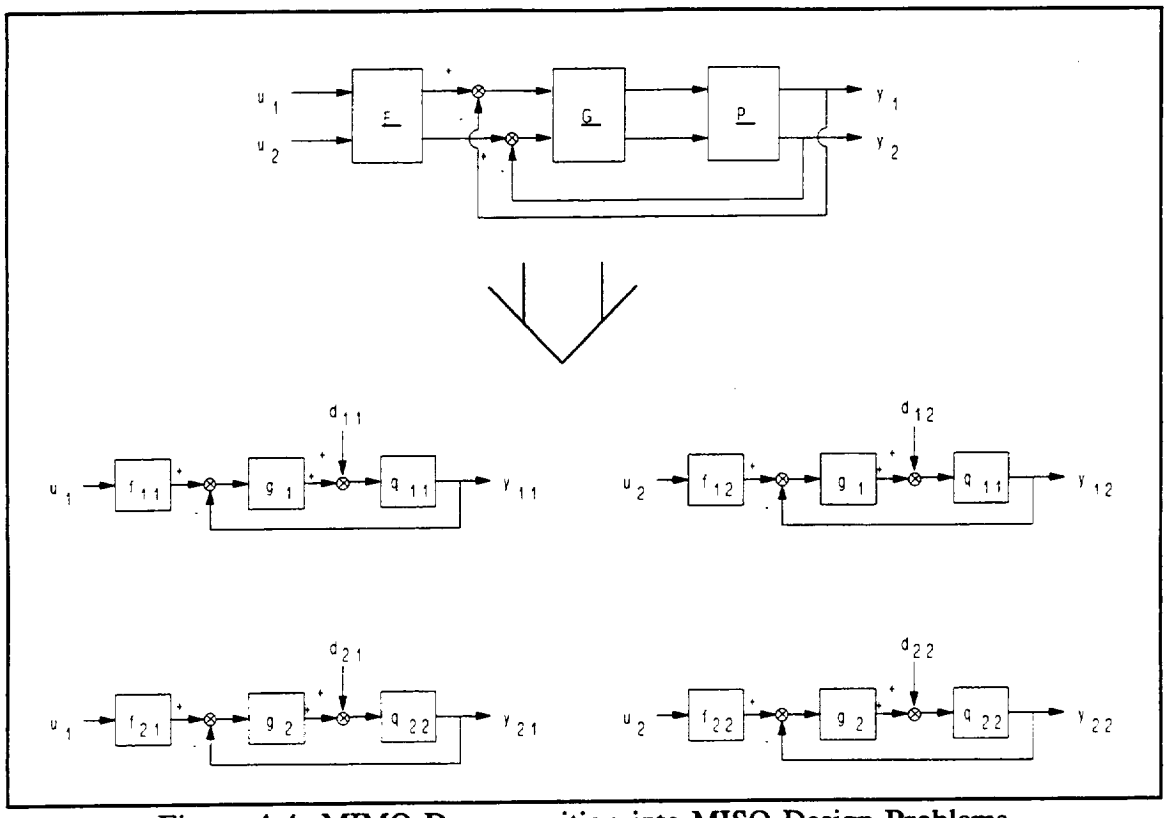

Figure 4.4 MIMO Decomposition into MISO Design Problems

$$(\underline{P}^{-1} + \underline{G})\underline{c} = \underline{GF}\underline{u} \tag{4.7}$$

which yields the constraint that $\underline{P}$ must be non-singular for all of P. Now, substituting $\underline{T}\,\underline{u}$, where $\underline{y} = \underline{T}\,\underline{u}$, into Eqn. 4.7 for $\underline{c}$, we see that

$$(\underline{P}^{-1} + \underline{G})\underline{T} = \underline{GF} \tag{4.8}$$

Let each of the elements of the $\underline{P}^{-1}$ matrix be denoted $1/Q_{ij}$ and require $\underline{G}$ to be diagonal. To solve this matrix equation, each of the elements of the left and right hand sides of the equation must be equated. With a little manipulation of these n^2 equations, a general expression results.

$$T_{ij}=\frac{F_{ij}G_iQ_{ii}+d_{ij}Q_{ii}}{1+G_iQ_{ii}},\quad d_{ij}=-\sum_{\alpha\neq i}\frac{T_{\alpha j}}{Q_{i\alpha}} \qquad (4.9)$$

This suggests a mapping for y_{ij} by replacing T_{ij} on the left hand side of Eqn. 4.9 with y_{ij}. The T_{ij} in the disturbance expression are replaced by the acceptable response boundaries, τ_{ij}, where τ_{ij} represents the upper performance boundary for the response of the i^{th} output to the j^{th} input. The form of Eqn. 4.9 may be depicted graphically by the four block diagrams in the lower half of Fig. 4.4 if the inputs , u_1 and u_2, are taken to be unit impulse functions. Notice that each is precisely equivalent to the MISO design problem shown in Fig. 4.1, so that the techniques employed for that problem may also be employed here. For diagonal $\underline{G}$ compensation, as is assumed here, there exists the additional stipulation that the elements of the $\underline{G}$ compensator matrix satisfy the performance bounds for each of the MISO design problems in its row (e.g., g_1 must satisfy the bounds for both of the upper two MISO design problems shown in the lower half of Fig. 4.4).

4.3 Plant Variation in the QFT Design Process

As was previously discussed, QFT is a design procedure which accounts for a quantifiable uncertainty in the dynamic properties of the plant. In the case of this flight control system design problem, the uncertainty was taken to be the variation in the dynamic characteristics of the rotorcraft at different flight conditions, from hover (0 kts) to 100 kts. The full 28 state non-linear UH-60 helicopter model defined in Chapter 3 was liearized about six (6) flight conditions: hover (0 kts); 20 kts; 40 kts; 60 kts; 80 kts;

and 100 kts. These six linear state-space models are listed in Appendix A, and constituted the set of possible plant dynamic models, P.

4.4 Performance Boundaries

Another necessary design specification for QFT is the set of boundaries on acceptable performance. As was indicated in Section 4.3, it is desired that the defined performance bounds relate to the handling qualities of the resulting FCS. Handling qualities (HQ) are defined in Ref.[31] as "those qualities or characteristics of an aircraft that govern the ease and precision with which a pilot is able to perform the tasks required in support of an aircraft role." A rating scale has been developed to standardize pilot evaluation of handling qualities (Fig.4.5)[32]

Using this standard, specifications have been developed which relate various dynamic response descriptors (bandwidth, time delays, etc.) with an expected handling qualities level [33]. These relations are presented in a graphical form for typical rotorcraft response considerations as shown in Fig. 4.6. The different "levels" of handling qualities corresponds to the three levels shown in Fig. 4.5, with Level 1 handling qualities representing the desired performance for the rotorcraft. These specifications were used to determine appropriate performance bounds by selecting a point in the Level 1 region of a given handling qualities specification plot as shown in Fig. 4.6. This point defines a phase delay, τ_p, and a bandwidth, ω_{BW}, of a transfer function which defines a lower limit for Level 1 handling qualities. Any higher

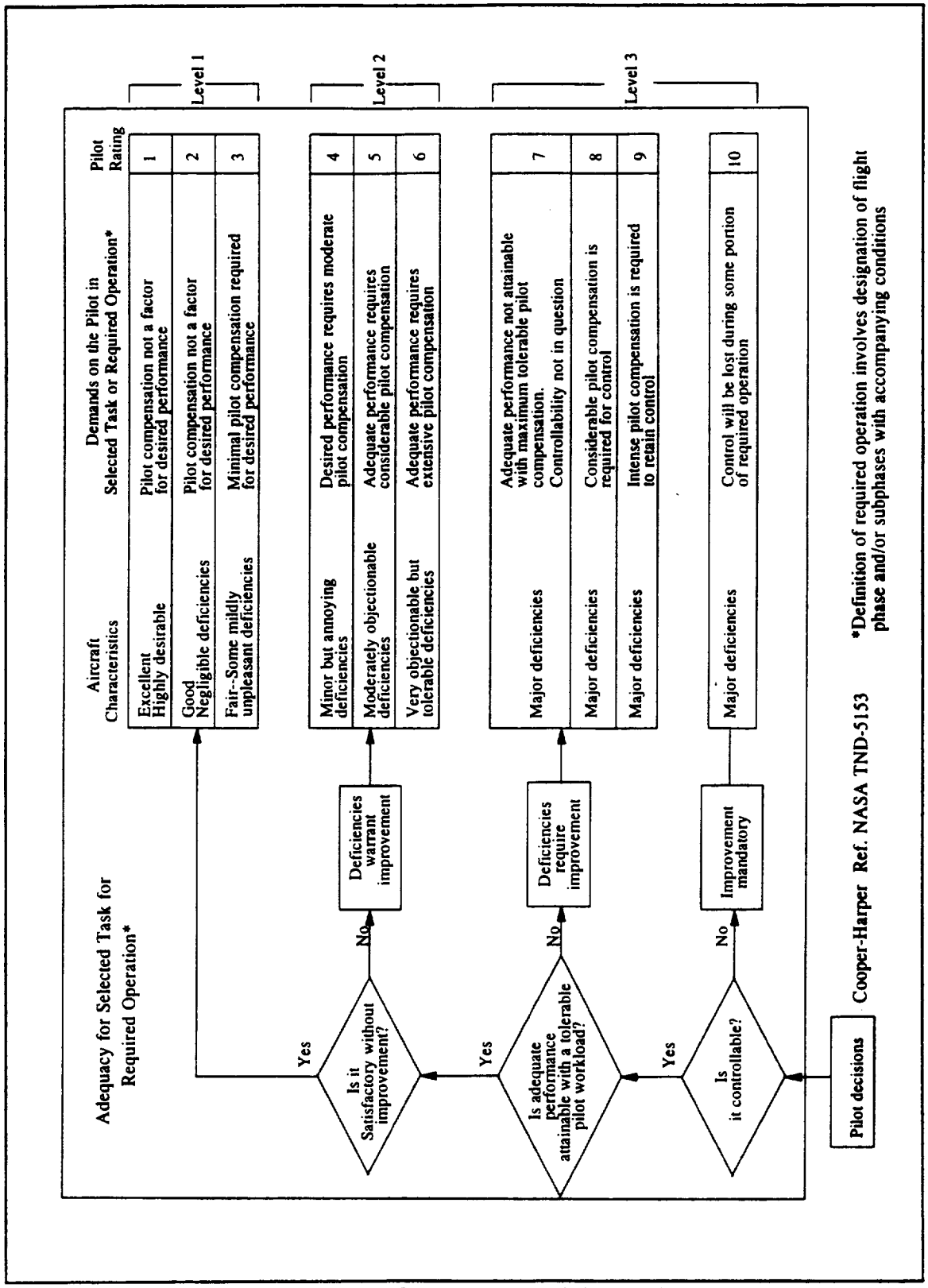

Figure 4.5 Cooper-Harper Pilot Opinion Rating Scale

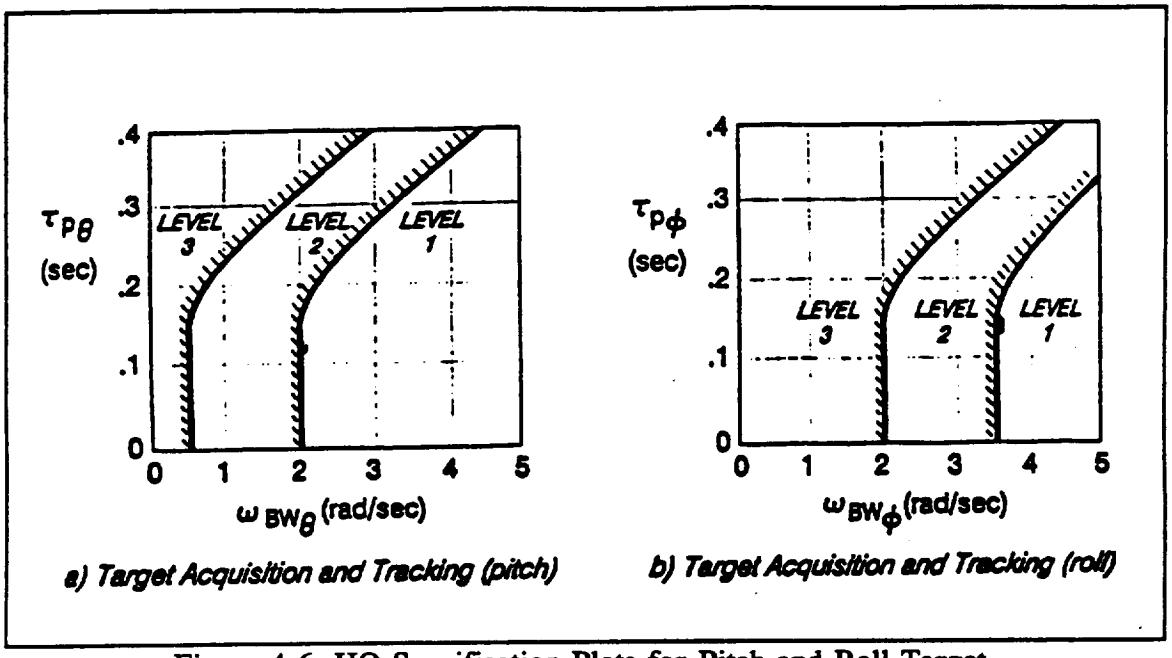

Figure 4.6 HQ Specification Plots for Pitch and Roll Target Acquisition and Tracking

bandwidth and/or lower phase delay will also result in Level 1 handling qualities. To determine a transfer function which has the required bandwidth and phase delay requires the use of Fig. 4.7, taken directly from Ref. [33]. The bandwidth of a given transfer function is defined as the lesser of the gain bandwidth, ω_{BWgain}, and the phase bandwidth, $\omega_{BWphase}$, and the phase delay is defined by the following expression.

$$\tau_p = \frac{\Delta\Phi 2\omega_{180}}{57.3(2\omega_{180})} \tag{4.10}$$

These specifications were, unfortunately, defined for use in an evaluation procedure; that is, one can easily use these specifications to determine if a given transfer function will likely result in Level 1 handling qualities. Because a given bandwidth and phase delay do not characterize a unique transfer function, it is less easy to use the

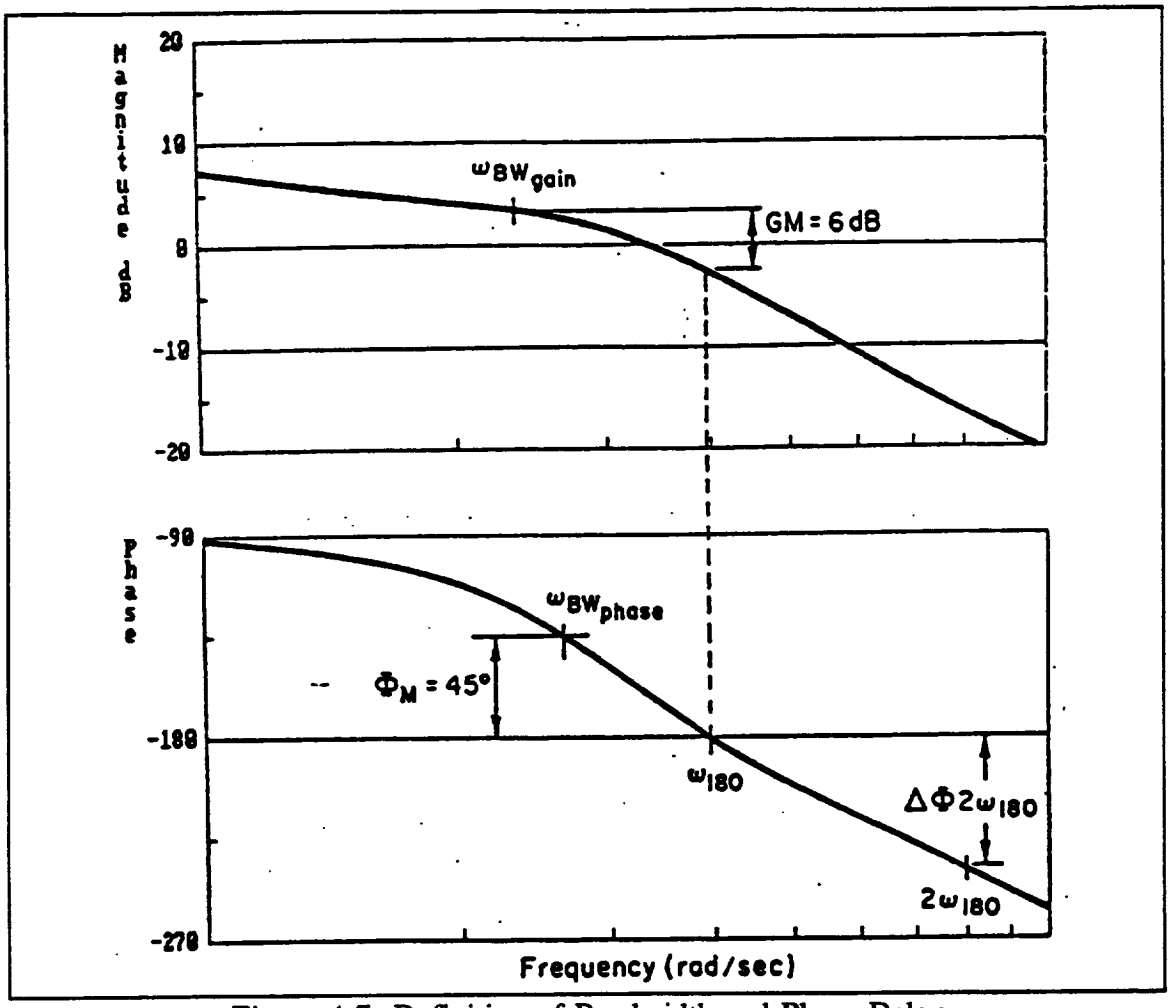

Figure 4.7 Definition of Bandwidth and Phase Delay

specifications in reverse, and determine a transfer function that likely will result in Level 1 handling qualities. Still worse, the handling qualities specifications for the cross coupling responses are even more ambiguous when used in design rather than to demonstrate compliance. A perfect example of this is depicted in Fig. 4.8, the handling qualities specification plot for yaw due to collective. Upon close inspection of this specification, one can see how a given yaw response due to collective input could be

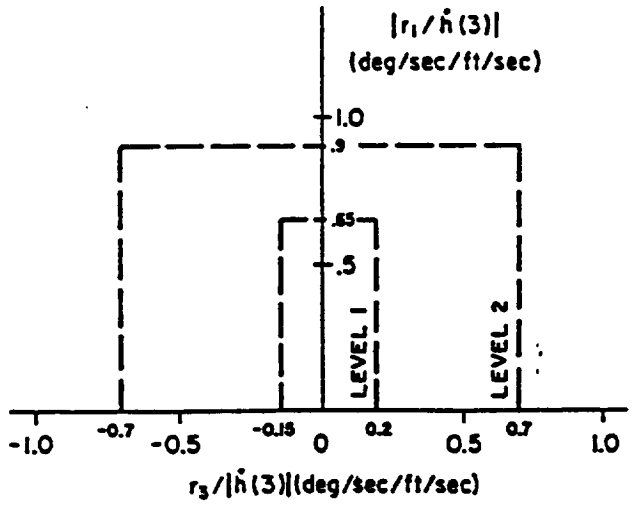

where:

r_1 = first peak (before 3 seconds) or r(1) if no peak occurs before 3 seconds

$$r_3 = \begin{cases} (r(3) - r_1) \text{ for } r_1 > 0 \\ (r_1 - r(3)) \text{ for } r_1 < 0 \end{cases}$$

r(1) and r(3) are yaw rate responses measured at 1 and 3 seconds, respectively, and $\dot{h}(3)$ is altitude rate response measured at 3 seconds, following a step collective input at t = 0

In the unlikely event of more than one peak before 3 seconds, the largest peak (by magnitude) should be designated as r_1.

Figure 4.8 Collective to Yaw Coupling Requirements

evaluated against this specification to determine the likely handling qualities level, but to determine a transfer function which could act as an upper limit on cross-coupling which would still likely yield Level 1 handling qualities based on this specification would be extremely difficult.

To determine bounds on cross-coupling performance, a classical "base-line" flight control system was designed about the 40 kt linear model. The cross-coupling responses of this FCS were evaluated against the handling qualities specifications, and where acceptable, these responses became the limits on cross-coupling performance. Where peak responses were above acceptable limits, the responses were scaled sufficiently to yield acceptable performance.

Also not covered in the handling qualities specification is an upper limit on acceptable performance. These upper limits were defined somewhat arbitrarily with an eye toward the impending design procedure. It is desirable, for example, to allow for a larger variation in performance at higher frequencies, i.e., that the upper and lower performance bounds diverge. To understand the benefit of this, recall Eqn.4.3, the performance robustness equation. Divergence of the performance boundaries facilitates compliance with this inequality at higher frequencies. Also, since both of the performance boundaries tend to diminish in magnitude with frequency at higher frequencies, albeit with T_L diminishing more quickly, the divergence of the performance boundaries has little effect on the resulting closed-loop system performance. Also, because a flight control system is being designed which simplifies the operation of the rotorcraft for the pilot (as opposed to an automatic pilot), it is unnecessary to ensure zero steady state error; the pilot will easily compensate for very low frequency offset errors. It must also be acknowledged, however, that there are physical constraints on the attainable response bandwidth of the flight control system. It is not acceptable, therefore,

to set the upper performance bound bandwidth above a reasonable level. With these considerations in mind, the upper performance bounds were established for each of the four axes.

The resulting performance boundaries utilized in the design process are shown in Tables 4.1 and 4.2.

Table 4.1 On-Axis Performance Boundaries

Roll Axis	$T_L = \frac{0.9}{(3.5)[.7;4.5](10)}$ $T_U = \frac{1.11(5)}{[.4;3.5](10)}$
Pitch Axis	$T_L = \frac{0.9}{(2.0)[.7;2.6](6)}$ $T_U = \frac{1.11(2.9)}{[.4;2.0](6)}$
Heave Axis	$T_L = \frac{0.9}{(.25)(1.0)}$ $T_U = \frac{1.11}{(1.0)}$

Yaw Axis	$T_L = \frac{0.9}{(3.5)[.7;4.5](10)}$ $T_U = \frac{1.11(5)}{[.4;3.5](10)}$

Table 4.2 Cross-Coupling Performance Boundaries

	Roll	Pitch	Heave	Yaw
Lat. Cyclic	X	$T_D = \frac{1.1(0)}{(0.3)(10)}$	$T_D = \frac{0.4(0)}{(0.8)(15)}$	$T_D = \frac{20.46(0)}{(0.2)(8)}$
Long. Cyclic	$T_D = \frac{1.42(0)}{(0.8)(6)}$	X	$T_D = \frac{0.71(0)(4)^2}{[.7;1.25][.3;12]}$	$T_D = \frac{33.95(0)}{(0.1)(20)}$
Collective	$T_D = \frac{1.83(0)}{(0.6)(6)}$	$T_D = \frac{1.68(0)}{(0.3)(5)}$	X	$T_D = \frac{-.06(0)}{[0.2;8.5]}$
Pedals	$T_D = \frac{1.83(0)}{(0.6)(6)}$	$T_D = \frac{1.05(0)}{(1)(10)}$	$T_D = \frac{0.39(0)}{(0.6)(8)}$	X

The nomenclature in the table is defined as follows, where s is the Laplace variable.

$$(\omega) \Rightarrow (s/\omega + 1) \qquad [\zeta;\omega] \Rightarrow \left(\frac{s}{\omega^2} + \frac{2\zeta s}{\omega} + 1\right)$$

Finally, in guaranteeing stability robustness, the following constraints were employed

$$|1 + GP| > -4\,\text{db}, \qquad P \in P$$

$$\left|\frac{GP}{1 + GP}\right| < 10\,\text{db}, \qquad P \in P$$

The former constraint is synonymous with gain and phase margins of 8.66 db and 39 deg.

4.5 The Quantitative Feedback Theory Design Procedure

To facilitate the QFT design process, a computer-aided design (CAD) package was employed [34] (hereafter referred to as QFT-CAD) in conjunction with the computer simulation package, ACSL [35], and MATLAB [36], a systems and controls computer package. QFT-CAD utilizes a menu to coordinate several programs. Using this menu, the user inputs the plant transfer function, including the variability of its parameters. The user then inputs the performance bounds, either as magnitudes at the specified frequencies or in transfer function form, as well as the stability criteria. QFT-CAD then uses this information to establish boundaries on the Nichols chart associated with each of the design frequencies and provides an interactive medium in which the user may derive a feedback compensator and prefilter in order to satisfy the design constraints.

QFT-CAD may alternatively be used in conjunction with MATLAB. In this case, the menu is foregone and instead the user provides the individual programs with data files necessary to perform their assigned tasks. For example, the BOUNDARY program, which defines the boundaries on the Nichols chart, requires a binary data file which defines the templates (see Section 4.2), as well as an ASCII data file which defines the performance boundaries, the disturbance rejection boundaries, and the stability criteria. The SHAPE program, which allows the user to design the feedback compensator, requires these boundaries as well as a binary data file defining the nominal loop transmission. MATLAB may be used to generate the requisite data files.

The ability to provide these data files, instead of requiring the use of the interactive input screen to define the plant specifications, is particularly useful when the plant model is cumbersome as was certainly the case in this instance. With a 30 state 4x4 MIMO design problem, each of the elements of the P matrix of transfer functions is 30th order. This implies that with no cancellations, the elements of the Q matrix, utilized in the extension of the MISO design technique to the MIMO design problem, would be 30*4 or 120th order. This is obviously too cumbersome to deal with, particularly due to the digital accuracy attainable using algebraic manipulation programs such as Mathematica.

To circumvent this problem, the $q_{ij}(s)$ transfer functions were evaluated and defined at specific frequencies as follows. First, the $p_{ij}(j\omega)$ is evaluated as follows:

$$\underline{P}(j\omega)=\underline{c}^t(j\omega\underline{I}-\underline{A})^{-1}\underline{b} \tag{4.11}$$

where p_{ij}, the elements of $\underline{P}$, equal $y_i(j\omega)/\delta_j(j\omega)$, and

$$\begin{aligned}\dot{\underline{x}}&=\underline{A}\,\underline{x}+\underline{b}\,\underline{\delta}\\ \underline{y}&=\underline{c}^t\underline{x}+D\,\underline{\delta}\end{aligned} \tag{4.12}$$

Next, for each frequency, the matrix $\underline{P}(j\omega)$ is inverted to obtain the $\underline{Q}'(j\omega)$ matrix at the given frequency. Finally, the $q_{ij}(j\omega)$ are calculated by inverting the elements of the $\underline{Q}'(j\omega)$ matrix. This complex number is then decomposed into a Bode magnitude and phase. Calculated over a large range of closely spaced frequencies, this technique provides the frequency response of $q_{ij}(j\omega)$. Appendix B contains a library of MATLAB script and function files which perform the operations described herein. Although the actual poles and zeros of the $q_{ij}(s)$ transfer functions are never determined (nor are they needed for the design procedure), it would be possible to fit the resulting frequency responses with an approximate transfer function representation should that be desired.

Figures 4.9 and 4.10 present Bode diagrams of the frequency responses of p_{11} and q_{11} and p_{22} and q_{22} for the rotorcraft model linearized about the hover flight condition. Notice that for the most part, the q_{ii}'s are similar to the p_{ii}'s. This is not true of the q_{ij}'s where $i \neq j$, as is shown in Fig. 4.11, the frequency response of p_{12} and q_{12} for the hover model.

The rotorcraft model linearized about the hover flight condition was arbitrarily

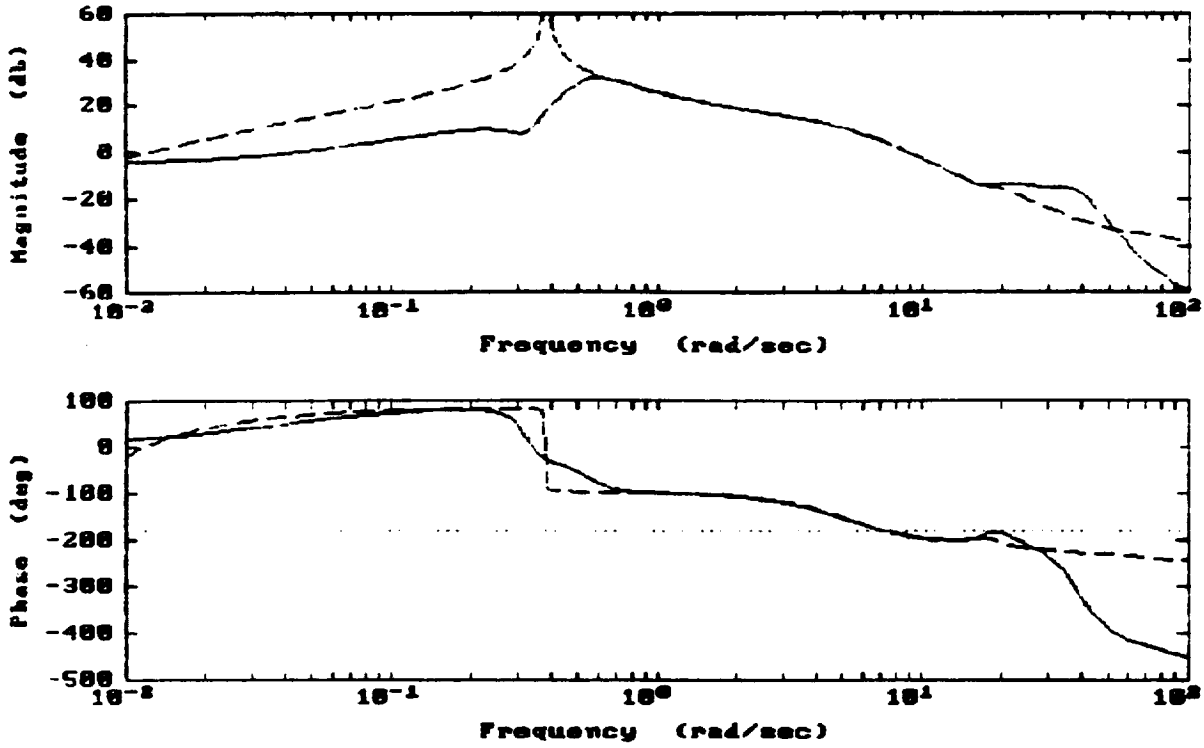

Figure 4.9 Comparison of p_{11} and q_{11} for the hover model

selected as the nominal plant dynamic model. The nominal plant data files, NOMPLANT.DAT, were calculated for the q_{ii} as described above and stored in the correct format for QFT-CAD using the matlab function SAV_NOM (Appendix B).

The selection of the design frequencies is based on the frequency range of interest for the given design problem. The set of design frequencies for this study was chosen as ω = [0.3, 0.5, 1.0, 3.0, 5.0, 10, 20, 40, 80]. Below 0.3 rad/sec was considered within the range of pilot compensation and so was not of importance to the FCS design,

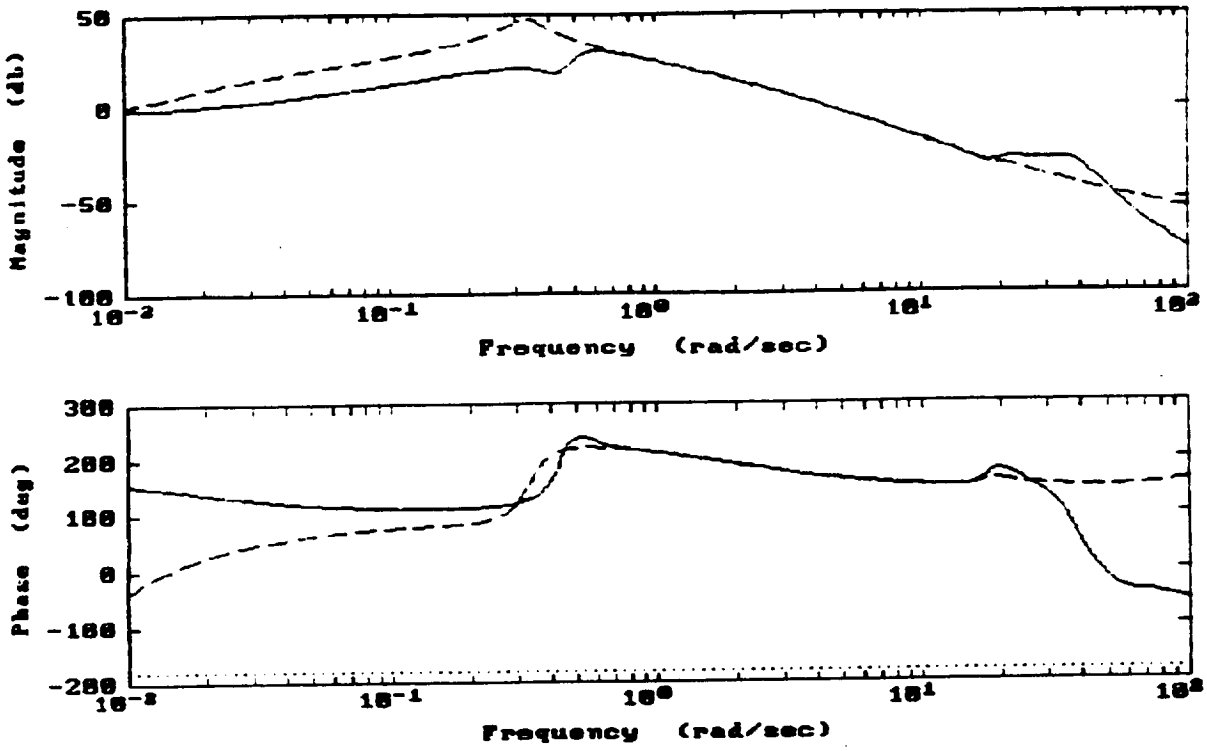

Figure 4.10 Comparison of p_{22} and q_{22} for the hover model

and above 80 rad/sec was deemed adequate for the purposes of ensuring stability and preventing control saturation.

The template for the k^{th} design frequency, which is used along with the performance criteria to define the boundary for that design frequency on the Nichols chart, consists of the set of Bode magnitudes and phases of $q_{ii}(j\omega_k)$ calculated for each of the six rotorcraft dynamic models. This information was generated using the same

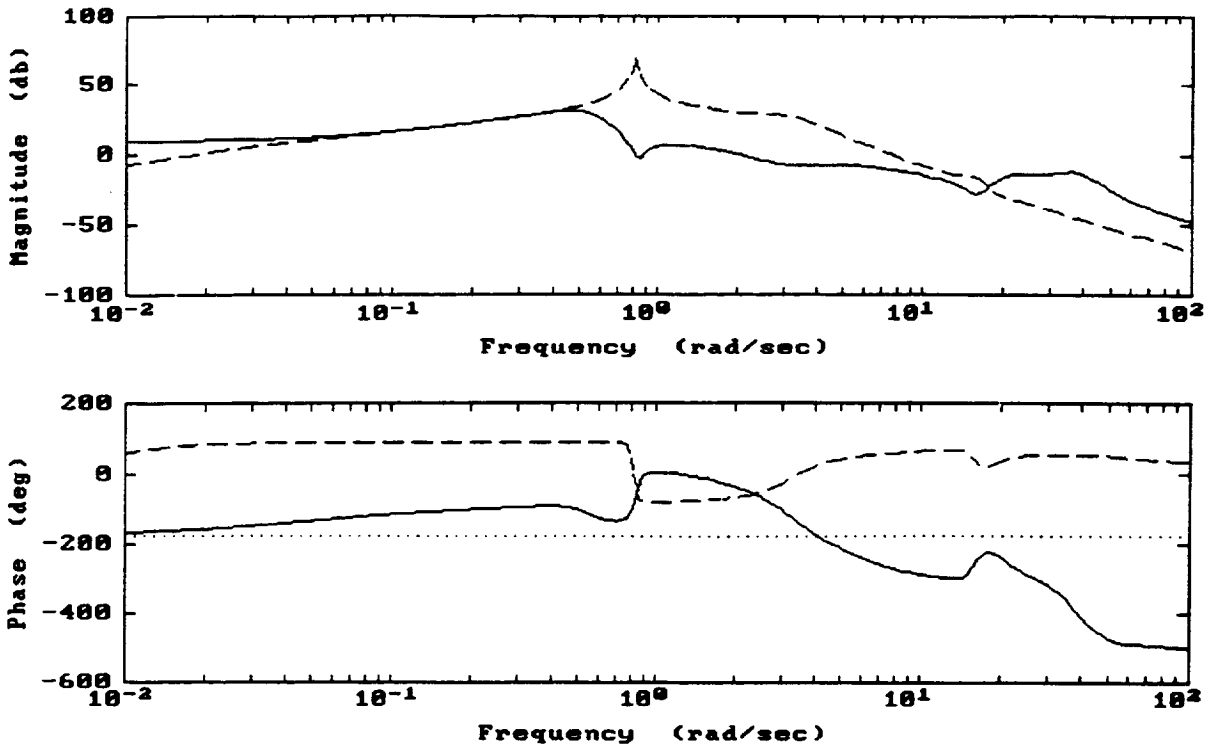

Figure 4.11 Comparison of p_{12} and q_{12} for the hover model

technique as was described for the calculation of the nominal plant data files, with the template data stored in TEMPLATE.DAT using the MATLAB function TEMPLATE (Appendix B).

The disturbance bounds in QFT-CAD are defined such that

$$\frac{|1+L|}{|P|} \geq No.(db) \tag{4.13}$$

where the input to the plant is the disturbance insertion point and *No.* is the number

expected by QFT-CAD in decibels (db) in the disturbance rejection portion of the performance specification file. For this MIMO design problem, therefore, the disturbance specification for the ijth design problem is determined as follows.

$$No.(db) = \frac{|d_{ij}|}{|\tau_{ij}|} \tag{4.14}$$

$$|d_{ij}| = \sum_{\alpha \neq i} - \frac{|\tau_{\alpha j}|}{|q_{i\alpha}|_{\min}} \tag{4.15}$$

where τ_{ij} is the upper bound on the acceptable response of the ith output to the jth input. This is a conservative estimate of the boundary, because the upper response boundaries are used as estimates of the actual off-axis responses in the calculation of the disturbance signal, d_{ij}. In reality, the αj frequency response magnitude could be significantly less than the upper acceptable bound. It is necessary to make this conservative estimate, however, because no information on the actual closed loop αj frequency response magnitude is available until after the design is complete. It is known, however, that if the design procedure is followed accurately the upper acceptable bound will limit the αj frequency response magnitude and thus that bound provides a worst case estimate.

With the above information, the sixteen (16) MISO design problems were addressed to arrive at a four (4) input - four (4) output flight control system for the UH-60 rotorcraft which would yield satisfactory handling qualities over the range of flight conditions from hover to 100 kts.

Figure 4.12 is a sample of the feedback compensator design environment in QFT-CAD. Appendix C provides aid in interpreting the figure. Included on the Nichols chart in various colors are the M-circles, the boundaries, and the nominal loop transmission. The user may vary the parameters in the feedback compensator (e.g., poles, zeros, damping constants, etc.) incrementally and observe the effect on the nominal loop transmission, thus enabling him to zero in on an optimal solution. Figure 4.12 is the design of the feedback compensator, g_3, for the 33 design problem, or the design for the response of the roll attitude (the 1st output) to a roll attitude command (the 1st input). Notice that the values of the nominal loop transmission at the design frequencies, indicated by the alpha-numeric labels, are above the appropriate boundaries. Thus, for this design problem, the design specifications are satisfied.

Due to the conservative nature in the specification of the disturbance boundaries, however, it was not possible to satisfy all of the design specifications for all sixteen (16) of the design problems. In these cases, as depicted in Fig. 13, a CAD plot of the 14 design problem, an attempt was made to minimize the deviation from the design specifications, but the design process was continued despite these deviations. It was left to discover the true ramifications of these deviations in the final simulation of the FCS to the full rotorcraft models.

Once the feedback compensator, g_i, for the i^{th} output variable has been optimized for the four (4) MISO design problems, ij with $j=1$ to 4, then the prefilter, f_{ii}, is

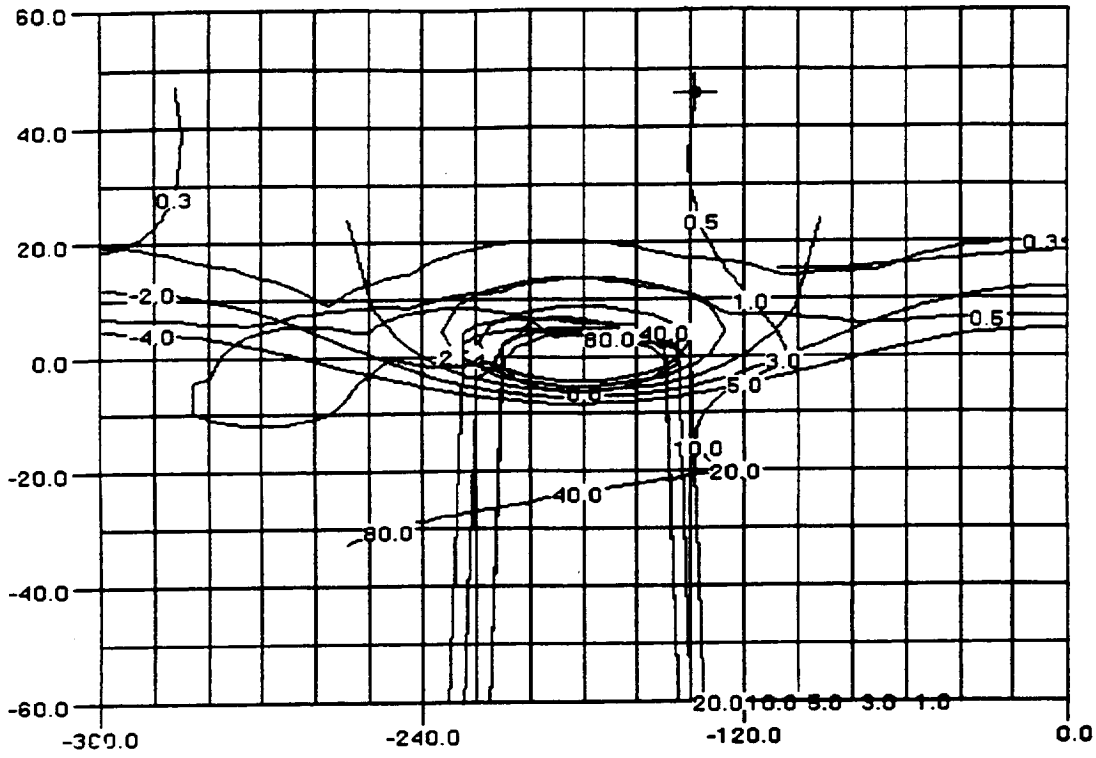

Figure 4.12 CAD Drawing of Feedback Compensator Design for Roll Response to Roll Command

designed. Because the four output to input relations are to be non-interacting, that is no cross-feeding of the pilot inputs are to be employed, the prefilter matrix, $\underline{F}$, is diagonal so that f_{ij} for $i \neq j$ is identically equal to zero. With this stipulation, the control loops are said to be Basically Non-Interacting Loops (BNIL). Figure 4.14 is an example of the prefilter design environment of QFT-CAD. The user may vary the parameters in the prefilter (e.g., poles, zeros, damping constants, etc.) incrementally and observe the effect on the closed loop frequency response for all of the plant dynamic models, thus enabling him to zero in on an optimal solution. Figure 4.14 is the design of the prefilter, f_{33}, for the 33 design problem. Appendix C contains a complete set of the design figures for this design.

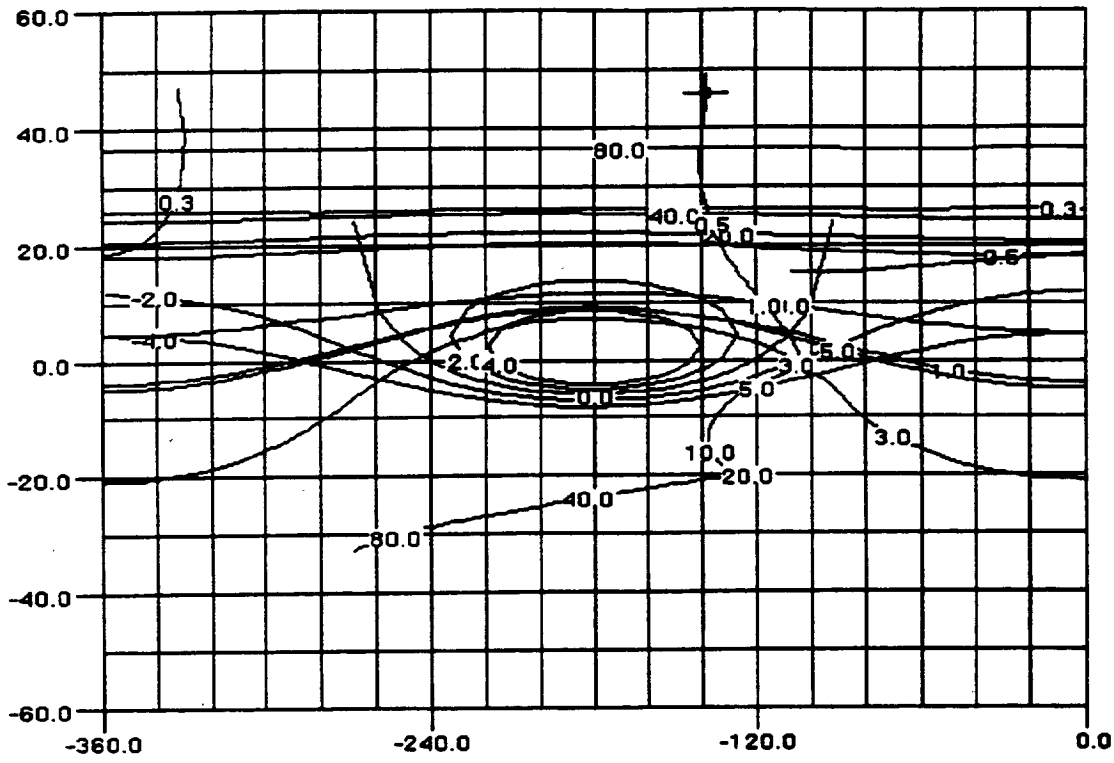

Figure 4.13 CAD Drawing of Feedback Compensator Design for Roll Response to Yaw Rate Command

The feedback compensators and prefilters designed utilizing the above described process are listed in Table 4.3 with the same nomenclature as used in the previous tables. Note that the maximum order of any of the compensators is only seven. Recalling that the model was of 30th order (28th order vehicle plus 2nd order actuators), the compensator simplicity afforded by the frequency-based QFT design is quite apparent. Large order compensators are frequent results of many modern FCS design techniques, e.g., [14].

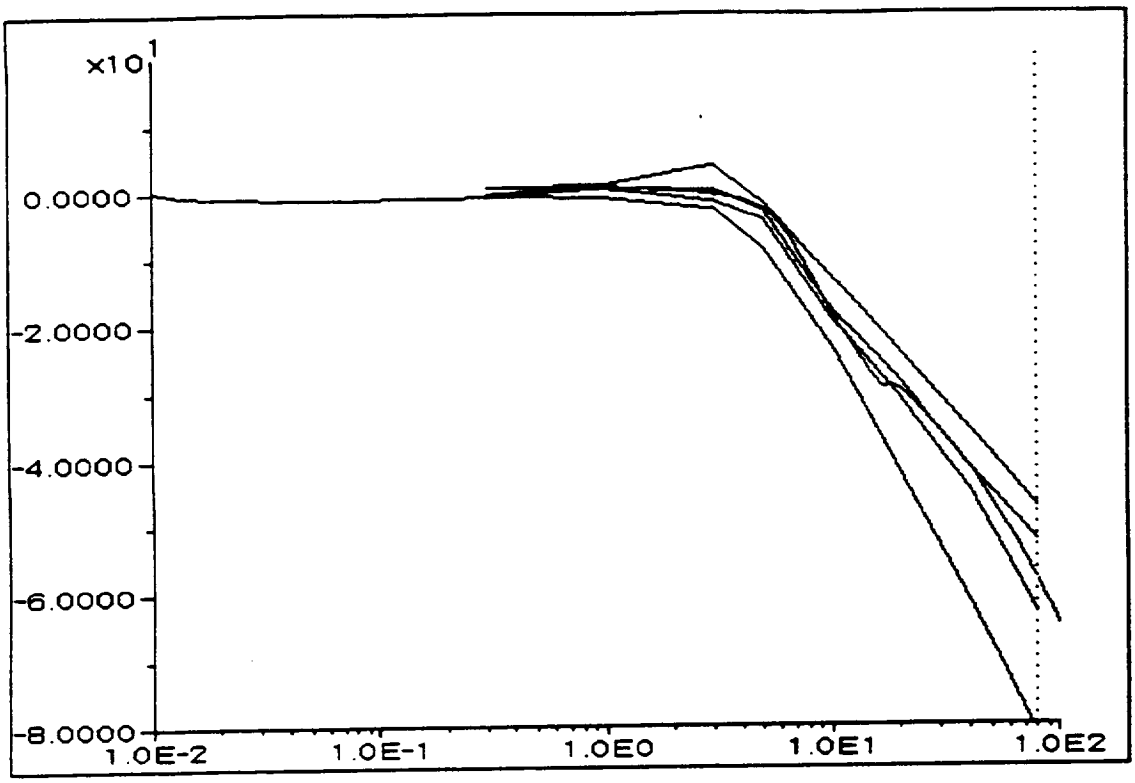

Figure 4.14 CAD Drawing of Prefilter Design for Roll Response to Roll Command

Table 4.3 Prefilters and Feedback Compensators of the FCS Design #1

Roll Attitude	$g_\phi = \frac{0.0257(0.5)(7.4)[.7;13.72][.7;30]}{(0)(20)[.7;40][.7;50](67.2)}$	$f_{\phi\phi_c} = \frac{(0.64)(2)}{(0.5)(7)[.7;10]}$
Pitch Attitude	$g_\theta = \frac{0.0185(0.15)(.7)(1)(1.6)[.7;30]}{(0)^2(6)(80)^2[.7;80]}$	$f_{\theta\theta_c} = \frac{1}{[.7;2.52]}$
Vertical Velocity	$g_h = \frac{0.306(0.5)}{(0)(60)}$	$f_{hh_c} = 1.0$
Yaw Rate	$g_\psi = \frac{0.4192(2)[.7;30]}{(0)(42)[.7;50](70)}$	$f_{\psi\psi_c} = \frac{1}{[.7;4.2]}$

4.6 Results

Figures 4.16 thru 4.21 depict some of the time histories resulting from the application of the above listed FCS in a manner shown in Fig. 4.15. Each of the rotorcraft dynamic models are represented by a solid line on each plot. On the ii responses (i.e., roll to roll command, pitch to pitch command, etc.) the performance boundary time histories are presented as dashed lines. Note that in the time domain, the bounds indicate limits on rise time, overshoot, settling time, etc., and should not be construed as absolute bounds that cannot be crossed by the actual response. The performance of all four responses was satisfactory based on the imposed performance criteria.

In addition, by applying the cross-coupling performance criteria from the handling qualities specification, the cross-coupling resulting from this FCS was also satisfactory. This is despite the fact that the design indicated that the cross-coupling performance bounds would be violated. Several reasons for this apparent inconsistency exist. First, the cross-coupling performance boundaries were overly restrictive. It may be possible to violate the imposed boundaries and still have "satisfactory" cross-coupling performance. Second, as was hinted at previously, the performance criteria as stated in the specification do not translate directly into frequency domain bounds. That is, the specifications do not dictate a maximum magnitude for a cross-coupling frequency response at a given frequency. As a result, many different boundaries could be drawn in the frequency domain, each of which would satisfy the performance criteria set forth

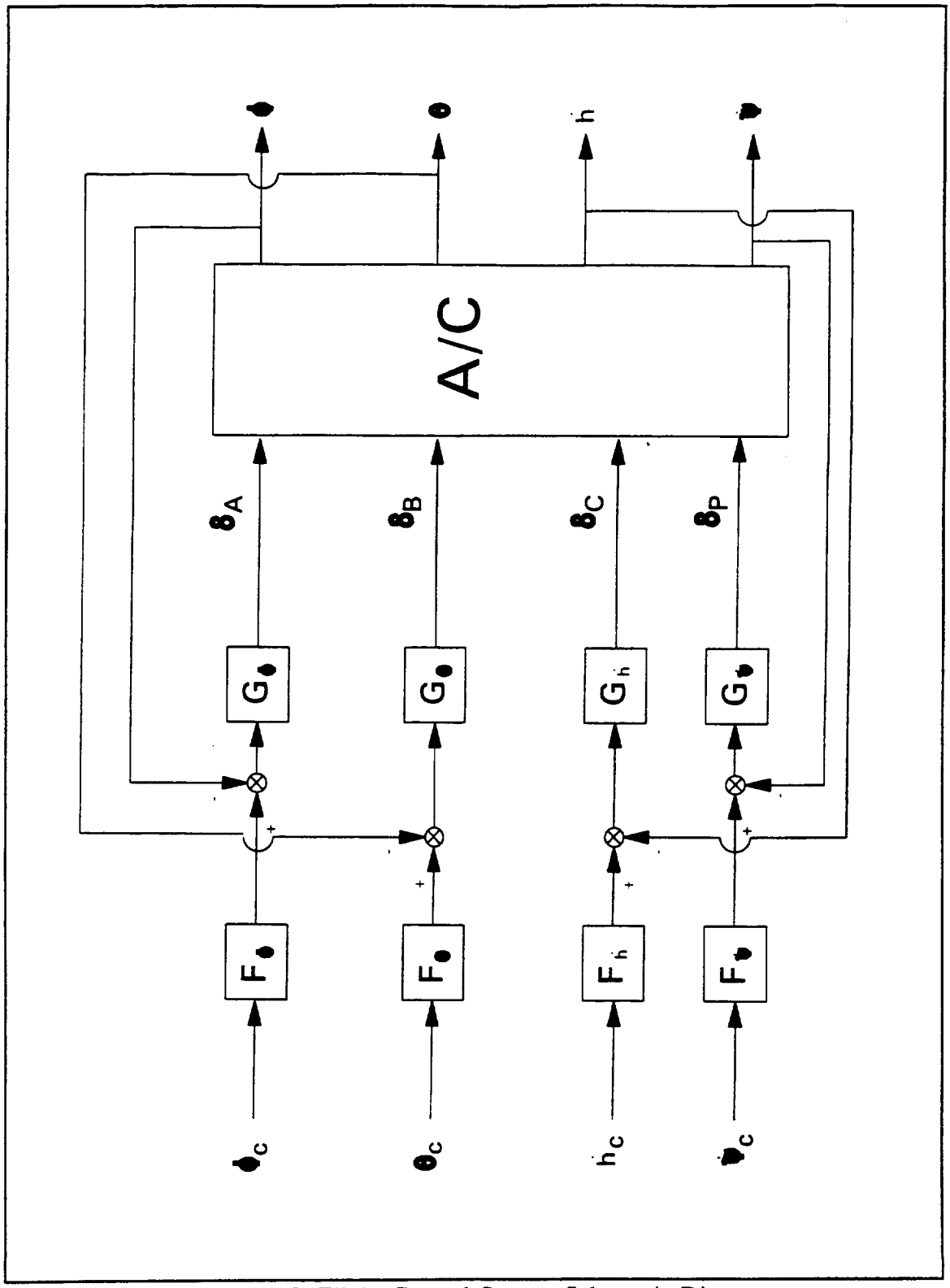

Figure 4.15 Flight Control System Schematic Diagram

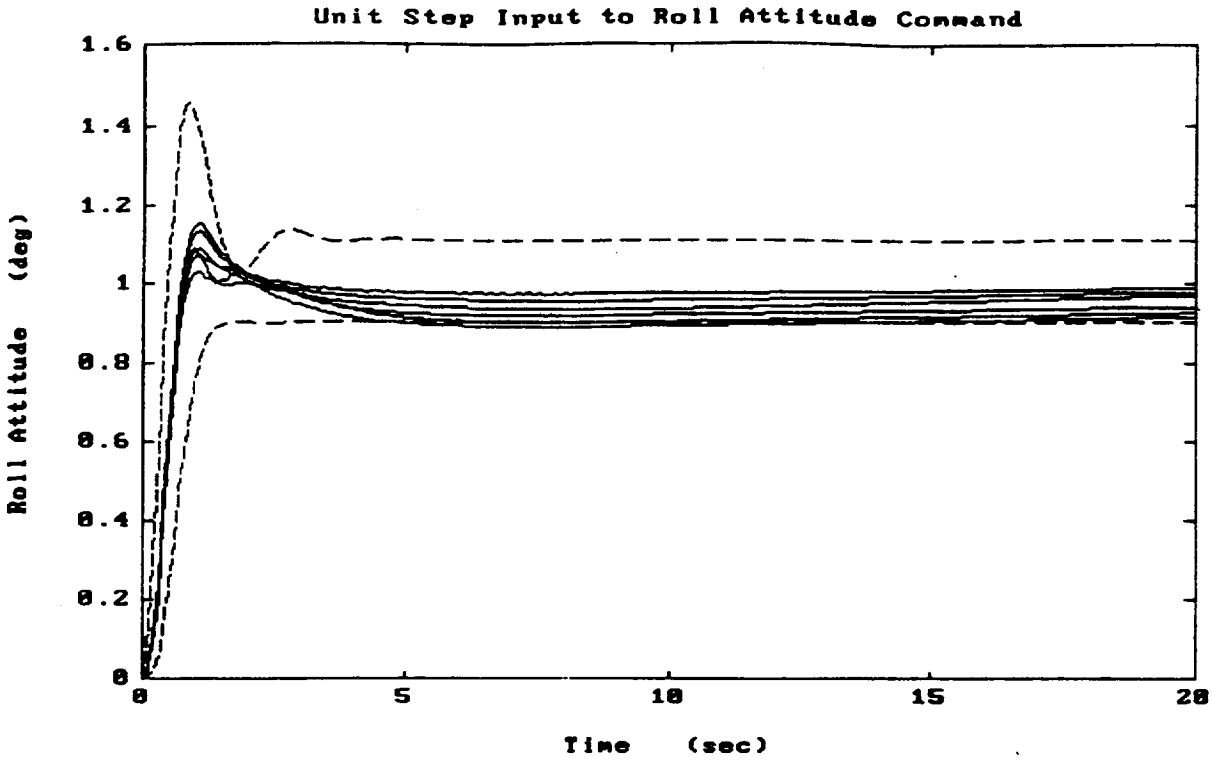

Figure 4.16 Roll Attitude Response to a Unit Step to Roll Attitude Command -

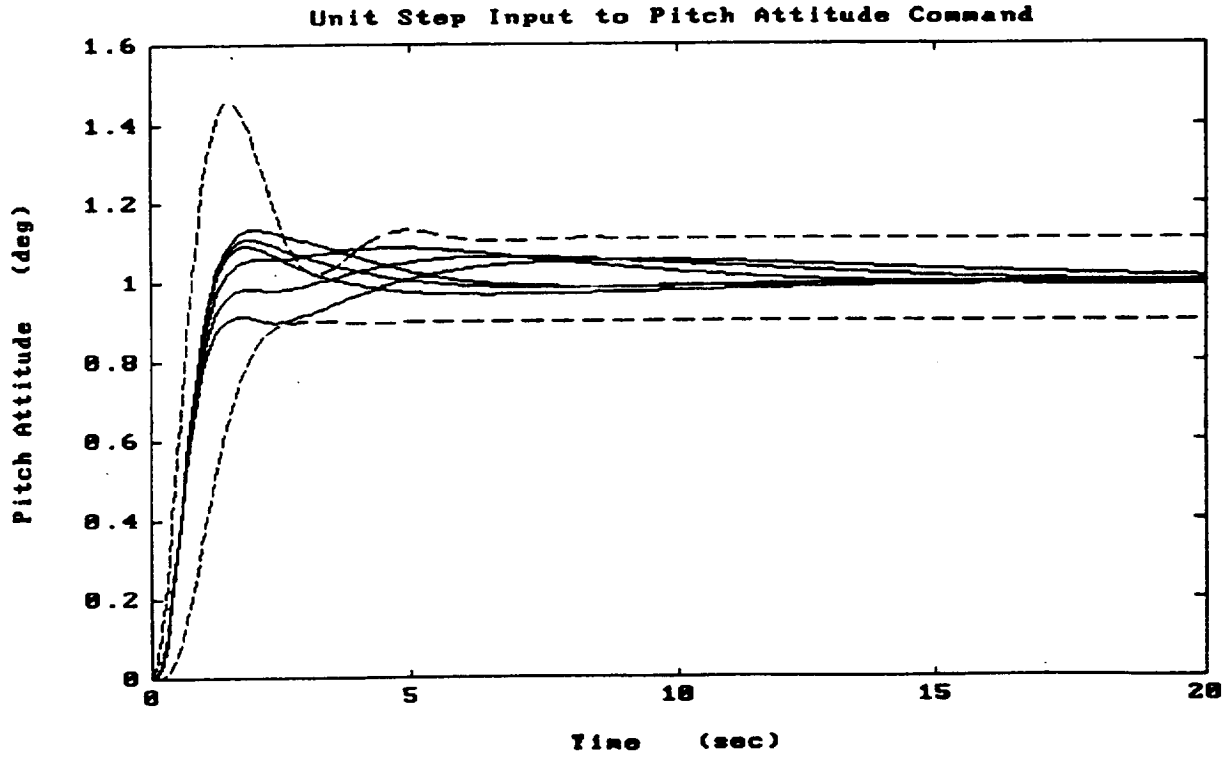

Figure 4.17 Pitch Attitude Response to a Unit Step to Pitch Attitude Command - Design #1

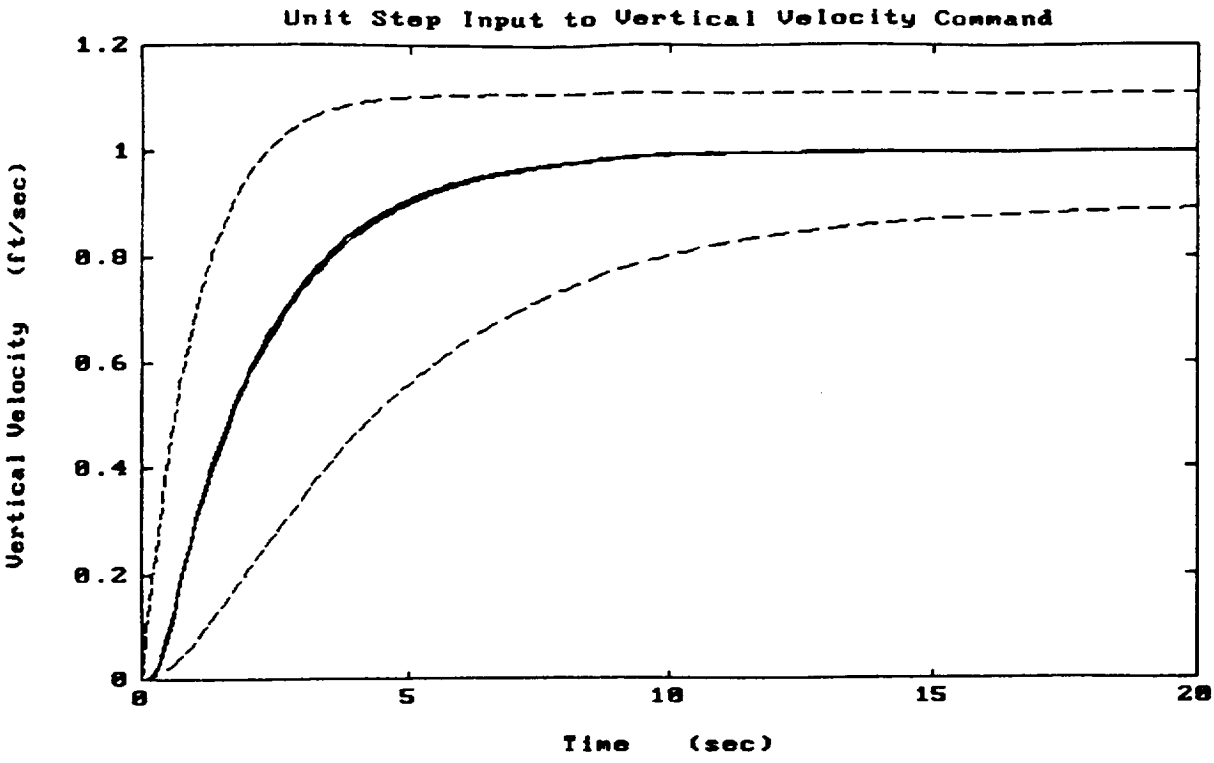

Figure 4.18 Vertical Velocity Response to a Unit Step to Vertical Velocity Command - Design #1

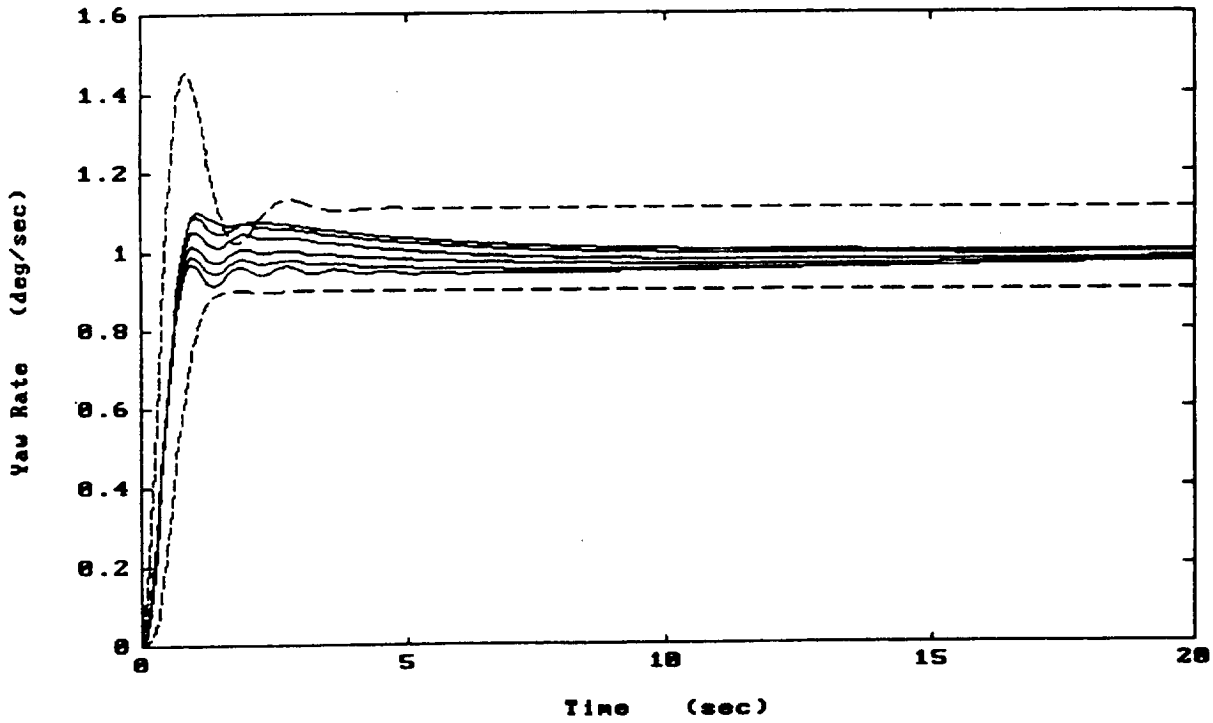

Figure 4.19 Yaw Rate Response to a Unit Step to Yaw Rate Command - Design #1

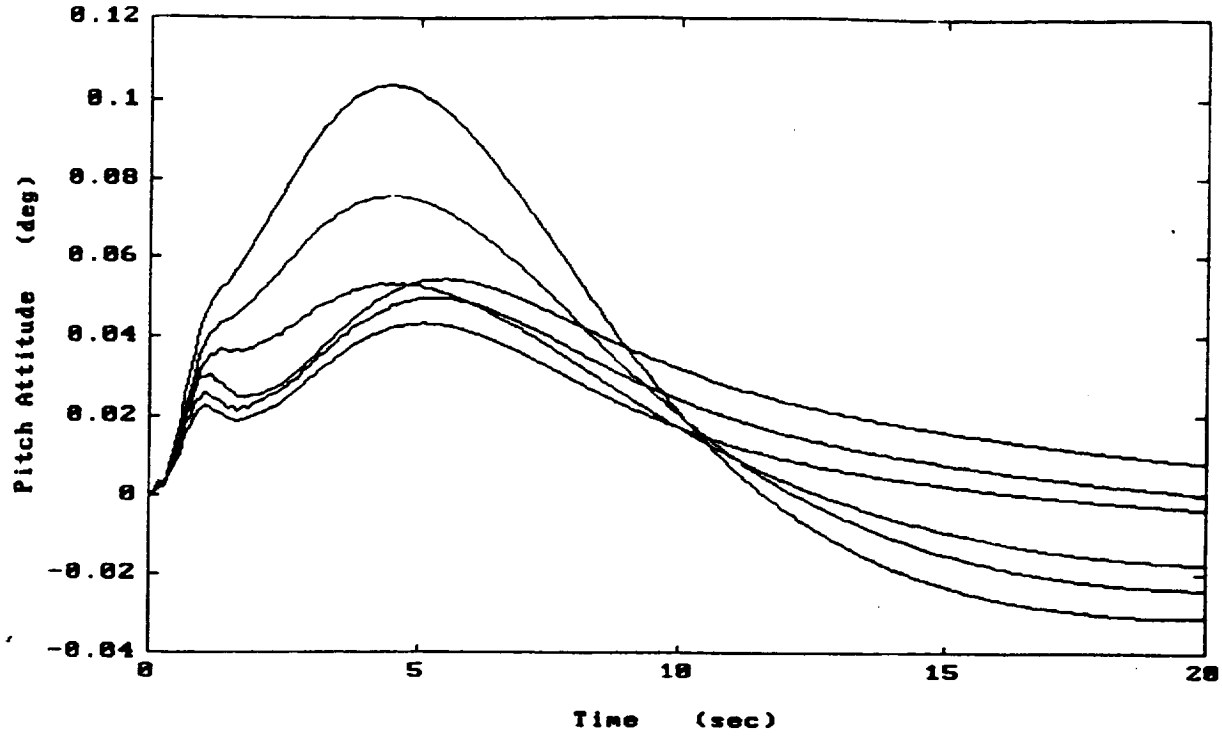

Figure 4.20 Pitch Attitude Response to a Unit Step to Roll Attitude Command - Design #1

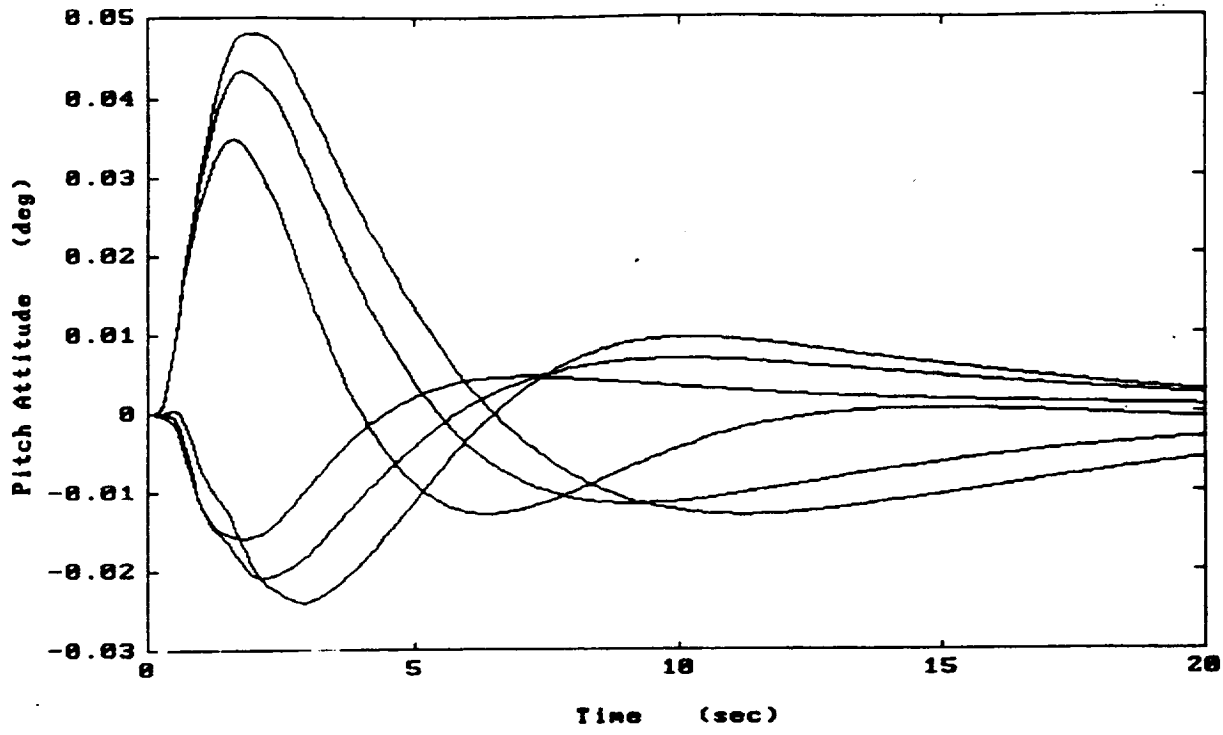

Figure 4.21 Pitch Attitude Response to a Unit Step to Vertical Velocity Command - Design #1

in the handling qualities specification. The third reason has to do with the conservative nature of the determination of the disturbance magnitude for the MISO design problems (Eqn. 4.13). It was unclear, because of this, whether actual performance bounds really are violated, or whether, instead, the conservative worst-case estimate of the cross-coupling bound is violated but the actual response is in compliance with the bound.

To investigate this further would necessitate closed loop frequency responses for the various control input to response transfer functions. An abbreviated form of the Golubev program was employed to this end [37]. Given input and output data sequences, this program computes a rational function approximation, H(s) = num(s)/den(s), such that OUT(s) = H(s)IN(s). Figure 4.22 presents a plot of the approximate closed loop frequency response of roll attitude due to yaw rate command for three (3) flight conditions: hover, 40 kts, and 100 kts. Also included on the plot as a dashed line is the cross coupling performance bound. Clearly, all three frequency responses are well below the imposed boundary at each of the design frequencies indicated by "+" marks in the figure. This is contrary to Fig. 4.13 which indicates that this cross coupling performance bound would be violated by the FCS design. This inconsistency must in large part be due to the overly conservative nature of the determination of the disturbance magnitude for the MISO design problems (Eqn. 4.13). Chapter 5 will investigate a means of addressing this limitation of the design methodology.

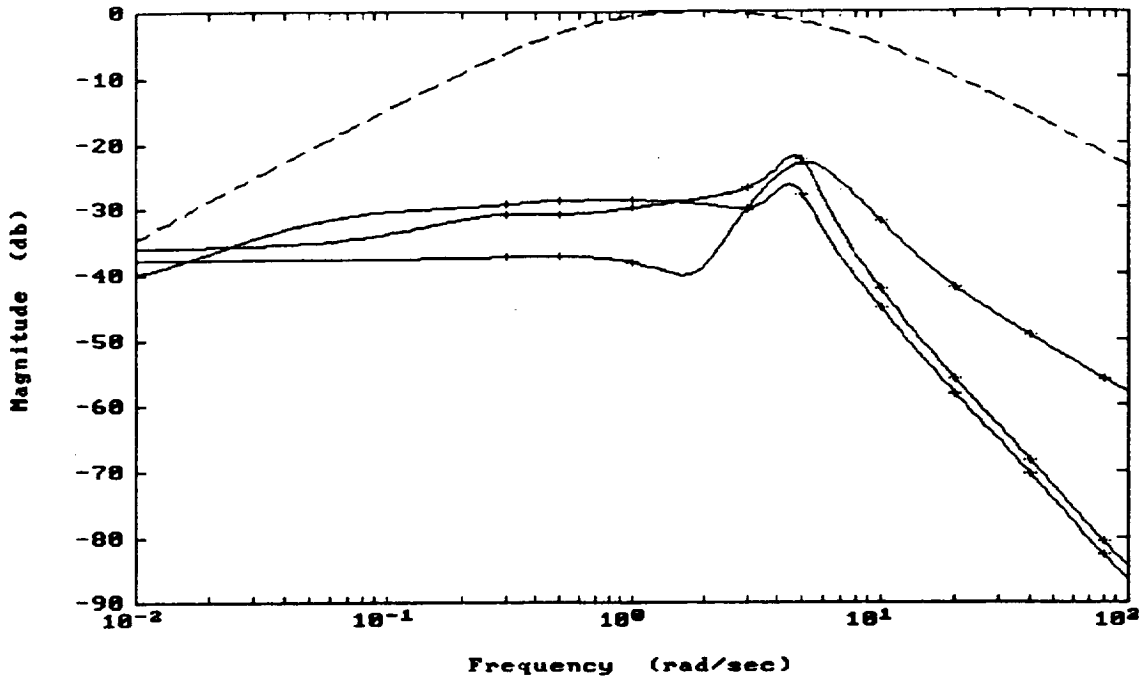

Figure 4.22 Approximate Frequency Response of Roll Attitude due to Yaw Rate Command - Design 1

CHAPTER 5

SEQUENTIAL LOOP CLOSURE

5.1 Introduction

One problem arising from the conservative determination of the disturbance signals for the MISO design problems is the fact that the resulting feedback compensator designs are overly conservative. A price paid for using this design technique for the robust disturbance rejection and tracking performance of the resulting control system is in the noise reduction characteristics of the system. This is termed by Horowitz the "cost of feedback," and is characterized by large Bode magnitudes in the feedback compensator at high frequency. Figures 5.1 thru 5.4 show Bode plots of the four feedback compensators listed in Table 4.3. Note that the high frequency magnitudes, particularly for the pitch and roll compensators, do not drop off quickly following the system feedback bandwidth, ω_{BW}, for each loop.

Another problem observed as a result of the conservative definition of the disturbance signal was enumerated in Section 4.7. Even though many performance bounds were unavoidably violated in the design process, adequate cross-coupling performance was attained. Although the fact that adequate cross-coupling performance was attained speaks well for the design methodology which was utilized in the creation of the FCS, it is unfortunate that this performance was not foreseen during the design

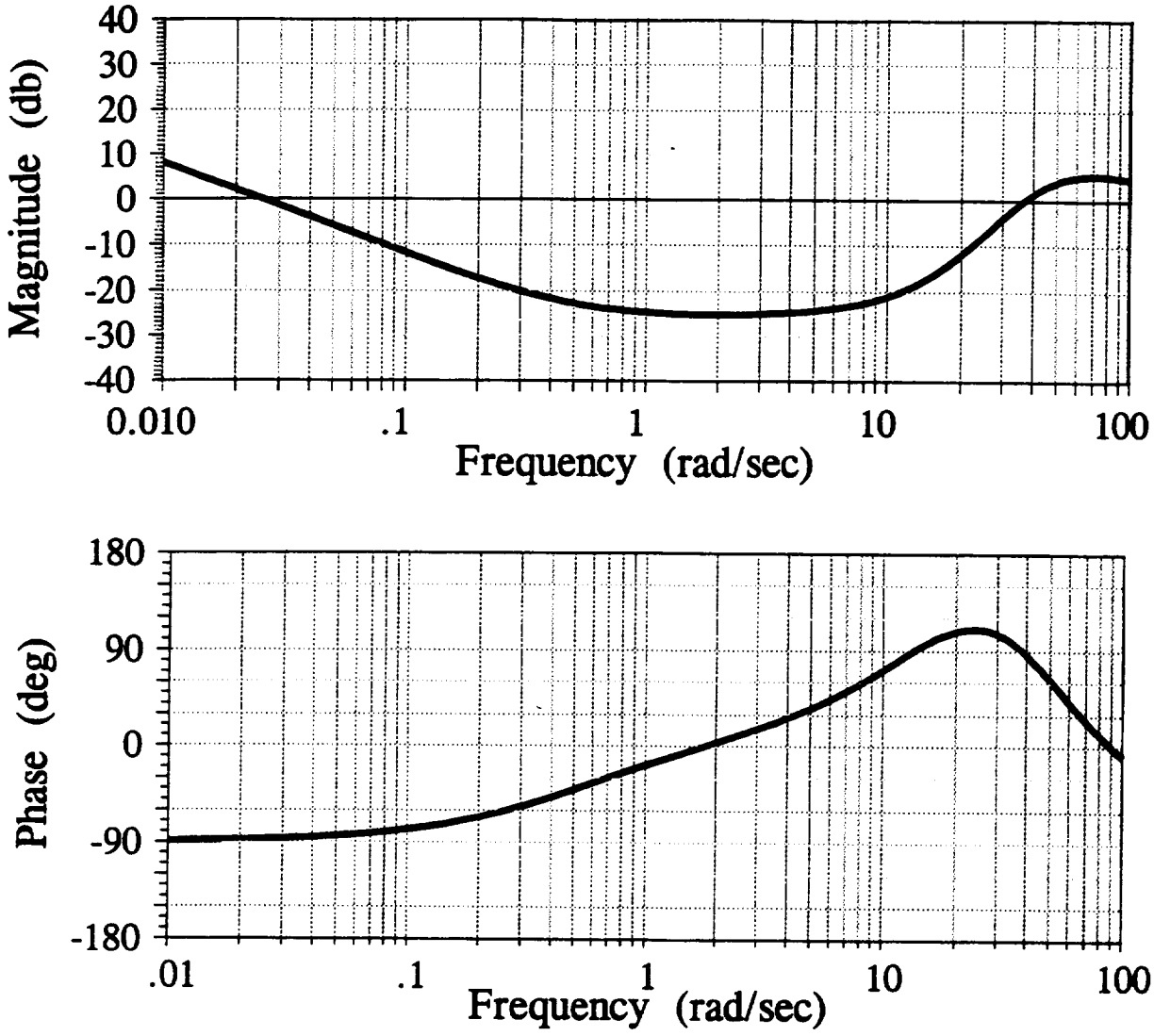

Figure 5.1 Bode Plot for Roll Feedback Compensator of Design #1

process. The QFT control system design methodology for the MIMO design problem is founded on the assumption that all of the bounds for all of the n^2 design problems are being met by the compensators. Without this, the mathematical foundation for the technique is violated and the proof of the equivalence between the n^2 MISO design problems and the original MIMO design problem no longer applies. A better design

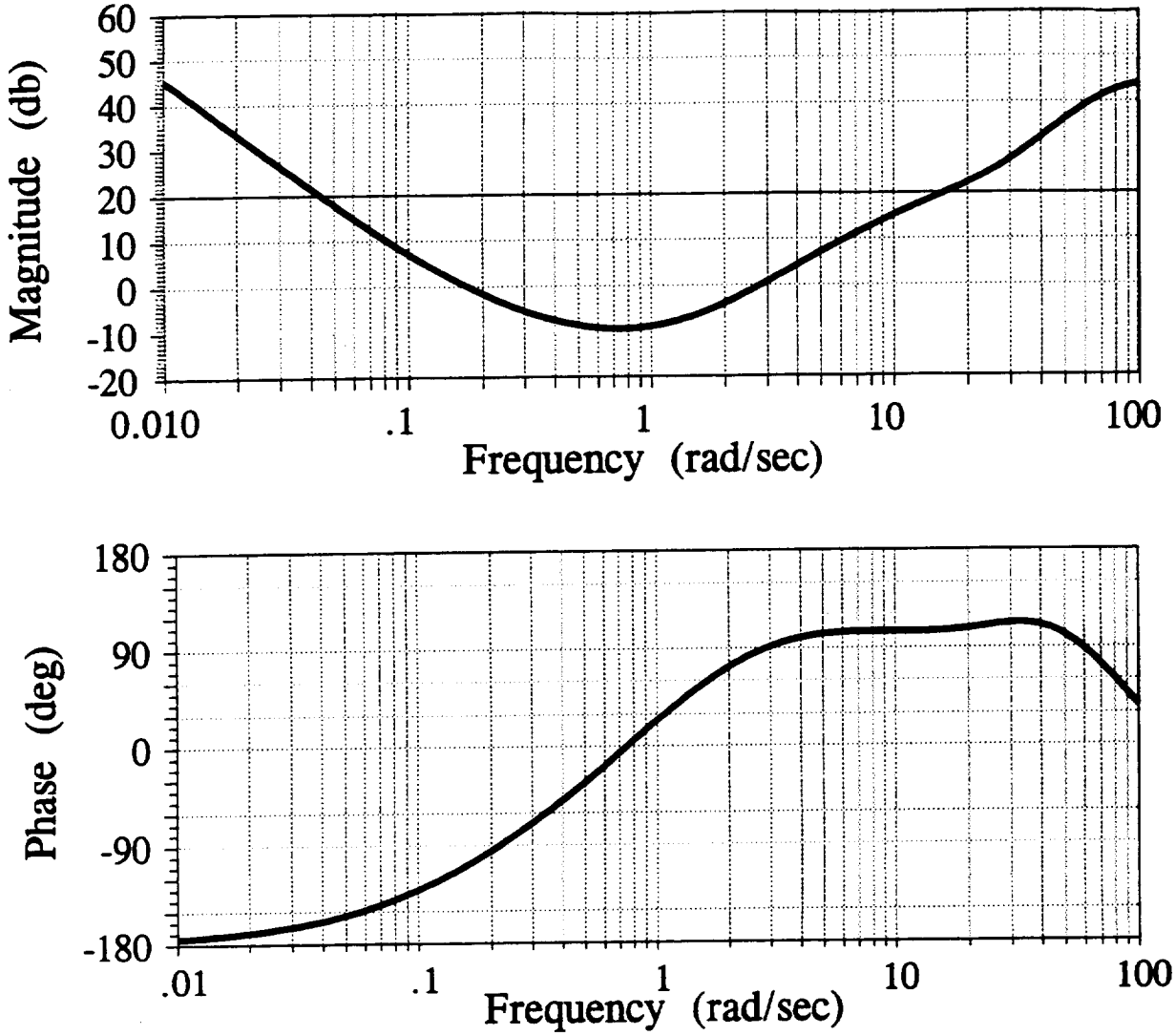

Figure 5.2 Bode Plot for Pitch Feedback Compensator of Design #1

approach is necessary for the design of a robust MIMO FCS for the UH-60 rotorcraft.

5.2 Sequential Loop Closure

One improvement to the extension of the MISO QFT technique to the MIMO control system design problem is offered in Ref. [7]. This method, termed Sequential

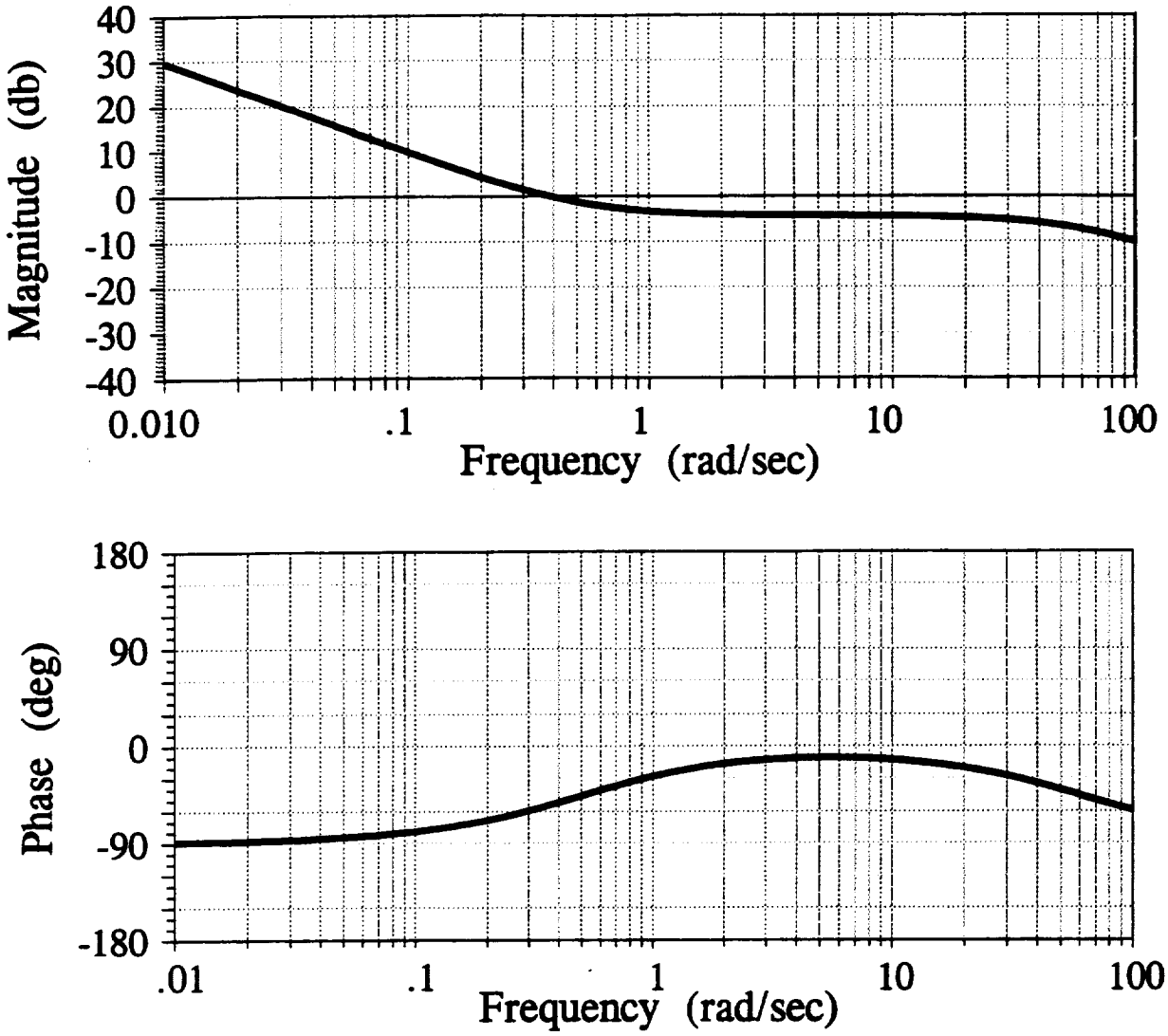

Figure 5.3 Bode Plot for Vertical Velocity Feedback Compensator of Design #1

Loop Closure, utilizes available cross coupling response information to reduce the over specification of the disturbance signal in the design of successive feedback compensators. For the n MISO design problems governing the feedback compensator, g_1, for loop No. 1, no information is available as to the final closed-loop response of the other output variables. This is exactly the same observation made in the previous method, and thus

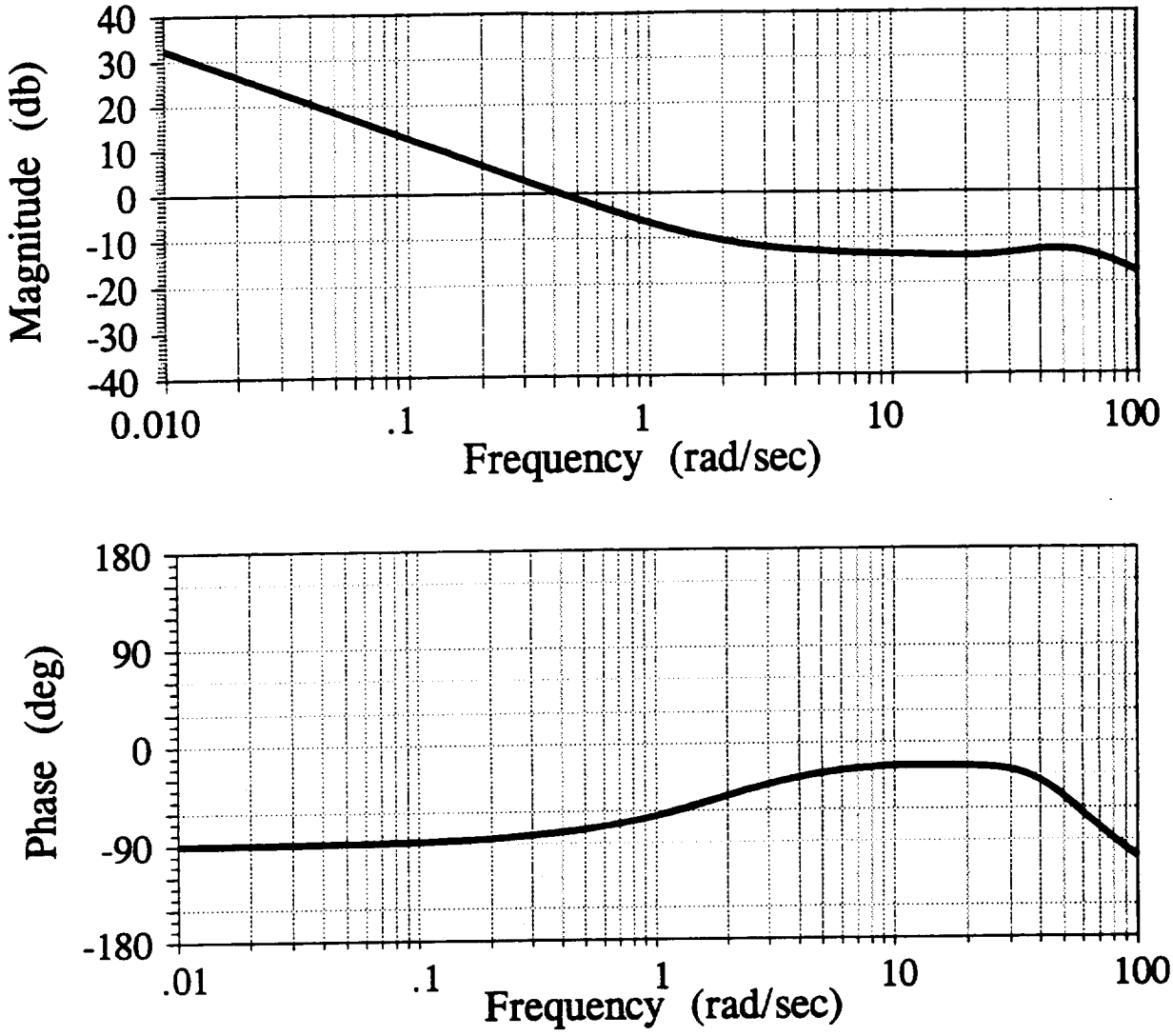

Figure 5.4 Bode Plot for Yaw Rate Feedback Compensator of Design #1

the disturbance signal contains the same amount of over specification indicated in Eqn. 4.9. Once this feedback compensator, g_1, has been designed, the first prefilter, f_{11}, is designed. Note that $f_{1j} = 0$ for $j \neq 1$ for this design problem. With g_1 and f_{11} determined, the final closed-loop responses of the first output variable to all of the inputs are fully defined. This information may be used in the design of the feedback

compensator for loop No. 2 to reduce some of the over specification of the disturbance signals. As each successive loop is closed, more information is available in the design of the feedback compensators for the remaining loops, until for the last loop, no over specification is present at all in the specification of the disturbance signals.

As an example of this process, consider the 2x2 MIMO design problem. Equations. 5.1-5.3, from the general expression of Eqn. 4.9, indicate the design problems governing the feedback compensator, g_1.

$$t_{1i} = \frac{f_{1i}L_1 + d_{1i}Q_{11}}{1 + L_1} \tag{5.1}$$

$$L_1 = g_1 Q_{11} \tag{5.2}$$

$$d_{1i} = -\frac{t_{2i}}{Q_{12}} \tag{5.3}$$

where the t_{2i} represent the closed loop response of the second output to the i^{th} input. For $i = 2$, for example, the closed loop response is defined by the following expression.

$$t_{12} = \frac{f_{12}L_1 - \dfrac{t_{22}}{Q_{12}}Q_{11}}{1 + L_1} \tag{5.4}$$

The bound imposed on this response is defined by τ_{12}. Since there is no knowledge of

the t_{22} closed loop response, the bounding value, τ_{22}, must be used. These two facts coupled with Eqn. 5.4 imply that g_1 must be designed such that for every plant dynamic model,

$$\frac{f_{12}L_1 - \frac{\tau_{22}}{Q_{12}}Q_{11}}{1+L_1} \le \tau_{12} \tag{5.5}$$

For the design of the second row problems, again from Eqn. 4.9, the design problems governing the feedback compensator, g_2, are

$$t_{2i} = \frac{f_{2i}L_2 + d_{2i}Q_{22}}{1+L_2} \le \tau_{2i} \tag{5.6}$$

The second row can now be designed with the advance knowledge of the first row results. For instance, the 22 design problem, or the design of the second output response to the second input, is given by

$$t_{22} = \frac{f_{22}L_2 - \frac{t_{12}}{Q_{21}}Q_{22}}{1+L_2} = \frac{f_{22}L_2 - \left(\frac{f_{12}L_1 - \frac{t_{22}}{Q_{12}}Q_{11}}{(1+L_1)Q_{21}}\right)Q_{22}}{1+L_2} \tag{5.7}$$

The following algebra leads to a new design equation for t_{22}.

$$t_{22}=\frac{f_{22}g_2Q_{22}(1+L_1)-f_{12}L_1\dfrac{Q_{22}}{Q_{21}}+t_{22}\dfrac{Q_{11}Q_{22}}{Q_{12}Q_{21}}}{(1+g_2Q_{22})(1+L_1)} \tag{5.8}$$

$$\left((1+g_2Q_{22})(1+L_1)-\frac{Q_{11}Q_{22}}{Q_{12}Q_{21}}\right)t_{22}=f_{22}g_2Q_{22}(1+L_1)-f_{12}L_1\frac{Q_{22}}{Q_{21}} \tag{5.9}$$

$$t_{22}=\frac{f_{22}g_2Q_{22}(1+L_1)-f_{12}L_1\dfrac{Q_{22}}{Q_{21}}}{1+L_1+g_2Q_{22}+g_2Q_{22}L_1-\dfrac{Q_{11}Q_{22}}{Q_{12}Q_{21}}} \tag{5.10}$$

We would now like to write the general second row design problem so as to resemble the design problem of Eqn. 5.1, or

$$t_{2i}=\frac{f_{2i}L_{2_e}+d_{2i}Q_{22_e}}{1+L_{2_e}} \tag{5.11}$$

Equating Eqns. 5.10 and 5.11, we see that

$$1+\frac{g_2Q_{22}(1+L_1)}{x}=\frac{1+L_1+g_2Q_{22}+g_2Q_{22}L_1-\dfrac{Q_{11}Q_{22}}{Q_{12}Q_{21}}}{x} \tag{5.12}$$

$$x+g_2Q_{22}(1+L_1)=1+L_1+g_2Q_{22}+g_2Q_{22}L_1-\frac{Q_{11}Q_{22}}{Q_{12}Q_{21}} \tag{5.13}$$

$$x=1+L_1-\frac{Q_{11}Q_{22}}{Q_{12}Q_{21}} \tag{5.14}$$

so that, in Eqn. 11,

$$L_{2_e} = g_2 Q_{22_e} = \frac{g_2 Q_{22}(1+L_1)}{1+L_1-\gamma_{12}} \tag{5.15}$$

$$d_{2i} = -\frac{f_{1i} L_1}{Q_{21}(1+L_1)} \tag{5.16}$$

$$\gamma_{ij} = \frac{Q_{ii} Q_{jj}}{Q_{ij} Q_{ji}} \tag{5.17}$$

Recall that with basically non-interacting loops (BNIL), as is the case in this investigation, the f_{ij} for i $\neq$ j are zero, implying the desire that one controller not effect the command to other than the desired controlled output. This means that $d_{22} = 0$ from Eqn. 5.16 so that the second row design problems reduce to SISO design problems, with the disturbance signal as the only input in the off-diagonal design problem (21), and the control input as the only input in the on-diagonal design problem (22). This process can be extended to an n x n MIMO control system design problem by applying the same logic shown above to each of the rows of MISO design problems in succession, utilizing the information about actual transfer functional relationships determined in the design of the previous rows.

In the case of this 4 x 4 MIMO design problem, the following defines the design equations for the successive loop closures.

For the first loop,

$$t_{1i} = \frac{f_{1i}L_1 + d_{1i}Q_{11}}{1 + L_1} \tag{5.18 a}$$

$$L_1 = g_1 Q_{11} \tag{5.18 b}$$

$$d_{1i} = -\frac{t_{2i}}{Q_{12}} - \frac{t_{3i}}{Q_{13}} - \frac{t_{4i}}{Q_{14}} \tag{5.18 c}$$

Having defined f_{11} and g_1 based on these equations, the following expressions govern the second loop.

$$t_{2i} = \frac{f_{2i}L_{2_e} + d_{2i}Q_{22_e}}{1 + L_{2_e}} \tag{5.19 a}$$

$$L_{2_e} = g_2 Q_{22_e} = \frac{g_2 Q_{22}(1 + L_1)}{1 + L_1 - \gamma_{12}} \tag{5.19 b}$$

$$d_{2i} = t_{3i}\left(\frac{Q_{11}}{Q_{13}Q_{21}(1 + L_1)} - \frac{1}{Q_{23}}\right) + t_{4i}\left(\frac{Q_{11}}{Q_{14}Q_{21}(1 + L_1)} - \frac{1}{Q_{24}}\right) - \frac{f_{1i}L_1}{Q_{21}(1 + L_1)} \tag{5.19 c}$$

$$\gamma_{12} = \frac{Q_{11}Q_{22}}{Q_{12}Q_{21}} \tag{5.19 d}$$

Now, f_{11}, f_{22}, g_1, and g_2 have been designed from the two previous steps. With this information, the following expressions govern the design of the compensation for the third loop.

$$t_{3i} = \frac{f_{3i}L_{3_e} + d_{3i}Q_{33_e}}{1 + L_{3_e}} \tag{5.20 a}$$

$$L_{3_e} = g_3 Q_{33_e} = \frac{g_3 Q_{33}\zeta_{12}}{\zeta_{12} - \Lambda_3} \tag{5.20 b}$$

$$\zeta_{ij} = (1 + L_i)(1 + L_j) - \gamma_{ij} \tag{5.20 c}$$

$$\Lambda_3 = \gamma_{23}(1 + L_1) + \gamma_{23}(1 + L_1) - (\gamma_{12}\mu_2 + \gamma_{13}\mu_3) \tag{5.20 d}$$

$$\mu_2 = \frac{Q_{21}Q_{33}}{Q_{23}Q_{31}} \tag{5.20 e}$$

$$\mu_3 = \frac{Q_{31}Q_{22}}{Q_{32}Q_{21}} \tag{5.20 f}$$

$$d_{3i} = \frac{f_{1i}L_1\eta_1 + f_{2i}L_2\eta_2 + t_{4i}\epsilon_3}{\zeta_{12}} \tag{5.20 g}$$

$$\eta_1 = \frac{Q_{22}}{Q_{21}Q_{32}} - \frac{1}{Q_{31}}(1 + L_2) \tag{5.20 h}$$

$$\eta_2 = \frac{Q_{11}}{Q_{12}Q_{31}} - \frac{1}{Q_{32}}(1 + L_1) \tag{5.20 i}$$

$$\epsilon_3 = \frac{Q_{11}}{Q_{14}Q_{21}}(1 + L_2) + \frac{Q_{22}}{Q_{24}Q_{32}}(1 + L_1) - \frac{1}{Q_{34}}\zeta_{12} - \gamma_{12}\left(\frac{Q_{21}}{Q_{24}Q_{31}} + \frac{Q_{12}}{Q_{14}Q_{32}}\right) \tag{5.20 j}$$

Lastly, with f_{11}, f_{22}, f_{33}, g_1, g_2, and g_3 defined, the following equations govern the design of the compensation for the fourth loop.

$$t_{4i} = \frac{f_{4i}L_{4_e} + d_{4i}Q_{44_e}}{1 + L_{4_e}} \tag{5.21 a}$$

$$L_{4_e} = g_4 Q_{44_e} = \frac{g_4 Q_{44} \mathrm{X}}{\mathrm{X} - \Lambda_4} \tag{5.21 b}$$

$$\mathrm{X} = (1 + L_3)\zeta_{12} - \Lambda_3 \tag{5.21 c}$$

$$\Lambda_4 = \gamma_{34}\zeta_{12} + \gamma_{24}\zeta_{13} + \gamma_{14}\zeta_{23} - \nu_1(1 + L_1) - \nu_2(1 + L_2) - \nu_3(1 + L_3) + \rho_{12} + \rho_{13} + \rho_{14} \tag{5.21 d}$$

$$\nu_i = \frac{Q_{jj}Q_{kk}Q_{ll}}{Q_{jk}Q_{kl}Q_{lj}} + \frac{Q_{jj}Q_{kk}Q_{ll}}{Q_{jl}Q_{kj}Q_{lk}}, \quad i \neq j \neq k \neq l \tag{5.21 e}$$

$$\rho_{12} = \frac{Q_{11}Q_{22}Q_{33}Q_{44}}{Q_{12}Q_{23}Q_{34}Q_{41}} + \frac{Q_{11}Q_{22}Q_{33}Q_{44}}{Q_{12}Q_{24}Q_{31}Q_{43}} \tag{5.21 f}$$

$$\rho_{13} = \frac{Q_{11}Q_{22}Q_{33}Q_{44}}{Q_{13}Q_{21}Q_{34}Q_{42}} + \frac{Q_{11}Q_{22}Q_{33}Q_{44}}{Q_{13}Q_{24}Q_{32}Q_{41}} \tag{5.21 g}$$

$$\rho_{14} = \frac{Q_{11}Q_{22}Q_{33}Q_{44}}{Q_{14}Q_{21}Q_{32}Q_{43}} + \frac{Q_{11}Q_{22}Q_{33}Q_{44}}{Q_{14}Q_{23}Q_{31}Q_{42}} \tag{5.21 h}$$

$$d_{4i} = \frac{f_{1i}L_1\lambda_1 + f_{2i}L_2\lambda_2 + f_{3i}L_3\lambda_3}{\mathrm{X}} \tag{5.21 i}$$

$$\lambda_1 = -\frac{1}{Q_{41}}\zeta_{23} + \frac{1}{Q_{42}}\left(\frac{Q_{22}}{Q_{21}}(1 + L_3) - \frac{Q_{22}Q_{33}}{Q_{23}Q_{31}}\right) + \frac{1}{Q_{43}}\left(\frac{Q_{33}}{Q_{31}}(1 + L_2) - \frac{Q_{22}Q_{33}}{Q_{21}Q_{32}}\right) \tag{5.21 j}$$

$$\lambda_2 = \frac{1}{Q_{41}}\left(\frac{Q_{11}}{Q_{12}}(1+L_3) - \frac{Q_{11}Q_{33}}{Q_{13}Q_{32}}\right) - \frac{1}{Q_{42}}\zeta_{13} + \frac{1}{Q_{43}}\left(\frac{Q_{33}}{Q_{32}}(1+L_1) - \frac{Q_{11}Q_{33}}{Q_{12}Q_{31}}\right) \quad (5.21\ k)$$

$$\lambda_3 = \frac{1}{Q_{41}}\left(\frac{Q_{11}}{Q_{13}}(1+L_2) - \frac{Q_{11}Q_{22}}{Q_{12}Q_{23}}\right) + \frac{1}{Q_{42}}\left(\frac{Q_{22}}{Q_{23}}(1+L_1) - \frac{Q_{11}Q_{22}}{Q_{13}Q_{21}}\right) - \frac{1}{Q_{43}}\zeta_{12} \quad (5.21\ l)$$

Appendix B contains MATLAB function and script files which perform the operations necessary to apply sequential loop closure to a 4x4 MIMO design problem. Note that the loops may be closed in any order. The numerical subscripts of the above derivation refer to the order of loop closure rather than the output number.

5.3 Plant Variation in the Sequential Loop Closure QFT Design Process

The plant variation is, of course, identical to that discussed in Section 4.3.

5.4 Performance Boundaries

The performance boundaries are identical to those discussed in Section 4.4.

5.5 The Sequential Loop Closure QFT Design Procedure

Once again, the QFT-CAD program was utilized in the design process. Recall that QFT-CAD may be used in conjunction with MATLAB with the user providing the individual programs with data files necessary to perform their assigned tasks. For

example, the BOUNDARY program, which defines the boundaries on the Nichols chart, requires a binary data file which defines the templates (see Section 4.2), as well as an ASCII data file which defines the performance boundaries, the disturbance rejection boundaries, and the stability criteria. For the sequential loop closure process, the nominal plant and templates are defined based on the Q_{iic} expressions of Eqns. 5.18b, 5.19b, 5.20b, and 5.21b. The disturbance signals of Eqns. 5.18c, 5.19c, 5.20g, and 5.21i effect the definition of the disturbance boundaries just as in Eqn. 4.14.

The order of loop closure is, as previously stated, arbitrary, and there is no guidance to aid the designer in selecting an order. Intuitively, it is obvious that as the over specification of the disturbance signal decreases, it becomes "easier" to satisfy the imposed disturbance rejection boundaries. Thus, if one is encountering difficulties in satisfying the disturbance rejection boundaries for a particular loop when using the design procedure described in Chapter 4, that loop should be closed later rather than earlier in the sequential process. Beyond this, however, there is no apparent way to choose the sequence.

Two different sequences for loop closure were attempted in this study. In both, the heave rate and yaw rate loops were closed first and second, respectively. For Sequence 1, the roll loop was closed prior to the pitch loop, and for Sequence 2., the opposite was true.

Utilizing the sequential loop closure technique, both sequences were used in the design of two new FCS's. With the sequence in which the roll loop was closed before the pitch loop, difficulties were encountered in satisfying the performance boundaries by the roll loop transmission. With the pitch loop closed before the roll loop, all performance boundaries were able to be satisfied in the FCS design. Appendix E contains the CAD design figures for this design. The feedback compensators and prefilters for this design are listed in Table 5.1 with the nomenclature described in Section 4.5.

Table 5.1 Prefilters and Feedback Compensators of the FCS

Sequential Loop Closure Design

Roll Attitude	$g_\phi = \frac{0.0257(0.5)[.9;.5](2.76)[.7;3][.7;30]}{(0)^2(2)^2(2.5)(6)^2[.7;50]}$	$f_{\phi\phi_c} = \frac{(0.25)(0.88)(1)}{(0.3)(0.36)(4.64)}$
Pitch Attitude	$g_\theta = \frac{0.0185(0.15)(.7)(1)(1.6)(10)[.7;30]}{(0)^2(6)(80)^2[.7;80]}$	$f_{\theta\theta_c} = \frac{1}{[.7;2.76]}$
Vertical Velocity	$g_{\dot{h}} = \frac{0.306(1)(32)}{(0)(8)}$	$f_{\dot{h}\dot{h}_c} = \frac{(10)}{(0.5)(5)}$
Yaw Rate	$g_\psi = \frac{0.4192(5.2)[.7;30]}{(0)[.7;50](70)}$	$f_{\psi\psi_c} = \frac{(2)}{[.7;2.5]}$

5.6 Results

Figures 5.5 thru 5.10 show sample time histories resulting from the application of this FCS in the manner shown in Fig. 4.15. The performance of this FCS is quite similar to that of the previous FCS design, shown in Figs. 4.16 thru 4.21. It was possible using this sequential loop closure technique to satisfy all of the imposed disturbance rejection and tracking performance bounds during the design process. Although the yaw rate to yaw rate command response is somewhat oscillatory, the responses themselves met the design criteria and were felt to be acceptable. To verify the compliance of the closed loop system to these constraints, the modified Golubev program described in Section 4.6 was employed once again. Figures 5.11 and 5.12 depict two sample frequency response comparisons with the appropriate disturbance or tracking performance bounds indicated in the figures as dashed lines. The three (3) solid lines in the figures represent three (3) flight conditions, hover, 40 kts, and 100 kts. Note that in Fig. 5.11 each of the lines remains between the upper and lower bounds at all of the design frequencies, as expected. Also, in Fig. 5.12, each of the lines remains below the cross coupling bound at all of the design frequencies.

Note the magnitude of the roll attitude to yaw rate command cross coupling frequency response is significantly greater with the sequential loop closure design (Fig. 5.12) than the design of Chapter 4 (Fig. 4.22). Both, however, satisfy the imposed cross coupling performance specifications. One important difference between this and the previous FCS design is their respective sensor noise reduction characteristics. Figures

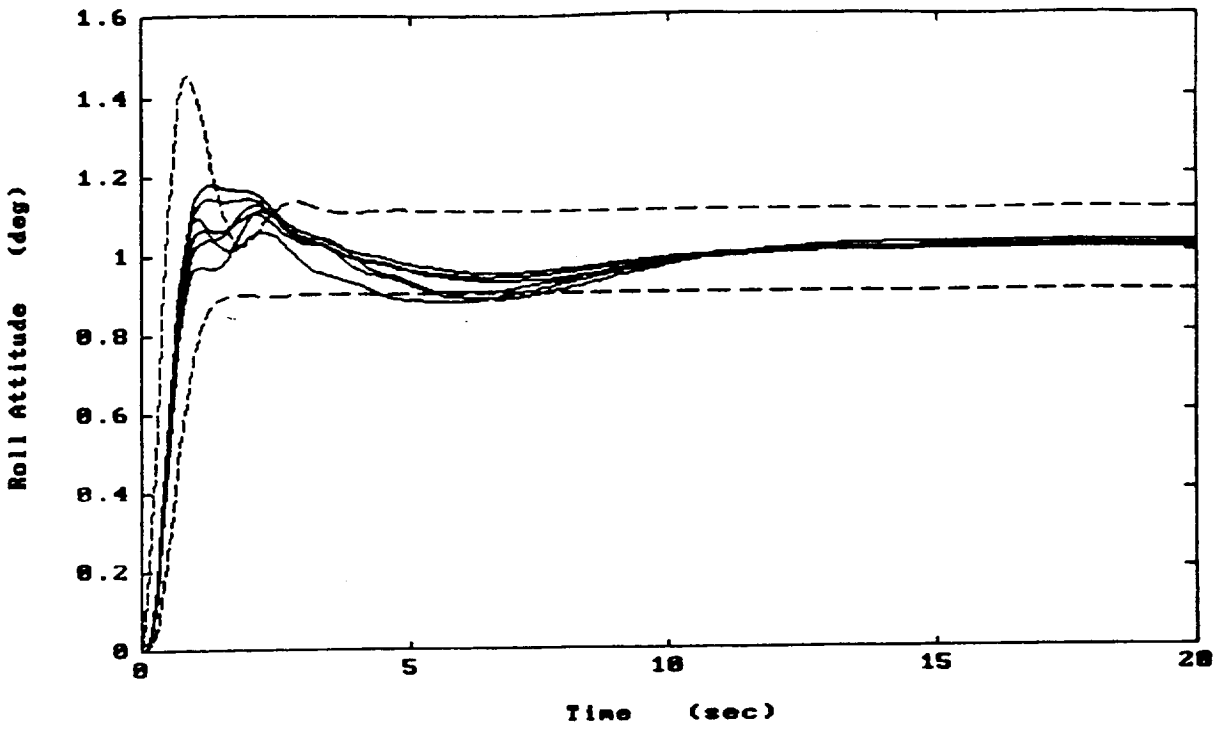

Figure 5.5 Roll Attitude Response to a Unit Step to Roll Attitude Command - Sequential Loop Closure Design

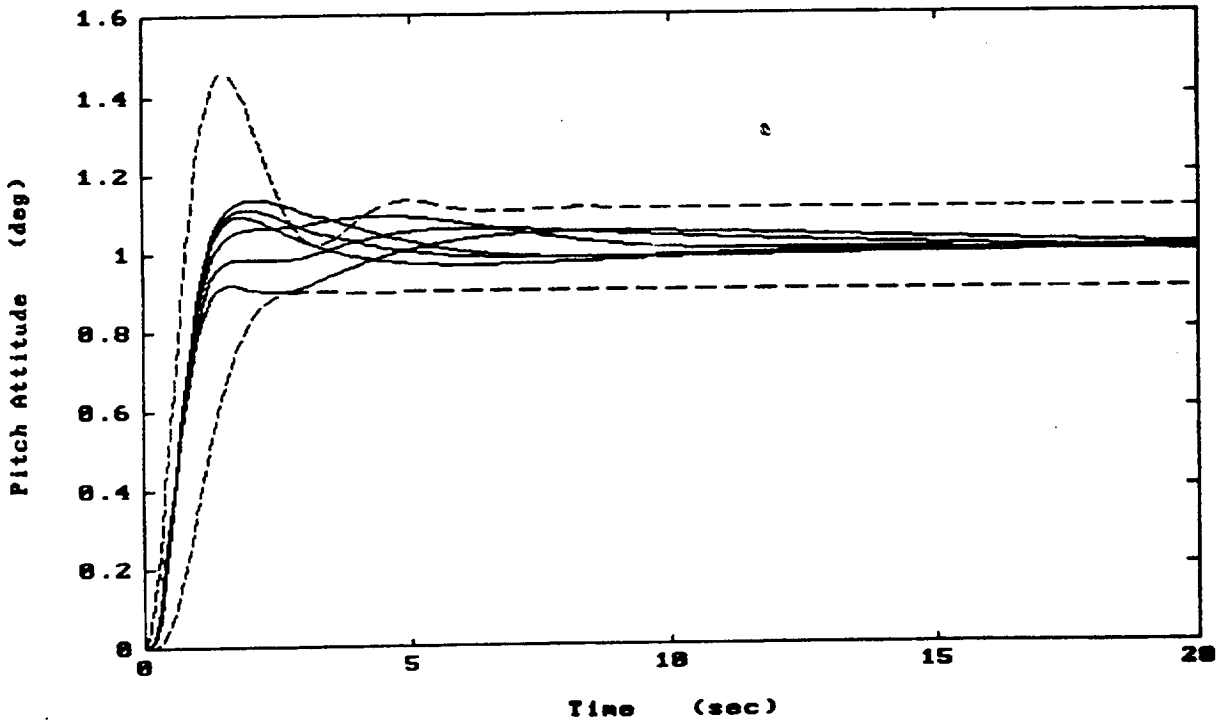

Figure 5.6 Pitch Attitude Response to a Unit Step to Pitch Attitude Command - Sequential Loop Closure Design

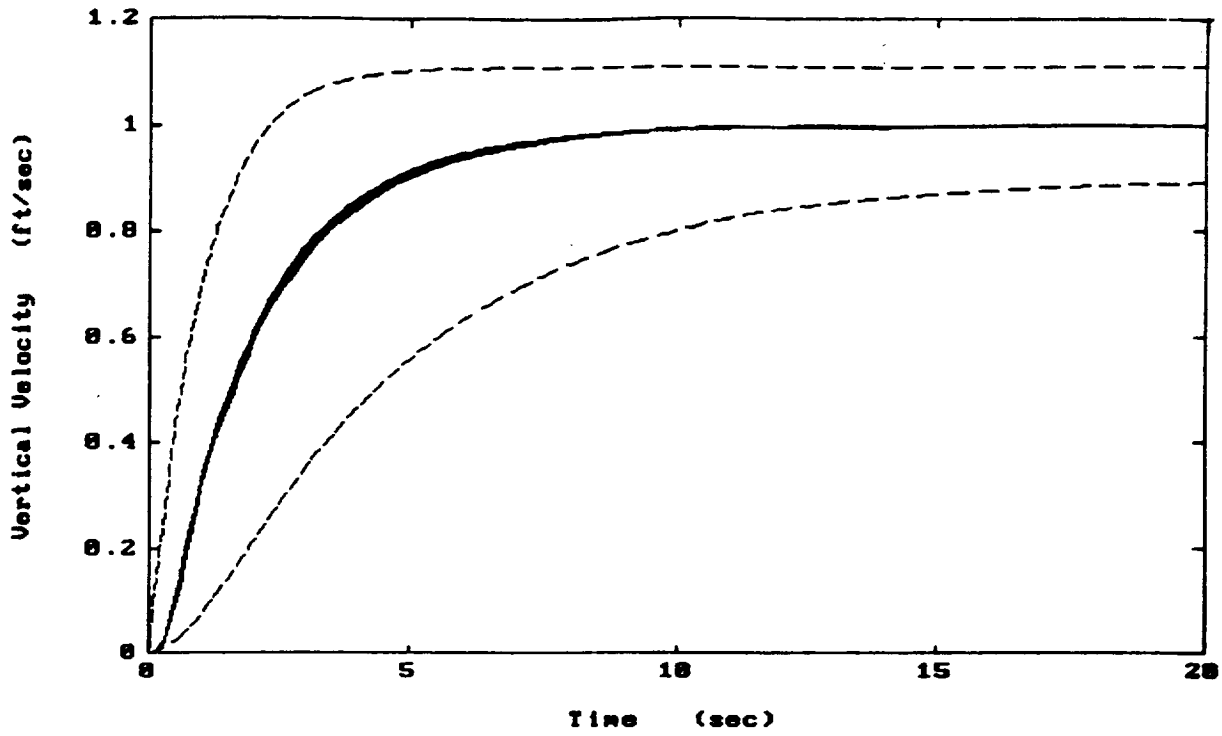

Figure 5.7 Vertical Velocity Response to a Unit Step to Vertical Velocity Command Sequential Loop Closure Design

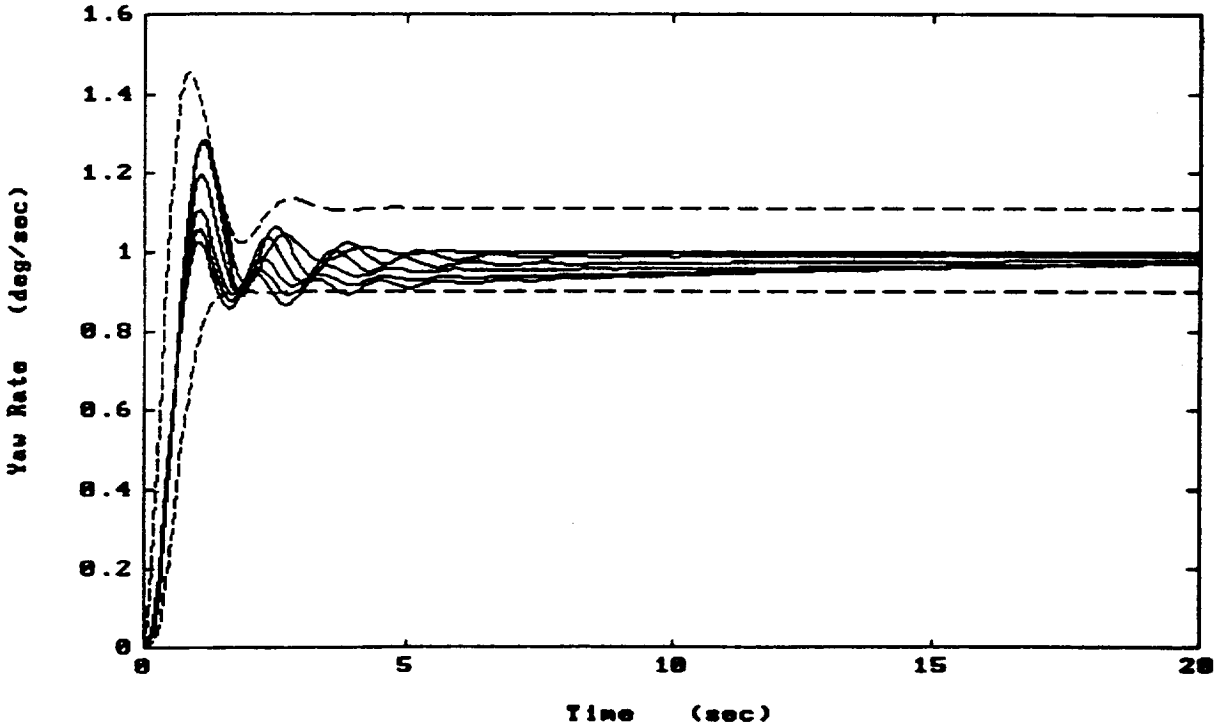

Figure 5.8 Yaw Rate Response to a Unit Step to Yaw Rate Command - Sequential Loop Closure Design

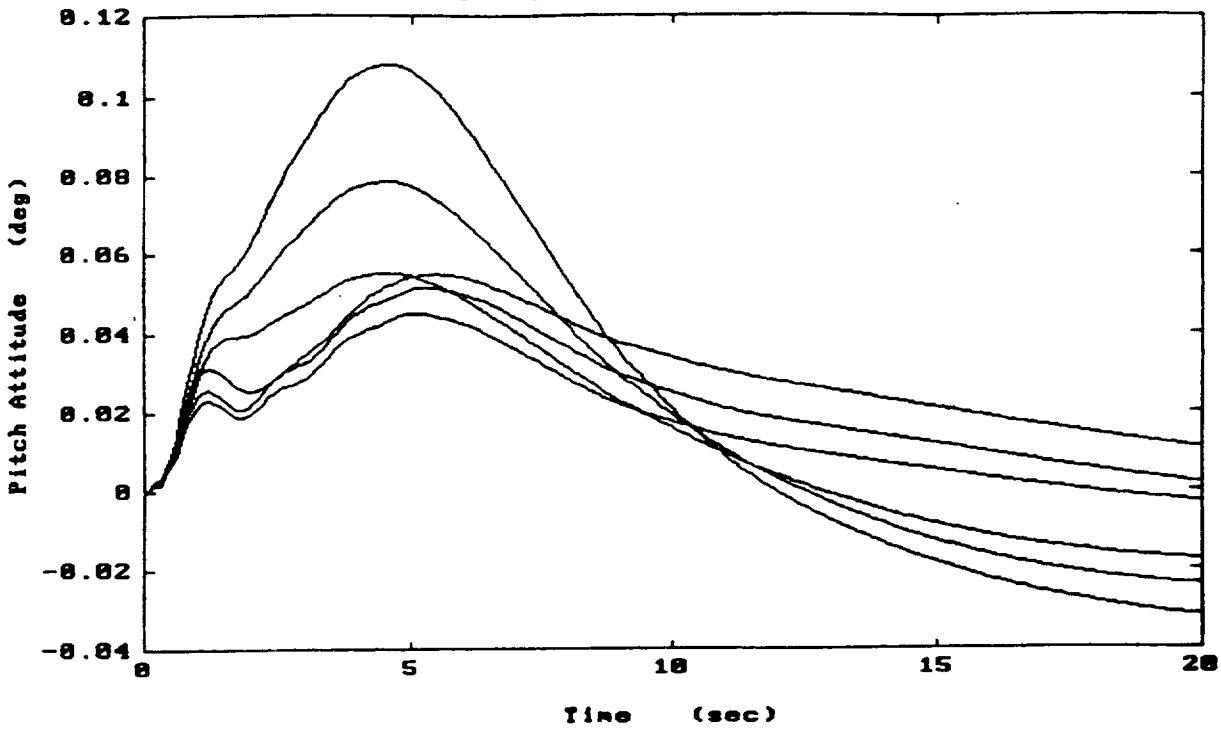

Figure 5.9 Pitch Attitude Response to a Unit Step to Roll Attitude Command - Sequential Loop Closure Design

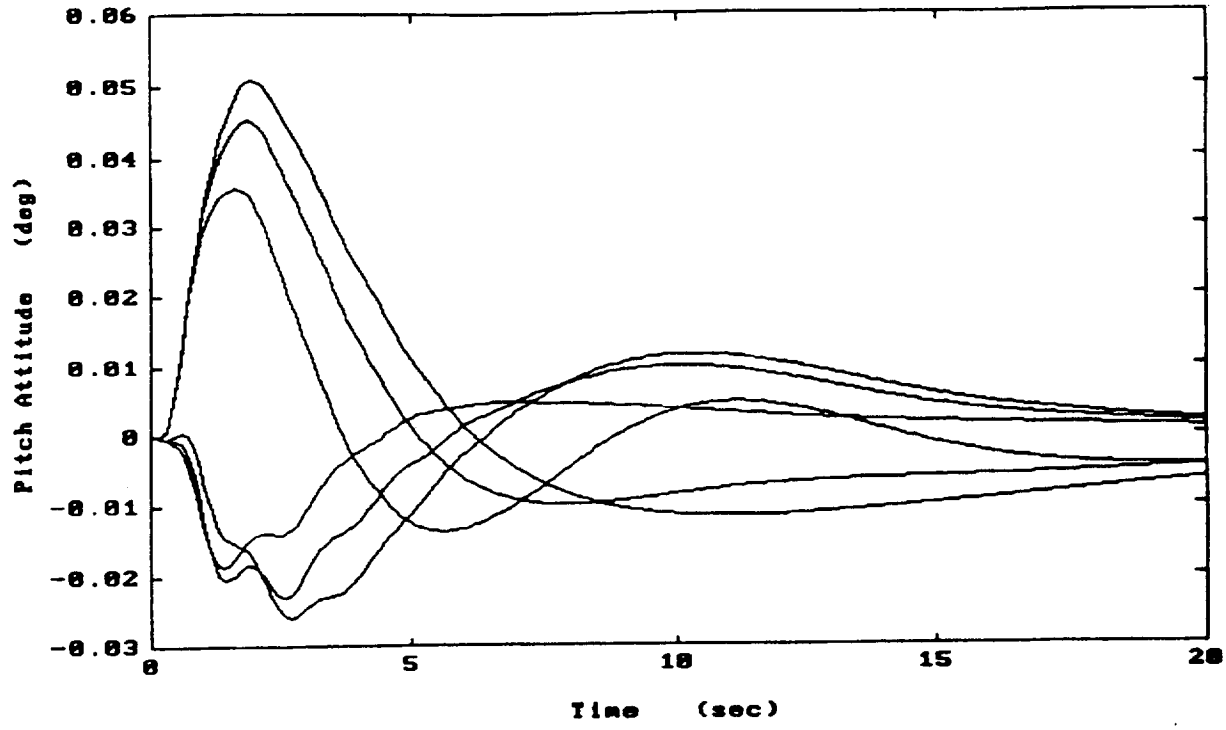

Figure 5.10 Pitch Attitude Response to a Unit Step to Vertical Velocity Command - Sequential Loop Closure Design

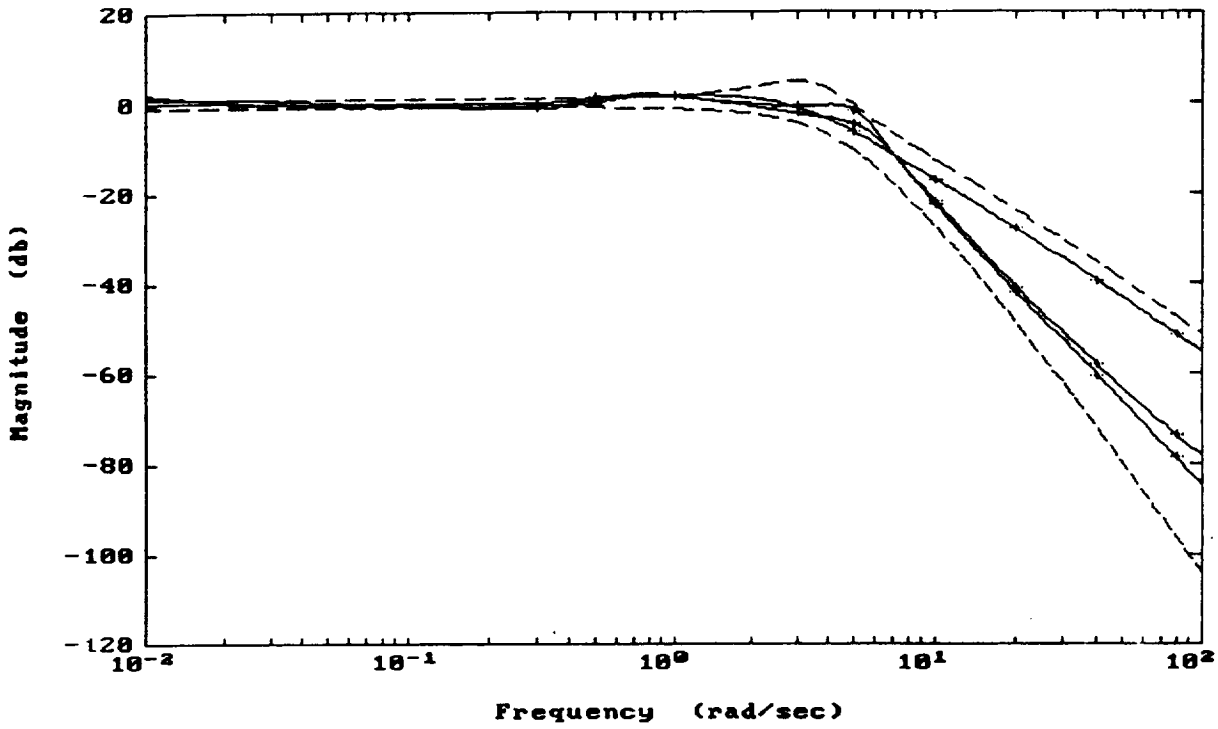

Figure 5.11 Approximate Frequency Response of Roll Attitude due to Roll Attitude Command - Sequential Loop Closure Design

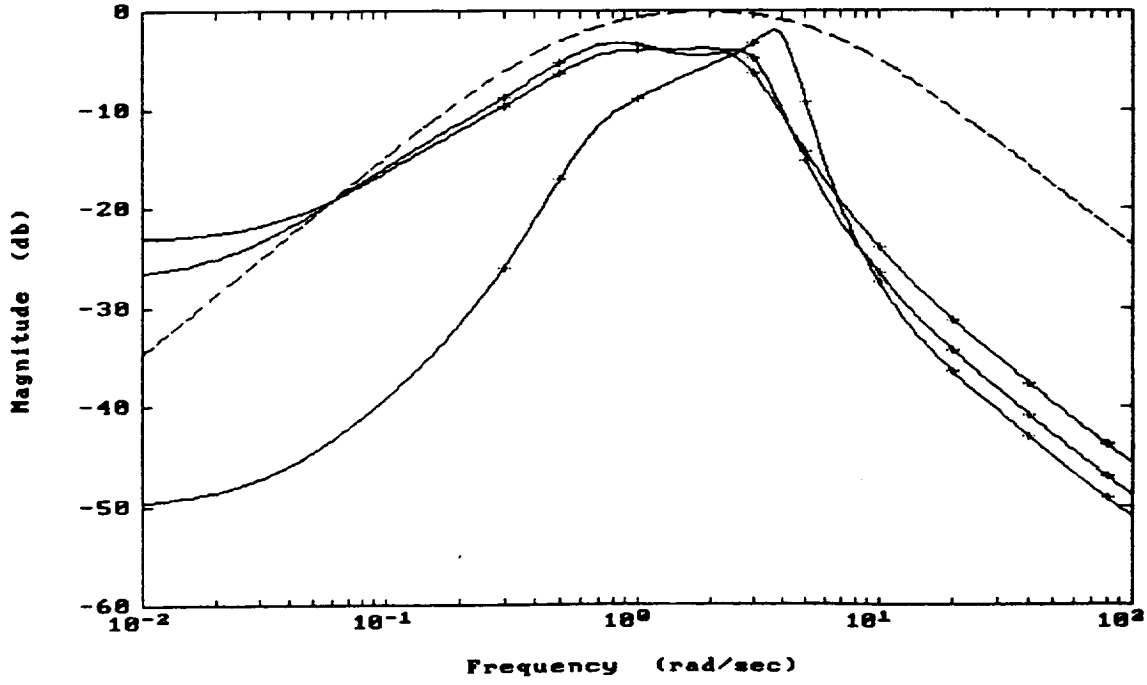

Figure 5.12 Approximate Frequency Response of Roll Attitude due to Yaw Rate Command - Sequential Loop Closure Design

5.13 thru 5.16 show a comparison between the four feedback compensators of the two designs. The pitch feedback compensator was identical for the two designs, so no enhancement of the noise reduction characteristics for that loop were realized. For the other loops, however, the shaded areas in the figures illustrate the improvement of the noise reduction characteristics in the FCS designed utilizing the sequential loop closure technique. The shaded area of Fig. 5.13 indicates the reduced "cost" of the improved roll attitude compensator.

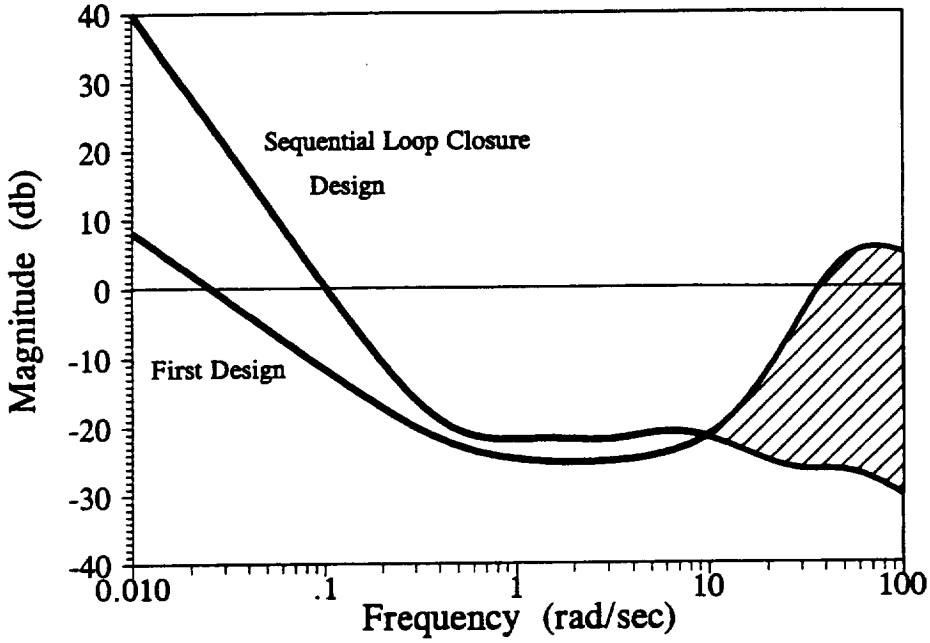

Figure 5.13 Comparison of Feedback Compensators for Design #1 and Sequential Loop Closure Design - Roll Loop

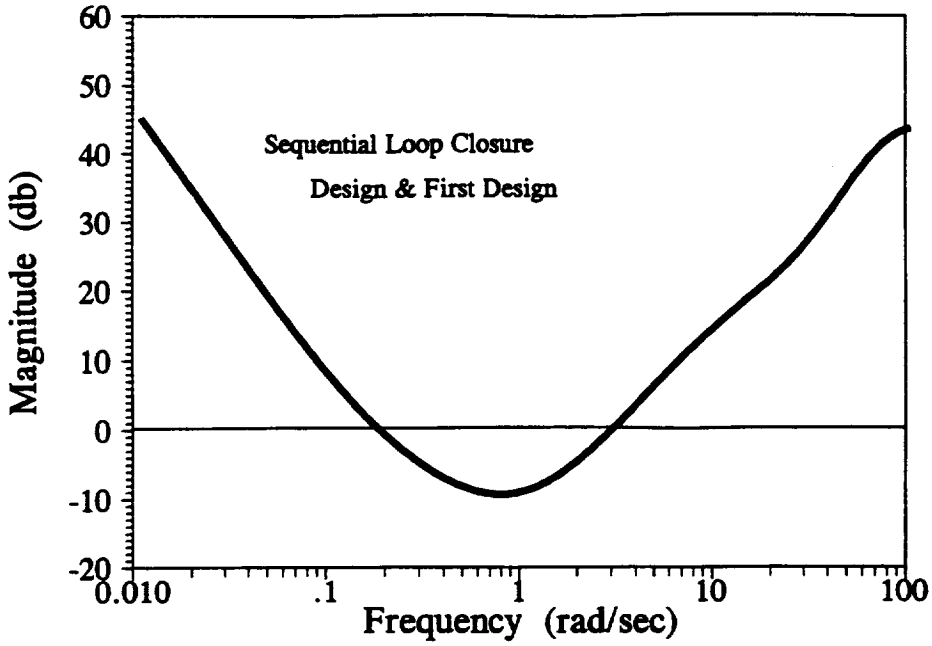

Figure 5.14 Comparison of Feedback Compensators for Design #1 and Sequential Loop Closure Design -Pitch Loop

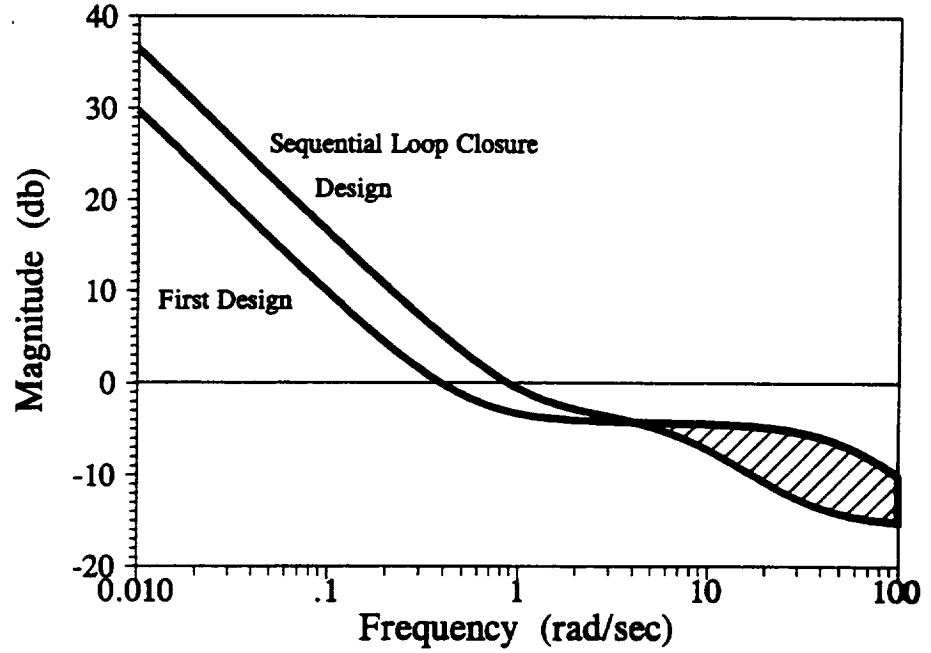

Figure 5.15 Comparison of Feedback Compensators for Design #1 and Sequential Loop Closure Design - Vertical Velocity Loop

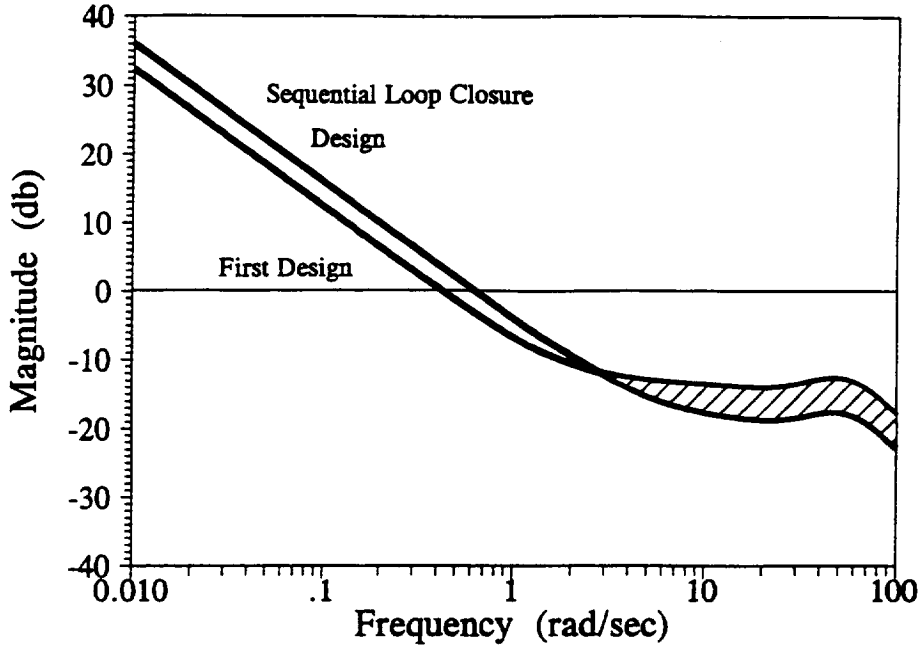

Figure 5.16 Comparison of Feedback Compensators for Design #1 and Sequential Loop Closure Design - Yaw Rate Loop

CHAPTER 6

CONCLUSIONS

The purpose of the research described herein was to develop a robust rotorcraft flight control system (FCS) design methodology utilizing Quantitative Feedback Theory (QFT). This research intended to develop a methodology for the design of robust rotorcraft flight control systems using Quantitative Feedback Theory (QFT). QFT was developed to address a Multiple-Input-Single-Output (MISO) design problem, and utilizes two degrees of freedom to satisfy the design criteria.

Two techniques were examined for extending the QFT MISO technique to the design of a Multiple-Input-Multiple-Output (MIMO) flight control system (FCS) for a UH-60 Black Hawk Helicopter. In the first, a set of MISO systems, mathematically equivalent to the MIMO system, is determined. QFT is applied to each member of the set simultaneously. In the second, the same set of equivalent MISO systems are analyzed sequentially, with closed loop response information from each utilized in subsequent MISO designs. Several conclusions resulted from this endeavor.

First, as a requirement of QFT, boundaries on acceptable performance must be defined for all input-output combinations. Handling qualities specifications published by the U.S. Army as a guide to military helicopter manufacturers proved very useful in the

determination of these bounds for the control responses (pitch to pitch command, etc.). These guidelines provide a means of designing a FCS that will likely yield acceptable handling qualities. The published handling qualities specifications were not very useful in determining the bounds on acceptable cross-coupling performance (pitch to roll command, etc.), however. Determined as a means of evaluating existing FCS, these guidelines did not lend themselves to the specification of boundaries on acceptable cross-coupling performance. One area of future research should be in this area. To be useful in the QFT design process, frequency responses which yield barely acceptable handling qualities for each cross-coupling combination must be determined.

Another conclusion drawn from this study was that the extension of the MISO QFT design technique to a MIMO design problem results in an overly conservative control system design. It was not even possible to satisfy all of the QFT design criteria in the test case due to the over-specification of the performance bounds associated with this technique. This problem is more acute with greater numbers of inputs and outputs. To address this problem in the 4x4 MIMO test case, a technique denoted Sequential Loop Closure (SLC) was utilized. With this technique, the over-specification of the performance boundaries is reduced with each successive loop closure, allowing for a less conservative FCS design.

Another possible means of alleviating the over design issue in the MIMO design technique would be to address the cross coupling characteristics of the MIMO system

directly since it is the cross-coupling characteristics of the MIMO system which result in the over-specification of the performance boundaries in the extension of the MISO design technique. This could be accomplished in at least two ways: 1) non-diagonal G compensation, 2) the implementation of a robust decoupling technique [15].

In the first, the non-diagonal elements of the $\underline{G}$ feedback compensator matrix are used to reduce the magnitude of the cross coupling responses. If the derivation of Section 4.2 is pursued without the assumption of a diagonal $\underline{G}$ compensator matrix, Eqn. 4.9 becomes

$$T_{ij} = \frac{F_{ij}G_{ii}Q_{ii} + d_{ij}Q_{ii}}{1 + G_{ii}Q_{ii}}, \quad d_{ij} = \sum_{\alpha \neq i} T_{\alpha j}\left(G_{i\alpha} - \frac{1}{Q_{i\alpha}}\right) \tag{6.22}$$

Clearly, if the off-diagonal elements of $\underline{G}$ are determined so as to minimize the magnitude

$$\min\left(\left|G_{ij} - \frac{1}{Q_{ij}}\right|\right) \tag{6.23}$$

then the adverse effects of the disturbance signal on the design process can be minimized. Unfortunately, as can be seen in Fig. 4.11, the magnitude of Q_{ij} tends to diminish at higher frequencies. Thus, to satisfy Eqn. 6.2, the magnitude of G_{ij} must increase at higher frequencies which results in undesirable noise reduction characteristics of the system.

The second technique involves the application of a robust decoupling scheme to the MIMO system prior to its decomposition into equivalent MISO design problems. Ideally, a completely decoupled MIMO system decomposes identically into n SISO systems since no loop is dependent on any other. Any reduction in the cross-coupling characteristics of the original MIMO system would reduce the magnitude of the disturbance signal of Eqn. 4.9 and, thus, aid in the successful design of a FCS utilizing QFT.

Overall, Quantitative Feedback Theory does provide a good means of designing a robust rotorcraft flight control system, particularly when sequential loop closure is utilized. The FCS designed utilizing this technique demonstrated acceptable dynamic responses for a wide range of flight conditions. With improvements discussed previously, it could be an even more powerful tool in the development of the next generation helicopters' high response-bandwidth flight control systems.

REFERENCES

1. Tischler, M. B., "Digital Control of Highly Augmented Combat Rotorcraft," NASA TM-88344, May 1987.

2. Chen, Robert T. N., and William S. Hindson, "Influence of High-Order Dynamics on Helicopter Flight-Control System Bandwidth," *Journal of Guidance*, Vol. 9, No. 2, Sept. 1985.

3. Horowitz, I., "Quantitative Feedback Theory (QFT)," Proceedings of the 1988 American Control Conference, Vol. 3, p. 2032-2037, 15-17 June, 1988.

4. Horowitz, Isaac M., and Marcel Sidi, "Synthesis of Feedback Systems with Large Plant Ignorance for Prescribed Time-Domain Tolerances," *International Journal of Control*, Vol. 53, No. 2, p. 287-309, 1972.

5. Horowitz, Isaac, "Survey of Quantitative Feedback Theory (QFT)," *International Journal of Control*, Vol. 53, No. 2, p. 255-291, 1972.

6. Horowitz, I., and C. Loecher, "Design of a 3x3 Multivariable Feedback System with Large Plant Uncertainty," *International Journal of Control*, Vol. 33, No. 4, p. 677-699, 1981.

7. Horowitz, I., "Improved Design Technique for Uncertain Multiple-Input-Multiple-Output Feedback Systems," *International Journal of Control*, Vol. 36, No. 6, p. 977-988, 1982.

8. Horowitz, Isaac, Oded Yaniv, Boris Golubev, and Linda Neumann, "A Synthesis Technique for Highly Uncertain and Interacting Multivariable Flight Control Systems," IEEE, 1981.

9. Landis, Kenneth H., and Steven I. Glusman, "Development of ADOCS Controllers and Control Laws," NASA Contractor Report No. 177339, 1985.

10. Kaletka, J., and W. Grunhagen, "Identification of Mathematical Derivative Models for the Design of a Model Following Control System," Proceedings of the 45th Annual Forum of the American Helicopter Society, p. 655-668, May

1989.

11. Hall, W. E., Jr., and A. E. Bryson Jr., "Inclusion of Rotor Dynamics in Controller Design for Helicopters," *Journal of Aircraft*, Vol. 10, No. 4., April 1973.

12. Yue, Andrew, and Ian Postlethwaite, "H^{∞} - Optimal Design for Helicopter Control," Proceedings of the 1988 American Control Conference, Vol. 2, p. 1679-1684, 15-17 June, 1988.

13. Yue, A., I. Postlethwaite, and G. Padfield, "H-infinity Design and the Improvement of Helicopter Handling Qualities," *Vertica*, Vol. 13, No. 2, p. 119-132, 1989.

14. Takahashi, Mark D., "Helicopter Flight-Control Design Using an *H2* Method," Proceedings of the AIAA Guidance, Navigation and Control Conference, Vol. 3, p. 1392-1416, 1991.

15. Catapang, David R., Mark B. Tischler, and Daniel J. Biezad, "Robust Crossfeed Design for Hovering Rotorcraft," Presented at the Symposium and Tutorial on Quantitative Feedback Theory, Dayton, Ohio, Aug. 3-4 1992.

16. Gerrard, William L., and Bradley S. Liebst, "Design of a Multivariable Helicopter Flight Control System for Handling Qualities Enhancement," Proceedings of the 43rd Annual Forum of the American Helicopter Society, Vol. 2., p. 677-696, 18-20 May, 1987.

17. Manness, M. A., and D. J. Murray-Smith, "Aspects of Multivariable Flight Control Law Design for Helicopters Using Eigenstructure Assignment,"

18. Ekblad, Mark, "Reduced-Order Modeling and Control Design for a High-Performance Helicopter," *Journal of Guidance*, Vol. 13, No. 3, May-June 1990.

19. Hall, Steven R., and Norman M. Wereley, "Linear Control Issues in the Higher Harmonic Control of Helicopter Vibrations," Proceedings of the 45th Annual

Forum of the American Helicopter Society, p. 955-971, 22-24 May, 1989.

20. Ham, Norman D., Norman M. Wereley, and Karl D. von Ellenrieder, "Active Control of Gust- and Interference-Induced Vibration of Tilt-Rotor Aircraft,"

21. McKillop, Robert M., "Periodic Control of the Individual Blade Control Helicopter Rotor," *Vertica*, vol. 9, p. 199-225, 1989.

22. McKillop, Robert M., "Kinematic Observers for Active Control of Helicopter Rotor Vibration," *Vertica*, Vol. 12, No. 1/2, p. 1-11, 1988.

23. Stevens, Brian L., and Frank L. Lewis, Aircraft Control and Simulation, Ch. 4, John Wiley and sons, 1992.

24. Seddon, J., Basic Helicopter Aerodynamics, BSP Professional Books, 1990

25. Prouty, R. W., Military Helicopter Design Technology, Jane's Defence Data, 1989

26. Prouty, R. W., Helicopter Performance, Stability, and Control, PWS Engineering, 1986

27. Prouty, R. W., Helicopter Aerodynamics, PJS Publications Inc., 1985

28. Prouty, R. W., Practical Helicopter Aerodynamics, PJS Publications Inc., 1982

29. Takahashi, M. D., "A Flight-Dynamic Helicopter Mathematical Model with a Single Flap-Lag-Torsion Main Rotor," NASA Technical Memorandum 102267, February 1990.

30. Howlett, J. J., "UH-60A Black Hawk Engineering Simulation Program, Vol. 1 - Math Model," NASA CR-166309, Dec. 1981.

31. Harper, Robert P., and George E. Cooper, "Handling Qualities and Pilot Evaluation," *Journal of Guidance*, Vol. 1, No. 5, p. 515-529, Sept.-Oct. 1986.

32. Cooper, George E., and Robert P. Harper, "The Use of Pilot Rating in the Evaluation of Aircraft Handling Qualities," NASA TN D-5153, April 1969.

33. Anon., "Handling Qualities Requirements for Military Rotorcraft," US Army Aviation Systems Command, ADS-33C, Aug. 1989.

34. Yaniv, Oded, "Multiple Input Single Output (MISO) QFT - CAD User Manual," Department of Electrical Engineering - Systems, Tel-Aviv University, July 1992.

35. Anon., Advanced Continuous Simulation Language (ACSL) - User Guide/Reference Manual, Mitchell and Gauthier, Assoc., Inc., 1981.

36. Anon., The Student Edition of MATLAB, The Math Works, Inc., 1992.

37. Golubev, B., and I. Horowitz, "Plant Rational Transfer Function Approximation from Input-Output Data," *Int. J. Control*, vol. 36, p. 711-23, 1982

APPENDIX A

THE LINEARIZED UH-60A HELICOPTER MODEL

The full 28 state non-linear UH-60A helicopter model (before actuator dynamics are added) described in Chapter 3 was linearized about six (6) flight conditions: hover (0 kts); 20 kts; 40 kts; 60 kts; 80 kts; 100 kts. The form of the linearized model is the state-space representation

$$\dot{\underline{x}} = \underline{A}\underline{x} + \underline{B}\underline{u}$$

$$\underline{y} = \underline{C}^t\underline{x}$$

where the 28 states in the vector $\underline{x}$ are listed in Table A-1, the 4 inputs in $\underline{u}$ are listed in Table A-2, and the 4 outputs in the vector $\underline{y}$ are listed in Table A-3.

Tables A-4 thru A-21 list the $\underline{A}$, $\underline{B}$, and $\underline{C}$ matrices for the six (6) linear models. Note that it is the transpose of the $\underline{C}$ matrices listed in the tables which appears in the state equations above.

Table A-1 List of States for Linearized Helicopter Model

1-3	p, q, and r	Attitude Rates (deg/sec)
4-6	U, V, and W	Body Axis Velocities (ft/sec)
7-9	ϕ, θ, and ψ	Euler angles (deg)
10-13	$\dot{\beta}_0$, $\dot{\beta}_D$, $\dot{\beta}_{1S}$, and $\dot{\beta}_{1C}$	Rotor Flapping Rates (deg/sec)
14-17	$\dot{\zeta}_0$, $\dot{\zeta}_D$, $\dot{\zeta}_{1S}$, and $\dot{\zeta}_{1C}$	Rotor Lead-Lag Rates (deg/sec)
18-21	β_0 , β_D , β_{1S} , and β_{1C}	Rotor Flapping Angles (deg)
22-25	ζ_0 , ζ_D , ζ_{1S} , and ζ_{1C}	Rotor Lead-Lag Angles (deg)
26-28	λ_0 , λ_{1S} , and λ_{1C}	Inflow Velocities (ft/sec)

Table A-2 List of Inputs to the Linearized Helicopter Model

1-2	δ_A and δ_B	Lateral and Longitudinal Cyclic (in)
3	δ_C	Collective (in)
4	δ_P	Pedals (in)

Table A-3 List of Outputs of the Linearized Helicopter Model

1	ϕ	Roll Attitude (deg)
2	θ	Pitch Attitude (deg)
3	$\dot{h}$	Inertial Vertical Velocity (ft/sec)
4	r	Yaw Rate (deg/sec)

Table A-4 Hover Model A Matrix

	1	2	3	4
1	-8.5101700e-002	-3.3899400e-001	4.6771900e-001	-1.6206400e-001
2	7.0595500e-002	-3.2382500e-002	-6.4793300e-002	-1.3452800e-002
3	2.8364700e-002	-8.6021200e-002	-2.7568100e-001	-1.1739300e-002
4	-1.7290900e-002	-1.1726000e-003	-3.8738800e-003	-4.8635700e-003
5	4.0808000e-004	-1.5210100e-002	-2.2435100e-002	6.0371900e-004
6	-2.3368500e-003	2.9695600e-002	3.9809500e-002	-3.3852600e-004
7	1.0000000e+000	-2.3598400e-003	4.8930300e-002	0.0000000e+000
8	0.0000000e+000	9.9883900e-001	4.8172700e-002	0.0000000e+000
9	0.0000000e+000	-4.8230400e-002	1.0000400e+000	0.0000000e+000
10	2.2881900e-001	-1.0133400e+000	-1.5925600e+000	-3.2056000e+000
11	0.0000000e+000	0.0000000e+000	0.0000000e+000	0.0000000e+000
12	2.8066300e+001	-5.6340700e+001	2.9308000e+000	1.4941300e+001
13	5.5990600e+001	2.8239000e+001	2.5003400e+000	-5.1921500e+000
14	-4.7410900e-001	-2.3792400e-001	-2.9856900e-001	1.0979600e-001
15	0.0000000e+000	0.0000000e+000	0.0000000e+000	0.0000000e+000
16	-5.4498000e-001	4.1246400e-002	-6.1028400e-002	-1.4838100e+000
17	-1.2446600e-002	-4.2928500e-001	-1.5458900e-001	3.8461100e-001
18	0.0000000e+000	0.0000000e+000	0.0000000e+000	0.0000000e+000
19	0.0000000e+000	0.0000000e+000	0.0000000e+000	0.0000000e+000
20	0.0000000e+000	0.0000000e+000	0.0000000e+000	0.0000000e+000
21	0.0000000e+000	0.0000000e+000	0.0000000e+000	0.0000000e+000
22	0.0000000e+000	0.0000000e+000	0.0000000e+000	0.0000000e+000
23	0.0000000e+000	0.0000000e+000	0.0000000e+000	0.0000000e+000
24	0.0000000e+000	0.0000000e+000	0.0000000e+000	0.0000000e+000
25	0.0000000e+000	0.0000000e+000	0.0000000e+000	0.0000000e+000
26	1.6216000e-003	-5.4827800e-003	-1.4736100e-002	-2.6986000e-002
27	7.4406900e-002	-2.5661800e-003	-2.9328200e-003	7.5749500e-002
28	3.7469900e-003	7.3100800e-002	-9.9735200e-005	3.3256600e-001

Table A-4 Hover Model A Matrix (cont.)

	5	6	7	8
1	-5.6588300e-001	8.7724300e-002	0.0000000e+000	0.0000000e+000
2	9.5968700e-002	-6.5614200e-002	0.0000000e+000	0.0000000e+000
3	3.2865900e-001	-1.1052400e-001	0.0000000e+000	0.0000000e+000
4	1.4393300e-003	1.9730000e-003	0.0000000e+000	-5.5958000e-001
5	-1.4611000e-002	3.4663100e-003	5.5893000e-001	1.3205200e-003
6	3.7400100e-003	-3.3945200e-002	2.6956400e-002	-2.7380400e-002
7	0.0000000e+000	0.0000000e+000	0.0000000e+000	0.0000000e+000
8	0.0000000e+000	0.0000000e+000	0.0000000e+000	0.0000000e+000
9	0.0000000e+000	0.0000000e+000	0.0000000e+000	0.0000000e+000
10	1.1991600e+000	6.4015000e+001	0.0000000e+000	0.0000000e+000
11	0.0000000e+000	0.0000000e+000	0.0000000e+000	0.0000000e+000
12	4.6389400e+000	9.4320200e-001	0.0000000e+000	0.0000000e+000
13	1.5299400e+001	-7.3259100e-001	0.0000000e+000	0.0000000e+000
14	1.9950700e-001	-2.0309800e+000	0.0000000e+000	0.0000000e+000
15	0.0000000e+000	0.0000000e+000	0.0000000e+000	0.0000000e+000
16	-2.1569900e-001	-2.5693700e-001	0.0000000e+000	0.0000000e+000
17	-1.2989300e+000	-1.1849400e+000	0.0000000e+000	0.0000000e+000
18	0.0000000e+000	0.0000000e+000	0.0000000e+000	0.0000000e+000
19	0.0000000e+000	0.0000000e+000	0.0000000e+000	0.0000000e+000
20	0.0000000e+000	0.0000000e+000	0.0000000e+000	0.0000000e+000
21	0.0000000e+000	0.0000000e+000	0.0000000e+000	0.0000000e+000
22	0.0000000e+000	0.0000000e+000	0.0000000e+000	0.0000000e+000
23	0.0000000e+000	0.0000000e+000	0.0000000e+000	0.0000000e+000
24	0.0000000e+000	0.0000000e+000	0.0000000e+000	0.0000000e+000
25	0.0000000e+000	0.0000000e+000	0.0000000e+000	0.0000000e+000
26	7.7857200e-003	3.9034700e-001	0.0000000e+000	0.0000000e+000
27	-3.3206300e-001	1.4248600e-002	-1.5674500e-002	0.0000000e+000
28	7.5352900e-002	3.0775300e-002	7.2873100e-003	0.0000000e+000

Table A-4 Hover Model A Matrix (cont.)

	9	10	11	12
1	0.0000000e+000	-1.1441900e-002	0.0000000e+000	-6.8253500e-002
2	0.0000000e+000	3.4737500e-002	0.0000000e+000	2.1120200e-004
3	0.0000000e+000	2.8146800e-003	0.0000000e+000	6.1290900e-003
4	0.0000000e+000	-5.2587800e-003	0.0000000e+000	5.6276600e-005
5	0.0000000e+000	-1.4856700e-004	0.0000000e+000	-1.4793300e-004
6	0.0000000e+000	-1.5648100e-002	0.0000000e+000	-7.3440500e-005
7	0.0000000e+000	0.0000000e+000	0.0000000e+000	0.0000000e+000
8	0.0000000e+000	0.0000000e+000	0.0000000e+000	0.0000000e+000
9	0.0000000e+000	0.0000000e+000	0.0000000e+000	0.0000000e+000
10	0.0000000e+000	-2.0916500e+001	0.0000000e+000	-2.4130500e-002
11	0.0000000e+000	0.0000000e+000	-2.0864500e+001	0.0000000e+000
12	0.0000000e+000	-5.5776800e-002	0.0000000e+000	-2.0940400e+001
13	0.0000000e+000	1.5697300e-001	0.0000000e+000	-5.3991900e+001
14	0.0000000e+000	3.6154700e+000	0.0000000e+000	5.6213100e-001
15	0.0000000e+000	0.0000000e+000	3.6106600e+000	0.0000000e+000
16	0.0000000e+000	1.1369200e+000	0.0000000e+000	3.6169800e+000
17	0.0000000e+000	2.5128000e-001	0.0000000e+000	2.5934900e-002
18	0.0000000e+000	1.0000000e+000	0.0000000e+000	0.0000000e+000
19	0.0000000e+000	0.0000000e+000	1.0000000e+000	0.0000000e+000
20	0.0000000e+000	0.0000000e+000	0.0000000e+000	1.0000000e+000
21	0.0000000e+000	0.0000000e+000	0.0000000e+000	0.0000000e+000
22	0.0000000e+000	0.0000000e+000	0.0000000e+000	0.0000000e+000
23	0.0000000e+000	0.0000000e+000	0.0000000e+000	0.0000000e+000
24	0.0000000e+000	0.0000000e+000	0.0000000e+000	0.0000000e+000
25	0.0000000e+000	0.0000000e+000	0.0000000e+000	0.0000000e+000
26	0.0000000e+000	-5.6299700e-002	0.0000000e+000	-6.1535700e-005
27	0.0000000e+000	-2.3855900e-004	0.0000000e+000	-9.9368000e-002
28	0.0000000e+000	4.0717000e-004	0.0000000e+000	-9.7842900e-003

Table A-4 Hover Model A Matrix (cont.)

	13	14	15	16
1	1.2372500e-003	7.0573600e-001	0.0000000e+000	1.0143700e+001
2	-8.6147200e-003	-7.1209100e-002	0.0000000e+000	-1.6052000e-001
3	-1.3365600e-004	-1.5606600e+000	0.0000000e+000	2.2584600e-001
4	3.9514800e-004	1.8957900e-003	0.0000000e+000	3.2705100e-002
5	5.9215300e-005	2.2608200e-004	0.0000000e+000	2.7918300e-001
6	-3.1911200e-004	-2.5843700e-002	0.0000000e+000	-2.9409100e-003
7	0.0000000e+000	0.0000000e+000	0.0000000e+000	0.0000000e+000
8	0.0000000e+000	0.0000000e+000	0.0000000e+000	0.0000000e+000
9	0.0000000e+000	0.0000000e+000	0.0000000e+000	0.0000000e+000
10	5.7814900e-002	2.5604000e+000	0.0000000e+000	-3.2695800e-001
11	0.0000000e+000	0.0000000e+000	2.6416200e+000	0.0000000e+000
12	5.4001100e+001	-4.1413100e-002	0.0000000e+000	1.3896900e+001
13	-2.0871600e+001	4.2985700e-001	0.0000000e+000	-1.2790200e+000
14	1.2480400e-001	-1.1406200e+001	0.0000000e+000	-4.4494500e-001
15	0.0000000e+000	0.0000000e+000	-9.6979400e+000	0.0000000e+000
16	-4.1861900e-003	-2.7860500e-001	0.0000000e+000	-1.2494200e+001
17	3.6084400e+000	-6.1799700e-001	0.0000000e+000	-5.8591800e+001
18	0.0000000e+000	0.0000000e+000	0.0000000e+000	0.0000000e+000
19	0.0000000e+000	0.0000000e+000	0.0000000e+000	0.0000000e+000
20	0.0000000e+000	0.0000000e+000	0.0000000e+000	0.0000000e+000
21	1.0000000e+000	0.0000000e+000	0.0000000e+000	0.0000000e+000
22	0.0000000e+000	1.0000000e+000	0.0000000e+000	0.0000000e+000
23	0.0000000e+000	0.0000000e+000	1.0000000e+000	0.0000000e+000
24	0.0000000e+000	0.0000000e+000	0.0000000e+000	1.0000000e+000
25	0.0000000e+000	0.0000000e+000	0.0000000e+000	0.0000000e+000
26	1.5831900e-004	1.3804700e-002	0.0000000e+000	1.9902200e-004
27	9.6965900e-003	-5.6062700e-004	0.0000000e+000	-1.3243100e-002
28	-9.9543300e-002	2.4080000e-003	0.0000000e+000	1.8659700e-002

Table A-4 Hover Model A Matrix (cont.)

	17	18	19	20
1	4.2679700e-001	-7.5895700e+000	0.0000000e+000	-5.4186700e+001
2	1.3436200e+000	5.8215700e+000	0.0000000e+000	-5.8526900e-001
3	3.8778300e-002	-5.3377400e-002	0.0000000e+000	-6.2560900e-001
4	-3.1393700e-001	4.9554200e-001	0.0000000e+000	8.6851700e-002
5	6.3273400e-003	-2.2240100e-001	0.0000000e+000	-5.4237000e-001
6	-1.4630600e-002	-9.2654300e+000	0.0000000e+000	1.7492400e-002
7	0.0000000e+000	0.0000000e+000	0.0000000e+000	0.0000000e+000
8	0.0000000e+000	0.0000000e+000	0.0000000e+000	0.0000000e+000
9	0.0000000e+000	0.0000000e+000	0.0000000e+000	0.0000000e+000
10	2.2820100e-001	-7.8865400e+002	0.0000000e+000	8.3194800e-001
11	0.0000000e+000	0.0000000e+000	-7.5794500e+002	0.0000000e+000
12	6.0513400e-001	-8.5848000e+000	0.0000000e+000	-9.1350700e+001
13	3.8795400e+000	5.7654000e+000	0.0000000e+000	-5.6851200e+002
14	-2.0194600e-001	-9.6268800e-001	0.0000000e+000	8.4479500e+000
15	0.0000000e+000	0.0000000e+000	-1.3796100e+000	0.0000000e+000
16	5.5623700e+001	7.7275600e+000	0.0000000e+000	6.1577200e-001
17	-7.9082700e+000	3.0381200e+001	0.0000000e+000	1.2063800e+002
18	0.0000000e+000	0.0000000e+000	0.0000000e+000	0.0000000e+000
19	0.0000000e+000	0.0000000e+000	0.0000000e+000	0.0000000e+000
20	0.0000000e+000	0.0000000e+000	0.0000000e+000	0.0000000e+000
21	0.0000000e+000	0.0000000e+000	0.0000000e+000	0.0000000e+000
22	0.0000000e+000	0.0000000e+000	0.0000000e+000	0.0000000e+000
23	0.0000000e+000	0.0000000e+000	0.0000000e+000	0.0000000e+000
24	0.0000000e+000	0.0000000e+000	0.0000000e+000	0.0000000e+000
25	1.0000000e+000	0.0000000e+000	0.0000000e+000	0.0000000e+000
26	5.1847200e-004	4.6744800e-002	0.0000000e+000	6.2140500e-005
27	-3.4365500e-003	1.4784900e-002	0.0000000e+000	5.0104700e-001
28	2.3011300e-002	-2.1999300e-002	0.0000000e+000	-2.7789300e+000

Table A-4 Hover Model A Matrix (cont.)

	21	22	23	24
1	4.0339900e+000	3.9331700e+000	0.0000000e+000	2.6797500e+001
2	-7.3994700e+000	-4.0863700e-001	0.0000000e+000	1.7869500e+001
3	-3.8783100e-001	-9.1045100e+000	0.0000000e+000	4.0150700e-001
4	7.3554100e-001	-5.7496700e-003	0.0000000e+000	-4.0131300e+000
5	7.3632200e-002	-3.7370000e-003	0.0000000e+000	6.2434100e-001
6	4.0568100e-002	-7.0128700e-003	0.0000000e+000	-1.6542400e-001
7	0.0000000e+000	0.0000000e+000	0.0000000e+000	0.0000000e+000
8	0.0000000e+000	0.0000000e+000	0.0000000e+000	0.0000000e+000
9	0.0000000e+000	0.0000000e+000	0.0000000e+000	0.0000000e+000
10	3.1545500e-001	2.8098400e+000	0.0000000e+000	8.2328400e+000
11	0.0000000e+000	0.0000000e+000	2.8129900e+000	0.0000000e+000
12	5.7720200e+002	5.9431500e+000	0.0000000e+000	3.3667200e+001
13	-4.1049700e+001	-9.6799000e-001	0.0000000e+000	8.2360500e+001
14	-2.0747600e+000	-6.2173600e+001	0.0000000e+000	-7.8323400e+000
15	0.0000000e+000	0.0000000e+000	-5.2210100e+001	-7.0628100e-005
16	-1.0393900e+002	-1.5515400e+000	0.0000000e+000	6.9835100e+002
17	-2.3653600e+000	-1.3539000e+000	0.0000000e+000	-2.1843000e+002
18	0.0000000e+000	0.0000000e+000	0.0000000e+000	0.0000000e+000
19	0.0000000e+000	0.0000000e+000	0.0000000e+000	0.0000000e+000
20	0.0000000e+000	0.0000000e+000	0.0000000e+000	0.0000000e+000
21	0.0000000e+000	0.0000000e+000	0.0000000e+000	0.0000000e+000
22	0.0000000e+000	0.0000000e+000	0.0000000e+000	0.0000000e+000
23	0.0000000e+000	0.0000000e+000	0.0000000e+000	0.0000000e+000
24	0.0000000e+000	0.0000000e+000	0.0000000e+000	0.0000000e+000
25	0.0000000e+000	0.0000000e+000	0.0000000e+000	0.0000000e+000
26	-7.3247200e-003	9.6620200e-003	0.0000000e+000	1.6730500e-002
27	2.6898000e+000	3.4446200e-003	0.0000000e+000	-1.1196500e-001
28	3.4327200e-001	-1.9778900e-003	0.0000000e+000	4.4438300e-001

Table A-4 Hover Model A Matrix (conc.)

	25	26	27	28
1	-1.3967600e+002	4.7023500e-001	-3.4986400e+000	-9.8567600e-002
2	6.5856500e+000	-5.0607700e-001	1.0607300e-002	-4.7654900e-001
3	-2.5036600e+000	-1.7361400e-001	-2.8356200e-002	-1.1057600e-002
4	-1.3893200e+000	-4.4965200e-002	7.3150600e-003	2.0700800e-002
5	-3.5496400e+000	1.0621400e-002	-8.1640600e-003	7.7523800e-003
6	5.9388200e-002	8.0600200e-001	1.6365800e-003	8.3143500e-004
7	0.0000000e+000	0.0000000e+000	0.0000000e+000	0.0000000e+000
8	0.0000000e+000	0.0000000e+000	0.0000000e+000	0.0000000e+000
9	0.0000000e+000	0.0000000e+000	0.0000000e+000	0.0000000e+000
10	9.1022800e+000	-1.7202000e+003	-1.9750400e+000	6.6468800e-001
11	0.0000000e+000	0.0000000e+000	0.0000000e+000	0.0000000e+000
12	-2.2875800e+002	-4.8596000e+000	-1.2692600e+003	-1.2526100e+002
13	2.5463200e+001	2.6026300e+000	1.2549900e+002	-1.2658500e+003
14	8.0900700e+000	5.1123100e+001	5.8311000e-001	1.2000200e+001
15	-4.1755100e-005	0.0000000e+000	0.0000000e+000	0.0000000e+000
16	3.3311800e+002	4.0151700e+000	3.5044600e+001	3.2110600e+000
17	7.3705000e+002	3.1839000e+001	-2.0700100e+000	3.4956500e+001
18	0.0000000e+000	0.0000000e+000	0.0000000e+000	0.0000000e+000
19	0.0000000e+000	0.0000000e+000	0.0000000e+000	0.0000000e+000
20	0.0000000e+000	0.0000000e+000	0.0000000e+000	0.0000000e+000
21	0.0000000e+000	0.0000000e+000	0.0000000e+000	0.0000000e+000
22	0.0000000e+000	0.0000000e+000	0.0000000e+000	0.0000000e+000
23	0.0000000e+000	0.0000000e+000	0.0000000e+000	0.0000000e+000
24	0.0000000e+000	0.0000000e+000	0.0000000e+000	0.0000000e+000
25	0.0000000e+000	0.0000000e+000	0.0000000e+000	0.0000000e+000
26	-5.4394800e-003	-1.5857100e+001	-6.1002500e-003	-4.1557400e-002
27	7.9770800e-002	-2.2406200e-001	-1.8935300e+001	-8.6821600e-003
28	-2.4559700e-001	-6.1757600e-003	4.1364800e-003	-1.8953900e+001

Table A-5 Hover Model B Matrix

	1	2	3	4
1	7.3815949e+000	3.0310794e+001	5.8040552e+000	-5.9389811e+001
2	-3.3713605e+000	6.6923719e-001	-3.5082624e+000	1.2517254e+001
3	-4.4687608e-001	2.5048593e-001	-8.8439862e+000	3.0757570e+001
4	6.2601385e-001	6.0955812e-002	-1.9254555e-001	2.0059216e-002
5	-8.1123922e-003	6.0291051e-001	2.2352018e-001	-1.4115710e+000
6	3.9690844e-002	6.1286339e-003	4.6863503e-001	4.5400206e-001
7	0.0000000e+000	0.0000000e+000	0.0000000e+000	0.0000000e+000
8	0.0000000e+000	0.0000000e+000	0.0000000e+000	0.0000000e+000
9	0.0000000e+000	0.0000000e+000	0.0000000e+000	0.0000000e+000
10	2.3403859e+000	5.3446868e+000	9.6905013e+002	-2.3197243e+000
11	0.0000000e+000	0.0000000e+000	0.0000000e+000	0.0000000e+000
12	-1.0221121e+002	1.7376796e+003	-2.5228385e+002	-1.0432116e+003
13	-9.6761194e+002	-2.0437016e+002	1.7925029e+002	1.3599632e+002
14	6.3429075e+000	-5.3046699e+000	-1.1148624e+002	3.8583914e+001
15	1.9980171e-005	-3.2063092e-005	2.0601603e-006	1.8467435e-005
16	-9.5888873e+001	-2.0916885e+002	4.9303912e+001	1.2687659e+002
17	1.1012274e+002	-1.0619265e+002	-2.3877811e+001	7.7705239e+001
18	0.0000000e+000	0.0000000e+000	0.0000000e+000	0.0000000e+000
19	0.0000000e+000	0.0000000e+000	0.0000000e+000	0.0000000e+000
20	0.0000000e+000	0.0000000e+000	0.0000000e+000	0.0000000e+000
21	0.0000000e+000	0.0000000e+000	0.0000000e+000	0.0000000e+000
22	0.0000000e+000	0.0000000e+000	0.0000000e+000	0.0000000e+000
23	0.0000000e+000	0.0000000e+000	0.0000000e+000	0.0000000e+000
24	0.0000000e+000	0.0000000e+000	0.0000000e+000	0.0000000e+000
25	0.0000000e+000	0.0000000e+000	0.0000000e+000	0.0000000e+000
26	1.6480684e-003	1.5168876e-002	2.6351853e+000	-8.7368439e-003
27	-1.6899842e-001	8.1219441e+000	-1.3122544e+000	-4.5509835e+000
28	-4.6389595e+000	-2.1754900e-001	7.9154728e-001	6.6245671e-002

Table A-6 Hover Model $\underline{C}$ Matrix

	1	2	3	4
1	0.0000000e+000	0.0000000e+000	0.0000000e+000	0.0000000e+000
2	0.0000000e+000	0.0000000e+000	0.0000000e+000	-4.8230400e-002
3	0.0000000e+000	0.0000000e+000	0.0000000e+000	1.0000400e+000
4	0.0000000e+000	0.0000000e+000	4.8928500e-002	0.0000000e+000
5	0.0000000e+000	0.0000000e+000	4.8115000e-002	0.0000000e+000
6	0.0000000e+000	0.0000000e+000	-9.9764300e-001	0.0000000e+000
7	1.0000000e+000	0.0000000e+000	0.0000000e+000	0.0000000e+000
8	0.0000000e+000	1.0000000e+000	2.9461200e-002	0.0000000e+000
9	0.0000000e+000	0.0000000e+000	0.0000000e+000	0.0000000e+000
10	0.0000000e+000	0.0000000e+000	0.0000000e+000	0.0000000e+000
11	0.0000000e+000	0.0000000e+000	0.0000000e+000	0.0000000e+000
12	0.0000000e+000	0.0000000e+000	0.0000000e+000	0.0000000e+000
13	0.0000000e+000	0.0000000e+000	0.0000000e+000	0.0000000e+000
14	0.0000000e+000	0.0000000e+000	0.0000000e+000	0.0000000e+000
15	0.0000000e+000	0.0000000e+000	0.0000000e+000	0.0000000e+000
16	0.0000000e+000	0.0000000e+000	0.0000000e+000	0.0000000e+000
17	0.0000000e+000	0.0000000e+000	0.0000000e+000	0.0000000e+000
18	0.0000000e+000	0.0000000e+000	0.0000000e+000	0.0000000e+000
19	0.0000000e+000	0.0000000e+000	0.0000000e+000	0.0000000e+000
20	0.0000000e+000	0.0000000e+000	0.0000000e+000	0.0000000e+000
21	0.0000000e+000	0.0000000e+000	0.0000000e+000	0.0000000e+000
22	0.0000000e+000	0.0000000e+000	0.0000000e+000	0.0000000e+000
23	0.0000000e+000	0.0000000e+000	0.0000000e+000	0.0000000e+000
24	0.0000000e+000	0.0000000e+000	0.0000000e+000	0.0000000e+000
25	0.0000000e+000	0.0000000e+000	0.0000000e+000	0.0000000e+000
26	0.0000000e+000	0.0000000e+000	0.0000000e+000	0.0000000e+000
27	0.0000000e+000	0.0000000e+000	0.0000000e+000	0.0000000e+000
28	0.0000000e+000	0.0000000e+000	0.0000000e+000	0.0000000e+000

Table A-7 20 kt Model A Matrix

	1	2	3	4
1	-1.1164700e-001	-3.6074600e-001	5.0028200e-001	4.6337100e-001
2	7.7308600e-002	-4.6735100e-002	-9.2467300e-002	-3.1028300e-001
3	4.8881100e-002	-5.9585800e-002	-3.5449800e-001	-4.8165800e-001
4	-1.6894500e-002	-2.5516200e-002	-4.6312100e-003	-1.1370200e-002
5	2.3457100e-002	-1.5755600e-002	-5.7880800e-001	1.6307700e-002
6	-1.5064000e-003	5.8774200e-001	3.8585500e-002	-1.5724600e-002
7	1.0000000e+000	-1.5346400e-003	4.2896300e-002	0.0000000e+000
8	0.0000000e+000	9.9936100e-001	3.5752800e-002	0.0000000e+000
9	0.0000000e+000	-3.5785800e-002	1.0002800e+000	0.0000000e+000
10	9.6249000e-001	-9.9927900e-001	-1.2949600e+000	-3.4257200e+000
11	0.0000000e+000	0.0000000e+000	0.0000000e+000	0.0000000e+000
12	2.7528800e+001	-5.6627300e+001	2.5030600e+000	1.4543200e+001
13	5.6223700e+001	2.7672700e+001	2.0642900e+000	-5.1676600e+000
14	-2.1401800e-001	-4.3827900e-001	-3.8674500e-001	-4.0210200e-001
15	0.0000000e+000	0.0000000e+000	0.0000000e+000	0.0000000e+000
16	-3.1393400e-001	6.5163000e-002	-7.7495500e-002	-1.3827600e+000
17	-2.2712000e-002	-1.3394500e-001	-3.6221600e-002	1.2417900e-001
18	0.0000000e+000	0.0000000e+000	0.0000000e+000	0.0000000e+000
19	0.0000000e+000	0.0000000e+000	0.0000000e+000	0.0000000e+000
20	0.0000000e+000	0.0000000e+000	0.0000000e+000	0.0000000e+000
21	0.0000000e+000	0.0000000e+000	0.0000000e+000	0.0000000e+000
22	0.0000000e+000	0.0000000e+000	0.0000000e+000	0.0000000e+000
23	0.0000000e+000	0.0000000e+000	0.0000000e+000	0.0000000e+000
24	0.0000000e+000	0.0000000e+000	0.0000000e+000	0.0000000e+000
25	0.0000000e+000	0.0000000e+000	0.0000000e+000	0.0000000e+000
26	9.5692900e-002	1.3102300e-001	-3.7203700e-001	-3.1676500e+000
27	2.3555900e+000	-6.9810800e-002	2.5785300e-002	1.8525900e+000
28	1.0219800e-001	2.3240700e+000	-7.4898800e-002	4.4542900e+000

Table A-7 20 kt Model A Matrix (cont.)

	5	6	7	8
1	-6.9408400e-001	9.3339900e-002	0.0000000e+000	0.0000000e+000
2	1.2717500e-001	-6.9889300e-002	0.0000000e+000	0.0000000e+000
3	4.2497000e-001	-1.5522600e-001	0.0000000e+000	0.0000000e+000
4	1.5365800e-003	1.3234500e-003	0.0000000e+000	-5.5973500e-001
5	-3.2608300e-002	4.3254100e-003	5.5937700e-001	8.5899400e-004
6	5.3431000e-003	-4.8660300e-002	2.0012100e-002	-2.4010600e-002
7	0.0000000e+000	0.0000000e+000	0.0000000e+000	0.0000000e+000
8	0.0000000e+000	0.0000000e+000	0.0000000e+000	0.0000000e+000
9	0.0000000e+000	0.0000000e+000	0.0000000e+000	0.0000000e+000
10	1.6089300e+000	6.4138900e+001	0.0000000e+000	0.0000000e+000
11	0.0000000e+000	0.0000000e+000	0.0000000e+000	0.0000000e+000
12	4.2963800e+000	5.1768500e+000	0.0000000e+000	0.0000000e+000
13	1.4580900e+001	-1.3400600e+000	0.0000000e+000	0.0000000e+000
14	1.7302300e-001	-1.2736400e+000	0.0000000e+000	0.0000000e+000
15	0.0000000e+000	0.0000000e+000	0.0000000e+000	0.0000000e+000
16	-1.1801000e-001	-5.4791200e-001	0.0000000e+000	0.0000000e+000
17	-1.0388700e+000	-2.4487100e+000	0.0000000e+000	0.0000000e+000
18	0.0000000e+000	0.0000000e+000	0.0000000e+000	0.0000000e+000
19	0.0000000e+000	0.0000000e+000	0.0000000e+000	0.0000000e+000
20	0.0000000e+000	0.0000000e+000	0.0000000e+000	0.0000000e+000
21	0.0000000e+000	0.0000000e+000	0.0000000e+000	0.0000000e+000
22	0.0000000e+000	0.0000000e+000	0.0000000e+000	0.0000000e+000
23	0.0000000e+000	0.0000000e+000	0.0000000e+000	0.0000000e+000
24	0.0000000e+000	0.0000000e+000	0.0000000e+000	0.0000000e+000
25	0.0000000e+000	0.0000000e+000	0.0000000e+000	0.0000000e+000
26	1.7534400e-001	8.5772200e+000	0.0000000e+000	0.0000000e+000
27	-5.2676500e+000	8.5162300e-001	-3.3463800e-001	0.0000000e+000
28	2.0096500e+000	5.5319900e+000	8.8854900e-003	0.0000000e+000

Table A-7 20 kt Model A Matrix (cont.)

	9	10	11	12
1	0.0000000e+000	9.0442300e-004	-3.0992000e-005	-6.3172700e-002
2	0.0000000e+000	1.9754000e-002	0.0000000e+000	1.2432300e-004
3	0.0000000e+000	3.6122100e-004	-1.7383100e-005	1.8518500e-004
4	0.0000000e+000	-1.6750700e-003	0.0000000e+000	-7.6822400e-005
5	0.0000000e+000	-2.6202300e-005	0.0000000e+000	-1.0928500e-004
6	0.0000000e+000	-1.5412700e-002	0.0000000e+000	2.0647900e-004
7	0.0000000e+000	0.0000000e+000	0.0000000e+000	0.0000000e+000
8	0.0000000e+000	0.0000000e+000	0.0000000e+000	0.0000000e+000
9	0.0000000e+000	0.0000000e+000	0.0000000e+000	0.0000000e+000
10	0.0000000e+000	-2.0964800e+001	0.0000000e+000	-6.4668400e-001
11	0.0000000e+000	0.0000000e+000	-2.0913700e+001	0.0000000e+000
12	0.0000000e+000	-1.2915800e+000	-3.3959900e-005	-2.0987400e+001
13	0.0000000e+000	3.2333800e-001	-1.9674000e-005	-5.3992800e+001
14	0.0000000e+000	3.3198100e+000	-1.0996900e-004	2.8851400e-001
15	0.0000000e+000	-9.3096600e-005	3.3192600e+000	-1.0239900e-005
16	0.0000000e+000	5.8507000e-001	-2.0926400e-005	3.3391700e+000
17	0.0000000e+000	6.8765100e-001	2.0755800e-004	2.1266400e-002
18	0.0000000e+000	1.0000000e+000	0.0000000e+000	0.0000000e+000
19	0.0000000e+000	0.0000000e+000	1.0000000e+000	0.0000000e+000
20	0.0000000e+000	0.0000000e+000	0.0000000e+000	1.0000000e+000
21	0.0000000e+000	0.0000000e+000	0.0000000e+000	0.0000000e+000
22	0.0000000e+000	0.0000000e+000	0.0000000e+000	0.0000000e+000
23	0.0000000e+000	0.0000000e+000	0.0000000e+000	0.0000000e+000
24	0.0000000e+000	0.0000000e+000	0.0000000e+000	0.0000000e+000
25	0.0000000e+000	0.0000000e+000	0.0000000e+000	0.0000000e+000
26	0.0000000e+000	-1.5141400e+000	0.0000000e+000	-5.1424100e-002
27	0.0000000e+000	-1.7784800e-001	0.0000000e+000	-2.6759000e+000
28	0.0000000e+000	1.9774300e-002	0.0000000e+000	-2.3438200e-001

Table A-7 20 kt Model A Matrix (cont.)

	13	14	15	16
1	2.7943100e-003	2.9542800e-002	-1.0379700e-002	9.0061900e+000
2	-8.7658700e-003	-1.5014500e-002	3.2271300e-003	8.1951100e-002
3	-6.6793500e-004	-4.7671400e-001	8.0203800e-003	2.1406600e-001
4	4.2859700e-004	3.9421100e-003	-5.8078300e-004	-2.0974100e-002
5	8.0039200e-005	-3.8570700e-003	0.0000000e+000	2.7003300e-001
6	-1.4904300e-004	-3.3961800e-002	-8.4555200e-005	-3.6246600e-003
7	0.0000000e+000	0.0000000e+000	0.0000000e+000	0.0000000e+000
8	0.0000000e+000	0.0000000e+000	0.0000000e+000	0.0000000e+000
9	0.0000000e+000	0.0000000e+000	0.0000000e+000	0.0000000e+000
10	1.5064500e-001	1.5866500e+000	-4.9462200e-003	-2.0111000e-001
11	0.0000000e+000	-4.5755000e-003	1.6982700e+000	-4.9464100e-003
12	5.4003100e+001	-4.1229500e-001	-2.0343500e-002	1.1342400e+001
13	-2.0918300e+001	8.3892000e-001	4.5460900e-003	-8.8425900e-001
14	3.4379000e-001	-3.9212300e+000	5.4330400e-002	-4.3679000e-001
15	9.5793700e-005	4.5185900e-002	-3.4091300e+000	5.0936300e-002
16	-7.4010200e-003	-3.3047900e-001	1.0529700e-001	-1.9737500e+000
17	3.3013000e+000	5.3933900e-001	2.3623700e-004	-5.6875800e+001
18	0.0000000e+000	0.0000000e+000	0.0000000e+000	0.0000000e+000
19	0.0000000e+000	0.0000000e+000	0.0000000e+000	0.0000000e+000
20	0.0000000e+000	0.0000000e+000	0.0000000e+000	0.0000000e+000
21	1.0000000e+000	0.0000000e+000	0.0000000e+000	0.0000000e+000
22	0.0000000e+000	1.0000000e+000	0.0000000e+000	0.0000000e+000
23	0.0000000e+000	0.0000000e+000	1.0000000e+000	0.0000000e+000
24	0.0000000e+000	0.0000000e+000	0.0000000e+000	1.0000000e+000
25	0.0000000e+000	0.0000000e+000	0.0000000e+000	0.0000000e+000
26	1.1797900e-002	3.5046800e-001	0.0000000e+000	1.5975600e-003
27	2.3406800e-001	-6.4994000e-003	5.1223000e-004	-1.2545200e-001
28	-2.6785700e+000	1.0388900e-001	-1.3601000e-005	6.7686300e-002

Table A-7 20 kt Model A Matrix (cont.)

	17	18	19	20
1	-7.2725200e-002	-3.8463500e+000	6.8134600e-005	-5.3931300e+001
2	1.3515500e+000	5.8791300e+000	-3.4493500e-004	-5.5197100e-001
3	1.2481900e-001	6.6753300e-002	-2.3807800e-003	-7.2749900e-001
4	-3.1978200e-001	4.9616700e-001	3.2997500e-005	7.7673900e-002
5	-2.6800300e-003	-9.7728100e-002	-2.7263300e-005	-5.3614300e-001
6	-1.5592100e-002	-9.2665700e+000	1.6212100e-005	1.9669400e-002
7	0.0000000e+000	0.0000000e+000	0.0000000e+000	0.0000000e+000
8	0.0000000e+000	0.0000000e+000	0.0000000e+000	0.0000000e+000
9	0.0000000e+000	0.0000000e+000	0.0000000e+000	0.0000000e+000
10	3.6617600e-001	-7.8829900e+002	1.2814100e-003	1.4694900e+000
11	0.0000000e+000	1.2189300e-003	-7.5758200e+002	-1.1518400e-004
12	-5.0054800e-002	-3.9379400e+000	1.7046200e-004	-9.0240500e+001
13	3.4085900e+000	-2.8386500e+001	-1.0024200e-003	-5.6915000e+002
14	3.9561700e-001	-2.1701800e-001	-1.5899100e-002	1.3159100e+001
15	-1.4212300e-003	-1.3347600e-002	-5.2551000e-001	-1.3740200e-004
16	5.6949900e+001	4.8977900e+000	-5.6611300e-003	1.1015800e+000
17	-5.2650200e+000	1.2386700e+001	5.7655800e-003	1.1230800e+002
18	0.0000000e+000	0.0000000e+000	0.0000000e+000	0.0000000e+000
19	0.0000000e+000	0.0000000e+000	0.0000000e+000	0.0000000e+000
20	0.0000000e+000	0.0000000e+000	0.0000000e+000	0.0000000e+000
21	0.0000000e+000	0.0000000e+000	0.0000000e+000	0.0000000e+000
22	0.0000000e+000	0.0000000e+000	0.0000000e+000	0.0000000e+000
23	0.0000000e+000	0.0000000e+000	0.0000000e+000	0.0000000e+000
24	0.0000000e+000	0.0000000e+000	0.0000000e+000	0.0000000e+000
25	1.0000000e+000	0.0000000e+000	0.0000000e+000	0.0000000e+000
26	2.8707900e-002	1.3124800e+000	0.0000000e+000	7.9283000e-002
27	-3.9585000e-002	5.3767000e-001	4.0973600e-005	1.1915800e+001
28	5.6425800e-001	-4.8387200e+000	0.0000000e+000	-7.2755200e+001

Table A-7 20 kt Model A Matrix (cont.)

	21	22	23	24
1	3.7581600e+000	3.9020000e+000	-4.8648300e-004	1.1630700e+001
2	-7.3769500e+000	-3.5901600e-001	3.0007100e-004	1.8054700e+001
3	-2.9974800e-001	-9.1160300e+000	2.1473600e-003	2.8003400e+000
4	7.2936500e-001	-1.4359800e-002	-3.0732500e-005	-4.1661100e+000
5	6.6246300e-002	-6.8350900e-003	1.5287300e-005	3.3300000e-001
6	4.7509700e-002	-7.6125700e-003	-1.4771100e-005	-1.8667200e-001
7	0.0000000e+000	0.0000000e+000	0.0000000e+000	0.0000000e+000
8	0.0000000e+000	0.0000000e+000	0.0000000e+000	0.0000000e+000
9	0.0000000e+000	0.0000000e+000	0.0000000e+000	0.0000000e+000
10	-1.0419100e+000	4.0674900e+000	-1.1635800e-003	2.0568300e+001
11	-3.3299700e-004	-1.1063100e-003	4.0735200e+000	-2.8740900e-004
12	5.7571900e+002	2.3170600e+001	-7.0043200e-004	1.5626400e+001
13	-3.9663800e+001	6.0679400e+000	7.4335800e-004	6.9885100e+001
14	-2.7625600e+000	-6.2389600e+001	1.4418200e-002	9.0375900e+000
15	3.0387000e-003	1.2092700e-002	-5.2415600e+001	-3.4826900e-002
16	-9.5859000e+001	-5.4029100e-001	5.4654900e-003	7.3406700e+002
17	-1.3776200e+000	-1.6933200e+000	-3.1609500e-003	-1.4663800e+002
18	0.0000000e+000	0.0000000e+000	0.0000000e+000	0.0000000e+000
19	0.0000000e+000	0.0000000e+000	0.0000000e+000	0.0000000e+000
20	0.0000000e+000	0.0000000e+000	0.0000000e+000	0.0000000e+000
21	0.0000000e+000	0.0000000e+000	0.0000000e+000	0.0000000e+000
22	0.0000000e+000	0.0000000e+000	0.0000000e+000	0.0000000e+000
23	0.0000000e+000	0.0000000e+000	0.0000000e+000	0.0000000e+000
24	0.0000000e+000	0.0000000e+000	0.0000000e+000	0.0000000e+000
25	0.0000000e+000	0.0000000e+000	0.0000000e+000	0.0000000e+000
26	-2.2875100e+000	3.5745400e-001	0.0000000e+000	1.4845500e+000
27	7.2144600e+001	2.2547000e+000	0.0000000e+000	-1.0402100e+000
28	5.3453100e+000	1.0154600e+000	0.0000000e+000	9.9565200e+000

Table A-7 20 kt Model A Matrix (conc.)

	25	26	27	28
1	-1.0880700e+002	7.4637100e-002	-1.3032300e-001	-1.1439100e-002
2	-1.7006700e-001	-1.6904500e-002	1.0452000e-003	-1.7608800e-002
3	-2.1438700e+000	-2.9174400e-003	-6.3432600e-004	-4.8895500e-004
4	1.1420200e-001	-2.3882900e-003	-6.7132200e-005	7.5652200e-004
5	-3.2992200e+000	9.4219400e-004	-3.0076400e-004	1.8752100e-005
6	6.8361200e-002	3.0408500e-002	7.4399000e-004	-6.4699300e-005
7	0.0000000e+000	0.0000000e+000	0.0000000e+000	0.0000000e+000
8	0.0000000e+000	0.0000000e+000	0.0000000e+000	0.0000000e+000
9	0.0000000e+000	0.0000000e+000	0.0000000e+000	0.0000000e+000
10	8.9701700e+000	-6.4293400e+001	-1.5376800e+000	1.3967700e-001
11	1.3370000e-001	0.0000000e+000	0.0000000e+000	0.0000000e+000
12	-1.5961600e+002	-4.3234900e+000	-4.7485800e+001	-4.1940900e+000
13	1.7371300e+001	8.7987700e-001	4.1928400e+000	-4.7345400e+001
14	7.7010100e+000	1.1027200e+000	1.2158400e-001	9.0241600e-001
15	-1.3763900e+000	0.0000000e+000	0.0000000e+000	0.0000000e+000
16	4.9418900e+001	4.5048900e-001	8.1284800e-001	6.6123200e-002
17	6.9058000e+002	2.4047900e+000	-1.2293700e-002	7.7167700e-001
18	0.0000000e+000	0.0000000e+000	0.0000000e+000	0.0000000e+000
19	0.0000000e+000	0.0000000e+000	0.0000000e+000	0.0000000e+000
20	0.0000000e+000	0.0000000e+000	0.0000000e+000	0.0000000e+000
21	0.0000000e+000	0.0000000e+000	0.0000000e+000	0.0000000e+000
22	0.0000000e+000	0.0000000e+000	0.0000000e+000	0.0000000e+000
23	0.0000000e+000	0.0000000e+000	0.0000000e+000	0.0000000e+000
24	0.0000000e+000	0.0000000e+000	0.0000000e+000	0.0000000e+000
25	0.0000000e+000	0.0000000e+000	0.0000000e+000	0.0000000e+000
26	2.7724300e-001	-1.4493600e+001	-1.2513500e-001	-1.0845600e+000
27	-1.5125600e+000	-7.6445500e-001	-1.5816000e+001	-8.9318000e-003
28	-5.4408500e-001	2.4747200e+000	5.7361500e-004	-1.8589900e+001

Table A-8 20 kt Model B Matrix

	1	2	3	4
1	-2.4523310e+000	1.6619089e+001	9.4664442e+000	-5.1240372e+001
2	-9.2065093e-001	1.4166203e+000	-4.2250211e+000	1.2501061e+001
3	-2.0169079e-001	7.6747289e-001	-9.0466648e+000	3.0789041e+001
4	9.9535746e-002	-1.8219487e-001	-6.4458402e-002	1.8911911e-001
5	-7.0872401e-002	3.5591408e-001	2.7766929e-001	-1.2825103e+000
6	6.3849525e-003	-6.8020018e-002	4.7563209e-001	5.2928322e-001
7	0.0000000e+000	0.0000000e+000	0.0000000e+000	0.0000000e+000
8	0.0000000e+000	0.0000000e+000	0.0000000e+000	0.0000000e+000
9	0.0000000e+000	0.0000000e+000	0.0000000e+000	0.0000000e+000
10	-1.3511384e+000	1.0603951e+002	9.5561387e+002	-6.0188341e+001
11	-3.9572014e-002	-1.4784946e-002	1.3633268e-002	8.5157220e-003
12	-1.2295494e+002	1.7237557e+003	-1.3199912e+002	-1.0350369e+003
13	-9.6606833e+002	-2.0854473e+002	1.6860839e+002	1.3836840e+002
14	1.8272031e+001	-2.5819666e+000	-1.0181140e+002	3.7293885e+001
15	4.0791827e-001	1.2101203e-001	-1.3591362e-001	-6.9699576e-002
16	-6.0051321e-001	-1.3750479e+002	1.2723333e+001	8.5441028e+001
17	1.0880151e+002	-5.7937083e+001	-4.9804849e+001	4.9854107e+001
18	0.0000000e+000	0.0000000e+000	0.0000000e+000	0.0000000e+000
19	0.0000000e+000	0.0000000e+000	0.0000000e+000	0.0000000e+000
20	0.0000000e+000	0.0000000e+000	0.0000000e+000	0.0000000e+000
21	0.0000000e+000	0.0000000e+000	0.0000000e+000	0.0000000e+000
22	0.0000000e+000	0.0000000e+000	0.0000000e+000	0.0000000e+000
23	0.0000000e+000	0.0000000e+000	0.0000000e+000	0.0000000e+000
24	0.0000000e+000	0.0000000e+000	0.0000000e+000	0.0000000e+000
25	0.0000000e+000	0.0000000e+000	0.0000000e+000	0.0000000e+000
26	-1.4276980e-001	8.5799328e+000	6.9573218e+001	-4.9418103e+000
27	-5.0457843e+000	2.2004450e+002	-2.0064217e+001	-1.2404511e+002
28	-1.2482656e+002	-9.2325574e+000	2.1260469e+001	5.2461272e+000

Table A-9 20 kt Model C Matrix

	1	2	3	4
1	0.0000000e+000	0.0000000e+000	0.0000000e+000	0.0000000e+000
2	0.0000000e+000	0.0000000e+000	0.0000000e+000	-3.5785800e-002
3	0.0000000e+000	0.0000000e+000	0.0000000e+000	1.0002800e+000
4	0.0000000e+000	0.0000000e+000	4.2884200e-002	0.0000000e+000
5	0.0000000e+000	0.0000000e+000	3.5719900e-002	0.0000000e+000
6	0.0000000e+000	0.0000000e+000	-9.9844100e-001	0.0000000e+000
7	1.0000000e+000	0.0000000e+000	0.0000000e+000	0.0000000e+000
8	0.0000000e+000	1.0000000e+000	5.8922300e-001	0.0000000e+000
9	0.0000000e+000	0.0000000e+000	0.0000000e+000	0.0000000e+000
10	0.0000000e+000	0.0000000e+000	0.0000000e+000	0.0000000e+000
11	0.0000000e+000	0.0000000e+000	0.0000000e+000	0.0000000e+000
12	0.0000000e+000	0.0000000e+000	0.0000000e+000	0.0000000e+000
13	0.0000000e+000	0.0000000e+000	0.0000000e+000	0.0000000e+000
14	0.0000000e+000	0.0000000e+000	0.0000000e+000	0.0000000e+000
15	0.0000000e+000	0.0000000e+000	0.0000000e+000	0.0000000e+000
16	0.0000000e+000	0.0000000e+000	0.0000000e+000	0.0000000e+000
17	0.0000000e+000	0.0000000e+000	0.0000000e+000	0.0000000e+000
18	0.0000000e+000	0.0000000e+000	0.0000000e+000	0.0000000e+000
19	0.0000000e+000	0.0000000e+000	0.0000000e+000	0.0000000e+000
20	0.0000000e+000	0.0000000e+000	0.0000000e+000	0.0000000e+000
21	0.0000000e+000	0.0000000e+000	0.0000000e+000	0.0000000e+000
22	0.0000000e+000	0.0000000e+000	0.0000000e+000	0.0000000e+000
23	0.0000000e+000	0.0000000e+000	0.0000000e+000	0.0000000e+000
24	0.0000000e+000	0.0000000e+000	0.0000000e+000	0.0000000e+000
25	0.0000000e+000	0.0000000e+000	0.0000000e+000	0.0000000e+000
26	0.0000000e+000	0.0000000e+000	0.0000000e+000	0.0000000e+000
27	0.0000000e+000	0.0000000e+000	0.0000000e+000	0.0000000e+000
28	0.0000000e+000	0.0000000e+000	0.0000000e+000	0.0000000e+000

Table A-10 40 kt Model A Matrix

	1	2	3	4
1	-1.8362400e-001	-2.2543800e-001	7.3415100e-001	1.8243400e-001
2	8.9462000e-002	-1.1000300e-001	-1.7907800e-001	-3.4601100e-001
3	1.0293100e-001	-1.4180200e-001	-5.7335800e-001	-2.7386200e-001
4	-1.6157600e-002	-3.0960600e-002	-4.0876100e-003	-1.6030100e-002
5	2.6560800e-002	-1.2366200e-002	-1.1601200e+000	8.8174300e-003
6	-1.0052000e-003	1.1742000e+000	3.4909500e-002	-2.0616700e-002
7	1.0000000e+000	-6.7217700e-004	2.5693400e-002	0.0000000e+000
8	0.0000000e+000	9.9965800e-001	2.6152500e-002	0.0000000e+000
9	0.0000000e+000	-2.6161100e-002	9.9998800e-001	0.0000000e+000
10	1.6509200e+000	-9.8004600e-001	-8.7730100e-001	-3.2871200e+000
11	0.0000000e+000	0.0000000e+000	0.0000000e+000	0.0000000e+000
12	2.6577900e+001	-5.6857000e+001	2.4252900e+000	1.2713600e+001
13	5.6566000e+001	2.6685600e+001	1.6274800e+000	-4.6088000e+000
14	-7.6828300e-002	-3.9464900e-001	-6.5131700e-001	-2.4822500e-001
15	0.0000000e+000	0.0000000e+000	0.0000000e+000	0.0000000e+000
16	3.0694900e-002	6.4518200e-002	-1.0634900e-001	-1.0455800e+000
17	-4.2185300e-003	2.3716900e-001	-1.3863600e-001	1.1012600e-001
18	0.0000000e+000	0.0000000e+000	0.0000000e+000	0.0000000e+000
19	0.0000000e+000	0.0000000e+000	0.0000000e+000	0.0000000e+000
20	0.0000000e+000	0.0000000e+000	0.0000000e+000	0.0000000e+000
21	0.0000000e+000	0.0000000e+000	0.0000000e+000	0.0000000e+000
22	0.0000000e+000	0.0000000e+000	0.0000000e+000	0.0000000e+000
23	0.0000000e+000	0.0000000e+000	0.0000000e+000	0.0000000e+000
24	0.0000000e+000	0.0000000e+000	0.0000000e+000	0.0000000e+000
25	0.0000000e+000	0.0000000e+000	0.0000000e+000	0.0000000e+000
26	1.4695500e-001	1.2193000e-001	-3.3604400e-001	-2.7134700e+000
27	2.6514300e+000	-7.3184500e-002	1.0385100e-001	1.6391200e+000
28	8.1481900e-002	2.6591600e+000	-7.7762100e-002	1.1564400e+000

Table A-10 40 kt Model A Matrix (cont.)

	5	6	7	8
1	-1.1515900e+000	1.8874400e-001	0.0000000e+000	0.0000000e+000
2	2.5276000e-001	-8.1356200e-002	0.0000000e+000	0.0000000e+000
3	7.7799100e-001	-2.5912100e-001	0.0000000e+000	0.0000000e+000
4	1.9686400e-003	1.9225200e-003	0.0000000e+000	-5.6006600e-001
5	-6.0042800e-002	7.3434600e-003	5.5987400e-001	3.7646300e-004
6	1.0832400e-002	-6.4838200e-002	1.4647100e-002	-1.4390000e-002
7	0.0000000e+000	0.0000000e+000	0.0000000e+000	0.0000000e+000
8	0.0000000e+000	0.0000000e+000	0.0000000e+000	0.0000000e+000
9	0.0000000e+000	0.0000000e+000	0.0000000e+000	0.0000000e+000
10	1.5189500e+000	6.4354700e+001	0.0000000e+000	0.0000000e+000
11	0.0000000e+000	0.0000000e+000	0.0000000e+000	0.0000000e+000
12	3.4160500e+000	9.6943100e+000	0.0000000e+000	0.0000000e+000
13	1.3537800e+001	-1.4886700e+000	0.0000000e+000	0.0000000e+000
14	6.0972500e-001	-1.5401000e-001	0.0000000e+000	0.0000000e+000
15	0.0000000e+000	0.0000000e+000	0.0000000e+000	0.0000000e+000
16	5.4564400e-002	-1.0198400e+000	0.0000000e+000	0.0000000e+000
17	-5.0318300e-001	-2.5763500e+000	0.0000000e+000	0.0000000e+000
18	0.0000000e+000	0.0000000e+000	0.0000000e+000	0.0000000e+000
19	0.0000000e+000	0.0000000e+000	0.0000000e+000	0.0000000e+000
20	0.0000000e+000	0.0000000e+000	0.0000000e+000	0.0000000e+000
21	0.0000000e+000	0.0000000e+000	0.0000000e+000	0.0000000e+000
22	0.0000000e+000	0.0000000e+000	0.0000000e+000	0.0000000e+000
23	0.0000000e+000	0.0000000e+000	0.0000000e+000	0.0000000e+000
24	0.0000000e+000	0.0000000e+000	0.0000000e+000	0.0000000e+000
25	0.0000000e+000	0.0000000e+000	0.0000000e+000	0.0000000e+000
26	1.4393000e-001	7.0914700e+000	0.0000000e+000	0.0000000e+000
27	-2.3241100e+000	1.3398100e+000	-1.8604600e-001	0.0000000e+000
28	1.8195400e+000	5.3436500e+000	3.6538500e-003	0.0000000e+000

Table A-10 40 kt Model A Matrix (cont.)

	9	10	11	12
1	0.0000000e+000	6.7673400e-002	4.3005800e-004	-6.3048200e-002
2	0.0000000e+000	1.2854800e-002	3.2674400e-005	1.1876500e-003
3	0.0000000e+000	1.9274700e-004	-1.9926800e-004	8.2836500e-004
4	0.0000000e+000	2.2995500e-005	0.0000000e+000	-3.7519800e-004
5	0.0000000e+000	1.9066100e-003	1.0276400e-005	-1.1049800e-004
6	0.0000000e+000	-1.5258300e-002	0.0000000e+000	3.2843300e-004
7	0.0000000e+000	0.0000000e+000	0.0000000e+000	0.0000000e+000
8	0.0000000e+000	0.0000000e+000	0.0000000e+000	0.0000000e+000
9	0.0000000e+000	0.0000000e+000	0.0000000e+000	0.0000000e+000
10	0.0000000e+000	-2.1035500e+001	1.1396800e-004	-1.3079400e+000
11	0.0000000e+000	1.1153500e-004	-2.0985000e+001	-3.9409800e-005
12	0.0000000e+000	-2.5432000e+000	3.8046100e-004	-2.1057700e+001
13	0.0000000e+000	3.6166900e-001	1.9780800e-004	-5.3992700e+001
14	0.0000000e+000	2.8538800e+000	-1.4326100e-003	1.9669300e-001
15	0.0000000e+000	-1.1953800e-003	2.8570800e+000	4.2153600e-004
16	0.0000000e+000	3.8993200e-001	8.6081900e-004	2.9099100e+000
17	0.0000000e+000	3.4767100e-001	-2.2757100e-003	2.6370800e-002
18	0.0000000e+000	1.0000000e+000	0.0000000e+000	0.0000000e+000
19	0.0000000e+000	0.0000000e+000	1.0000000e+000	0.0000000e+000
20	0.0000000e+000	0.0000000e+000	0.0000000e+000	1.0000000e+000
21	0.0000000e+000	0.0000000e+000	0.0000000e+000	0.0000000e+000
22	0.0000000e+000	0.0000000e+000	0.0000000e+000	0.0000000e+000
23	0.0000000e+000	0.0000000e+000	0.0000000e+000	0.0000000e+000
24	0.0000000e+000	0.0000000e+000	0.0000000e+000	0.0000000e+000
25	0.0000000e+000	0.0000000e+000	0.0000000e+000	0.0000000e+000
26	0.0000000e+000	-1.5201000e+000	0.0000000e+000	-1.0392300e-001
27	0.0000000e+000	-3.5243800e-001	-1.5969200e-005	-2.6905100e+000
28	0.0000000e+000	1.8020500e-002	0.0000000e+000	-1.9197500e-001

Table A-10 40 kt Model A Matrix (cont.)

	13	14	15	16
1	4.5464200e-003	1.4325600e-001	5.3338700e-002	8.9448000e+000
2	-8.6611800e-003	3.0995000e-003	4.0782100e-003	4.9766400e-002
3	-1.7282900e-003	-4.7637000e-001	-2.2556900e-002	2.3982300e-001
4	4.1089700e-004	1.4079000e-003	-7.0338800e-004	-1.3692700e-002
5	1.2074000e-004	-4.1284300e-004	1.2881900e-003	2.6862700e-001
6	-5.2141500e-005	-3.4040600e-002	1.1699700e-004	-1.9529900e-003
7	0.0000000e+000	0.0000000e+000	0.0000000e+000	0.0000000e+000
8	0.0000000e+000	0.0000000e+000	0.0000000e+000	0.0000000e+000
9	0.0000000e+000	0.0000000e+000	0.0000000e+000	0.0000000e+000
10	1.7661000e-001	1.1772200e+000	1.3037000e-002	-1.0413000e-001
11	9.7362600e-005	1.2776600e-002	1.2894100e+000	-4.7481400e-003
12	5.4005300e+001	-8.4449100e-002	4.7600400e-002	1.0888900e+001
13	-2.0990300e+001	1.2169600e+000	2.4586200e-002	-7.4043500e-001
14	1.8771300e-001	-3.7932300e+000	-1.6316100e-001	-2.0882300e-001
15	-1.0456400e-003	-1.3604800e-001	-3.2756300e+000	5.0539800e-002
16	-1.9532900e-003	1.6891900e-002	1.0320800e-001	-2.1329300e+000
17	2.8063800e+000	-1.5168200e-001	-2.8480000e-001	-5.6460700e+001
18	0.0000000e+000	0.0000000e+000	0.0000000e+000	0.0000000e+000
19	0.0000000e+000	0.0000000e+000	0.0000000e+000	0.0000000e+000
20	0.0000000e+000	0.0000000e+000	0.0000000e+000	0.0000000e+000
21	1.0000000e+000	0.0000000e+000	0.0000000e+000	0.0000000e+000
22	0.0000000e+000	1.0000000e+000	0.0000000e+000	0.0000000e+000
23	0.0000000e+000	0.0000000e+000	1.0000000e+000	0.0000000e+000
24	0.0000000e+000	0.0000000e+000	0.0000000e+000	1.0000000e+000
25	0.0000000e+000	0.0000000e+000	0.0000000e+000	0.0000000e+000
26	1.3973700e-002	3.1860400e-001	0.0000000e+000	1.2424600e-004
27	1.9174700e-001	-2.7570700e-002	-1.9995400e-003	1.2018900e-001
28	-2.6911900e+000	1.0272900e-001	3.9269900e-005	4.6212700e-002

Table A-10 40 kt Model A Matrix (cont.)

	17	18	19	20
1	3.4879900e-002	-1.8258900e+000	9.0993100e-004	-5.3559100e+001
2	1.3496800e+000	6.2417200e+000	6.1291400e-004	-4.8323600e-001
3	7.0415000e-002	1.6595400e-001	-8.6520100e-004	-7.2074700e-001
4	-3.2195700e-001	4.0860900e-001	-1.1804300e-004	6.2745800e-002
5	4.5332300e-004	-3.2684400e-002	4.8486500e-005	-5.2452700e-001
6	-1.3497800e-002	-9.2773800e+000	0.0000000e+000	1.3819600e-002
7	0.0000000e+000	0.0000000e+000	0.0000000e+000	0.0000000e+000
8	0.0000000e+000	0.0000000e+000	0.0000000e+000	0.0000000e+000
9	0.0000000e+000	0.0000000e+000	0.0000000e+000	0.0000000e+000
10	5.5238800e-001	-7.8761200e+002	4.8027400e-004	2.2753400e+000
11	1.2088100e-002	4.9583000e-004	-7.5685500e+002	1.6404500e-003
12	4.6560700e-002	-1.8549800e+000	-9.7696000e-004	-8.8446300e+001
13	2.9706500e+000	-6.6326700e+001	1.8756900e-003	-5.7087800e+002
14	9.2290700e-003	8.5991900e-001	-6.2837400e-003	1.2863700e+001
15	-1.3089400e-001	-5.3169000e-003	5.8207300e-001	-1.8373900e-002
16	5.7323400e+001	1.3532500e+001	2.0301100e-002	1.8132000e+000
17	-4.8124300e+000	2.2653000e-001	-1.0835600e-002	9.9248200e+001
18	0.0000000e+000	0.0000000e+000	0.0000000e+000	0.0000000e+000
19	0.0000000e+000	0.0000000e+000	0.0000000e+000	0.0000000e+000
20	0.0000000e+000	0.0000000e+000	0.0000000e+000	0.0000000e+000
21	0.0000000e+000	0.0000000e+000	0.0000000e+000	0.0000000e+000
22	0.0000000e+000	0.0000000e+000	0.0000000e+000	0.0000000e+000
23	0.0000000e+000	0.0000000e+000	0.0000000e+000	0.0000000e+000
24	0.0000000e+000	0.0000000e+000	0.0000000e+000	0.0000000e+000
25	1.0000000e+000	0.0000000e+000	0.0000000e+000	0.0000000e+000
26	2.8154200e-002	1.4024500e+000	0.0000000e+000	1.8365500e-001
27	-3.0128500e-002	6.9160100e-001	-3.9682700e-005	9.3479100e+000
28	5.0734400e-001	-9.7064500e+000	0.0000000e+000	-7.3029600e+001

Table A-10 40 kt Model A Matrix (cont.)

	21	22	23	24
1	3.4221200e+000	3.9362800e+000	3.3194700e-004	1.1939300e+001
2	-7.3284000e+000	-3.7969600e-001	-4.4065100e-004	1.7961100e+001
3	-3.4630000e-001	-9.1276100e+000	3.6842000e-004	1.2534200e+000
4	7.1732100e-001	-1.1821900e-002	8.9150100e-005	-4.2154400e+000
5	5.5089500e-002	-4.3163900e-003	-1.4806400e-005	3.4049900e-001
6	4.3833300e-002	-7.0180500e-003	0.0000000e+000	-1.3004600e-001
7	0.0000000e+000	0.0000000e+000	0.0000000e+000	0.0000000e+000
8	0.0000000e+000	0.0000000e+000	0.0000000e+000	0.0000000e+000
9	0.0000000e+000	0.0000000e+000	0.0000000e+000	0.0000000e+000
10	-2.3915700e+000	5.2791600e+000	-2.1783000e-004	2.7684700e+001
11	1.6944300e-003	-2.3390000e-004	5.2820500e+000	3.2692600e-001
12	5.7214800e+002	2.7299500e+001	1.9056000e-003	1.6960200e+001
13	-3.7328100e+001	1.3172100e+001	-1.0257500e-003	5.8276300e+001
14	-5.9093100e+000	-6.2586200e+001	2.6410500e-003	-1.1429300e+000
15	-1.6565300e-002	2.2741900e-003	-5.2612700e+001	-3.5391500e+000
16	-8.2830900e+001	-3.4960300e-001	-1.5703300e-002	7.4413500e+002
17	-3.0458800e-001	-1.9849400e+000	3.3805000e-003	-1.3365600e+002
18	0.0000000e+000	0.0000000e+000	0.0000000e+000	0.0000000e+000
19	0.0000000e+000	0.0000000e+000	0.0000000e+000	0.0000000e+000
20	0.0000000e+000	0.0000000e+000	0.0000000e+000	0.0000000e+000
21	0.0000000e+000	0.0000000e+000	0.0000000e+000	0.0000000e+000
22	0.0000000e+000	0.0000000e+000	0.0000000e+000	0.0000000e+000
23	0.0000000e+000	0.0000000e+000	0.0000000e+000	0.0000000e+000
24	0.0000000e+000	0.0000000e+000	0.0000000e+000	0.0000000e+000
25	0.0000000e+000	0.0000000e+000	0.0000000e+000	0.0000000e+000
26	-2.6276900e+000	4.4784200e-001	0.0000000e+000	1.6353100e+000
27	7.2059200e+001	2.7557200e+000	0.0000000e+000	-1.4965500e-001
28	1.2945600e+000	1.9747700e+000	0.0000000e+000	8.6090500e+000

Table A-10 40 kt Model A Matrix (conc.)

	25	26	27	28
1	-1.0689700e+002	1.2957700e-001	-1.3004100e-001	-2.3600700e-002
2	3.5036300e-001	-1.5069000e-002	2.2018800e-003	-1.7358300e-002
3	-2.8387100e+000	2.0285600e-003	-8.9758600e-005	-9.8785700e-004
4	4.9200600e-003	-3.0257900e-003	-5.7191600e-004	7.1566100e-004
5	-3.2532300e+000	1.3472000e-003	-3.0115100e-004	-4.1101200e-004
6	1.5466900e-002	3.1129800e-002	1.5009400e-003	-1.3198800e-004
7	0.0000000e+000	0.0000000e+000	0.0000000e+000	0.0000000e+000
8	0.0000000e+000	0.0000000e+000	0.0000000e+000	0.0000000e+000
9	0.0000000e+000	0.0000000e+000	0.0000000e+000	0.0000000e+000
10	9.7128900e+000	-6.4541300e+001	-3.0695400e+000	1.4936800e-001
11	1.2789200e-001	0.0000000e+000	0.0000000e+000	0.0000000e+000
12	-1.4724700e+002	-8.7957400e+000	-4.7719000e+001	-3.4203800e+000
13	1.6783500e+001	1.1613800e+000	3.4002300e+000	-4.7580400e+001
14	1.8206600e+000	-1.3528400e-001	3.4016200e-001	9.2646000e-001
15	-1.3622500e+000	0.0000000e+000	0.0000000e+000	0.0000000e+000
16	5.4375400e+001	9.3870100e-001	5.3236600e-002	5.8184400e-003
17	6.7931600e+002	2.4556300e+000	6.4801000e-002	-5.4024300e-002
18	0.0000000e+000	0.0000000e+000	0.0000000e+000	0.0000000e+000
19	0.0000000e+000	0.0000000e+000	0.0000000e+000	0.0000000e+000
20	0.0000000e+000	0.0000000e+000	0.0000000e+000	0.0000000e+000
21	0.0000000e+000	0.0000000e+000	0.0000000e+000	0.0000000e+000
22	0.0000000e+000	0.0000000e+000	0.0000000e+000	0.0000000e+000
23	0.0000000e+000	0.0000000e+000	0.0000000e+000	0.0000000e+000
24	0.0000000e+000	0.0000000e+000	0.0000000e+000	0.0000000e+000
25	0.0000000e+000	0.0000000e+000	0.0000000e+000	0.0000000e+000
26	6.5430500e-001	-1.3391300e+001	-2.4904200e-001	-3.3759900e+000
27	-3.7341400e+000	-1.2771900e+000	-1.4601400e+001	-5.3579400e-003
28	-9.9417900e-002	1.2544500e+001	-6.7473200e-003	-2.2963800e+001

Table A-11 40 kt Model B Matrix

	1	2	3	4
1	-2.8642937e+000	1.4581876e+001	1.1545106e+001	-5.7125229e+001
2	-9.5051136e-001	1.2891848e+000	-4.7022775e+000	1.4393963e+001
3	1.5828826e-001	-7.8199390e-002	-1.0658744e+001	3.7056562e+001
4	1.1243252e-001	-1.8723584e-001	-7.4629772e-002	2.0579225e-001
5	-7.8663231e-002	3.0100414e-001	3.4025880e-001	-1.4490329e+000
6	4.8081226e-003	-1.1865391e-001	4.4773931e-001	6.4429648e-001
7	0.0000000e+000	0.0000000e+000	0.0000000e+000	0.0000000e+000
8	0.0000000e+000	0.0000000e+000	0.0000000e+000	0.0000000e+000
9	0.0000000e+000	0.0000000e+000	0.0000000e+000	0.0000000e+000
10	-7.0768768e+000	2.1439690e+002	9.4515494e+002	-1.2239074e+002
11	-6.2866438e-002	1.7567784e-001	-1.8147460e-002	-1.0118572e-001
12	-1.2432595e+002	1.7380381e+003	-9.7093712e+000	-1.0507508e+003
13	-9.6938279e+002	-2.1203974e+002	1.6240772e+002	1.4214980e+002
14	2.1196622e+001	-1.3646268e+001	-8.3894471e+001	5.0060672e+001
15	6.7189370e-001	-1.9011595e+000	1.9822052e-001	1.0950169e+000
16	-4.1598055e+000	-1.0171380e+002	6.5327238e-001	6.5334015e+001
17	9.1767148e+001	-5.1501677e+001	-4.8380317e+001	4.8996372e+001
18	0.0000000e+000	0.0000000e+000	0.0000000e+000	0.0000000e+000
19	0.0000000e+000	0.0000000e+000	0.0000000e+000	0.0000000e+000
20	0.0000000e+000	0.0000000e+000	0.0000000e+000	0.0000000e+000
21	0.0000000e+000	0.0000000e+000	0.0000000e+000	0.0000000e+000
22	0.0000000e+000	0.0000000e+000	0.0000000e+000	0.0000000e+000
23	0.0000000e+000	0.0000000e+000	0.0000000e+000	0.0000000e+000
24	0.0000000e+000	0.0000000e+000	0.0000000e+000	0.0000000e+000
25	0.0000000e+000	0.0000000e+000	0.0000000e+000	0.0000000e+000
26	-5.4809328e-001	1.7299403e+001	6.8784447e+001	-9.9639905e+000
27	-7.1903180e+000	2.2271390e+002	-3.9013445e+000	-1.2652655e+002
28	-1.2514994e+002	-1.2813219e+001	2.1775375e+001	7.3456581e+000

Table A-12 40 kt Model C Matrix

	1	2	3	4
1	0.0000000e+000	0.0000000e+000	0.0000000e+000	0.0000000e+000
2	0.0000000e+000	0.0000000e+000	0.0000000e+000	-2.6161100e-002
3	0.0000000e+000	0.0000000e+000	0.0000000e+000	9.9998800e-001
4	0.0000000e+000	0.0000000e+000	2.5693700e-002	0.0000000e+000
5	0.0000000e+000	0.0000000e+000	2.6143900e-002	0.0000000e+000
6	0.0000000e+000	0.0000000e+000	-9.9932800e-001	0.0000000e+000
7	1.0000000e+000	0.0000000e+000	0.0000000e+000	0.0000000e+000
8	0.0000000e+000	1.0000000e+000	1.1784500e+000	0.0000000e+000
9	0.0000000e+000	0.0000000e+000	0.0000000e+000	0.0000000e+000
10	0.0000000e+000	0.0000000e+000	0.0000000e+000	0.0000000e+000
11	0.0000000e+000	0.0000000e+000	0.0000000e+000	0.0000000e+000
12	0.0000000e+000	0.0000000e+000	0.0000000e+000	0.0000000e+000
13	0.0000000e+000	0.0000000e+000	0.0000000e+000	0.0000000e+000
14	0.0000000e+000	0.0000000e+000	0.0000000e+000	0.0000000e+000
15	0.0000000e+000	0.0000000e+000	0.0000000e+000	0.0000000e+000
16	0.0000000e+000	0.0000000e+000	0.0000000e+000	0.0000000e+000
17	0.0000000e+000	0.0000000e+000	0.0000000e+000	0.0000000e+000
18	0.0000000e+000	0.0000000e+000	0.0000000e+000	0.0000000e+000
19	0.0000000e+000	0.0000000e+000	0.0000000e+000	0.0000000e+000
20	0.0000000e+000	0.0000000e+000	0.0000000e+000	0.0000000e+000
21	0.0000000e+000	0.0000000e+000	0.0000000e+000	0.0000000e+000
22	0.0000000e+000	0.0000000e+000	0.0000000e+000	0.0000000e+000
23	0.0000000e+000	0.0000000e+000	0.0000000e+000	0.0000000e+000
24	0.0000000e+000	0.0000000e+000	0.0000000e+000	0.0000000e+000
25	0.0000000e+000	0.0000000e+000	0.0000000e+000	0.0000000e+000
26	0.0000000e+000	0.0000000e+000	0.0000000e+000	0.0000000e+000
27	0.0000000e+000	0.0000000e+000	0.0000000e+000	0.0000000e+000
28	0.0000000e+000	0.0000000e+000	0.0000000e+000	0.0000000e+000

Table A-13 60 kt Model A Matrix

	1	2	3	4
1	-2.2482500e-001	-1.5704300e-001	8.8321000e-001	-3.2155500e-002
2	1.9677800e-001	-3.9413600e-001	-2.3343200e-001	-6.5061700e-001
3	1.4699100e-001	-2.3175500e-001	-7.4416600e-001	-4.6406800e-002
4	-1.3535200e-002	-5.3982900e-002	2.1941000e-001	-2.1959700e-002
5	4.2053400e-002	-9.0597500e-003	-1.7278400e+000	-6.5362300e-003
6	-2.2220200e-001	1.7357200e+000	3.2224600e-002	-3.7817600e-002
7	1.0000000e+000	0.0000000e+000	2.6818300e-002	0.0000000e+000
8	0.0000000e+000	1.0000000e+000	0.0000000e+000	0.0000000e+000
9	0.0000000e+000	0.0000000e+000	1.0003600e+000	0.0000000e+000
10	2.3410100e+000	-6.2294600e-001	-6.3359500e-001	-3.9937500e+000
11	0.0000000e+000	0.0000000e+000	0.0000000e+000	0.0000000e+000
12	2.6057500e+001	-5.6997700e+001	2.9573100e+000	1.1336500e+001
13	5.6839600e+001	2.5886300e+001	1.9053700e+000	-4.7647400e+000
14	5.7358000e-002	-6.0049000e-001	-8.4707700e-001	2.6839100e-002
15	0.0000000e+000	0.0000000e+000	0.0000000e+000	0.0000000e+000
16	2.5574600e-001	-6.0495400e-002	-1.4012000e-001	-1.0036000e+000
17	-3.6293700e-002	4.7511800e-001	-2.3560600e-001	1.9086200e-001
18	0.0000000e+000	0.0000000e+000	0.0000000e+000	0.0000000e+000
19	0.0000000e+000	0.0000000e+000	0.0000000e+000	0.0000000e+000
20	0.0000000e+000	0.0000000e+000	0.0000000e+000	0.0000000e+000
21	0.0000000e+000	0.0000000e+000	0.0000000e+000	0.0000000e+000
22	0.0000000e+000	0.0000000e+000	0.0000000e+000	0.0000000e+000
23	0.0000000e+000	0.0000000e+000	0.0000000e+000	0.0000000e+000
24	0.0000000e+000	0.0000000e+000	0.0000000e+000	0.0000000e+000
25	0.0000000e+000	0.0000000e+000	0.0000000e+000	0.0000000e+000
26	1.8127700e-001	9.9954300e-002	-3.1870900e-001	-2.1203200e+000
27	2.7481500e+000	-7.8802300e-002	1.8572100e-001	1.6581100e+000
28	6.2037000e-002	2.7760000e+000	-6.9114900e-002	1.3169900e-001

Table A-13 60 kt Model A Matrix (cont.)

	5	6	7	8
1	-9.8313400e-001	-7.1250100e-002	0.0000000e+000	0.0000000e+000
2	1.0764100e+000	-3.5271700e-002	0.0000000e+000	0.0000000e+000
3	1.1041900e+000	6.5923400e-001	0.0000000e+000	0.0000000e+000
4	1.7959500e-002	9.5132300e-003	0.0000000e+000	-5.6004900e-001
5	-9.0844200e-002	-3.4134400e-002	5.6004900e-001	0.0000000e+000
6	3.9801100e-002	-7.9713800e-002	0.0000000e+000	-1.5019600e-002
7	0.0000000e+000	0.0000000e+000	0.0000000e+000	0.0000000e+000
8	0.0000000e+000	0.0000000e+000	0.0000000e+000	0.0000000e+000
9	0.0000000e+000	0.0000000e+000	0.0000000e+000	0.0000000e+000
10	1.5241200e+000	6.4395300e+001	0.0000000e+000	0.0000000e+000
11	0.0000000e+000	0.0000000e+000	0.0000000e+000	0.0000000e+000
12	3.4333000e+000	1.4092000e+001	0.0000000e+000	0.0000000e+000
13	1.3885300e+001	1.5112000e-001	0.0000000e+000	0.0000000e+000
14	1.0117800e+000	1.5797300e+000	0.0000000e+000	0.0000000e+000
15	0.0000000e+000	0.0000000e+000	0.0000000e+000	0.0000000e+000
16	3.7116500e-001	-5.3587000e-001	0.0000000e+000	0.0000000e+000
17	-3.5881000e-001	-2.3302000e+000	0.0000000e+000	0.0000000e+000
18	0.0000000e+000	0.0000000e+000	0.0000000e+000	0.0000000e+000
19	0.0000000e+000	0.0000000e+000	0.0000000e+000	0.0000000e+000
20	0.0000000e+000	0.0000000e+000	0.0000000e+000	0.0000000e+000
21	0.0000000e+000	0.0000000e+000	0.0000000e+000	0.0000000e+000
22	0.0000000e+000	0.0000000e+000	0.0000000e+000	0.0000000e+000
23	0.0000000e+000	0.0000000e+000	0.0000000e+000	0.0000000e+000
24	0.0000000e+000	0.0000000e+000	0.0000000e+000	0.0000000e+000
25	0.0000000e+000	0.0000000e+000	0.0000000e+000	0.0000000e+000
26	-7.9579300e-002	6.6175600e+000	0.0000000e+000	0.0000000e+000
27	-1.3440100e+000	1.3331500e+000	-1.0033600e-001	-1.2868200e-002
28	1.6251200e+000	4.7826400e+000	-1.0610300e-002	-1.3607800e-003

Table A-13 60 kt Model A Matrix (cont.)

	9	10	11	12
1	0.0000000e+000	-4.1242500e-002	1.2230300e-004	-7.3676600e-002
2	0.0000000e+000	-1.4752500e-001	3.5320400e-005	-1.4802600e-002
3	0.0000000e+000	-1.9445800e-003	0.0000000e+000	3.5552600e-004
4	0.0000000e+000	-3.2667800e-003	0.0000000e+000	-9.8647000e-004
5	0.0000000e+000	9.1033600e-004	0.0000000e+000	-2.0889200e-004
6	0.0000000e+000	-2.2748600e-002	0.0000000e+000	-1.4565900e-004
7	0.0000000e+000	0.0000000e+000	0.0000000e+000	0.0000000e+000
8	0.0000000e+000	0.0000000e+000	0.0000000e+000	0.0000000e+000
9	0.0000000e+000	0.0000000e+000	0.0000000e+000	0.0000000e+000
10	0.0000000e+000	-2.1085000e+001	0.0000000e+000	-2.0011400e+000
11	0.0000000e+000	0.0000000e+000	-2.1018200e+001	-4.1979900e-005
12	0.0000000e+000	-4.0576500e+000	5.2212100e-005	-2.1103100e+001
13	0.0000000e+000	-2.7436600e-001	1.0511900e-004	-5.4013900e+001
14	0.0000000e+000	2.5907800e+000	0.0000000e+000	1.2639900e-001
15	0.0000000e+000	0.0000000e+000	2.5906100e+000	4.9839600e-004
16	0.0000000e+000	2.0414300e-001	1.0257800e-003	2.6543900e+000
17	0.0000000e+000	6.1036500e-001	-9.9780100e-004	6.3411800e-002
18	0.0000000e+000	1.0000000e+000	0.0000000e+000	0.0000000e+000
19	0.0000000e+000	0.0000000e+000	1.0000000e+000	0.0000000e+000
20	0.0000000e+000	0.0000000e+000	0.0000000e+000	1.0000000e+000
21	0.0000000e+000	0.0000000e+000	0.0000000e+000	0.0000000e+000
22	0.0000000e+000	0.0000000e+000	0.0000000e+000	0.0000000e+000
23	0.0000000e+000	0.0000000e+000	0.0000000e+000	0.0000000e+000
24	0.0000000e+000	0.0000000e+000	0.0000000e+000	0.0000000e+000
25	0.0000000e+000	0.0000000e+000	0.0000000e+000	0.0000000e+000
26	0.0000000e+000	-1.5230300e+000	0.0000000e+000	-1.5894600e-001
27	0.0000000e+000	-5.2157100e-001	0.0000000e+000	-2.6970600e+000
28	0.0000000e+000	-5.0073700e-002	0.0000000e+000	-1.7047400e-001

Table A-13 60 kt Model A Matrix (cont.)

	13	14	15	16
1	5.7375800e-003	7.6455100e-002	2.2352500e-002	8.9828800e+000
2	-8.5714600e-003	1.6843600e-002	6.2688200e-003	-1.0768000e-003
3	-5.2040000e-004	-4.4087500e-001	7.6670800e-003	1.9121100e-001
4	2.5567300e-004	5.4378900e-003	-9.9310300e-004	-3.5230300e-003
5	1.8957500e-004	-2.7703400e-003	8.6531100e-004	2.6755000e-001
6	-1.0148200e-005	-3.2551900e-002	-7.2923200e-005	-1.9297500e-003
7	0.0000000e+000	0.0000000e+000	0.0000000e+000	0.0000000e+000
8	0.0000000e+000	0.0000000e+000	0.0000000e+000	0.0000000e+000
9	0.0000000e+000	0.0000000e+000	0.0000000e+000	0.0000000e+000
10	-5.8502100e-002	9.3625600e-001	-2.2928300e-003	-2.9046600e-001
11	3.6976200e-005	-1.8958300e-003	1.0447000e+000	-6.5931200e-003
12	5.4002600e+001	-5.2046100e-001	1.2091300e-002	1.0745500e+001
13	-2.1024000e+001	8.8427200e-001	1.8957800e-002	-7.3604100e-001
14	2.9675000e-001	-3.4589800e+000	4.4693300e-002	-5.2497600e-001
15	-4.6762400e-004	3.7743200e-002	-2.9831400e+000	8.0872900e-002
16	3.1100500e-002	-4.7677600e-001	1.6654400e-001	-3.3724900e+000
17	2.5240500e+000	3.8477400e-001	-1.8800300e-001	-5.6167500e+001
18	0.0000000e+000	0.0000000e+000	0.0000000e+000	0.0000000e+000
19	0.0000000e+000	0.0000000e+000	0.0000000e+000	0.0000000e+000
20	0.0000000e+000	0.0000000e+000	0.0000000e+000	0.0000000e+000
21	1.0000000e+000	0.0000000e+000	0.0000000e+000	0.0000000e+000
22	0.0000000e+000	1.0000000e+000	0.0000000e+000	0.0000000e+000
23	0.0000000e+000	0.0000000e+000	1.0000000e+000	0.0000000e+000
24	0.0000000e+000	0.0000000e+000	0.0000000e+000	1.0000000e+000
25	0.0000000e+000	0.0000000e+000	0.0000000e+000	0.0000000e+000
26	-4.5901300e-003	3.0085200e-001	0.0000000e+000	-1.1315800e-002
27	1.6970500e-001	-7.5203200e-002	-6.0869200e-004	2.5564100e-001
28	-2.6970800e+000	8.8717200e-002	-6.4367500e-005	1.0122300e-002

Table A-13 60 kt Model A Matrix (cont.)

	17	18	19	20
1	-2.5172900e-001	-2.2362600e+000	2.9574700e-003	-5.3519200e+001
2	1.3453900e+000	6.1122900e+000	5.7158800e-004	-6.0143300e-001
3	1.0660800e-001	1.5472800e-001	2.1899100e-004	-6.9890500e-001
4	-3.2278500e-001	4.7291400e-001	-8.8681800e-005	5.1987700e-002
5	-5.8192600e-003	-4.0370500e-002	1.0599600e-004	-5.2104800e-001
6	-1.5126100e-002	-9.2710700e+000	0.0000000e+000	-1.9409000e-003
7	0.0000000e+000	0.0000000e+000	0.0000000e+000	0.0000000e+000
8	0.0000000e+000	0.0000000e+000	0.0000000e+000	0.0000000e+000
9	0.0000000e+000	0.0000000e+000	0.0000000e+000	0.0000000e+000
10	3.7379400e-001	-7.8737000e+002	1.8462300e-005	3.5661400e+000
11	6.7478200e-003	4.6374500e-005	-7.5662700e+002	1.3447400e-004
12	-2.9792300e-001	1.1505500e+001	1.5507900e-003	-8.6431400e+001
13	2.6767500e+000	-1.0510600e+002	2.1263100e-003	-5.7404700e+002
14	3.1552600e-001	1.7069900e+000	6.4449800e-004	1.2817000e+001
15	-8.8018800e-002	5.7613100e-004	1.4171100e+000	-5.6079300e-003
16	5.7619800e+001	7.2705600e+000	1.4438200e-002	2.5132000e+000
17	-2.8630200e+000	-9.5451800e-001	-2.2700100e-002	9.2203700e+001
18	0.0000000e+000	0.0000000e+000	0.0000000e+000	0.0000000e+000
19	0.0000000e+000	0.0000000e+000	0.0000000e+000	0.0000000e+000
20	0.0000000e+000	0.0000000e+000	0.0000000e+000	0.0000000e+000
21	0.0000000e+000	0.0000000e+000	0.0000000e+000	0.0000000e+000
22	0.0000000e+000	0.0000000e+000	0.0000000e+000	0.0000000e+000
23	0.0000000e+000	0.0000000e+000	0.0000000e+000	0.0000000e+000
24	0.0000000e+000	0.0000000e+000	0.0000000e+000	0.0000000e+000
25	1.0000000e+000	0.0000000e+000	0.0000000e+000	0.0000000e+000
26	2.5797400e-002	1.4409900e+000	0.0000000e+000	6.7343100e-001
27	-2.8657700e-002	2.8004600e+000	-7.4586300e-005	8.0593100e+000
28	4.8029000e-001	-1.4515400e+001	0.0000000e+000	-7.2283600e+001

Table A-13 60 kt Model A Matrix (cont.)

	21	22	23	24
1	3.2278200e+000	3.7821300e+000	-1.9759000e-003	2.8883400e+000
2	-7.3904100e+000	-3.2717600e-001	-4.2767500e-004	1.7898600e+001
3	-2.7288800e-001	-9.1394500e+000	0.0000000e+000	2.1910000e+000
4	7.0777000e-001	-1.0198300e-002	6.9471600e-005	-4.2318900e+000
5	4.8900100e-002	-6.6626300e-003	-7.1962400e-005	1.3111100e-001
6	4.1672500e-002	-4.3424300e-003	0.0000000e+000	-1.7011900e-001
7	0.0000000e+000	0.0000000e+000	0.0000000e+000	0.0000000e+000
8	0.0000000e+000	0.0000000e+000	0.0000000e+000	0.0000000e+000
9	0.0000000e+000	0.0000000e+000	0.0000000e+000	0.0000000e+000
10	-2.9775100e+000	6.3316300e+000	-1.1341700e-004	2.1034500e+001
11	1.9767800e-003	-1.3041900e-004	6.3291700e+000	1.8277500e-001
12	5.6776500e+002	2.3552500e+001	-8.8477200e-004	7.5548800e+000
13	-3.7652700e+001	2.3408900e+001	-1.5317700e-003	5.0327500e+001
14	-4.6105800e+000	-6.2661800e+001	5.2520800e-004	7.3603600e+000
15	-2.4064900e-002	4.2248800e-004	-5.2674900e+001	-2.3811500e+000
16	-7.5008000e+001	1.0514900e-001	-1.1442800e-002	7.5225700e+002
17	4.3488300e-001	-2.3875300e+000	1.5459900e-002	-8.0513300e+001
18	0.0000000e+000	0.0000000e+000	0.0000000e+000	0.0000000e+000
19	0.0000000e+000	0.0000000e+000	0.0000000e+000	0.0000000e+000
20	0.0000000e+000	0.0000000e+000	0.0000000e+000	0.0000000e+000
21	0.0000000e+000	0.0000000e+000	0.0000000e+000	0.0000000e+000
22	0.0000000e+000	0.0000000e+000	0.0000000e+000	0.0000000e+000
23	0.0000000e+000	0.0000000e+000	0.0000000e+000	0.0000000e+000
24	0.0000000e+000	0.0000000e+000	0.0000000e+000	0.0000000e+000
25	0.0000000e+000	0.0000000e+000	0.0000000e+000	0.0000000e+000
26	-2.9386200e+000	5.2805900e-001	0.0000000e+000	1.4292000e+000
27	7.2753800e+001	2.3102200e+000	4.9874400e-005	3.2803300e-001
28	-1.1125400e+000	3.2300200e+000	0.0000000e+000	8.0131100e+000

Table A-13 60 kt Model A Matrix (conc.)

	25	26	27	28
1	-1.0778300e+002	4.2062000e-001	-1.4697000e-001	-3.2181700e-002
2	1.6633400e+000	-6.0614400e-001	-3.6099300e-002	-2.1089800e-002
3	-1.5400000e+000	-1.0115300e+000	-1.5289500e-005	-1.2785700e-003
4	-2.2237900e-001	-2.3453600e-002	-1.6725500e-003	5.8789700e-004
5	-3.2206500e+000	4.5499200e-002	-2.5531300e-004	-6.4724300e-004
6	1.2641200e-002	5.1189800e-003	4.4582300e-004	-3.5726600e-005
7	0.0000000e+000	0.0000000e+000	0.0000000e+000	0.0000000e+000
8	0.0000000e+000	0.0000000e+000	0.0000000e+000	0.0000000e+000
9	0.0000000e+000	0.0000000e+000	0.0000000e+000	0.0000000e+000
10	1.9740400e+001	-6.4720500e+001	-4.5827600e+000	-4.4978300e-001
11	1.7743800e-001	0.0000000e+000	0.0000000e+000	0.0000000e+000
12	-1.4347200e+002	-1.3194900e+001	-4.7848100e+001	-3.0299200e+000
13	1.8814700e+001	-1.0716700e+000	2.9462900e+000	-4.7698400e+001
14	9.8238500e+000	-1.9713300e+000	2.0462500e-001	8.8188500e-001
15	-2.1764900e+000	0.0000000e+000	0.0000000e+000	0.0000000e+000
16	8.8321300e+001	3.0242900e-001	-4.2920300e-001	2.1241700e-002
17	6.7135200e+002	2.2042400e+000	1.4600700e-001	-5.3239500e-001
18	0.0000000e+000	0.0000000e+000	0.0000000e+000	0.0000000e+000
19	0.0000000e+000	0.0000000e+000	0.0000000e+000	0.0000000e+000
20	0.0000000e+000	0.0000000e+000	0.0000000e+000	0.0000000e+000
21	0.0000000e+000	0.0000000e+000	0.0000000e+000	0.0000000e+000
22	0.0000000e+000	0.0000000e+000	0.0000000e+000	0.0000000e+000
23	0.0000000e+000	0.0000000e+000	0.0000000e+000	0.0000000e+000
24	0.0000000e+000	0.0000000e+000	0.0000000e+000	0.0000000e+000
25	0.0000000e+000	0.0000000e+000	0.0000000e+000	0.0000000e+000
26	1.4163900e+000	-1.2689200e+001	4.6075200e-001	-6.5010700e+000
27	-4.8169900e+000	-5.3374900e+000	-1.6495100e+001	1.9754900e+000
28	5.4799900e-001	2.7009900e+001	1.9687000e+000	-3.1628200e+001

Table A-14 60 kt Model B Matrix

	1	2	3	4
1	-2.0858308e+000	9.7775454e+000	1.6829749e+001	-6.0455333e+001
2	-1.5041777e+000	3.7418950e+000	1.9455077e+000	1.5289453e+001
3	-1.6793716e-001	3.9015857e-001	-1.2123332e+001	4.1894126e+001
4	1.5779595e-001	-1.1365491e-001	5.4525074e-002	1.8610900e-001
5	-7.1299448e-002	1.5531167e-001	3.9413633e-001	-1.5443868e+000
6	6.4958910e-003	-4.6413158e-002	7.4249685e-001	6.9698409e-001
7	0.0000000e+000	0.0000000e+000	0.0000000e+000	0.0000000e+000
8	0.0000000e+000	0.0000000e+000	0.0000000e+000	0.0000000e+000
9	0.0000000e+000	0.0000000e+000	0.0000000e+000	0.0000000e+000
10	-3.6420484e+001	3.1833491e+002	9.4401964e+002	-1.8204003e+002
11	-6.3190429e-002	6.7873780e-002	-1.3198561e-003	-3.9093484e-002
12	-1.2730800e+002	1.7605643e+003	1.1755798e+002	-1.0700698e+003
13	-9.7518336e+002	-2.1006599e+002	2.1147604e+002	1.4347217e+002
14	1.7980676e+001	-2.5686487e+000	-7.5942213e+001	4.9572438e+001
15	7.7272781e-001	-8.9348189e-001	3.0510891e-002	5.1462169e-001
16	-1.4447435e+001	-7.8935637e+001	8.3106992e+000	5.2969670e+001
17	8.0726062e+001	-2.4669432e+001	-5.0880458e+001	3.5985967e+001
18	0.0000000e+000	0.0000000e+000	0.0000000e+000	0.0000000e+000
19	0.0000000e+000	0.0000000e+000	0.0000000e+000	0.0000000e+000
20	0.0000000e+000	0.0000000e+000	0.0000000e+000	0.0000000e+000
21	0.0000000e+000	0.0000000e+000	0.0000000e+000	0.0000000e+000
22	0.0000000e+000	0.0000000e+000	0.0000000e+000	0.0000000e+000
23	0.0000000e+000	0.0000000e+000	0.0000000e+000	0.0000000e+000
24	0.0000000e+000	0.0000000e+000	0.0000000e+000	0.0000000e+000
25	0.0000000e+000	0.0000000e+000	0.0000000e+000	0.0000000e+000
26	-2.8968327e+000	2.5641553e+001	6.8768486e+001	-1.4768845e+001
27	-8.7949109e+000	2.2652702e+002	1.1528252e+001	-1.2944567e+002
28	-1.2581631e+002	-1.4203529e+001	2.8121207e+001	8.2895081e+000

Table A-15 60 kt Model C Matrix

	1	2	3	4
1	0.0000000e+000	0.0000000e+000	0.0000000e+000	0.0000000e+000
2	0.0000000e+000	0.0000000e+000	0.0000000e+000	0.0000000e+000
3	0.0000000e+000	0.0000000e+000	0.0000000e+000	1.0003600e+000
4	0.0000000e+000	0.0000000e+000	2.6808700e-002	0.0000000e+000
5	0.0000000e+000	0.0000000e+000	0.0000000e+000	0.0000000e+000
6	0.0000000e+000	0.0000000e+000	-9.9964100e-001	0.0000000e+000
7	1.0000000e+000	0.0000000e+000	-2.2470300e-001	0.0000000e+000
8	0.0000000e+000	1.0000000e+000	1.7533200e+000	0.0000000e+000
9	0.0000000e+000	0.0000000e+000	0.0000000e+000	0.0000000e+000
10	0.0000000e+000	0.0000000e+000	0.0000000e+000	0.0000000e+000
11	0.0000000e+000	0.0000000e+000	0.0000000e+000	0.0000000e+000
12	0.0000000e+000	0.0000000e+000	0.0000000e+000	0.0000000e+000
13	0.0000000e+000	0.0000000e+000	0.0000000e+000	0.0000000e+000
14	0.0000000e+000	0.0000000e+000	0.0000000e+000	0.0000000e+000
15	0.0000000e+000	0.0000000e+000	0.0000000e+000	0.0000000e+000
16	0.0000000e+000	0.0000000e+000	0.0000000e+000	0.0000000e+000
17	0.0000000e+000	0.0000000e+000	0.0000000e+000	0.0000000e+000
18	0.0000000e+000	0.0000000e+000	0.0000000e+000	0.0000000e+000
19	0.0000000e+000	0.0000000e+000	0.0000000e+000	0.0000000e+000
20	0.0000000e+000	0.0000000e+000	0.0000000e+000	0.0000000e+000
21	0.0000000e+000	0.0000000e+000	0.0000000e+000	0.0000000e+000
22	0.0000000e+000	0.0000000e+000	0.0000000e+000	0.0000000e+000
23	0.0000000e+000	0.0000000e+000	0.0000000e+000	0.0000000e+000
24	0.0000000e+000	0.0000000e+000	0.0000000e+000	0.0000000e+000
25	0.0000000e+000	0.0000000e+000	0.0000000e+000	0.0000000e+000
26	0.0000000e+000	0.0000000e+000	0.0000000e+000	0.0000000e+000
27	0.0000000e+000	0.0000000e+000	0.0000000e+000	0.0000000e+000
28	0.0000000e+000	0.0000000e+000	0.0000000e+000	0.0000000e+000

Table A-16 80 kt Model A Matrix

	1	2	3	4
1	-2.9464200e-001	-1.5355400e-001	1.0033400e+000	-4.4444900e-002
2	1.7640700e-001	-5.8232300e-001	-2.7216700e-001	-5.0189000e-001
3	1.9994400e-001	-2.5682300e-001	-8.7111900e-001	-7.8525900e-002
4	-1.3744200e-002	-4.4247100e-002	1.5585400e-001	-1.8276500e-002
5	3.1810600e-002	-8.7002200e-003	-2.3213400e+000	-3.0710100e-003
6	-1.6057800e-001	2.3253800e+000	3.0310800e-002	-3.3288100e-002
7	1.0000000e+000	0.0000000e+000	1.6429800e-002	0.0000000e+000
8	0.0000000e+000	1.0000000e+000	0.0000000e+000	0.0000000e+000
9	0.0000000e+000	0.0000000e+000	1.0001300e+000	0.0000000e+000
10	3.0682600e+000	-6.6535600e-001	-5.7356500e-001	-4.1506700e+000
11	0.0000000e+000	0.0000000e+000	0.0000000e+000	0.0000000e+000
12	2.5906900e+001	-5.7073900e+001	3.2048000e+000	1.0763900e+001
13	5.6854700e+001	2.5611800e+001	1.9281500e+000	-4.4439000e+000
14	9.9087800e-002	-6.1978000e-001	-9.9134300e-001	-1.6735300e-002
15	0.0000000e+000	0.0000000e+000	0.0000000e+000	0.0000000e+000
16	2.5146900e-001	-1.5109600e-001	-1.5648000e-001	-9.2256700e-001
17	-3.2718600e-002	5.8623800e-001	-2.9399700e-001	1.6313100e-001
18	0.0000000e+000	0.0000000e+000	0.0000000e+000	0.0000000e+000
19	0.0000000e+000	0.0000000e+000	0.0000000e+000	0.0000000e+000
20	0.0000000e+000	0.0000000e+000	0.0000000e+000	0.0000000e+000
21	0.0000000e+000	0.0000000e+000	0.0000000e+000	0.0000000e+000
22	0.0000000e+000	0.0000000e+000	0.0000000e+000	0.0000000e+000
23	0.0000000e+000	0.0000000e+000	0.0000000e+000	0.0000000e+000
24	0.0000000e+000	0.0000000e+000	0.0000000e+000	0.0000000e+000
25	0.0000000e+000	0.0000000e+000	0.0000000e+000	0.0000000e+000
26	2.5266700e-001	6.3239700e-002	-3.0854700e-001	-1.7129700e+000
27	2.7925900e+000	-8.3555800e-002	2.2312900e-001	1.4960000e+000
28	6.8063400e-002	2.8218200e+000	-6.3124100e-002	-1.6445600e-001

Table A-16 80 kt Model A Matrix (cont.)

	5	6	7	8
1	-1.2411500e+000	-3.4235800e-001	0.0000000e+000	0.0000000e+000
2	9.6946300e-001	-3.2411600e-001	0.0000000e+000	0.0000000e+000
3	1.3730300e+000	4.9462000e-001	0.0000000e+000	0.0000000e+000
4	1.2407700e-002	8.5653400e-003	0.0000000e+000	-5.6017500e-001
5	-1.1652800e-001	-2.6193800e-002	5.6017500e-001	0.0000000e+000
6	3.7915600e-002	-1.0819100e-001	0.0000000e+000	-9.2035900e-003
7	0.0000000e+000	0.0000000e+000	0.0000000e+000	0.0000000e+000
8	0.0000000e+000	0.0000000e+000	0.0000000e+000	0.0000000e+000
9	0.0000000e+000	0.0000000e+000	0.0000000e+000	0.0000000e+000
10	1.5493400e+000	6.4332200e+001	0.0000000e+000	0.0000000e+000
11	0.0000000e+000	0.0000000e+000	0.0000000e+000	0.0000000e+000
12	3.1443300e+000	1.8307200e+001	0.0000000e+000	0.0000000e+000
13	1.3787100e+001	-8.5527000e-001	0.0000000e+000	0.0000000e+000
14	1.3225300e+000	1.5885600e+000	0.0000000e+000	0.0000000e+000
15	0.0000000e+000	0.0000000e+000	0.0000000e+000	0.0000000e+000
16	3.6827200e-001	-8.1683000e-001	0.0000000e+000	0.0000000e+000
17	-1.7689800e-001	-2.0654000e+000	0.0000000e+000	0.0000000e+000
18	0.0000000e+000	0.0000000e+000	0.0000000e+000	0.0000000e+000
19	0.0000000e+000	0.0000000e+000	0.0000000e+000	0.0000000e+000
20	0.0000000e+000	0.0000000e+000	0.0000000e+000	0.0000000e+000
21	0.0000000e+000	0.0000000e+000	0.0000000e+000	0.0000000e+000
22	0.0000000e+000	0.0000000e+000	0.0000000e+000	0.0000000e+000
23	0.0000000e+000	0.0000000e+000	0.0000000e+000	0.0000000e+000
24	0.0000000e+000	0.0000000e+000	0.0000000e+000	0.0000000e+000
25	0.0000000e+000	0.0000000e+000	0.0000000e+000	0.0000000e+000
26	5.2378700e-002	6.3428500e+000	0.0000000e+000	0.0000000e+000
27	-8.8550900e-001	2.2421200e+000	-6.0669800e-002	-4.1774500e-003
28	1.6901900e+000	3.9342600e+000	-2.6128600e-003	-1.7990700e-004

Table A-16 80 kt Model A Matrix (cont.)

	9	10	11	12
1	0.0000000e+000	-1.8060500e-002	-6.0483500e-005	-7.3247400e-002
2	0.0000000e+000	-1.4018400e-001	-3.9186400e-005	-1.8493400e-002
3	0.0000000e+000	-4.7860000e-002	1.5634800e-004	-6.0126700e-003
4	0.0000000e+000	-1.7098800e-003	0.0000000e+000	-1.1617900e-003
5	0.0000000e+000	2.5661200e-003	0.0000000e+000	1.8438600e-005
6	0.0000000e+000	-2.2283100e-002	0.0000000e+000	-1.1108600e-004
7	0.0000000e+000	0.0000000e+000	0.0000000e+000	0.0000000e+000
8	0.0000000e+000	0.0000000e+000	0.0000000e+000	0.0000000e+000
9	0.0000000e+000	0.0000000e+000	0.0000000e+000	0.0000000e+000
10	0.0000000e+000	-2.1088900e+001	-8.4395800e-005	-2.6759200e+000
11	0.0000000e+000	-8.3153700e-005	-2.1023000e+001	7.1142000e-005
12	-1.0331300e-005	-5.3845300e+000	8.2718800e-005	-2.1108500e+001
13	0.0000000e+000	-5.7295000e-002	-9.3707100e-005	-5.4018300e+001
14	0.0000000e+000	2.4625100e+000	1.0823000e-003	1.3468200e-001
15	0.0000000e+000	9.1167900e-004	2.5126800e+000	-7.6683800e-004
16	0.0000000e+000	2.3116500e-001	-1.5767000e-003	2.6062400e+000
17	0.0000000e+000	5.8440200e-001	5.5532400e-004	7.9584900e-002
18	0.0000000e+000	1.0000000e+000	0.0000000e+000	0.0000000e+000
19	0.0000000e+000	0.0000000e+000	1.0000000e+000	0.0000000e+000
20	0.0000000e+000	0.0000000e+000	0.0000000e+000	1.0000000e+000
21	0.0000000e+000	0.0000000e+000	0.0000000e+000	0.0000000e+000
22	0.0000000e+000	0.0000000e+000	0.0000000e+000	0.0000000e+000
23	0.0000000e+000	0.0000000e+000	0.0000000e+000	0.0000000e+000
24	0.0000000e+000	0.0000000e+000	0.0000000e+000	0.0000000e+000
25	0.0000000e+000	0.0000000e+000	0.0000000e+000	0.0000000e+000
26	0.0000000e+000	-1.5235700e+000	0.0000000e+000	-2.1252900e-001
27	0.0000000e+000	-6.9740600e-001	0.0000000e+000	-2.6986100e+000
28	0.0000000e+000	-3.1160800e-002	0.0000000e+000	-1.6726300e-001

Table A-16 80 kt Model A Matrix (cont.)

	13	14	15	16
1	1.2509500e-002	4.9843100e-002	-4.7843000e-003	9.0295000e+000
2	-7.5131400e-003	1.5879300e-002	-4.9032800e-003	-1.2060200e-002
3	-7.8191800e-005	-4.1294500e-001	1.9986300e-002	1.9138100e-001
4	2.2785100e-004	5.1426800e-003	1.1576300e-003	-9.2389900e-004
5	3.8298900e-004	-3.2557800e-003	-2.3164400e-004	2.6823800e-001
6	0.0000000e+000	-3.2457800e-002	-6.7357200e-005	-2.1541200e-003
7	0.0000000e+000	0.0000000e+000	0.0000000e+000	0.0000000e+000
8	0.0000000e+000	0.0000000e+000	0.0000000e+000	0.0000000e+000
9	0.0000000e+000	0.0000000e+000	0.0000000e+000	0.0000000e+000
10	4.6881600e-002	9.0019400e-001	-1.0702400e-002	-3.6425000e-001
11	-2.6650100e-005	-1.0540600e-002	1.0081700e+000	9.0925400e-003
12	5.4009900e+001	-6.8854700e-001	1.3787600e-002	1.0730800e+001
13	-2.1027600e+001	8.2169000e-001	-1.0960900e-002	-7.1551200e-001
14	2.8926700e-001	-3.3074100e+000	1.3777200e-001	-5.2582200e-001
15	2.6646300e-004	1.1612400e-001	-2.8628700e+000	-9.8207700e-002
16	4.8039300e-002	-4.6604200e-001	-2.0195300e-001	-3.7529700e+000
17	2.4122000e+000	4.3506700e-001	5.5038200e-002	-5.6294500e+001
18	0.0000000e+000	0.0000000e+000	0.0000000e+000	0.0000000e+000
19	0.0000000e+000	0.0000000e+000	0.0000000e+000	0.0000000e+000
20	0.0000000e+000	0.0000000e+000	0.0000000e+000	0.0000000e+000
21	1.0000000e+000	0.0000000e+000	0.0000000e+000	0.0000000e+000
22	0.0000000e+000	1.0000000e+000	0.0000000e+000	0.0000000e+000
23	0.0000000e+000	0.0000000e+000	1.0000000e+000	0.0000000e+000
24	0.0000000e+000	0.0000000e+000	0.0000000e+000	1.0000000e+000
25	0.0000000e+000	0.0000000e+000	0.0000000e+000	0.0000000e+000
26	3.8081800e-003	2.9675500e-001	0.0000000e+000	-1.4697700e-002
27	1.6640400e-001	-9.7585100e-002	4.4174800e-005	3.2352800e-001
28	-2.6977000e+000	8.5646500e-002	0.0000000e+000	2.6598500e-002

Table A-16 80 kt Model A Matrix (cont.)

	17	18	19	20
1	-3.5199600e-001	-2.3059300e+000	-1.5442900e-004	-5.3430400e+001
2	1.3369600e+000	6.0600100e+000	-3.4807700e-004	-4.8546200e-001
3	1.0773700e-001	1.8663100e-001	3.5969200e-003	-7.0318200e-001
4	-3.2194200e-001	4.8131000e-001	1.0630400e-004	5.3492100e-002
5	-8.4767800e-003	-4.2049200e-002	0.0000000e+000	-5.1899000e-001
6	-1.5287200e-002	-9.2728100e+000	-1.8186500e-005	-6.0290000e-004
7	0.0000000e+000	0.0000000e+000	0.0000000e+000	0.0000000e+000
8	0.0000000e+000	0.0000000e+000	0.0000000e+000	0.0000000e+000
9	0.0000000e+000	0.0000000e+000	0.0000000e+000	0.0000000e+000
10	3.4228900e-001	-7.8731300e+002	-2.0300800e-003	4.3559800e+000
11	-2.8590900e-003	-1.9704900e-003	-7.5656500e+002	4.6372700e-004
12	-3.8717000e-001	6.7645200e+000	2.3838800e-003	-8.6629800e+001
13	2.6646900e+000	-1.4469900e+002	-8.8652700e-004	-5.7792200e+002
14	3.4184400e-001	2.2876800e+000	2.4449500e-002	1.1861100e+001
15	2.6754500e-002	2.0592800e-002	1.9623200e+000	-1.8244300e-003
16	5.7500600e+001	5.7739700e+000	-1.8525300e-002	3.2008900e+000
17	-2.2019500e+000	-3.2744500e+000	2.0969100e-003	9.0573300e+001
18	0.0000000e+000	0.0000000e+000	0.0000000e+000	0.0000000e+000
19	0.0000000e+000	0.0000000e+000	0.0000000e+000	0.0000000e+000
20	0.0000000e+000	0.0000000e+000	0.0000000e+000	0.0000000e+000
21	0.0000000e+000	0.0000000e+000	0.0000000e+000	0.0000000e+000
22	0.0000000e+000	0.0000000e+000	0.0000000e+000	0.0000000e+000
23	0.0000000e+000	0.0000000e+000	0.0000000e+000	0.0000000e+000
24	0.0000000e+000	0.0000000e+000	0.0000000e+000	0.0000000e+000
25	1.0000000e+000	0.0000000e+000	0.0000000e+000	0.0000000e+000
26	2.4634300e-002	1.4559100e+000	0.0000000e+000	6.1540100e-001
27	-2.0164600e-002	2.5264400e+000	0.0000000e+000	7.6103300e+000
28	4.8052000e-001	-1.9615100e+001	0.0000000e+000	-7.3304600e+001

Table A-16 80 kt Model A Matrix (cont.)

	21	22	23	24
1	3.3215100e+000	3.7151800e+000	0.0000000e+000	-5.5395400e-002
2	-7.3631300e+000	-3.3192100e-001	3.6080900e-004	1.7669300e+001
3	-3.0874600e-001	-9.1179100e+000	-2.6415100e-003	2.2375000e+000
4	7.0352200e-001	-9.9453200e-003	-9.8688300e-005	-4.2090800e+000
5	5.1593800e-002	-7.1547700e-003	0.0000000e+000	5.2085200e-002
6	4.2308500e-002	-4.4207900e-003	1.2946600e-005	-1.7864400e-001
7	0.0000000e+000	0.0000000e+000	0.0000000e+000	0.0000000e+000
8	0.0000000e+000	0.0000000e+000	0.0000000e+000	0.0000000e+000
9	0.0000000e+000	0.0000000e+000	0.0000000e+000	0.0000000e+000
10	-4.1611900e+000	7.3005400e+000	1.5407300e-003	2.0440100e+001
11	-2.1663600e-003	1.5000100e-003	7.2985000e+000	-7.8234600e-002
12	5.6245900e+002	2.4037000e+001	-2.1870300e-003	5.8421400e+000
13	-3.6615500e+001	2.9941700e+001	8.6145400e-004	4.9667200e+001
14	-6.2492900e+000	-6.2701000e+001	-1.7986900e-002	8.0878700e+000
15	2.1818900e-002	-1.5160700e-002	-5.2739100e+001	7.3089800e-001
16	-7.2171600e+001	6.0031000e-002	1.7255300e-002	7.4903200e+002
17	7.7346400e-001	-2.8585900e+000	-2.1844000e-003	-6.2575500e+001
18	0.0000000e+000	0.0000000e+000	0.0000000e+000	0.0000000e+000
19	0.0000000e+000	0.0000000e+000	0.0000000e+000	0.0000000e+000
20	0.0000000e+000	0.0000000e+000	0.0000000e+000	0.0000000e+000
21	0.0000000e+000	0.0000000e+000	0.0000000e+000	0.0000000e+000
22	0.0000000e+000	0.0000000e+000	0.0000000e+000	0.0000000e+000
23	0.0000000e+000	0.0000000e+000	0.0000000e+000	0.0000000e+000
24	0.0000000e+000	0.0000000e+000	0.0000000e+000	0.0000000e+000
25	0.0000000e+000	0.0000000e+000	0.0000000e+000	0.0000000e+000
26	-3.2101400e+000	6.0471400e-001	0.0000000e+000	1.4455200e+000
27	7.1636000e+001	2.3682500e+000	0.0000000e+000	6.5117700e-001
28	-2.0475200e+000	4.0927400e+000	0.0000000e+000	8.1344800e+000

Table A-16 80 kt Model A Matrix (conc.)

	25	26	27	28
1	-1.0905900e+002	6.9771600e-001	-1.4459400e-001	-3.2001200e-002
2	1.9645200e+000	-5.2691800e-001	-4.6916900e-002	-1.9346100e-002
3	-1.5045300e+000	-9.6814000e-001	-1.4521700e-002	-2.1796600e-003
4	-2.8571700e-001	-1.8348400e-002	-1.5555600e-003	6.0641300e-004
5	-3.2403700e+000	4.2630000e-002	3.3021000e-004	-6.5411100e-004
6	9.5374400e-003	8.6389400e-003	7.3107700e-004	-6.5031600e-005
7	0.0000000e+000	0.0000000e+000	0.0000000e+000	0.0000000e+000
8	0.0000000e+000	0.0000000e+000	0.0000000e+000	0.0000000e+000
9	0.0000000e+000	0.0000000e+000	0.0000000e+000	0.0000000e+000
10	2.4923900e+001	-6.4737000e+001	-6.1280300e+000	-2.8400100e-001
11	-2.4523000e-001	0.0000000e+000	0.0000000e+000	0.0000000e+000
12	-1.4346700e+002	-1.7429900e+001	-4.7864100e+001	-2.9673400e+000
13	1.9478700e+001	-2.7710300e-001	2.8703600e+000	-4.7714200e+001
14	9.5930700e+000	-2.1103600e+000	2.8879800e-001	8.0640300e-001
15	2.6500200e+000	0.0000000e+000	0.0000000e+000	0.0000000e+000
16	9.8665100e+001	4.9598900e-001	-5.2466700e-001	5.2495100e-002
17	6.7480000e+002	1.9329200e+000	1.8736700e-001	-6.7417800e-001
18	0.0000000e+000	0.0000000e+000	0.0000000e+000	0.0000000e+000
19	0.0000000e+000	0.0000000e+000	0.0000000e+000	0.0000000e+000
20	0.0000000e+000	0.0000000e+000	0.0000000e+000	0.0000000e+000
21	0.0000000e+000	0.0000000e+000	0.0000000e+000	0.0000000e+000
22	0.0000000e+000	0.0000000e+000	0.0000000e+000	0.0000000e+000
23	0.0000000e+000	0.0000000e+000	0.0000000e+000	0.0000000e+000
24	0.0000000e+000	0.0000000e+000	0.0000000e+000	0.0000000e+000
25	0.0000000e+000	0.0000000e+000	0.0000000e+000	0.0000000e+000
26	1.8258200e+000	-1.2512700e+001	1.6557000e-001	-9.5802900e+000
27	-5.4182400e+000	-5.3622800e+000	-1.8863000e+001	1.5672700e+000
28	4.7754200e-001	4.2383700e+001	1.5592200e+000	-4.1473000e+001

Table A-17 80 kt Model B Matrix

	1	2	3	4
1	-1.4871865e+000	7.6297185e+000	1.6974572e+001	-6.4110727e+001
2	-1.5229235e+000	4.3881270e+000	1.0770644e+000	1.6889703e+001
3	-1.5209174e-001	1.4525589e+000	-1.1295919e+001	4.5435384e+001
4	1.7628732e-001	-1.0514672e-001	-2.8119397e-002	2.0772573e-001
5	-5.8046148e-002	6.8891627e-002	3.5742485e-001	-1.6412217e+000
6	3.9805888e-003	-6.6338427e-002	6.7034539e-001	7.9384853e-001
7	0.0000000e+000	0.0000000e+000	0.0000000e+000	0.0000000e+000
8	0.0000000e+000	0.0000000e+000	0.0000000e+000	0.0000000e+000
9	0.0000000e+000	0.0000000e+000	0.0000000e+000	0.0000000e+000
10	-3.5551805e+001	4.2961224e+002	9.4017555e+002	-2.4594047e+002
11	8.8881679e-002	-2.3646099e-002	-1.4831136e-002	1.3619537e-002
12	-1.2918534e+002	1.7977624e+003	2.3597287e+002	-1.0964776e+003
13	-9.8198151e+002	-2.1384366e+002	1.9219848e+002	1.4801354e+002
14	1.7306701e+001	-3.5678396e+000	-7.2042776e+001	5.4872125e+001
15	-9.5384755e-001	2.1990050e-001	1.6874986e-001	-1.2665699e-001
16	-1.6720195e+001	-7.5928029e+001	5.4635235e+000	5.1973635e+001
17	7.6577781e+001	-1.7339474e+001	-4.8273242e+001	3.3690310e+001
18	0.0000000e+000	0.0000000e+000	0.0000000e+000	0.0000000e+000
19	0.0000000e+000	0.0000000e+000	0.0000000e+000	0.0000000e+000
20	0.0000000e+000	0.0000000e+000	0.0000000e+000	0.0000000e+000
21	0.0000000e+000	0.0000000e+000	0.0000000e+000	0.0000000e+000
22	0.0000000e+000	0.0000000e+000	0.0000000e+000	0.0000000e+000
23	0.0000000e+000	0.0000000e+000	0.0000000e+000	0.0000000e+000
24	0.0000000e+000	0.0000000e+000	0.0000000e+000	0.0000000e+000
25	0.0000000e+000	0.0000000e+000	0.0000000e+000	0.0000000e+000
26	-2.7967725e+000	3.4581691e+001	6.8658673e+001	-1.9918124e+001
27	-9.2822091e+000	2.3178472e+002	2.7062034e+001	-1.3281334e+002
28	-1.2672673e+002	-1.4654089e+001	2.6602389e+001	8.4699795e+000

Table A-18 80 kt Model C Matrix

	1	2	3	4
1	0.0000000e+000	0.0000000e+000	0.0000000e+000	0.0000000e+000
2	0.0000000e+000	0.0000000e+000	0.0000000e+000	0.0000000e+000
3	0.0000000e+000	0.0000000e+000	0.0000000e+000	1.0001300e+000
4	0.0000000e+000	0.0000000e+000	1.6427600e-002	0.0000000e+000
5	0.0000000e+000	0.0000000e+000	0.0000000e+000	0.0000000e+000
6	0.0000000e+000	0.0000000e+000	-9.9986500e-001	0.0000000e+000
7	1.0000000e+000	0.0000000e+000	-1.6185900e-001	0.0000000e+000
8	0.0000000e+000	1.0000000e+000	2.3513300e+000	0.0000000e+000
9	0.0000000e+000	0.0000000e+000	0.0000000e+000	0.0000000e+000
10	0.0000000e+000	0.0000000e+000	0.0000000e+000	0.0000000e+000
11	0.0000000e+000	0.0000000e+000	0.0000000e+000	0.0000000e+000
12	0.0000000e+000	0.0000000e+000	0.0000000e+000	0.0000000e+000
13	0.0000000e+000	0.0000000e+000	0.0000000e+000	0.0000000e+000
14	0.0000000e+000	0.0000000e+000	0.0000000e+000	0.0000000e+000
15	0.0000000e+000	0.0000000e+000	0.0000000e+000	0.0000000e+000
16	0.0000000e+000	0.0000000e+000	0.0000000e+000	0.0000000e+000
17	0.0000000e+000	0.0000000e+000	0.0000000e+000	0.0000000e+000
18	0.0000000e+000	0.0000000e+000	0.0000000e+000	0.0000000e+000
19	0.0000000e+000	0.0000000e+000	0.0000000e+000	0.0000000e+000
20	0.0000000e+000	0.0000000e+000	0.0000000e+000	0.0000000e+000
21	0.0000000e+000	0.0000000e+000	0.0000000e+000	0.0000000e+000
22	0.0000000e+000	0.0000000e+000	0.0000000e+000	0.0000000e+000
23	0.0000000e+000	0.0000000e+000	0.0000000e+000	0.0000000e+000
24	0.0000000e+000	0.0000000e+000	0.0000000e+000	0.0000000e+000
25	0.0000000e+000	0.0000000e+000	0.0000000e+000	0.0000000e+000
26	0.0000000e+000	0.0000000e+000	0.0000000e+000	0.0000000e+000
27	0.0000000e+000	0.0000000e+000	0.0000000e+000	0.0000000e+000
28	0.0000000e+000	0.0000000e+000	0.0000000e+000	0.0000000e+000

Table A-19 100 kt Model A Matrix

	1	2	3	4
1	-3.5350700e-001	-1.5409800e-001	1.0976600e+000	-1.5598800e-002
2	1.7527700e-001	-7.5020400e-001	-2.9847800e-001	-3.2592900e-001
3	2.4747600e-001	-2.8331800e-001	-9.8353200e-001	-7.2865200e-002
4	-1.3160300e-002	-3.2713000e-002	1.3238000e-001	-1.8833400e-002
5	1.8931300e-002	-8.6344200e-003	-2.9087700e+000	-2.3660100e-003
6	-1.3850100e-001	2.9093900e+000	2.8859400e-002	-2.7029400e-002
7	1.0000000e+000	0.0000000e+000	9.2936900e-003	0.0000000e+000
8	0.0000000e+000	1.0000000e+000	0.0000000e+000	0.0000000e+000
9	0.0000000e+000	0.0000000e+000	1.0000400e+000	0.0000000e+000
10	3.8123700e+000	-6.1413600e-001	-6.0660900e-001	-4.7885400e+000
11	-3.4722300e-005	2.7947400e-005	-3.8222300e-005	-3.6884900e-004
12	2.6032800e+001	-5.7040800e+001	3.6544600e+000	1.0385400e+001
13	5.6797100e+001	2.5634500e+001	2.3071700e+000	-4.2172100e+000
14	2.1611500e-001	-8.5488700e-001	-1.1099800e+000	5.0096800e-002
15	-1.0866300e-004	2.5140800e-005	-5.3199800e-005	-5.0410000e-004
16	1.6867000e-001	-2.4798600e-001	-1.9109300e-001	-9.3225700e-001
17	-5.2196300e-002	6.2708300e-001	-3.2798600e-001	1.7842400e-001
18	0.0000000e+000	0.0000000e+000	0.0000000e+000	0.0000000e+000
19	0.0000000e+000	0.0000000e+000	0.0000000e+000	0.0000000e+000
20	0.0000000e+000	0.0000000e+000	0.0000000e+000	0.0000000e+000
21	0.0000000e+000	0.0000000e+000	0.0000000e+000	0.0000000e+000
22	0.0000000e+000	0.0000000e+000	0.0000000e+000	0.0000000e+000
23	0.0000000e+000	0.0000000e+000	0.0000000e+000	0.0000000e+000
24	0.0000000e+000	0.0000000e+000	0.0000000e+000	0.0000000e+000
25	0.0000000e+000	0.0000000e+000	0.0000000e+000	0.0000000e+000
26	3.1816400e-001	4.6297800e-002	-3.0823200e-001	-1.4850900e+000
27	2.8154300e+000	-9.1251900e-002	2.7727700e-001	1.4117200e+000
28	7.7858300e-002	2.8462500e+000	-6.5925600e-002	-2.9487300e-001

Table A-19 100 kt Model A Matrix (cont.)

	5	6	7	8
1	-1.2845200e+000	-3.3673700e-001	0.0000000e+000	0.0000000e+000
2	8.6215000e-001	-5.1267900e-001	1.8251700e-005	0.0000000e+000
3	1.5223400e+000	4.3448400e-001	2.5109300e-005	0.0000000e+000
4	1.1058400e-002	8.7804300e-003	0.0000000e+000	-5.6022900e-001
5	-1.3891600e-001	-2.4674000e-002	5.6022900e-001	0.0000000e+000
6	3.4140300e-002	-1.3258300e-001	0.0000000e+000	-5.2024200e-003
7	0.0000000e+000	0.0000000e+000	0.0000000e+000	0.0000000e+000
8	0.0000000e+000	0.0000000e+000	0.0000000e+000	0.0000000e+000
9	0.0000000e+000	0.0000000e+000	0.0000000e+000	0.0000000e+000
10	1.6791700e+000	6.4180300e+001	0.0000000e+000	1.3890300e-005
11	-2.0343900e-005	3.5023500e-004	0.0000000e+000	0.0000000e+000
12	3.2267800e+000	2.2872800e+001	0.0000000e+000	0.0000000e+000
13	1.4148400e+001	-1.6466600e+000	1.8415600e-005	0.0000000e+000
14	1.4872800e+000	1.4372300e+000	2.6992800e-005	-1.0177500e-005
15	-7.4246400e-005	1.0769500e-003	0.0000000e+000	0.0000000e+000
16	3.3276000e-001	-5.6315900e-001	0.0000000e+000	0.0000000e+000
17	-1.7394100e-001	-2.0141600e+000	0.0000000e+000	0.0000000e+000
18	0.0000000e+000	0.0000000e+000	0.0000000e+000	0.0000000e+000
19	0.0000000e+000	0.0000000e+000	0.0000000e+000	0.0000000e+000
20	0.0000000e+000	0.0000000e+000	0.0000000e+000	0.0000000e+000
21	0.0000000e+000	0.0000000e+000	0.0000000e+000	0.0000000e+000
22	0.0000000e+000	0.0000000e+000	0.0000000e+000	0.0000000e+000
23	0.0000000e+000	0.0000000e+000	0.0000000e+000	0.0000000e+000
24	0.0000000e+000	0.0000000e+000	0.0000000e+000	0.0000000e+000
25	0.0000000e+000	0.0000000e+000	0.0000000e+000	0.0000000e+000
26	1.0350400e-001	6.1145500e+000	0.0000000e+000	0.0000000e+000
27	-5.9828600e-001	2.9513700e+000	-3.9925200e-002	-1.8862000e-003
28	1.7755100e+000	3.2110700e+000	-7.3671500e-004	-3.4801900e-005

Table A-19 100 kt Model A Matrix (cont.)

	9	10	11	12
1	0.0000000e+000	-7.6181100e-002	0.0000000e+000	-7.3190200e-002
2	0.0000000e+000	-1.3975900e-001	-4.0619100e-005	-2.2478900e-002
3	0.0000000e+000	-7.5580500e-002	4.7129400e-005	-1.2898200e-002
4	0.0000000e+000	-1.2157100e-003	0.0000000e+000	-1.5355600e-003
5	0.0000000e+000	1.4059700e-003	0.0000000e+000	2.3854400e-004
6	0.0000000e+000	-2.2120900e-002	0.0000000e+000	-1.2866800e-005
7	0.0000000e+000	0.0000000e+000	0.0000000e+000	0.0000000e+000
8	0.0000000e+000	0.0000000e+000	0.0000000e+000	0.0000000e+000
9	0.0000000e+000	0.0000000e+000	0.0000000e+000	0.0000000e+000
10	0.0000000e+000	-2.1071100e+001	-5.4981200e-005	-3.3577800e+000
11	0.0000000e+000	-5.8684800e-005	-2.1005600e+001	7.1912000e-005
12	-1.2988300e-005	-6.8148700e+000	1.4895800e-004	-2.1093000e+001
13	0.0000000e+000	1.1373700e-001	-6.9492300e-005	-5.4024200e+001
14	0.0000000e+000	2.4677200e+000	2.3328400e-004	8.0001300e-002
15	0.0000000e+000	1.8315500e-004	2.5438900e+000	-4.0350600e-004
16	0.0000000e+000	1.3626600e-001	-8.5034700e-004	2.6707800e+000
17	1.4590700e-005	1.0379600e+000	1.7869300e-004	1.0210800e-001
18	0.0000000e+000	1.0000000e+000	0.0000000e+000	0.0000000e+000
19	0.0000000e+000	0.0000000e+000	1.0000000e+000	0.0000000e+000
20	0.0000000e+000	0.0000000e+000	0.0000000e+000	1.0000000e+000
21	0.0000000e+000	0.0000000e+000	0.0000000e+000	0.0000000e+000
22	0.0000000e+000	0.0000000e+000	0.0000000e+000	0.0000000e+000
23	0.0000000e+000	0.0000000e+000	0.0000000e+000	0.0000000e+000
24	0.0000000e+000	0.0000000e+000	0.0000000e+000	0.0000000e+000
25	0.0000000e+000	0.0000000e+000	0.0000000e+000	0.0000000e+000
26	0.0000000e+000	-1.5224500e+000	0.0000000e+000	-2.6662600e-001
27	0.0000000e+000	-8.7427900e-001	0.0000000e+000	-2.6959900e+000
28	0.0000000e+000	-2.2297700e-002	0.0000000e+000	-1.7733900e-001

Table A-19 100 kt Model A Matrix (cont.)

	13	14	15	16
1	2.3332800e-002	2.3313100e-002	3.0643900e-003	9.1259200e+000
2	-6.6721800e-003	1.3779900e-002	-5.0478200e-003	8.2940100e-003
3	9.1989100e-004	-2.9176900e-001	4.5891900e-003	1.7651300e-001
4	1.8852300e-004	6.6354300e-003	1.0420900e-003	-4.7774300e-003
5	6.9209500e-004	-3.0113500e-003	-1.5197700e-004	2.7107700e-001
6	0.0000000e+000	-3.2763700e-002	0.0000000e+000	-2.9627800e-003
7	0.0000000e+000	0.0000000e+000	0.0000000e+000	0.0000000e+000
8	0.0000000e+000	0.0000000e+000	0.0000000e+000	0.0000000e+000
9	0.0000000e+000	0.0000000e+000	0.0000000e+000	0.0000000e+000
10	1.2998500e-001	9.1617700e-001	-3.7406600e-003	-5.2925500e-001
11	-1.1767000e-005	-3.8021700e-003	1.0254300e+000	7.9112000e-003
12	5.4019700e+001	-1.0313900e+000	1.9040700e-002	1.0759700e+001
13	-2.1008700e+001	4.4168000e-001	-9.5878000e-003	-6.7784400e-001
14	5.0272800e-001	-2.5549600e+000	3.2807600e-002	-6.7461900e-001
15	8.9140100e-005	2.8086900e-002	-2.2411800e+000	-8.9377200e-002
16	7.0903700e-002	-6.5246200e-001	-1.8416400e-001	-3.3516500e+000
17	2.4049200e+000	3.5890900e-001	3.5808000e-002	-5.6910200e+001
18	0.0000000e+000	0.0000000e+000	0.0000000e+000	0.0000000e+000
19	0.0000000e+000	0.0000000e+000	0.0000000e+000	0.0000000e+000
20	0.0000000e+000	0.0000000e+000	0.0000000e+000	0.0000000e+000
21	1.0000000e+000	0.0000000e+000	0.0000000e+000	0.0000000e+000
22	0.0000000e+000	1.0000000e+000	0.0000000e+000	0.0000000e+000
23	0.0000000e+000	0.0000000e+000	1.0000000e+000	0.0000000e+000
24	0.0000000e+000	0.0000000e+000	0.0000000e+000	1.0000000e+000
25	0.0000000e+000	0.0000000e+000	0.0000000e+000	0.0000000e+000
26	1.0446800e-002	3.0056100e-001	0.0000000e+000	-2.3563300e-002
27	1.7629200e-001	-1.4096600e-001	-2.0009900e-005	3.6379900e-001
28	-2.6944100e+000	9.0505700e-002	0.0000000e+000	3.3880700e-002

Table A-19 100 kt Model A Matrix (cont.)

	17	18	19	20
1	-5.2702400e-001	-2.4173000e+000	1.0622800e-004	-5.3480500e+001
2	1.3149100e+000	5.6024500e+000	2.4176700e-005	-4.4823900e-001
3	9.6463400e-002	1.7116600e-001	1.7320100e-003	-7.2388600e-001
4	-3.1810300e-001	5.9124100e-001	0.0000000e+000	5.7503800e-002
5	-1.3937600e-002	-4.5728500e-002	0.0000000e+000	-5.2175900e-001
6	-1.7545700e-002	-9.2670500e+000	-1.2685900e-005	8.4988300e-004
7	0.0000000e+000	0.0000000e+000	0.0000000e+000	0.0000000e+000
8	0.0000000e+000	0.0000000e+000	0.0000000e+000	0.0000000e+000
9	0.0000000e+000	0.0000000e+000	0.0000000e+000	0.0000000e+000
10	1.5153300e-001	-7.8740400e+002	-1.1263100e-003	5.4787800e+000
11	-1.8545100e-003	-1.0855700e-003	-7.5668500e+002	3.8348700e-004
12	-5.1513200e-001	4.0232100e+000	1.6201000e-003	-8.7379400e+001
13	2.7637600e+000	-1.8413600e+002	-1.0406600e-003	-5.8262900e+002
14	3.0240600e-001	2.8636800e+000	1.1654000e-002	1.1724800e+001
15	1.8188600e-002	9.8053800e-003	2.5371400e+000	3.1890800e-003
16	5.6911600e+001	-6.8912000e+000	1.5642400e-003	4.0994400e+000
17	-1.2835300e+000	-3.5210300e+000	-2.5235300e-003	9.2018100e+001
18	0.0000000e+000	0.0000000e+000	0.0000000e+000	0.0000000e+000
19	0.0000000e+000	0.0000000e+000	0.0000000e+000	0.0000000e+000
20	0.0000000e+000	0.0000000e+000	0.0000000e+000	0.0000000e+000
21	0.0000000e+000	0.0000000e+000	0.0000000e+000	0.0000000e+000
22	0.0000000e+000	0.0000000e+000	0.0000000e+000	0.0000000e+000
23	0.0000000e+000	0.0000000e+000	0.0000000e+000	0.0000000e+000
24	0.0000000e+000	0.0000000e+000	0.0000000e+000	0.0000000e+000
25	1.0000000e+000	0.0000000e+000	0.0000000e+000	0.0000000e+000
26	2.6342000e-002	1.4464200e+000	0.0000000e+000	6.5475000e-001
27	-1.9290000e-002	2.5984100e+000	1.5873300e-005	7.6262500e+000
28	5.0025100e-001	-2.4660500e+001	2.2776500e-005	-7.4096400e+001

Table A-19 100 kt Model A Matrix (cont.)

	21	22	23	24
1	3.5366300e+000	3.5099400e+000	-1.6889900e-004	-4.2396200e+000
2	-7.3657600e+000	-3.2173800e-001	5.4312700e-005	1.7086400e+001
3	-2.9855100e-001	-9.1040800e+000	-1.7103100e-003	1.9758300e+000
4	7.0441000e-001	-1.0734800e-002	-1.2167700e-005	-4.1070100e+000
5	5.6917800e-002	-1.1780000e-002	0.0000000e+000	-7.9206300e-002
6	5.0290900e-002	-4.7793500e-003	1.3476800e-005	-2.4403000e-001
7	0.0000000e+000	0.0000000e+000	0.0000000e+000	0.0000000e+000
8	0.0000000e+000	0.0000000e+000	0.0000000e+000	0.0000000e+000
9	0.0000000e+000	0.0000000e+000	0.0000000e+000	0.0000000e+000
10	-4.9977000e+000	8.7087600e+000	1.2315700e-003	1.5819800e+001
11	-2.5240800e-003	1.1886000e-003	8.7086100e+000	-5.0793800e-002
12	5.5581800e+002	2.5062600e+001	-1.7373900e-003	4.2004600e+000
13	-3.5792400e+001	3.8849900e+001	1.2625400e-003	5.1895300e+001
14	-5.1330900e+000	-6.2798400e+001	-1.1739100e-002	7.0401900e+000
15	9.6362400e-003	-9.9187900e-003	-5.2847900e+001	4.9240500e-001
16	-7.2387200e+001	1.3932400e-001	2.8559700e-003	7.3310900e+002
17	1.0493500e+000	-3.5821900e+000	-8.9723400e-004	-3.7827500e+001
18	0.0000000e+000	0.0000000e+000	0.0000000e+000	0.0000000e+000
19	0.0000000e+000	0.0000000e+000	0.0000000e+000	0.0000000e+000
20	0.0000000e+000	0.0000000e+000	0.0000000e+000	0.0000000e+000
21	0.0000000e+000	0.0000000e+000	0.0000000e+000	0.0000000e+000
22	0.0000000e+000	0.0000000e+000	0.0000000e+000	0.0000000e+000
23	0.0000000e+000	0.0000000e+000	0.0000000e+000	0.0000000e+000
24	0.0000000e+000	0.0000000e+000	0.0000000e+000	0.0000000e+000
25	0.0000000e+000	0.0000000e+000	0.0000000e+000	0.0000000e+000
26	-3.3070100e+000	7.1808200e-001	0.0000000e+000	1.5617500e+000
27	7.0483500e+001	2.5146900e+000	0.0000000e+000	8.6149800e-001
28	-1.9845700e+000	5.2704500e+000	1.2763100e-005	8.7728800e+000

Table A-19 100 kt Model A Matrix (conc.)

	25	26	27	28
1	-1.1175600e+002	7.2676600e-001	-1.4289000e-001	-2.8641200e-002
2	1.5420100e+000	-5.3952000e-001	-5.9289300e-002	-1.8550200e-002
3	-1.0574700e+000	-9.8205200e-001	-2.8828400e-002	-2.3734300e-003
4	-2.0080100e-001	-1.7564700e-002	-1.5530400e-003	5.7879100e-004
5	-3.3202000e+000	4.3750900e-002	8.9668400e-004	-5.4505900e-004
6	2.2638100e-002	8.1635600e-003	8.7046500e-004	-8.1687600e-005
7	0.0000000e+000	0.0000000e+000	0.0000000e+000	0.0000000e+000
8	0.0000000e+000	0.0000000e+000	0.0000000e+000	0.0000000e+000
9	0.0000000e+000	0.0000000e+000	0.0000000e+000	0.0000000e+000
10	3.3779900e+001	-6.4700300e+001	-7.6624000e+000	-2.1182500e-001
11	-2.1299200e-001	-3.7125500e-004	7.4516500e-005	0.0000000e+000
12	-1.4473100e+002	-2.1897500e+001	-4.7824800e+001	-3.1478800e+000
13	1.9567200e+001	2.6316100e-001	3.0370300e+000	-4.7665600e+001
14	1.2709000e+001	-2.0367600e+000	1.7407800e-001	7.6909400e-001
15	2.4123700e+000	-1.1046900e-003	2.2221100e-004	0.0000000e+000
16	8.7786800e+001	1.5473600e-001	-4.7567800e-001	1.1006500e-001
17	6.9129100e+002	1.8734700e+000	2.4195200e-001	-6.3183200e-001
18	0.0000000e+000	0.0000000e+000	0.0000000e+000	0.0000000e+000
19	0.0000000e+000	0.0000000e+000	0.0000000e+000	0.0000000e+000
20	0.0000000e+000	0.0000000e+000	0.0000000e+000	0.0000000e+000
21	0.0000000e+000	0.0000000e+000	0.0000000e+000	0.0000000e+000
22	0.0000000e+000	0.0000000e+000	0.0000000e+000	0.0000000e+000
23	0.0000000e+000	0.0000000e+000	0.0000000e+000	0.0000000e+000
24	0.0000000e+000	0.0000000e+000	0.0000000e+000	0.0000000e+000
25	0.0000000e+000	0.0000000e+000	0.0000000e+000	0.0000000e+000
26	2.4670600e+000	-1.3077400e+001	-3.3925000e-002	-1.2321100e+001
27	-5.7750900e+000	-5.6770300e+000	-2.1675500e+001	1.3828800e+000
28	5.7219300e-001	5.6162800e+001	1.3761400e+000	-5.0815800e+001

Table A-20 100 kt Model B Matrix

	1	2	3	4
1	-4.2439068e-001	5.2850175e+000	1.7333749e+001	-6.6596138e+001
2	-1.3639288e+000	4.9963952e+000	6.1362317e-001	1.8367169e+001
3	-2.6342458e-001	2.3886316e+000	-1.1028558e+001	4.8270091e+001
4	1.5114006e-001	-5.7920469e-002	-6.2827846e-002	2.1134425e-001
5	-2.6741816e-002	-2.6366194e-002	3.4406241e-001	-1.7064297e+000
6	5.6293319e-004	-8.0915292e-002	6.0427420e-001	8.8343311e-001
7	0.0000000e+000	0.0000000e+000	0.0000000e+000	0.0000000e+000
8	0.0000000e+000	0.0000000e+000	0.0000000e+000	0.0000000e+000
9	0.0000000e+000	0.0000000e+000	0.0000000e+000	0.0000000e+000
10	-3.7109689e+001	5.3940085e+002	9.4102109e+002	-3.0897681e+002
11	7.4640661e-002	-1.0528751e-002	-1.4659653e-002	6.0642945e-003
12	-1.3189507e+002	1.8457624e+003	3.5203727e+002	-1.1278915e+003
13	-9.9029338e+002	-2.1872067e+002	1.7890734e+002	1.5328913e+002
14	1.6438250e+001	1.2077052e+000	-7.2909403e+001	5.6183578e+001
15	-8.0215367e-001	1.1153066e-001	1.6212682e-001	-6.4238844e-002
16	-1.1310328e+001	-8.0145912e+001	9.4359813e+000	5.5200727e+001
17	7.3085387e+001	-8.0320305e+000	-4.9248710e+001	2.9811644e+001
18	0.0000000e+000	0.0000000e+000	0.0000000e+000	0.0000000e+000
19	0.0000000e+000	0.0000000e+000	0.0000000e+000	0.0000000e+000
20	0.0000000e+000	0.0000000e+000	0.0000000e+000	0.0000000e+000
21	0.0000000e+000	0.0000000e+000	0.0000000e+000	0.0000000e+000
22	0.0000000e+000	0.0000000e+000	0.0000000e+000	0.0000000e+000
23	0.0000000e+000	0.0000000e+000	0.0000000e+000	0.0000000e+000
24	0.0000000e+000	0.0000000e+000	0.0000000e+000	0.0000000e+000
25	0.0000000e+000	0.0000000e+000	0.0000000e+000	0.0000000e+000
26	-2.8996347e+000	4.3373600e+001	6.8987391e+001	-2.4982027e+001
27	-9.2180901e+000	2.3845201e+002	4.1992122e+001	-1.3685649e+002
28	-1.2793830e+002	-1.4019059e+001	2.5982338e+001	8.0835288e+000

Table A-21 100 kt Model C Matrix

	1	2	3	4
1	0.0000000e+000	0.0000000e+000	0.0000000e+000	0.0000000e+000
2	0.0000000e+000	0.0000000e+000	0.0000000e+000	0.0000000e+000
3	0.0000000e+000	0.0000000e+000	0.0000000e+000	1.0000400e+000
4	0.0000000e+000	0.0000000e+000	9.2932900e-003	0.0000000e+000
5	0.0000000e+000	0.0000000e+000	0.0000000e+000	0.0000000e+000
6	0.0000000e+000	0.0000000e+000	-9.9995700e-001	0.0000000e+000
7	1.0000000e+000	0.0000000e+000	-1.3902000e-001	0.0000000e+000
8	0.0000000e+000	1.0000000e+000	2.9428300e+000	0.0000000e+000
9	0.0000000e+000	0.0000000e+000	0.0000000e+000	0.0000000e+000
10	0.0000000e+000	0.0000000e+000	0.0000000e+000	0.0000000e+000
11	0.0000000e+000	0.0000000e+000	0.0000000e+000	0.0000000e+000
12	0.0000000e+000	0.0000000e+000	0.0000000e+000	0.0000000e+000
13	0.0000000e+000	0.0000000e+000	0.0000000e+000	0.0000000e+000
14	0.0000000e+000	0.0000000e+000	0.0000000e+000	0.0000000e+000
15	0.0000000e+000	0.0000000e+000	0.0000000e+000	0.0000000e+000
16	0.0000000e+000	0.0000000e+000	0.0000000e+000	0.0000000e+000
17	0.0000000e+000	0.0000000e+000	0.0000000e+000	0.0000000e+000
18	0.0000000e+000	0.0000000e+000	0.0000000e+000	0.0000000e+000
19	0.0000000e+000	0.0000000e+000	0.0000000e+000	0.0000000e+000
20	0.0000000e+000	0.0000000e+000	0.0000000e+000	0.0000000e+000
21	0.0000000e+000	0.0000000e+000	0.0000000e+000	0.0000000e+000
22	0.0000000e+000	0.0000000e+000	0.0000000e+000	0.0000000e+000
23	0.0000000e+000	0.0000000e+000	0.0000000e+000	0.0000000e+000
24	0.0000000e+000	0.0000000e+000	0.0000000e+000	0.0000000e+000
25	0.0000000e+000	0.0000000e+000	0.0000000e+000	0.0000000e+000
26	0.0000000e+000	0.0000000e+000	0.0000000e+000	0.0000000e+000
27	0.0000000e+000	0.0000000e+000	0.0000000e+000	0.0000000e+000
28	0.0000000e+000	0.0000000e+000	0.0000000e+000	0.0000000e+000

APPENDIX B

LIBRARY OF MATLAB SCRIPT AND FUNCTION FILES

In this appendix are listed a number of MATLAB script and function files that were created to facilitate the operational tasks of the flight control system design processes employed in this project. Table B-1 contains a list of these and the pages on which they begin.

Table B-1 List of MATLAB Functions and Script Files

MODINV - creates the q_{ii} for the QFT MIMO design process

```
% This m-file takes the state space representation of a
% continuous MIMO system and generates the BODE diagram for
% both the transfer function matrix, P, and its inverse with
% inverted elements, Q.  The magnitude and phase of the Q matrix
% elements at specified frequencies are necessary in the
% application of QFT to the MIMO system.
%
% a, b, c, and d are the state matrices such that
%       x-dot = a x + b u
%       y     = c x + d u
%
% w is the vector of frequencies at which the magnitude and phase
%       are calculated
%
% pmagij magnitude vector for the ijth element of the transfer
%       function matrix, P.
% pphsij phase vector for the ijth element of the transfer
%       function matrix, P.
% qmagij magnitude vector for the ijth element of the Q matrix.
% qphsij phase vector for the ijth element of the Q matrix.
%

x=size(w);
imax=max(x);
pmag11=zeros(1,imax);
pmag22=zeros(1,imax);
pmag33=zeros(1,imax);
pmag44=zeros(1,imax);
qmag11=zeros(1,imax);
qmag22=zeros(1,imax);
qmag33=zeros(1,imax);
qmag44=zeros(1,imax);
pphs11=zeros(1,imax);
pphs22=zeros(1,imax);
pphs33=zeros(1,imax);
pphs44=zeros(1,imax);
qphs11=zeros(1,imax);
qphs22=zeros(1,imax);
qphs33=zeros(1,imax);
qphs44=zeros(1,imax);
for i=1:imax
   omeg=w(i);
```

```
tmp1=j*omeg*ones(1,28);
tmp2=diag(tmp1,0);
sima=tmp2-a;
simai=eye(28,28)/sima;
bodmgph=c*simai*b;
bodmgphi=eye(4,4)/bodmgph;
p11=bodmgph(1,1);
p22=bodmgph(2,2);
p33=bodmgph(3,3);
p44=bodmgph(4,4);
q11=1./bodmgphi(1,1);
q22=1./bodmgphi(2,2);
q33=1./bodmgphi(3,3);
q44=1./bodmgphi(4,4);
pmag11(i)=20*log10(abs(p11));
pmag22(i)=20*log10(abs(p22));
pmag33(i)=20*log10(abs(p33));
pmag44(i)=20*log10(abs(p44));
qmag11(i)=20*log10(abs(q11));
qmag22(i)=20*log10(abs(q22));
qmag33(i)=20*log10(abs(q33));
qmag44(i)=20*log10(abs(q44));
pphs11(i)=180*atan2(imag(p11),real(p11))/pi;
pphs22(i)=180*atan2(imag(p22),real(p22))/pi;
pphs33(i)=180*atan2(imag(p33),real(p33))/pi;
pphs44(i)=180*atan2(imag(p44),real(p44))/pi;
qphs11(i)=180*atan2(imag(q11),real(q11))/pi;
qphs22(i)=180*atan2(imag(q22),real(q22))/pi;
qphs33(i)=180*atan2(imag(q33),real(q33))/pi;
qphs44(i)=180*atan2(imag(q44),real(q44))/pi;
if i>1
   if pphs11(i)>pphs11(i-1)+300
      pphs11(i)=pphs11(i)-360;
   elseif pphs11(i)<pphs11(i-1)-300
      pphs11(i)=pphs11(i)+360;
   end
   if pphs22(i)>pphs22(i-1)+300
      pphs22(i)=pphs22(i)-360;
   elseif pphs22(i)<pphs22(i-1)-300
      pphs22(i)=pphs22(i)+360;
   end
   if pphs33(i)>pphs33(i-1)+300
      pphs33(i)=pphs33(i)-360;
   elseif pphs33(i)<pphs33(i-1)-300
```

```
            pphs33(i)=pphs33(i)+360;
        end
        if pphs44(i)>pphs44(i-1)+300
            pphs44(i)=pphs44(i)-360;
        elseif pphs44(i)<pphs44(i-1)-300
            pphs44(i)=pphs44(i)+360;
        end
        if qphs11(i)>qphs11(i-1)+300
            qphs11(i)=qphs11(i)-360;
        elseif qphs11(i)<qphs11(i-1)-300
            qphs11(i)=qphs11(i)+360;
        end
        if qphs22(i)>qphs22(i-1)+300
            qphs22(i)=qphs22(i)-360;
        elseif qphs22(i)<qphs22(i-1)-300
            qphs22(i)=qphs22(i)+360;
        end
        if qphs33(i)>qphs33(i-1)+300
            qphs33(i)=qphs33(i)-360;
        elseif qphs33(i)<qphs33(i-1)-300
            qphs33(i)=qphs33(i)+360;
        end
        if qphs44(i)>qphs44(i-1)+300
            qphs44(i)=qphs44(i)-360;
        elseif qphs44(i)<qphs44(i-1)-300
            qphs44(i)=qphs44(i)+360;
        end
    end
end
subplot(212)
plot(w,pphs11,'-r',w,qphs11,'--g',[.01 100],[-180 -180],':w')
semilogx
xlabel('Frequency  (rad/sec)')
ylabel('Phase  (deg)')
subplot(211)
plot(w,pmag11,'-r',w,qmag11,'--g')
semilogx
xlabel('Frequency  (rad/sec)')
ylabel('Magnitude  (db)')
pause
clg
subplot(212)
plot(w,pphs22,'-r',w,qphs22,'--g',[.01 100],[-180 -180],':w')
semilogx
```

```
xlabel('Frequency  (rad/sec)')
ylabel('Phase  (deg)')
subplot(211)
plot(w,pmag22,'-r',w,qmag22,'--g')
semilogx
xlabel('Frequency  (rad/sec)')
ylabel('Magnitude  (db)')
pause
clg
subplot(212)
plot(w,pphs33,'-r',w,qphs33,'--g',[.01  100],[-180 -180],':w')
semilogx
xlabel('Frequency  (rad/sec)')
ylabel('Phase  (deg)')
subplot(211)
plot(w,pmag33,'-r',w,qmag33,'--g')
semilogx
xlabel('Frequency  (rad/sec)')
ylabel('Magnitude  (db)')
pause
clg
subplot(212)
plot(w,pphs44,'-r',w,qphs44,'--g',[.01  100],[-180 -180],':w')
semilogx
xlabel('Frequency  (rad/sec)')
ylabel('Phase  (deg)')
subplot(211)
plot(w,pmag44,'-r',w,qmag44,'--g')
semilogx
xlabel('Frequency  (rad/sec)')
ylabel('Magnitude  (db)')
```

SAV_NOM - Saves the nominal plant data file in the proper format

```
%function sav_nom(w,m,p,type,ext,tsamp)
%
% Save frequency response of nominal plant, to be used by the QFT package.
%
% type : 0 for 'DISCRETE' or 1 for 'CONTINUOUS'.
% tsamp: Sampling time for discrete systems
% w    : Frequency vector at which the nominal plant has been evaluated.
% m    : Magnitude vector in db.
% p    : Phase vector in deg.
```

```
% ext  : File name extension for nomplant (default='dat')
%
% The file nomplant.dat is deleted if it exists.
%
%
%

function  nompl(w,m,p,type,ext,tsamp)
if nargin == 4
   filename='nomplant.dat';
else
   filename=['nomplant.' ext];
end

if type == 0,
   disp('Writing nominal DISCRETE TIME plant.') ;
   typeinfo=sprintf('DISC T=%-12.5g',tsamp) ;
elseif  type == 1 ,
   disp('Writing nominal CONTINUOUS plant.') ;
   typeinfo = 'CONTINUOUS          ';
else ,
   disp ('Error in nompl: type must be DISCRETE or CONTINUOUS .');
   return ;
end
!if exist nomplant.dat del nomplant.dat
class = ['OMEGA                ';typeinfo];

[mw,nw] = size(w) ;
if nw ~= 1, w = w';
   [mw,nw] = size(w) ;
   if nw ~= 1, error('w MUST be a row or column vector.') ; end
end

if size(m) ~= size(w) ,
   m=m';
   if size(m) ~= size(w), error('m is badly dimensioned.') ; end
end

if size(p) ~= size(w) ,
   p=p';
   if size(p) ~= size(w), error('p is badly dimensioned.') ; end
end

dat=[w,m,p] ;
```

```
%keyboard
save_pac(filename,dat,...
                    ['OMEGA   ';'GAIN[Db]';'Ph[Deg] '],class);
end;
```

TEMPLATE - Saves the template data in a file of proper format

```
function  template(imax,m,p,type,ext,tsamp)
% function  template(imax,m,p,type,ext,tsamp)
%
% This function creates the Template data file for use
% in the QFT CAD software.  If a file named template.dat
% already exists, it is deleted.
%
% imax:  Number of templates
% m:     Matrix of magnitude data -
%          Row indices indicate model
%          Column indices indicate frequency
% p:     Matrix of phase data -
%          Row indices indicate model
%          Column indices indicate frequency
% type:  System type - 1 for continuous, 0 for discrete
% ext:   Extension for template file name (default=.dat)
% tsamp: Sampling interval for discrete systems
%
if ext == 0
   filename='template.dat';
else
   filename=['template.' ext];
end

if type == 0,
   disp('Writing nominal DISCRETE TIME plant.') ;
   typeinfo=sprintf('DISC T=%-12.5g',tsamp) ;
elseif  type == 1 ,
   disp('Writing nominal CONTINUOUS plant.') ;
   typeinfo = '/CONTINUOUS';
else ,
   disp ('Error in nompl: type must be DISCRETE or CONTINUOUS .');
   return ;
end
!if exist template.dat del template.dat
class = ['Template  ';typeinfo];
```

```
for i = 1:imax,
   dat=[m(:,i),p(:,i)] ;
   save_pac(filename,dat,['GAIN[Db]';'Ph[Deg] '],class);
end

end;
```

SAV_PAC - Used in SAV_NOM and TEMPLATE

```
function save_pac(filename,data,titles,class)
%
%  Save MATLAB variables as a Package file.
%  using program SAVE_PAC
%  filename = name of Package data file.
%  Data = A matrix containing the data
%  titles = a matrix of text labels for tha data columns
%  class  = a matrix with list class and source.
%           class is defaulted to ['MATLAB  ';'MATLAB  '] .
%  Many lists may be generated in the same file by a repeated use of save_pac.
%
%  Example:
%  save_pac('pac.dat',[1 2 3;4 5 6],['title1 ';'title2 '];['class';'source'])
%
%  Yahali Theodor
%
if nargin < 4 ,
 class=['MATLAB  ';'MATLAB  '];
else
 [m,n]=size(class) ;
 if  m ~= 2 | n > 20 | isstr(class) == 0 ,
    error('Bad dimension or type of class.') ; end
end
if nargin < 3 , error('Need at least 3 input variables.') ; end
junkfile = 'r75yyfhh';
if exist([junkfile,'.mat']) ~= 0 ,
  disp(' A file named r75yyfhh.mat exists. ') ;
  junkfile=input('Enter another name for temporary scratch file.') ;
end
command=['save ',junkfile,' class titles data '] ;
eval(command) ;
command=['!save_pac ',junkfile,'.mat ',filename,' MATLAB']  ;
eval(command) ;
command = ['!del ',junkfile,'.mat'];
```

```
eval(command) ;
end
```

LOAD_PAC - Loads files stored by SAV_PAC

```
%  Just type load_pac .
%  Load a Package data file into MATLAB by using the external file
%  converter READ_BIN.
%  The user is asked interactivelly for the package file name.
%
%  Each list in the data file loads as 3 variables:
%  classn = Text , class and source of list.
%  titlesn = Text , column titles
%  listdatn = Numeric matrix with numeric data.
%  where n is the list number in the Package data file.
%
%  Yahali Theodor.
%
command ='AAAAA' ;
while exist(command) ~= 0 ,
   command  = rndname(1) ;
end
input('Enter name of package data file. ') ;
eval(['!read_bin ',ans,' ',command,'.mat MATLAB']) ;
eval(['load  ',command]) ;
command = ['!del ',command,'.mat'] ;
eval(command) ;
clear command ;
```

DIJGEN - Generates the diturbance boundaries for the MIMO QFT

```
% This M-file takes the |tij|max |qij|min vectors and calculates
% the disturbance vectors, dij.
%
d11=(b21./q12min+b31./q13min+b41./q14min)./t11d;
d12=(b22./q12min+b32./q13min+b42./q14min)./b12;
d13=(b23./q12min+b33./q13min+b43./q14min)./b13;
d14=(b24./q12min+b34./q13min+b44./q14min)./b14;
d21=(b11./q21min+b31./q23min+b41./q24min)./b21;
d22=(b12./q21min+b32./q23min+b42./q24min)./t22d;
d23=(b13./q21min+b33./q23min+b43./q24min)./b23;
d24=(b14./q21min+b34./q23min+b44./q24min)./b24;
```

```
d31=(b11./q31min+b21./q32min+b41./q34min)./b31;
d32=(b12./q31min+b22./q32min+b42./q34min)./b32;
d33=(b13./q31min+b23./q32min+b43./q34min)./t33d;
d34=(b14./q31min+b24./q32min+b44./q34min)./b34;
d41=(b11./q41min+b21./q42min+b31./q43min)./b41;
d42=(b12./q41min+b22./q42min+b32./q43min)./b42;
d43=(b13./q41min+b23./q42min+b33./q43min)./b43;
d44=(b14./q41min+b24./q42min+b34./q43min)./t44d;

d11=20*log10(d11);
d12=20*log10(d12);
d13=20*log10(d13);
d14=20*log10(d14);
d21=20*log10(d21);
d22=20*log10(d22);
d23=20*log10(d23);
d24=20*log10(d24);
d31=20*log10(d31);
d32=20*log10(d32);
d33=20*log10(d33);
d34=20*log10(d34);
d41=20*log10(d41);
d42=20*log10(d42);
d43=20*log10(d43);
d44=20*log10(d44);
save dijs d11 d12 d13 d14 d21 d22 d23 d24 ...
        d31 d32 d33 d34 d41 d42 d43 d44
```

DIJ_SAV - Saves the disturbance boundaries in ASCII format

```
load dijs
w=[.3 .5 1 3 5 10 20 40 80]';
d11t = [w -d11'];
d12t = [w -d12'];
d13t = [w -d13'];
d14t = [w -d14'];
d21t = [w -d21'];
d22t = [w -d22'];
d23t = [w -d23'];
d24t = [w -d24'];
d31t = [w -d31'];
d32t = [w -d32'];
d33t = [w -d33'];
```

```
d34t = [w -d34'];
d41t = [w -d41'];
d42t = [w -d42'];
d43t = [w -d43'];
d44t = [w -d44'];

save d11.dat d11t /ascii
save d12.dat d12t /ascii
save d13.dat d13t /ascii
save d14.dat d14t /ascii
save d21.dat d21t /ascii
save d22.dat d22t /ascii
save d23.dat d23t /ascii
save d24.dat d24t /ascii
save d31.dat d31t /ascii
save d32.dat d32t /ascii
save d33.dat d33t /ascii
save d34.dat d34t /ascii
save d41.dat d41t /ascii
save d42.dat d42t /ascii
save d43.dat d43t /ascii
save d44.dat d44t /ascii
```

GNORM - Normalizes feedback compensator transfer functions

```
function num1 = gnorm(num,den,n,w)
% function num1 = gnorm(num,den,n,w)
%
% This function provides a gain to num such that
% the magnitude of the resulting transfer function at
% the specified frequency is equal to the specified gain.
%
% This is necessary because QFT-CAD uses a nomalized
% gain at a specified frequency in the feedback compensator
% design process.
%
% num and den are the original transfer function coefficient
%     vectors
%
% n is the gain in db.
%
% w is the specified frequency
%
```

```
% num1 is num multiplied by a gain
%
m1=bode(num,den,w);
m2=10^(n/20)/m1;
num1=m2*num;
```

NOM1SEQ - Creates nominal plant data file for first loop of sequential process

```
function [nommag,nomphs]=nom1seq(a,b,c,w,n,sav)
% function [nommag,nomphs]=nom1seq(a,b,c,w,n,sav)
%
% This function calculates the nominal plant magnitude and
% phase at the frequencies designated in w.
%
% a, b, and c are the state matrices such that
%       x-dot = a x + b u
%       y     = c x
%
% w is the vector of frequencies at which the magnitude and phase
%       are calculated
%
% n is the array of indices of the loop sequence
%
% nommag and nomphs are the magnitude and phase vectors,
%       respectively
%
% if sav = 1, then the sav_nom function is called to save the
%       data in nomplant.qn1
%
x=size(w);
imax=max(x);
nommag=zeros(1,imax);
nomphs=zeros(1,imax);
for i=1:imax
   omeg=w(i);
   tmp1=j*omeg*ones(1,28);
   tmp2=diag(tmp1,0);
   sima=tmp2-a;
   simai=eye(28,28)/sima;
   bodmgph=c*simai*b;
   bodmgphi=eye(4,4)/bodmgph;
   q=1./bodmgphi(n(1),n(1));
   nommag(i)=20*log10(abs(q));
```

```
    nomphs(i)=180*atan2(imag(q),real(q))/pi;
    if i>1
       if nomphs(i)>nomphs(i-1)+300
          nomphs(i)=nomphs(i)-360;
       elseif nomphs(i)<nomphs(i-1)-300
          nomphs(i)=nomphs(i)+360;
       end
    end
end
if nargin == 6
    if sav == 1
       ext=[ 'q' int2str(n(1)) '1' ]
       sav_nom(w,nommag,nomphs,1,ext)
    end
end
```

TEMP1SEQ - Creates template data files for first loop of sequential process

```
% This script file utilizes the function NOM1SEQ to determine
% the templates for the first loop of the sequential process.
% Be sure to set n to the vector indices of the loop sequence.
%
load model01m
w=[.3 .5 1 3 5 10 20 40 80];
[mag1,phs1]=nom1seq(a,b,c,w,n);
[nr,nc]=size(mag1);
if nr == 1
    tmag=mag1;
    tphs=phs1;
else
    tmag=mag1';
    tphs=phs1';
end
save temp w tmag tphs n
clear
load model20m
load temp
[mag1,phs1]=nom1seq(a,b,c,w,n);
[nr,nc]=size(mag1);
if nr == 1
    tmag=[tmag;mag1];
    tphs=[tphs;phs1];
else
    tmag=[tmag;mag1'];
```

```
    tphs=[tphs;phs1'];
end
save temp w tmag tphs n
clear
load model40m
load temp
[mag1,phs1]=nom1seq(a,b,c,w,n);
[nr,nc]=size(mag1);
if nr == 1
    tmag=[tmag;mag1];
    tphs=[tphs;phs1];
else
    tmag=[tmag;mag1'];
    tphs=[tphs;phs1'];
end
save temp w tmag tphs n
clear
load model60m
load temp
[mag1,phs1]=nom1seq(a,b,c,w,n);
[nr,nc]=size(mag1);
if nr == 1
    tmag=[tmag;mag1];
    tphs=[tphs;phs1];
else
    tmag=[tmag;mag1'];
    tphs=[tphs;phs1'];
end
save temp w tmag tphs n
clear
load model80m
load temp
[mag1,phs1]=nom1seq(a,b,c,w,n);
[nr,nc]=size(mag1);
if nr == 1
    tmag=[tmag;mag1];
    tphs=[tphs;phs1];
else
    tmag=[tmag;mag1'];
    tphs=[tphs;phs1'];
end
save temp w tmag tphs n
clear
load modl100m
```

```
load temp
[mag1,phs1]=nom1seq(a,b,c,w,n);
[nr,nc]=size(mag1);
if nr == 1
    tmag=[tmag;mag1];
    tphs=[tphs;phs1];
else
    tmag=[tmag;mag1'];
    tphs=[tphs;phs1'];
end
save temp w tmag tphs n
clear
load temp
x=size(w);
imax=max(x);
ext=[ 'q' int2str(n(1)) '1' ]
template(imax,tmag,tphs,1,ext)
```

DIST1SEQ - Creates the disturbance boundaries for the first loop of the sequential process

```
% This script file utilizes the function DIST1 to determine
% the disturbance bounds for the first loop of the
% sequential process.  Be sure to set n to the array of indices
% indicating the sequence of loop closure.  TBNDS.MAT contains
% the bound matrices.
%
load tbnds
load model01m
w=[.3 .5 1 3 5 10 20 40 80];
[d1a,d1b,d1c]=dist1(a,b,c,w,n,t1,t2,t3,t4);
save temp w d1a d1b d1c n t1 t2 t3 t4
clear
load model20m
load temp
[d1ap,d1bp,d1cp]=dist1(a,b,c,w,n,t1,t2,t3,t4);
for i=1:4
    for j=1:max(size(w))
        if d1a(i,j) < d1ap(i,j)
            d1a(i,j)=d1ap(i,j);
        end
        if d1b(i,j) < d1bp(i,j)
            d1b(i,j)=d1bp(i,j);
```

```
        end
        if d1c(i,j) < d1cp(i,j)
            d1c(i,j)=d1cp(i,j);
        end
    end
end
save temp w d1a d1b d1c n t1 t2 t3 t4
clear
load model40m
load temp
[d1ap,d1bp,d1cp]=dist1(a,b,c,w,n,t1,t2,t3,t4);
for i=1:4
    for j=1:max(size(w))
        if d1a(i,j) < d1ap(i,j)
            d1a(i,j)=d1ap(i,j);
        end
        if d1b(i,j) < d1bp(i,j)
            d1b(i,j)=d1bp(i,j);
        end
        if d1c(i,j) < d1cp(i,j)
            d1c(i,j)=d1cp(i,j);
        end
    end
end
save temp w d1a d1b d1c n t1 t2 t3 t4
clear
load model60m
load temp
[d1ap,d1bp,d1cp]=dist1(a,b,c,w,n,t1,t2,t3,t4);
for i=1:4
    for j=1:max(size(w))
        if d1a(i,j) < d1ap(i,j)
            d1a(i,j)=d1ap(i,j);
        end
        if d1b(i,j) < d1bp(i,j)
            d1b(i,j)=d1bp(i,j);
        end
        if d1c(i,j) < d1cp(i,j)
            d1c(i,j)=d1cp(i,j);
        end
    end
end
save temp w d1a d1b d1c n t1 t2 t3 t4
clear
```

```
load model80m
load temp
[d1ap,d1bp,d1cp]=dist1(a,b,c,w,n,t1,t2,t3,t4);
for i=1:4
    for j=1:max(size(w))
        if d1a(i,j) < d1ap(i,j)
            d1a(i,j)=d1ap(i,j);
        end
        if d1b(i,j) < d1bp(i,j)
            d1b(i,j)=d1bp(i,j);
        end
        if d1c(i,j) < d1cp(i,j)
            d1c(i,j)=d1cp(i,j);
        end
    end
end
save temp w d1a d1b d1c n t1 t2 t3 t4
clear
load modl100m
load temp
[d1ap,d1bp,d1cp]=dist1(a,b,c,w,n,t1,t2,t3,t4);
for i=1:4
    for j=1:max(size(w))
        if d1a(i,j) < d1ap(i,j)
            d1a(i,j)=d1ap(i,j);
        end
        if d1b(i,j) < d1bp(i,j)
            d1b(i,j)=d1bp(i,j);
        end
        if d1c(i,j) < d1cp(i,j)
            d1c(i,j)=d1cp(i,j);
        end
    end
end
save temp w d1a d1b d1c n
clear
load temp
dn1n1=[w' 20*log10(d1a(1,:)+d1b(1,:)+d1c(1,:))'];
dn1n2=[w' 20*log10(d1a(2,:)+d1b(2,:)+d1c(2,:))'];
dn1n3=[w' 20*log10(d1a(3,:)+d1b(3,:)+d1c(3,:))'];
dn1n4=[w' 20*log10(d1a(4,:)+d1b(4,:)+d1c(4,:))'];
```

DIST1 - Calculates elements of the distuebance boundary for the first loop of the sequential process

```
function [d1a,d1b,d1c]=dist1(a,b,c,w,n,t1,t2,t3,t4)
% function [d1a,d1b,d1c]=dist1(a,b,c,w,n,t1,t2,t3,t4)
%
% This function calculates the elements of the disturbance
% signal at the frequencies specified in w.
%
% a, b, and c are the state matrices such that
%       x-dot = a x + b u
%       y     = c x
%
% w is the vector of frequencies at which the magnitude and phase
%       are calculated
%
% n is the array of loop indeces indicating the order
%       of the sequential process
%
% d1a, d1b, and d1c are the components of the disturbance signal
%       such that d1=d1a+d1b+d1c.  DIST1SEQ will use this info
%       from each model to determine the maximum possible dist.
%
x=size(w);
imax=max(x);
for i=1:imax
   omeg=w(i);
   tmp1=j*omeg*ones(1,28);
   tmp2=diag(tmp1,0);
   sima=tmp2-a;
   simai=eye(28,28)/sima;
   bodmgph=c*simai*b;
   bodmgphi=eye(4,4)/bodmgph;
   p12=bodmgphi(n(1),n(2));
   p13=bodmgphi(n(1),n(3));
   p14=bodmgphi(n(1),n(4));
  d1a(:,i)=abs(p12)*t2(:,i)./t1(:,i);
  d1b(:,i)=abs(p13)*t3(:,i)./t1(:,i);
  d1c(:,i)=abs(p14)*t4(:,i)./t1(:,i);
end
```

NOM2SEQ - Creates nominal plant data file for second loop of sequential process

```
function [nommag,nomphs]=nom2seq(a,b,c,w,n,g1,sav)
% function [nommag,nomphs]=nom2seq(a,b,c,w,n,g1,sav)
%
% This function calculates the nominal plant magnitude and
% phase at the frequencies designated in w.
%
% a, b, and c are the state matrices such that
%       x-dot = a x + b u
%       y     = c x
%
% w is the vector of frequencies at which the magnitude and phase
%       are calculated
%
% n is the array of loop indeces indicating the order
%       of the sequential process
%
% g1 is the first feedback compensator evaluated at the specified
%       frequencies
%
% nommag and nomphs are the magnitude and phase vectors,
%       respectively
%
% if sav = 1, then the sav_nom function is called to save the
%       data in nomplant.qn1
%
x=size(w);
imax=max(x);
nommag=zeros(1,imax);
nomphs=zeros(1,imax);
for i=1:imax
   omeg=w(i);
   tmp1=j*omeg*ones(1,28);
   tmp2=diag(tmp1,0);
   sima=tmp2-a;
   simai=eye(28,28)/sima;
   bodmgph=c*simai*b;
   bodmgphi=eye(4,4)/bodmgph;
   q11=1./bodmgphi(n(1),n(1));
   q12=1./bodmgphi(n(1),n(2));
   q21=1./bodmgphi(n(2),n(1));
   q22=1./bodmgphi(n(2),n(2));
  gamma12=q11*q22/q12/q21;
```

```
   L1=g1(i)*q11;
   q=q22*(1+L1)/(1+L1-gamma12);
    nommag(i)=20*log10(abs(q));
    nomphs(i)=180*atan2(imag(q),real(q))/pi;
    if i>1
       if nomphs(i)>nomphs(i-1)+300
          nomphs(i)=nomphs(i)-360;
       elseif nomphs(i)<nomphs(i-1)-300
          nomphs(i)=nomphs(i)+360;
       end
    end
end
if nargin == 7
    if sav == 1
        ext=[ 'q' int2str(n(2)) '2' ]
        sav_nom(w,nommag,nomphs,1,ext)
    end
end
```

TEMP2SEQ - Creates template data files for second loop of sequential process

```
% This script file utilizes the function NOM2SEQ to determine
% the templates for the first loop of the sequential process.
% Be sure n is defined as the array of indeces indicating the
% order of the sequential loop process.  Also, g1num and g1den
% must be defined as the numerator and denominator coefficient
% vectors of the first feedback compensator.
%
load model01m
w=[.3 .5 1 3 5 10 20 40 80];
[mag1,phs1]=nom2seq(a,b,c,w,n,g1);
[nr,nc]=size(mag1);
if nr == 1
    tmag=mag1;
    tphs=phs1;
else
    tmag=mag1';
    tphs=phs1';
end
save temp w tmag tphs n g1
clear
load model20m
load temp
```

```
[mag1,phs1]=nom2seq(a,b,c,w,n,g1);
[nr,nc]=size(mag1);
if nr == 1
    tmag=[tmag;mag1];
    tphs=[tphs;phs1];
else
    tmag=[tmag;mag1'];
    tphs=[tphs;phs1'];
end
save temp w tmag tphs n g1
clear
load model40m
load temp
[mag1,phs1]=nom2seq(a,b,c,w,n,g1);
[nr,nc]=size(mag1);
if nr == 1
    tmag=[tmag;mag1];
    tphs=[tphs;phs1];
else
    tmag=[tmag;mag1'];
    tphs=[tphs;phs1'];
end
save temp w tmag tphs n g1
clear
load model60m
load temp
[mag1,phs1]=nom2seq(a,b,c,w,n,g1);
[nr,nc]=size(mag1);
if nr == 1
    tmag=[tmag;mag1];
    tphs=[tphs;phs1];
else
    tmag=[tmag;mag1'];
    tphs=[tphs;phs1'];
end
save temp w tmag tphs n g1
clear
load model80m
load temp
[mag1,phs1]=nom2seq(a,b,c,w,n,g1);
[nr,nc]=size(mag1);
if nr == 1
    tmag=[tmag;mag1];
    tphs=[tphs;phs1];
```

```
else
    tmag=[tmag;mag1'];
    tphs=[tphs;phs1'];
end
save temp w tmag tphs n g1
clear
load modl100m
load temp
[mag1,phs1]=nom2seq(a,b,c,w,n,g1);
[nr,nc]=size(mag1);
if nr == 1
    tmag=[tmag;mag1];
    tphs=[tphs;phs1];
else
    tmag=[tmag;mag1'];
    tphs=[tphs;phs1'];
end
save temp w tmag tphs n g1
clear
load temp
x=size(w);
imax=max(x);
ext=[ 'q' int2str(n(2)) '2' ]
template(imax,tmag,tphs,1,ext)
```

DIST2SEQ - Creates the disturbance boundaries for the second loop of the sequential process

```
% This script file utilizes the function DIST2 to determine
% the disturbance bounds for the first loop of the
% sequential process.  Be sure to set n to the array of indices
% indicating the sequence of loop closure.  TBNDS.MAT contains
% the bound matrices.
%
load tbnds
load model01m
w=[.3 .5 1 3 5 10 20 40 80];
[d2a,d2b,d2c]=dist2(a,b,c,w,n,t2,t3,t4,g1,f1);
save temp w d2a d2b d2c n t2 t3 t4 g1 f1
clear
load model20m
load temp
[d2ap,d2bp,d2cp]=dist2(a,b,c,w,n,t2,t3,t4,g1,f1);
```

```
for i=1:4
    for j=1:max(size(w))
        if d2a(i,j) < d2ap(i,j)
            d2a(i,j)=d2ap(i,j);
        end
        if d2b(i,j) < d2bp(i,j)
            d2b(i,j)=d2bp(i,j);
        end
        if d2c(i,j) < d2cp(i,j)
            d2c(i,j)=d2cp(i,j);
        end
    end
end
save temp w d2a d2b d2c n t2 t3 t4 g1 f1
clear
load model40m
load temp
[d2ap,d2bp,d2cp]=dist2(a,b,c,w,n,t2,t3,t4,g1,f1);
for i=1:4
    for j=1:max(size(w))
        if d2a(i,j) < d2ap(i,j)
            d2a(i,j)=d2ap(i,j);
        end
        if d2b(i,j) < d2bp(i,j)
            d2b(i,j)=d2bp(i,j);
        end
        if d2c(i,j) < d2cp(i,j)
            d2c(i,j)=d2cp(i,j);
        end
    end
end
save temp w d2a d2b d2c n t2 t3 t4 g1 f1
clear
load model60m
load temp
[d2ap,d2bp,d2cp]=dist2(a,b,c,w,n,t2,t3,t4,g1,f1);
for i=1:4
    for j=1:max(size(w))
        if d2a(i,j) < d2ap(i,j)
            d2a(i,j)=d2ap(i,j);
        end
        if d2b(i,j) < d2bp(i,j)
            d2b(i,j)=d2bp(i,j);
        end
```

```
        if d2c(i,j) < d2cp(i,j)
            d2c(i,j)=d2cp(i,j);
        end
    end
end
save temp w d2a d2b d2c n t2 t3 t4 g1 f1
clear
load model80m
load temp
[d2ap,d2bp,d2cp]=dist2(a,b,c,w,n,t2,t3,t4,g1,f1);
for i=1:4
    for j=1:max(size(w))
        if d2a(i,j) < d2ap(i,j)
            d2a(i,j)=d2ap(i,j);
        end
        if d2b(i,j) < d2bp(i,j)
            d2b(i,j)=d2bp(i,j);
        end
        if d2c(i,j) < d2cp(i,j)
            d2c(i,j)=d2cp(i,j);
        end
    end
end
save temp w d2a d2b d2c n t2 t3 t4 g1 f1
clear
load modl100m
load temp
[d2ap,d2bp,d2cp]=dist2(a,b,c,w,n,t2,t3,t4,g1,f1);
for i=1:4
    for j=1:max(size(w))
        if d2a(i,j) < d2ap(i,j)
            d2a(i,j)=d2ap(i,j);
        end
        if d2b(i,j) < d2bp(i,j)
            d2b(i,j)=d2bp(i,j);
        end
        if d2c(i,j) < d2cp(i,j)
            d2c(i,j)=d2cp(i,j);
        end
    end
end
save temp w d2a d2b d2c n t2 t3 t4 g1 f1
clear
load temp
```

```
dn2n1=[w' 20*log10(d2a(1,:)+d2b(1,:)+d2c(1,:))'];
dn2n2=[w' 20*log10(d2a(2,:)+d2b(2,:)+d2c(2,:))'];
dn2n3=[w' 20*log10(d2a(3,:)+d2b(3,:)+d2c(3,:))'];
dn2n4=[w' 20*log10(d2a(4,:)+d2b(4,:)+d2c(4,:))'];
```

DIST2 - Calculates elements of the distuebance boundary for the second loop of the sequential process

```
function [d2a,d2b,d2c]=dist2(a,b,c,w,n,t2,t3,t4,g1,f1)
% function [d2a,d2b,d2c]=dist2(a,b,c,w,n,t2,t3,t4,g1,f1)
%
% This function calculates the elements of the disturbance
% signal at the frequencies specified in w for the second
% loop of the sequence.
%
% a, b, and c are the state matrices such that
%       x-dot = a x + b u
%       y     = c x
%
% w is the vector of frequencies at which the magnitude and phase
%       are calculated
%
% n is the array of loop indeces indicating the order
%       of the sequential process
%
% t2,t3, and t4 are the boundary matrices
%
% g1 and f1 are the feedback compensator and prefilters for the
%      first loop of the sequence evaluated at the specified
%      frequencies.
%
% d2a, d2b, and d2c are the components of the disturbance signal
%      such that d2=d2a+d2b+d2c.  DIST2SEQ will use this info
%      from each model to determine the maximum possible dist.
%
x=size(w);
imax=max(x);
for i=1:imax
   omeg=w(i);
   tmp1=j*omeg*ones(1,28);
   tmp2=diag(tmp1,0);
   sima=tmp2-a;
   simai=eye(28,28)/sima;
```

```
    bodmgph=c*simai*b;
    bodmgphi=eye(4,4)/bodmgph;
    p13=bodmgphi(n(1),n(3));
    p14=bodmgphi(n(1),n(4));
    p21=bodmgphi(n(2),n(1));
    p23=bodmgphi(n(2),n(3));
    p24=bodmgphi(n(2),n(4));
    q11=1.0 / bodmgphi(n(1),n(1));
    d2at=q11*p13*p21/(1+g1(i)*q11)-p23;
    d2bt=q11*p14*p21/(1+g1(i)*q11)-p24;
    d2ct=p21*g1(i)*q11/(1+g1(i)*q11);
    d2a(:,i)=abs(d2at)*t3(:,i)./t2(:,i);
    d2b(:,i)=abs(d2bt)*t4(:,i)./t2(:,i);
    d2c(:,i)=abs(d2ct*f1(:,i))./t2(:,i);
end
```

NOM3SEQ - Creates nominal plant data file for third loop of sequential process

```
function [nommag,nomphs]=nom3seq(a,b,c,w,n,g1,g2,sav)
% function [nommag,nomphs]=nom3seq(a,b,c,w,n,g1,g2,sav)
%
% This function calculates the nominal plant magnitude and
% phase at the frequencies designated in w.
%
% a, b, and c are the state matrices such that
%       x-dot = a x + b u
%       y     = c x
%
% w is the vector of frequencies at which the magnitude and phase
%       are calculated
%
% n is the array of loop indeces indicating the order
%       of the sequential process
%
% g1 and g2 are the first two feedback compensators evaluated at
%      the specified frequencies
%
% nommag and nomphs are the magnitude and phase vectors,
%       respectively
%
% if sav = 1, then the sav_nom function is called to save the
%       data in nomplant.qn3
```

```
%
x=size(w);
imax=max(x);
nommag=zeros(1,imax);
nomphs=zeros(1,imax);
for i=1:imax
    omeg=w(i);
    tmp1=j*omeg*ones(1,28);
    tmp2=diag(tmp1,0);
    sima=tmp2-a;
    simai=eye(28,28)/sima;
    bodmgph=c*simai*b;
    bodmgphi=eye(4,4)/bodmgph;
    q11=1./bodmgphi(n(1),n(1));
    q12=1./bodmgphi(n(1),n(2));
    q13=1./bodmgphi(n(1),n(3));
    q14=1./bodmgphi(n(1),n(4));
    q21=1./bodmgphi(n(2),n(1));
    q22=1./bodmgphi(n(2),n(2));
    q23=1./bodmgphi(n(2),n(3));
    q24=1./bodmgphi(n(2),n(4));
    q31=1./bodmgphi(n(3),n(1));
    q32=1./bodmgphi(n(3),n(2));
    q33=1./bodmgphi(n(3),n(3));
    q34=1./bodmgphi(n(3),n(4));
    gamma12=q11*q22/q12/q21;
    gamma13=q11*q33/q13/q31;
    gamma23=q22*q33/q23/q32;
    mu2=q21*q33/q23/q31;
    mu3=q31*q22/q32/q21;

    L1=g1(i)*q11;
    L2=g2(i)*q22;
    zeta12=(1+L1)*(1+L2)-gamma12;
    Lam3=gamma23*(1+L1)+gamma13*(1+L2)-(gamma12*mu2+gamma13*mu3);
    q=q33*zeta12/(zeta12-Lam3);
    nommag(i)=20*log10(abs(q));
    nomphs(i)=180*atan2(imag(q),real(q))/pi;
    if i>1
        if nomphs(i)>nomphs(i-1)+300
            nomphs(i)=nomphs(i)-360;
        elseif nomphs(i)<nomphs(i-1)-300
            nomphs(i)=nomphs(i)+360;
        end
```

```
   end
end
if nargin == 8
    if sav == 1
        ext=[ 'q' int2str(n(3)) '3' ]
        sav_nom(w,nommag,nomphs,1,ext)
    end
end
```

TEMP3SEQ - Creates template data files for third loop of sequential process

```
% This script file utilizes the function NOM3SEQ to determine
% the templates for the first loop of the sequential process.
% Be sure n is defined as the array of indeces indicating the
% order of the sequential loop process.  Also, g1 and g2
% must be defined as the feedback compensators for the first
% two loops evaluated at the specified frequencies.
%
load model01m
w=[.3 .5 1 3 5 10 20 40 80];
[mag1,phs1]=nom3seq(a,b,c,w,n,g1,g2);
[nr,nc]=size(mag1);
if nr == 1
    tmag=mag1;
    tphs=phs1;
else
    tmag=mag1';
    tphs=phs1';
end
save temp w tmag tphs n g1 g2
clear
load model20m
load temp
[mag1,phs1]=nom3seq(a,b,c,w,n,g1,g2);
[nr,nc]=size(mag1);
if nr == 1
    tmag=[tmag;mag1];
    tphs=[tphs;phs1];
else
    tmag=[tmag;mag1'];
    tphs=[tphs;phs1'];
end
save temp w tmag tphs n g1 g2
```

```
clear
load model40m
load temp
[mag1,phs1]=nom3seq(a,b,c,w,n,g1,g2);
[nr,nc]=size(mag1);
if nr == 1
    tmag=[tmag;mag1];
    tphs=[tphs;phs1];
else
    tmag=[tmag;mag1'];
    tphs=[tphs;phs1'];
end
save temp w tmag tphs n g1 g2
clear
load model60m
load temp
[mag1,phs1]=nom3seq(a,b,c,w,n,g1,g2);
[nr,nc]=size(mag1);
if nr == 1
    tmag=[tmag;mag1];
    tphs=[tphs;phs1];
else
    tmag=[tmag;mag1'];
    tphs=[tphs;phs1'];
end
save temp w tmag tphs n g1 g2
clear
load model80m
load temp
[mag1,phs1]=nom3seq(a,b,c,w,n,g1,g2);
[nr,nc]=size(mag1);
if nr == 1
    tmag=[tmag;mag1];
    tphs=[tphs;phs1];
else
    tmag=[tmag;mag1'];
    tphs=[tphs;phs1'];
end
save temp w tmag tphs n g1 g2
clear
load modl100m
load temp
[mag1,phs1]=nom3seq(a,b,c,w,n,g1,g2);
[nr,nc]=size(mag1);
```

```
if nr == 1
    tmag=[tmag;mag1];
    tphs=[tphs;phs1];
else
    tmag=[tmag;mag1'];
    tphs=[tphs;phs1'];
end
save temp w tmag tphs n g1 g2
clear
load temp
x=size(w);
imax=max(x);
ext=[ 'q' int2str(n(3)) '3' ]
template(imax,tmag,tphs,1,ext)
```

DIST3SEQ - Creates the disturbance boundaries for the third loop of the sequential process

```
% This script file utilizes the function DIST3 to determine
% the disturbance bounds for the first loop of the
% sequential process.  Be sure to set n to the array of indices
% indicating the sequence of loop closure.  TBNDS.MAT contains
% the bound matrices.
%
load tbnds
load model01m
w=[.3 .5 1 3 5 10 20 40 80];
[d3a,d3b,d3c]=dist3(a,b,c,w,n,t3,t4,g1,f1,g2,f2);
save temp w d3a d3b d3c n t3 t4 g1 f1 g2 f2
clear
load model20m
load temp
[d3ap,d3bp,d3cp]=dist3(a,b,c,w,n,t3,t4,g1,f1,g2,f2);
for i=1:4
    for j=1:max(size(w))
        if d3a(i,j) < d3ap(i,j)
            d3a(i,j)=d3ap(i,j);
        end
        if d3b(i,j) < d3bp(i,j)
            d3b(i,j)=d3bp(i,j);
        end
        if d3c(i,j) < d3cp(i,j)
            d3c(i,j)=d3cp(i,j);
```

```
        end
    end
end
save temp w d3a d3b d3c n t3 t4 g1 f1 g2 f2
clear
load model40m
load temp
[d3ap,d3bp,d3cp]=dist3(a,b,c,w,n,t3,t4,g1,f1,g2,f2);
for i=1:4
    for j=1:max(size(w))
        if d3a(i,j) < d3ap(i,j)
            d3a(i,j)=d3ap(i,j);
        end
        if d3b(i,j) < d3bp(i,j)
            d3b(i,j)=d3bp(i,j);
        end
        if d3c(i,j) < d3cp(i,j)
            d3c(i,j)=d3cp(i,j);
        end
    end
end
save temp w d3a d3b d3c n t3 t4 g1 f1 g2 f2
clear
load model60m
load temp
[d3ap,d3bp,d3cp]=dist3(a,b,c,w,n,t3,t4,g1,f1,g2,f2);
for i=1:4
    for j=1:max(size(w))
        if d3a(i,j) < d3ap(i,j)
            d3a(i,j)=d3ap(i,j);
        end
        if d3b(i,j) < d3bp(i,j)
            d3b(i,j)=d3bp(i,j);
        end
        if d3c(i,j) < d3cp(i,j)
            d3c(i,j)=d3cp(i,j);
        end
    end
end
save temp w d3a d3b d3c n t3 t4 g1 f1 g2 f2
clear
load model80m
load temp
[d3ap,d3bp,d3cp]=dist3(a,b,c,w,n,t3,t4,g1,f1,g2,f2);
```

```
for i=1:4
    for j=1:max(size(w))
        if d3a(i,j) < d3ap(i,j)
            d3a(i,j)=d3ap(i,j);
        end
        if d3b(i,j) < d3bp(i,j)
            d3b(i,j)=d3bp(i,j);
        end
        if d3c(i,j) < d3cp(i,j)
            d3c(i,j)=d3cp(i,j);
        end
    end
end
save temp w d3a d3b d3c n t3 t4 g1 f1 g2 f2
clear
load mod1100m
load temp
[d3ap,d3bp,d3cp]=dist3(a,b,c,w,n,t3,t4,g1,f1,g2,f2);
for i=1:4
    for j=1:max(size(w))
        if d3a(i,j) < d3ap(i,j)
            d3a(i,j)=d3ap(i,j);
        end
        if d3b(i,j) < d3bp(i,j)
            d3b(i,j)=d3bp(i,j);
        end
        if d3c(i,j) < d3cp(i,j)
            d3c(i,j)=d3cp(i,j);
        end
    end
end
save temp w d3a d3b d3c n
clear
load temp
dn3n1=[w' 20*log10(d3a(1,:)+d3b(1,:)+d3c(1,:))'];
dn3n2=[w' 20*log10(d3a(2,:)+d3b(2,:)+d3c(2,:))'];
dn3n3=[w' 20*log10(d3a(3,:)+d3b(3,:)+d3c(3,:))'];
dn3n4=[w' 20*log10(d3a(4,:)+d3b(4,:)+d3c(4,:))'];
```

DIST3 - Calculates elements of the distuebance boundary for the third loop of the sequential process

```
function [d3a,d3b,d3c]=dist3(a,b,c,w,n,t3,t4,g1,f1,g2,f2)
% function [d3a,d3b,d3c]=dist3(a,b,c,w,n,t3,t4,g1,f1,g2,f2)
%
% This function calculates the elements of the disturbance
% signal at the frequencies specified in w for the second
% loop of the sequence.
%
% a, b, and c are the state matrices such that
%       x-dot = a x + b u
%       y     = c x
%
% w is the vector of frequencies at which the magnitude and phase
%       are calculated
%
% n is the array of loop indeces indicating the order
%       of the sequential process
%
% t3 and t4 are the boundary matrices
%
% g1, g2, f1 and f2 are the feedback compensator and prefilters
%       for the first two loops of the sequence evaluated at the
%       specified frequencies.
%
% d3a, d3b, and d3c are the components of the disturbance signal
%       such that d3=d3a+d3b+d3c.  DIST3SEQ will use this info
%       from each model to determine the maximum possible dist.
%
x=size(w);
imax=max(x);
for i=1:imax
   omeg=w(i);
   tmp1=j*omeg*ones(1,28);
   tmp2=diag(tmp1,0);
   sima=tmp2-a;
   simai=eye(28,28)/sima;
   bodmgph=c*simai*b;
   bodmgphi=eye(4,4)/bodmgph;
   q11=1.0 / bodmgphi(n(1),n(1));
   q12=1.0 / bodmgphi(n(1),n(2));
   q13=1.0 / bodmgphi(n(1),n(3));
   q14=1.0 / bodmgphi(n(1),n(4));
```

```
    q21=1.0 / bodmgphi(n(2),n(1));
    q22=1.0 / bodmgphi(n(2),n(2));
    q23=1.0 / bodmgphi(n(2),n(3));
    q24=1.0 / bodmgphi(n(2),n(4));
    q31=1.0 / bodmgphi(n(3),n(1));
    q32=1.0 / bodmgphi(n(3),n(2));
    q33=1.0 / bodmgphi(n(3),n(3));
    q34=1.0 / bodmgphi(n(3),n(4));
    gamma12=q11*q22/q12/q21;
    gamma13=q11*q33/q13/q31;
    gamma23=q22*q33/q23/q32;
    L1=g1(i)*q11;
    L2=g2(i)*q22;
    zeta12=(1+L1)*(1+L2)-gamma12;
    eta1=q22/q21/q32-(1+L2)/q31;
    eta2=q11/q31/q12-(1+L1)/q32;
    beta4=q21/q31/q24+q12/q32/q14;
    eps3=q11*(1+L2)/q31/q14+q22*(1+L1)/q32/q24- ...
       zeta12/q34-gamma12*beta4;
    d3ct=eps3/zeta12;
    d3at=L1*eta1/zeta12;
    d3bt=L2*eta2/zeta12;
    d3a(:,i)=abs(d3at*f1(:,i))./t3(:,i);
    d3b(:,i)=abs(d3bt*f2(:,i))./t3(:,i);
    d3c(:,i)=abs(d3ct)*t4(:,i)./t3(:,i);
end
```

NOM4SEQ - Creates nominal plant data file for fourth loop of sequential process

```
function [nommag,nomphs]=nom4seq(a,b,c,w,n,g1,g2,g3,sav)
% function [nommag,nomphs]=nom4seq(a,b,c,w,n,g1,g2,g3,sav)
%
% This function calculates the nominal plant magnitude and
% phase at the frequencies designated in w.
%
% a, b, and c are the state matrices such that
%       x-dot = a x + b u
%       y     = c x
%
% w is the vector of frequencies at which the magnitude and phase
%       are calculated
%
% n is the array of loop indeces indicating the order
```

```
%       of the sequential process
%
% g1, g2, and g3 are the first three feedback compensators
%       evaluated at the specified frequencies
%
% nommag and nomphs are the magnitude and phase vectors,
%       respectively
%
% if sav = 1, then the sav_nom function is called to save the
%       data in nomplant.qn3
%
x=size(w);
imax=max(x);
nommag=zeros(1,imax);
nomphs=zeros(1,imax);
for i=1:imax
    omeg=w(i);
    tmp1=j*omeg*ones(1,28);
    tmp2=diag(tmp1,0);
    sima=tmp2-a;
    simai=eye(28,28)/sima;
    bodmgph=c*simai*b;
    bodmgphi=eye(4,4)/bodmgph;
    q11=1./bodmgphi(n(1),n(1));
    q12=1./bodmgphi(n(1),n(2));
    q13=1./bodmgphi(n(1),n(3));
    q14=1./bodmgphi(n(1),n(4));
    q21=1./bodmgphi(n(2),n(1));
    q22=1./bodmgphi(n(2),n(2));
    q23=1./bodmgphi(n(2),n(3));
    q24=1./bodmgphi(n(2),n(4));
    q31=1./bodmgphi(n(3),n(1));
    q32=1./bodmgphi(n(3),n(2));
    q33=1./bodmgphi(n(3),n(3));
    q34=1./bodmgphi(n(3),n(4));
    q41=1./bodmgphi(n(4),n(1));
    q42=1./bodmgphi(n(4),n(2));
    q43=1./bodmgphi(n(4),n(3));
    q44=1./bodmgphi(n(4),n(4));
    gamma12=q11*q22/q12/q21;
    gamma13=q11*q33/q13/q31;
    gamma14=q11*q44/q14/q41;
    gamma23=q22*q33/q23/q32;
    gamma24=q22*q44/q24/q42;
```

```
    gamma34=q33*q44/q34/q43;
    mu2=q21*q33/q23/q31;
    mu3=q31*q22/q32/q21;
    L1=g1(i)*q11;
    L2=g2(i)*q22;
    L3=g3(i)*q33;
    zeta12=(1+L1)*(1+L2)-gamma12;
    zeta13=(1+L1)*(1+L3)-gamma13;
    zeta23=(1+L2)*(1+L3)-gamma23;
    Lam3=gamma23*(1+L1)+gamma13*(1+L2)-(gamma12*mu2+gamma13*mu3);
    Xi=(1+L3)*zeta12-Lam3;
    rho41=q11*q22*q33*q44/(q12*q23*q34*q41);
    rho42=q11*q22*q33*q44/(q12*q24*q31*q43);
    rho43=q11*q22*q33*q44/(q13*q21*q34*q42);
    rho44=q11*q22*q33*q44/(q13*q24*q32*q41);
    rho45=q11*q22*q33*q44/(q14*q21*q32*q43);
    rho46=q11*q22*q33*q44/(q14*q23*q31*q42);
    rho4=rho41+rho42+rho43+rho44+rho45+rho46;
    nu1=q22*q33*q44/(q23*q34*q42)+q22*q33*q44/(q24*q32*q43);
    nu2=q11*q33*q44/(q13*q34*q41)+q11*q33*q44/(q14*q31*q43);
    nu3=q11*q22*q44/(q12*q24*q41)+q11*q22*q44/(q14*q21*q42);
    Lam41=gamma34*zeta12+gamma24*zeta13+gamma14*zeta23;
    Lam42=(1+L1)*nu1+(1+L2)*nu2+(1+L3)*nu3;
    Lam4=Lam41-Lam42+rho4;
    q=q44*Xi/(Xi-Lam4);
    nommag(i)=20*log10(abs(q));
    nomphs(i)=180*atan2(imag(q),real(q))/pi;
    if i>1
       if nomphs(i)>nomphs(i-1)+300
          nomphs(i)=nomphs(i)-360;
       elseif nomphs(i)<nomphs(i-1)-300
          nomphs(i)=nomphs(i)+360;
       end
    end
end
if nargin == 9
    if sav == 1
       ext=[ 'q' int2str(n(4)) '4' ]
       sav_nom(w,nommag,nomphs,1,ext)
    end
end
```

TEMP4SEQ - Creates template data files for fourth loop of sequential process

```
% This script file utilizes the function NOM4SEQ to determine
% the templates for the first loop of the sequential process.
% Be sure n is defined as the array of indeces indicating the
% order of the sequential loop process.  Also, g1, g2, and g3
% must be defined as the feedback compensators for the first
% three loops evaluated at the specified frequencies.
%
load model01m
w=[.3 .5 1 3 5 10 20 40 80];
[mag1,phs1]=nom4seq(a,b,c,w,n,g1,g2,g3);
[nr,nc]=size(mag1);
if nr == 1
    tmag=mag1;
    tphs=phs1;
else
    tmag=mag1';
    tphs=phs1';
end
save temp w tmag tphs n g1 g2 g3
clear
load model20m
load temp
[mag1,phs1]=nom4seq(a,b,c,w,n,g1,g2,g3);
[nr,nc]=size(mag1);
if nr == 1
    tmag=[tmag;mag1];
    tphs=[tphs;phs1];
else
    tmag=[tmag;mag1'];
    tphs=[tphs;phs1'];
end
save temp w tmag tphs n g1 g2 g3
clear
load model40m
load temp
[mag1,phs1]=nom4seq(a,b,c,w,n,g1,g2,g3);
[nr,nc]=size(mag1);
if nr == 1
    tmag=[tmag;mag1];
    tphs=[tphs;phs1];
else
    tmag=[tmag;mag1'];
```

```
    tphs=[tphs;phs1'];
end
save temp w tmag tphs n g1 g2 g3
clear
load model60m
load temp
[mag1,phs1]=nom4seq(a,b,c,w,n,g1,g2,g3);
[nr,nc]=size(mag1);
if nr == 1
    tmag=[tmag;mag1];
    tphs=[tphs;phs1];
else
    tmag=[tmag;mag1'];
    tphs=[tphs;phs1'];
end
save temp w tmag tphs n g1 g2 g3
clear
load model80m
load temp
[mag1,phs1]=nom4seq(a,b,c,w,n,g1,g2,g3);
[nr,nc]=size(mag1);
if nr == 1
    tmag=[tmag;mag1];
    tphs=[tphs;phs1];
else
    tmag=[tmag;mag1'];
    tphs=[tphs;phs1'];
end
save temp w tmag tphs n g1 g2 g3
clear
load modl100m
load temp
[mag1,phs1]=nom4seq(a,b,c,w,n,g1,g2,g3);
[nr,nc]=size(mag1);
if nr == 1
    tmag=[tmag;mag1];
    tphs=[tphs;phs1];
else
    tmag=[tmag;mag1'];
    tphs=[tphs;phs1'];
end
save temp w tmag tphs n g1 g2 g3
clear
load temp
```

```
x=size(w);
imax=max(x);
ext=[ 'q' int2str(n(4)) '4' ]
template(imax,tmag,tphs,1,ext)
```

DIST4SEQ - Creates the disturbance boundaries for the fourth loop of the sequential process

```
% This script file utilizes the function DIST4 to determine
% the disturbance bounds for the first loop of the
% sequential process.  Be sure to set n to the array of indices
% indicating the sequence of loop closure.  TBNDS.MAT contains
% the bound matrices.
%
load tbnds
load model01m
w=[.3 .5 1 3 5 10 20 40 80];
[d4a,d4b,d4c]=dist4(a,b,c,w,n,t4,g1,f1,g2,f2,g3,f3);
save temp w d4a d4b d4c n t4 g1 f1 g2 f2 g3 f3
clear
load model20m
load temp
[d4ap,d4bp,d4cp]=dist4(a,b,c,w,n,t4,g1,f1,g2,f2,g3,f3);
for i=1:4
    for j=1:max(size(w))
        if d4a(i,j) < d4ap(i,j)
            d4a(i,j)=d4ap(i,j);
        end
        if d4b(i,j) < d4bp(i,j)
            d4b(i,j)=d4bp(i,j);
        end
        if d4c(i,j) < d4cp(i,j)
            d4c(i,j)=d4cp(i,j);
        end
    end
end
save temp w d4a d4b d4c n t4 g1 f1 g2 f2 g3 f3
clear
load model40m
load temp
[d4ap,d4bp,d4cp]=dist4(a,b,c,w,n,t4,g1,f1,g2,f2,g3,f3);
for i=1:4
    for j=1:max(size(w))
```

```
        if d4a(i,j) < d4ap(i,j)
            d4a(i,j)=d4ap(i,j);
        end
        if d4b(i,j) < d4bp(i,j)
            d4b(i,j)=d4bp(i,j);
        end
        if d4c(i,j) < d4cp(i,j)
            d4c(i,j)=d4cp(i,j);
        end
    end
end
save temp w d4a d4b d4c n t4 g1 f1 g2 f2 g3 f3
clear
load model60m
load temp
[d4ap,d4bp,d4cp]=dist4(a,b,c,w,n,t4,g1,f1,g2,f2,g3,f3);
for i=1:4
    for j=1:max(size(w))
        if d4a(i,j) < d4ap(i,j)
            d4a(i,j)=d4ap(i,j);
        end
        if d4b(i,j) < d4bp(i,j)
            d4b(i,j)=d4bp(i,j);
        end
        if d4c(i,j) < d4cp(i,j)
            d4c(i,j)=d4cp(i,j);
        end
    end
end
save temp w d4a d4b d4c n t4 g1 f1 g2 f2 g3 f3
clear
load model80m
load temp
[d4ap,d4bp,d4cp]=dist4(a,b,c,w,n,t4,g1,f1,g2,f2,g3,f3);
for i=1:4
    for j=1:max(size(w))
        if d4a(i,j) < d4ap(i,j)
            d4a(i,j)=d4ap(i,j);
        end
        if d4b(i,j) < d4bp(i,j)
            d4b(i,j)=d4bp(i,j);
        end
        if d4c(i,j) < d4cp(i,j)
            d4c(i,j)=d4cp(i,j);
```

```
        end
    end
end
save temp w d4a d4b d4c n t4 g1 f1 g2 f2 g3 f3
clear
load modl100m
load temp
[d4ap,d4bp,d4cp]=dist4(a,b,c,w,n,t4,g1,f1,g2,f2,g3,f3);
for i=1:4
    for j=1:max(size(w))
        if d4a(i,j) < d4ap(i,j)
            d4a(i,j)=d4ap(i,j);
        end
        if d4b(i,j) < d4bp(i,j)
            d4b(i,j)=d4bp(i,j);
        end
        if d4c(i,j) < d4cp(i,j)
            d4c(i,j)=d4cp(i,j);
        end
    end
end
save temp w d4a d4b d4c n
clear
load temp
d41=(d4a(1,:)+d4b(1,:)+d4c(1,:))';
d42=(d4a(2,:)+d4b(2,:)+d4c(2,:))';
d43=(d4a(3,:)+d4b(3,:)+d4c(3,:))';
d44=(d4a(4,:)+d4b(4,:)+d4c(4,:))';
imax=max(size(w));
for i=1:imax
            if d41(i) > .00001
                ld41(i,1)=20*log10(d41(i));
            else
                ld41(i,1)=-100.;
            end
            if d42(i) > .00001
                ld42(i,1)=20*log10(d42(i));
            else
                ld42(i,1)=-100.;
            end
            if d43(i) > .00001
                ld43(i,1)=20*log10(d43(i));
            else
                ld43(i,1)=-100.;
```

```
        end
        if d44(i) > .00001
            ld44(i,1)=20*log10(d44(i));
        else
            ld44(i,1)=-100.;
        end
end
dn4n1=[w' ld41];
dn4n2=[w' ld42];
dn4n3=[w' ld43];
dn4n4=[w' ld44];
```

DIST4 - Calculates elements of the distuebance boundary for the fourth loop of the sequential process

```
function [d4a,d4b,d4c]=dist4(a,b,c,w,n,t4,g1,f1,g2,f2,g3,f3)
% function [d4a,d4b,d4c]=dist4(a,b,c,w,n,t4,g1,f1,g2,f2,g3,f3)
%
% This function calculates the elements of the disturbance
% signal at the frequencies specified in w for the second
% loop of the sequence.
%
% a, b, and c are the state matrices such that
%       x-dot = a x + b u
%       y     = c x
%
% w is the vector of frequencies at which the magnitude and phase
%       are calculated
%
% n is the array of loop indeces indicating the order
%       of the sequential process
%
% t3 and t4 are the boundary matrices
%
% g1, g2, g3, f1, f2 and f3 are the feedback compensator and
%       prefilters for the first three loops of the sequence
%       evaluated at the specified frequencies.
%
% d4a, d4b, and d4c are the components of the disturbance signal
%       such that d4=d4a+d4b+d4c.  DIST4SEQ will use this info
%       from each model to determine the maximum possible dist.
%
x=size(w);
```

```
imax=max(x);
for i=1:imax
    omeg=w(i);
    tmp1=j*omeg*ones(1,28);
    tmp2=diag(tmp1,0);
    sima=tmp2-a;
    simai=eye(28,28)/sima;
    bodmgph=c*simai*b;
    bodmgphi=eye(4,4)/bodmgph;
    q11=1./bodmgphi(n(1),n(1));
    q12=1./bodmgphi(n(1),n(2));
    q13=1./bodmgphi(n(1),n(3));
    q14=1./bodmgphi(n(1),n(4));
    q21=1./bodmgphi(n(2),n(1));
    q22=1./bodmgphi(n(2),n(2));
    q23=1./bodmgphi(n(2),n(3));
    q24=1./bodmgphi(n(2),n(4));
    q31=1./bodmgphi(n(3),n(1));
    q32=1./bodmgphi(n(3),n(2));
    q33=1./bodmgphi(n(3),n(3));
    q34=1./bodmgphi(n(3),n(4));
    q41=1./bodmgphi(n(4),n(1));
    q42=1./bodmgphi(n(4),n(2));
    q43=1./bodmgphi(n(4),n(3));
    q44=1./bodmgphi(n(4),n(4));
    gamma12=q11*q22/q12/q21;
    gamma13=q11*q33/q13/q31;
    gamma14=q11*q44/q14/q41;
    gamma23=q22*q33/q23/q32;
    gamma24=q22*q44/q24/q42;
    gamma34=q33*q44/q34/q43;
    mu2=q21*q33/q23/q31;
    mu3=q31*q22/q32/q21;
    L1=g1(i)*q11;
    L2=g2(i)*q22;
    L3=g3(i)*q33;
    zeta12=(1+L1)*(1+L2)-gamma12;
    zeta13=(1+L1)*(1+L3)-gamma13;
    zeta23=(1+L2)*(1+L3)-gamma23;
    Lam3=gamma23*(1+L1)+gamma13*(1+L2)-(gamma12*mu2+gamma13*mu3);
    Xi=(1+L3)*zeta12-Lam3;
    lamb11=-zeta23/q41;
    lamb12=(q22/q21*(1+L3)-q22*q33/q23/q31)/q42;
    lamb13=(q33/q31*(1+L2)-q22*q33/q21/q32)/q43;
```

```
    lamb1=lamb11+lamb12+lamb13;
    lamb21=(q11/q12*(1+L3)-q11*q22/q12/q23)/q41;
    lamb22=-zeta13/q42;
    lamb23=(q33/q31*(1+L1)-q11*q33/q12/q31)/q43;
    lamb2=lamb21+lamb22+lamb23;
    lamb31=(q11/q13*(1+L2)-q11*q22/q12/q23)/q41;
    lamb32=(q22/q23*(1+L1)-q11*q22/q13/q21)/q42;
    lamb33=-zeta12/q43;
    lamb3=lamb31+lamb32+lamb33;
    d4at=L1*lamb1/Xi;
    d4bt=L2*lamb2/Xi;
    d4ct=L3*lamb3/Xi;
    d4a(:,i)=abs(d4at*f1(:,i))./t4(:,i);
    d4b(:,i)=abs(d4bt*f2(:,i))./t4(:,i);
    d4c(:,i)=abs(d4ct*f3(:,i))./t4(:,i);
end
```

SEQ_BNDS - Creates boundary matrix for Sequential Loop Closure

```
% seq_bnds is an M-file that takes the boundary information in TBNDINFO.MAT
% and creates the boundary matrices t1, t2, t3, and t4 for use in the
% sequential loop closure process.  n must be defined as the array indicating
% the sequence of loop closure.
%
load tbndinfo
ind1=(n(1)-1)*4;
ind2=(n(2)-1)*4;
ind3=(n(3)-1)*4;
ind4=(n(4)-1)*4;
t1=[tbnd_info(ind1+n(1),:);tbnd_info(ind1+n(2),:); ...
    tbnd_info(ind1+n(3),:);tbnd_info(ind1+n(4),:)];
t2=[tbnd_info(ind2+n(1),:);tbnd_info(ind2+n(2),:); ...
    tbnd_info(ind2+n(3),:);tbnd_info(ind2+n(4),:)];
t3=[tbnd_info(ind3+n(1),:);tbnd_info(ind3+n(2),:); ...
    tbnd_info(ind3+n(3),:);tbnd_info(ind3+n(4),:)];
t4=[tbnd_info(ind4+n(1),:);tbnd_info(ind4+n(2),:); ...
    tbnd_info(ind4+n(3),:);tbnd_info(ind4+n(4),:)];
save tbnds t1 t2 t3 t4
```

GOLUBEV - Transfer function approximation given input and output sequences

```
function [num,den]=golubev(degn,degd,in,out,stepsz,imp)
% function [num,den]=golubev(degn,degd,in,out,stepsz,imp)
%
% This is a shortened modification of the Golubev program
% (Golubev, B., and I. Horowitz, Plant Rational Transfer Function
% Approximation from Input-Output Data, Int. J. Control, vol. 36,
% 1982, 711-23). Given input(t), output(t) sequences, it gives a
% rational function approximation, H(s)=num(s)/den(s), such that
% OUT(s)=H(s)IN(s).
%
% degn, degd: Degree of the numerator and denominator
% in, out:    Input and output time series
% stepsz:     Time step between samples of in and out
% imp:        If imp<>0, ignore input and use impulse input

if ((size(in) ~= size(out)) ~= [0 0]) .* (imp==0),
disp('ftf: in and out arrays must be same size');
return;
end

[npoint,roworcol]=max(size(out));
N=npoint;
if (roworcol == 1)
    out=out';
    in=in';
end

% find the integral of x^(-n) of t
mx=degn+degd+1;
if imp == 0
    integrals(degd+1,:)=in;
    for k=degd:-1:1
        integrals(k,:)=ftfint(stepsz,integrals(k+1,:));
    end
end

% find integrals y^(-n) of t
integrals(mx+1,:)=out;
for k=mx:-1:degn+2
    integrals(k,:)=ftfint(stepsz,integrals(k+1,:));
end
```

```
% if using impulse input, find integral x^(-n) of t
% for impulse input
if imp ~= 0
    vk(1)=1;
    vk(2)=1;
    for k=3:degd
        vk(k)=vk(k-1)*vk(k-1);
    end
    for k=degn+1:-1:1
        l=degd-k;
        integrals(k,1:npoint)=[0:stepsz:stepsz*(npoint-1)].^(l)/vk(1+l);
    end
end

% load the A and b matrices to do the least squares fit
A=[];
b=[];
for k=1:mx
    b(k)=sum(integrals(mx+1,:).*integrals(k,:));
    for l=k:mx
        A(k,l)=sum(integrals(l,:).*integrals(k,:));
        A(l,k)=A(k,l);
    end
end

% solve Ax=b & check condition of A
rcon=rcond(A);
c=A\b';
num=c(degn+1:-1:1)';
den=[1;-c(mx:-1:degn+2)]';
t=0:stepsz:(N-1)*stepsz;
if imp ~= 0
     disp('Sorry, no impulse function in Student Version');
%    outchk=impulse(num,den,t);
else
    outchk=step(num,den,t);
end
if size(out) ~= size(t)
    out=out';
end
if size(outchk) ~= size(t)
    outchk=outchk';
end
plot(t,out,t,outchk)
```

```
%rn=roots(num);
%rd=roots(den);
%err=sqrt(sum((integrals(mx+1,:) - ...
%     sum((c(1:mx)*ones(1,npoint)) ...
%     .* integrals(1:mx,:))).^2)/(npoint-mx));
return
```

FTFINT - Trapazoidal integration routine

```
function [sx]=ftfint(stepsz,x)
% Trapazoidal integration routine, integrating x * sx.
% Used in the gobulev function.
sx=([0 x]+[x 0])*stepsz/2;
sx(1)=0;
sx=cumsum(sx(1:max(size(x))));
```

WARP - Use with GOLUBEV to improve results

```
function out=warp(in,f);
% For use in the golubev function.  May improve results.
out=(2*f*atan(abs(in*3.1416/f))).*(cos(angle(in))+ ...
    sin(angle(in)*sqrt(-1));
```

APPENDIX C

CAD FIGURES FOR DESIGN 1

These figures are captured screen images from the QFT-CAD software package. As a result, the Nichols chart figures (Figs. C-1 thru C-16) are difficult to decipher. The ordinate on these plots is the open loop magnitude in decibels (db) and the abscissa is open loop phase in degrees. On a color VGA display, the lines denoting the M-circles, the performance and stability boundaries, and the nominal loop transmission are much more easily distinguishable than in these black-and-white figures. Offered here is a discription of the features in the figures as a means of facilitating the reader's interpretation thereof.

M-Circles - The M-Circles appear with digital identification markings on the left hand side of the figure. In the center of the figure, they appear as concentric ellipses, the largest labelled 0.0 db. The M-Circles of magnitude less than 0 db do not enclose the (0 db, -180 deg) point, but fan out to both sides of the figure and are, again, labelled on the left side.

Performance/Stability Bounds - The performance bounds as lines extending from one edge of the figure to the other, and the frequency corresponding to each bound is indicated on the right hand side of the figure. In cases where the

performance bound extends below the lower limit of the displayed open loop magnitude, the frequency label is located on the bottom edge of the plot. The stability bounds encircle the (0 db, -180 deg) point in the figures. As with the performance boundaries, the frequencies associated with these boundaries is indicated on the right hand side.

Nominal Loop Transmission - The nominal loop transmission is represented in the figures as a line broken up by intermittent frequency labels. Sometimes, the line is not continuous on the plot. This is either because of an abrupt phase shift caused by a pair of lightly-damped poles or zeros or because of the "phase-wrap" feature of QFT-CAD. The nominal loop transmission phase is presented between 0° and -360°, so that if phase passes above 0° or below -360°, 360° is added or subtracted to keep the presented phase between the those limits. Figure C-1 demonstrates both of these occurances in the nominal loop transmission of the roll response loop. There exists in the nominal plant dynamic model a very lightly damped pair of zeros between 0.3 rad/sec and 0.5 rad/sec accounting for the discontinuity of the nominal loop transmission. Also, below 0.3 rad/sec, the phase drops below -360° and the tail of the nominal loop transmission extends into the figure from the right hand side.

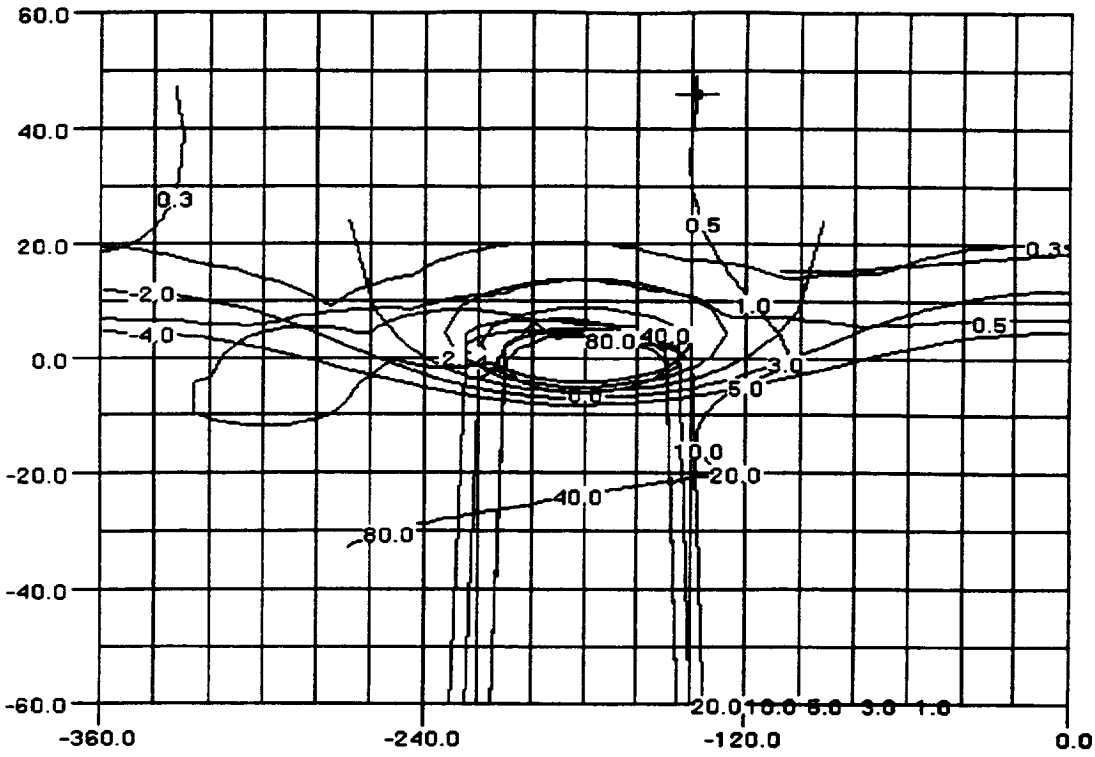

Figure C-1 CAD Drawing of Feedback Compensator Design for Roll

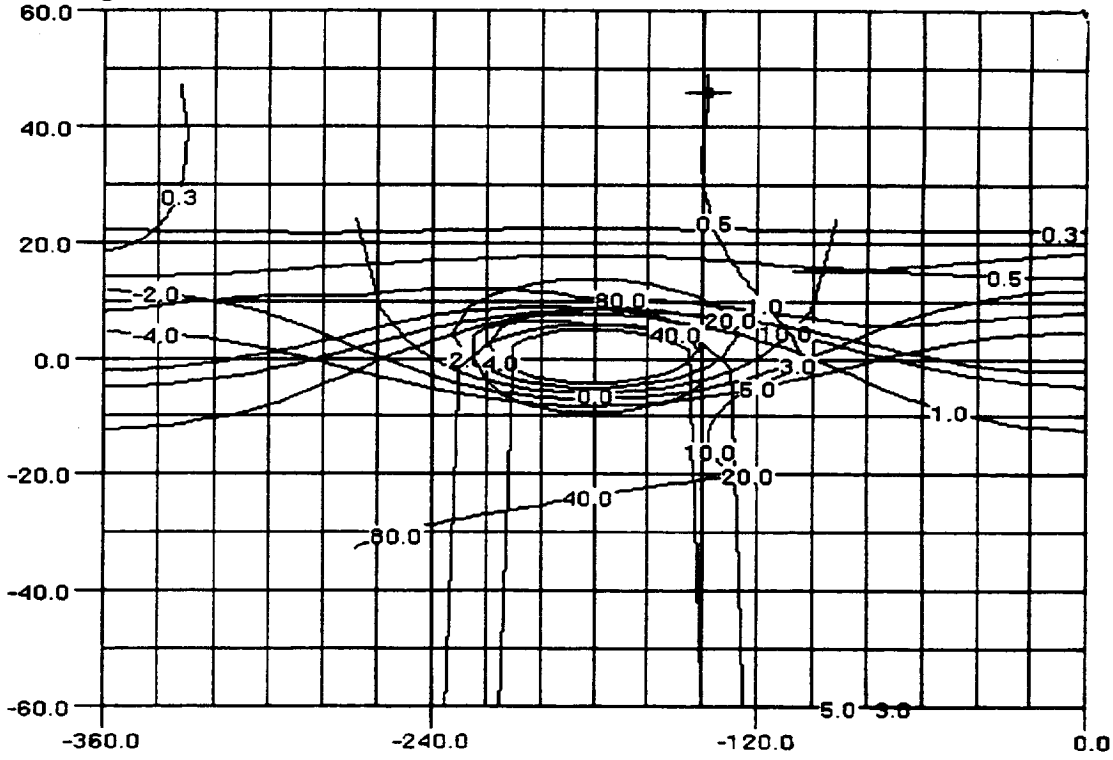

Figure C-2 CAD Drawing of Feedback Compensator Design for Roll Response to Pitch Command

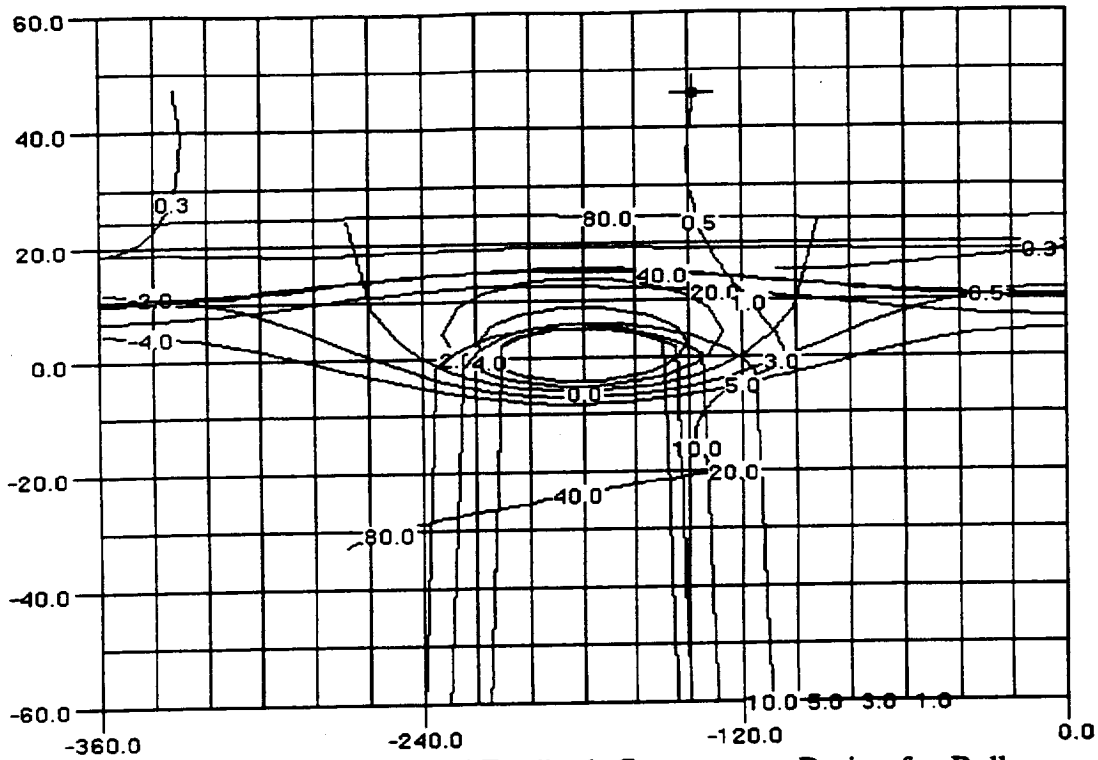

Figure C-3 CAD Drawing of Feedback Compensator Design for Roll Response to Vertical Velocity Command

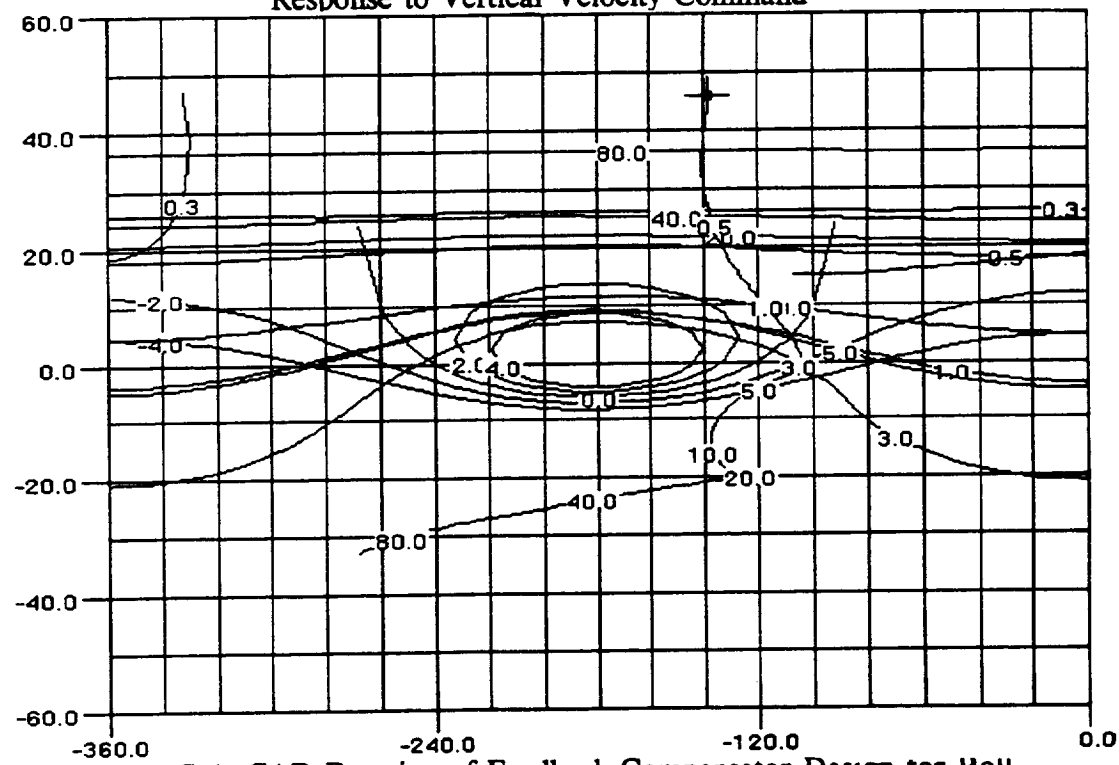

Figure C-4 CAD Drawing of Feedback Compensator Design for Roll Response to Yaw Rate Command

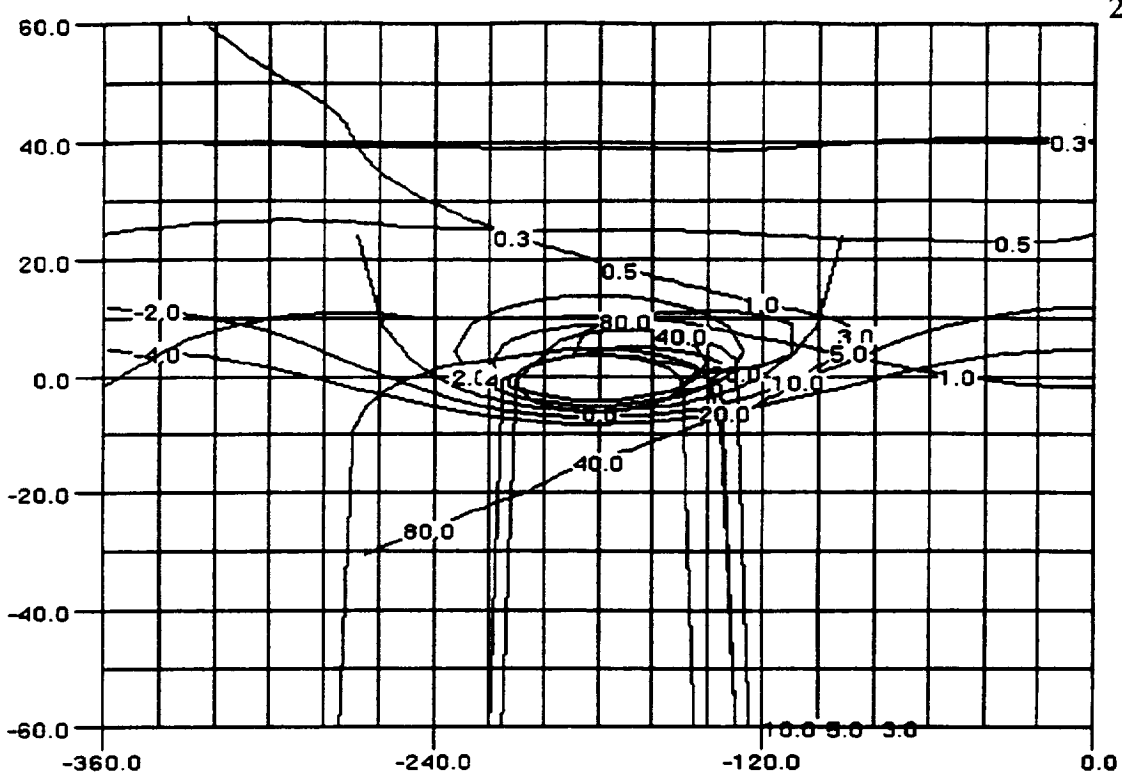

Figure C-5 CAD Drawing of Feedback Compensator Design for Pitch Response to Roll Command

Figure C-6 CAD Drawing of Feedback Compensator Design for Pitch Response to Pitch Command

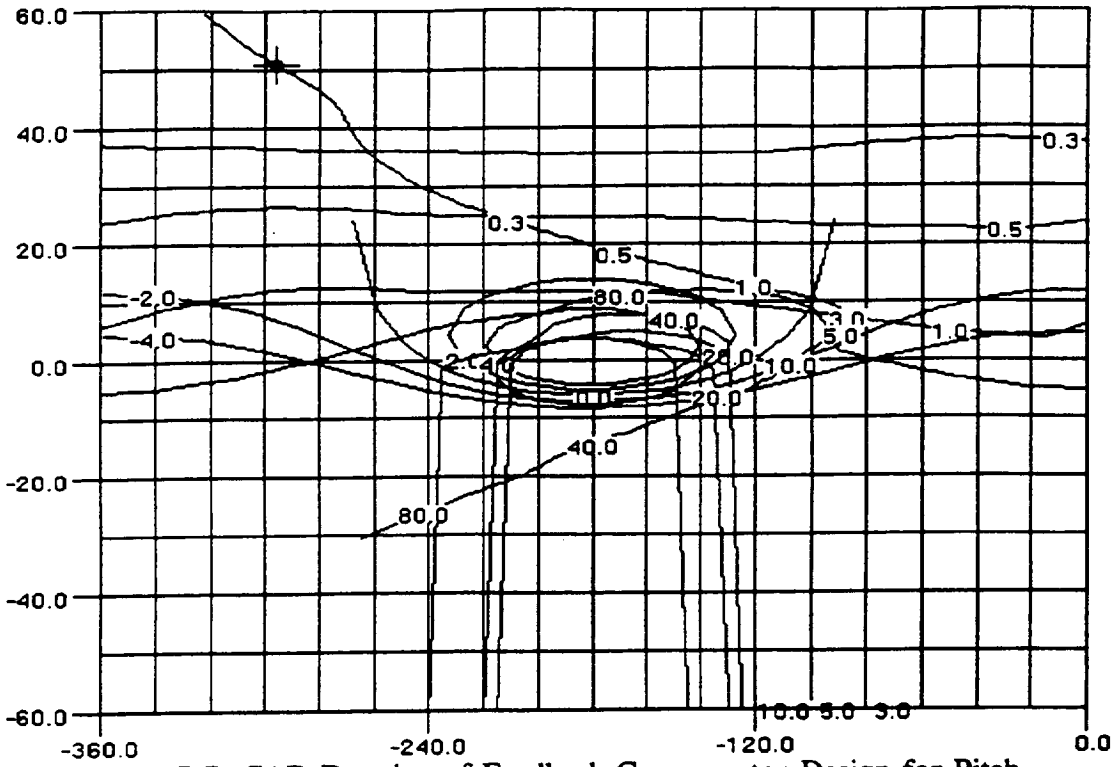

Figure C-7 CAD Drawing of Feedback Compensator Design for Pitch Response to Vertical Velocity Command

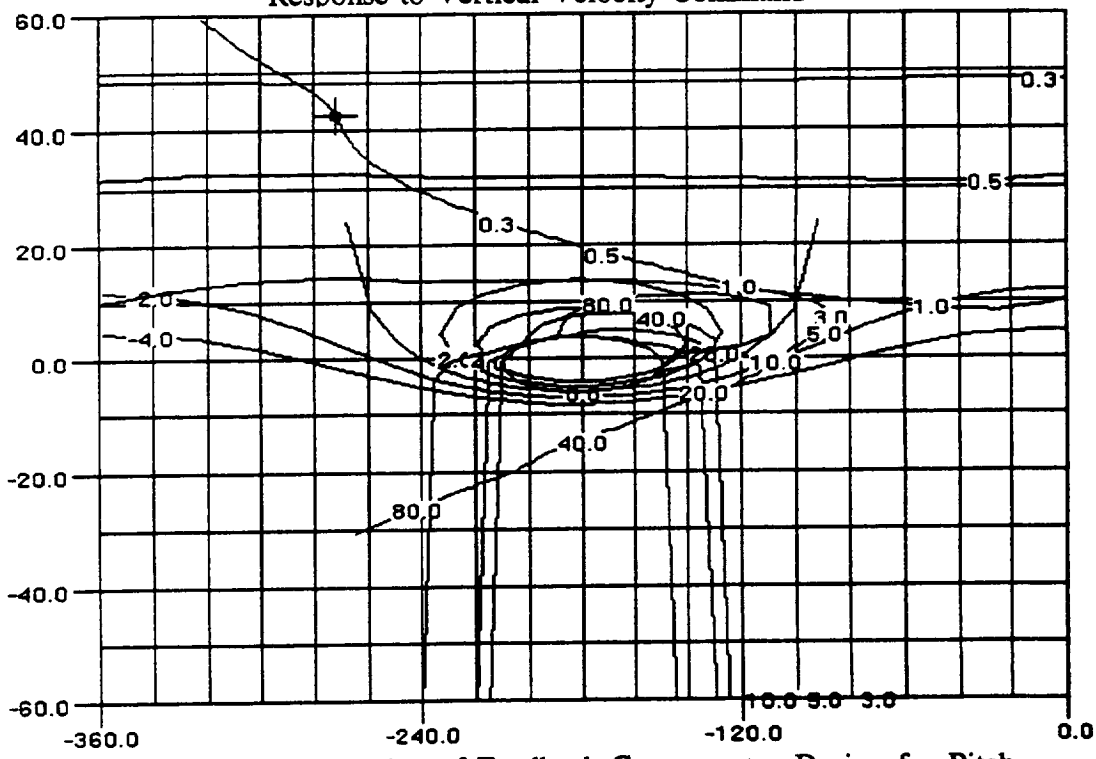

Figure C-8 CAD Drawing of Feedback Compensator Design for Pitch Response to Yaw Rate Command

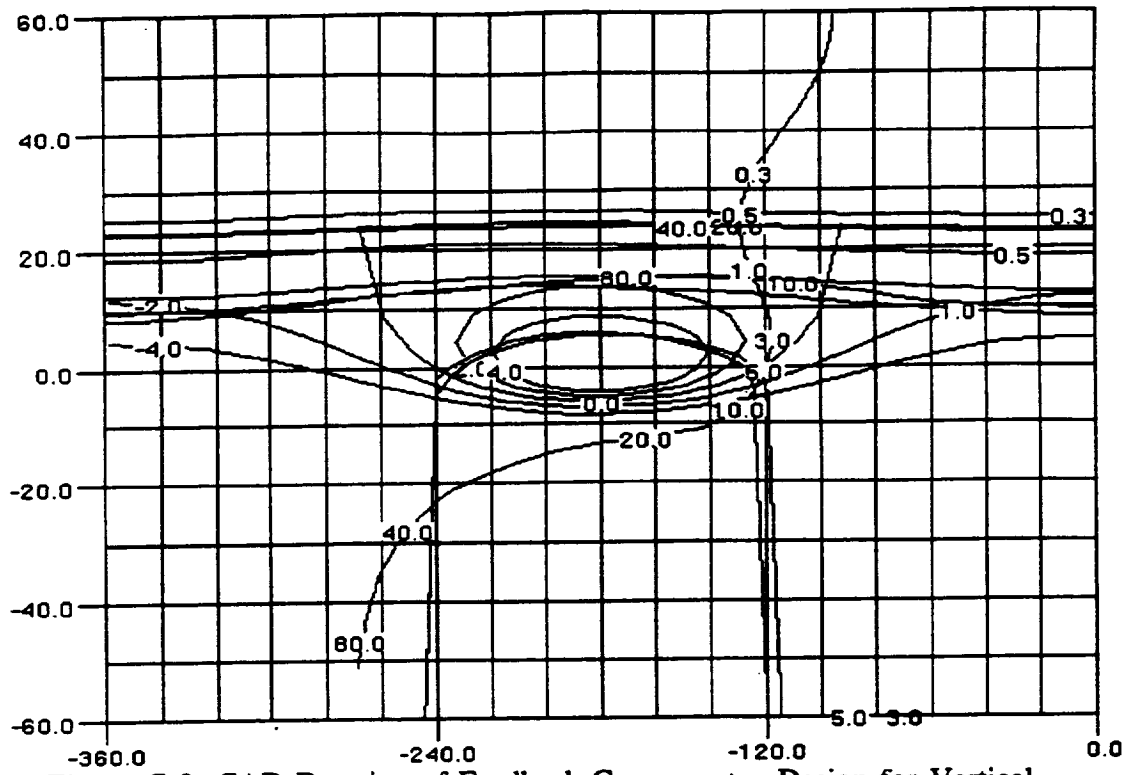

Figure C-9 CAD Drawing of Feedback Compensator Design for Vertical Velocity Response to Roll Command

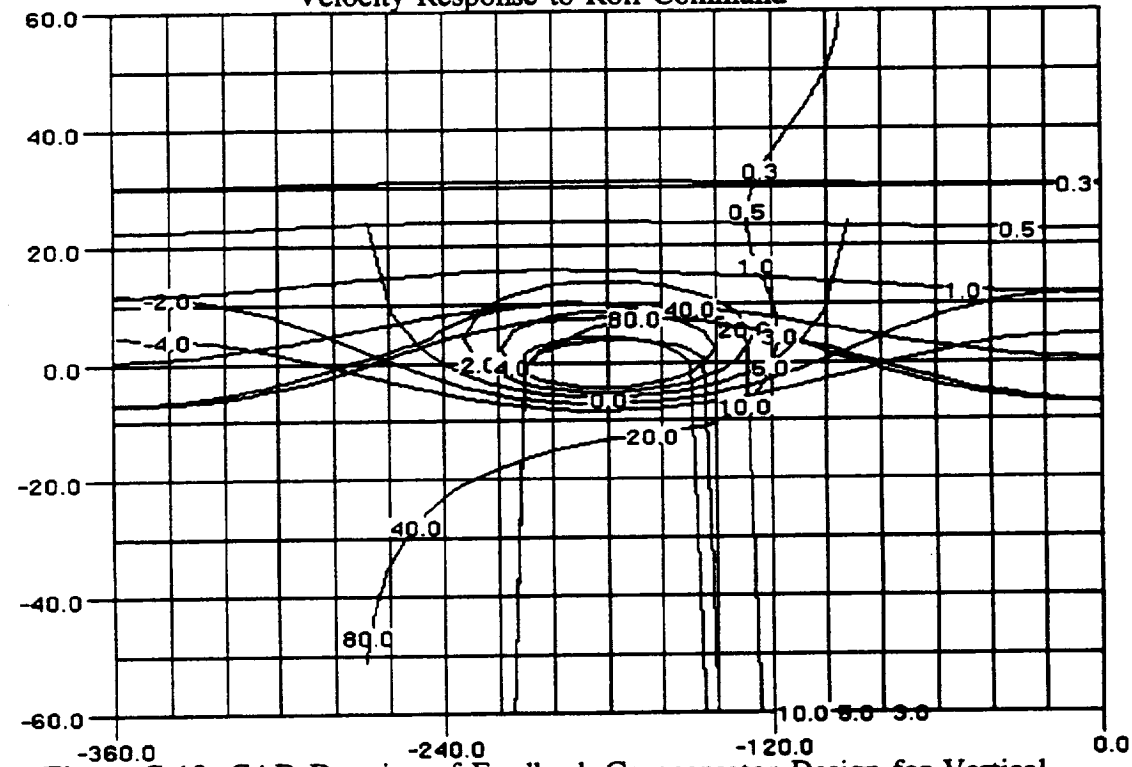

Figure C-10 CAD Drawing of Feedback Compensator Design for Vertical Velocity Response to Pitch Command

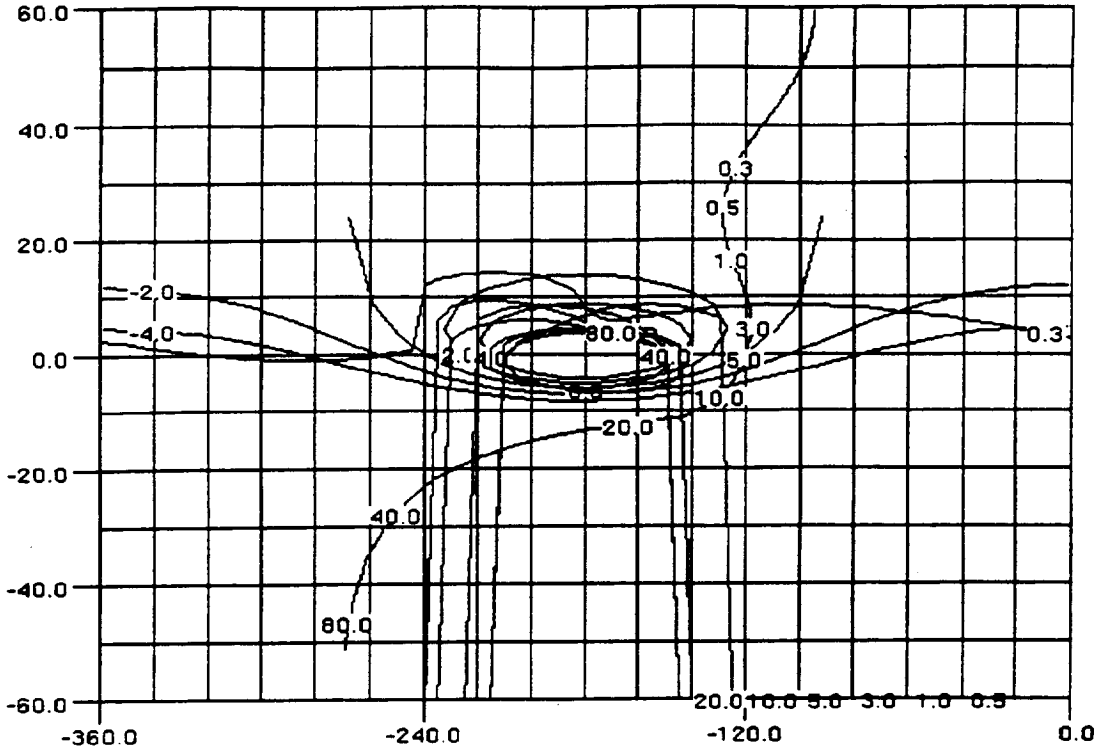

Figure C-11 CAD Drawing of Feedback Compensator Design for Vertical Velocity Response to Vertical Velocity Command

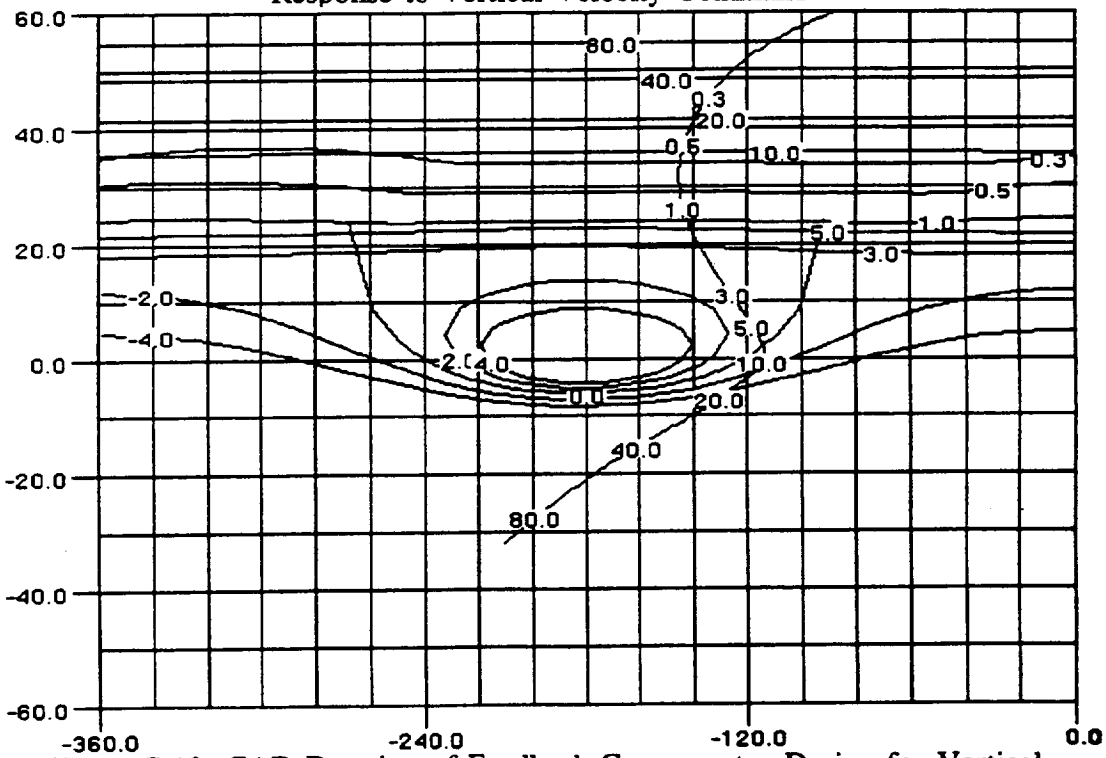

Figure C-12 CAD Drawing of Feedback Compensator Design for Vertical Velocity Response to Yaw Rate Command

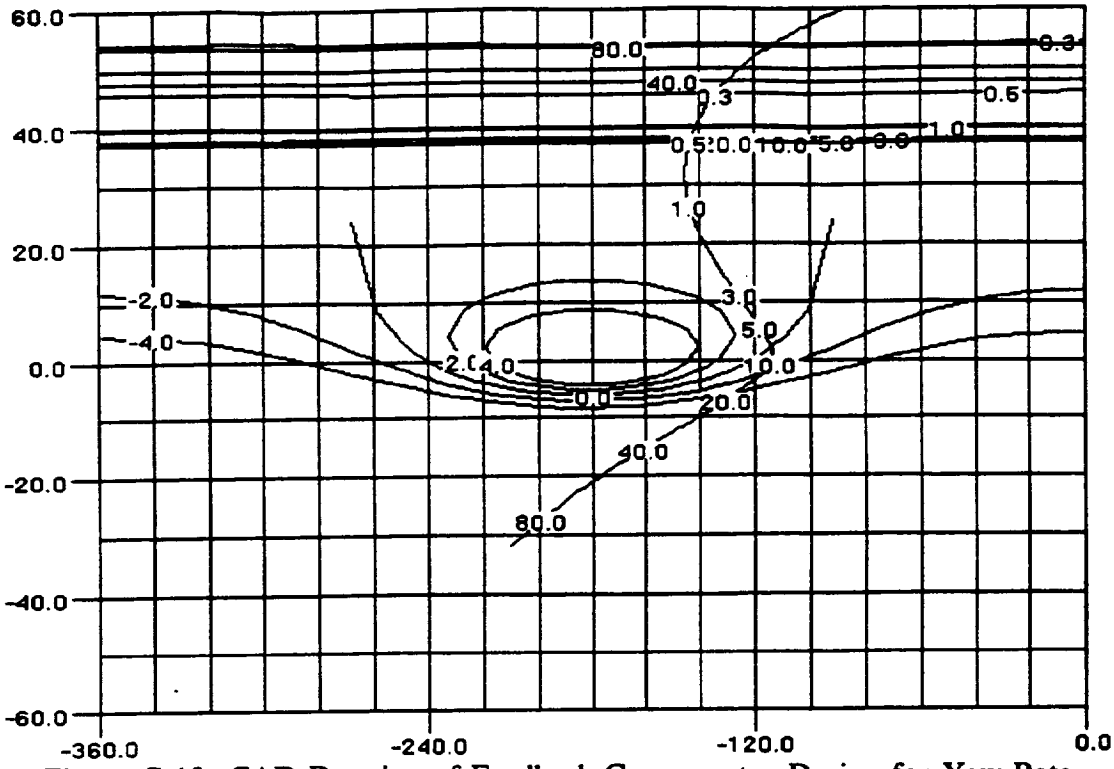

Figure C-13 CAD Drawing of Feedback Compensator Design for Yaw Rate Response to Roll Command

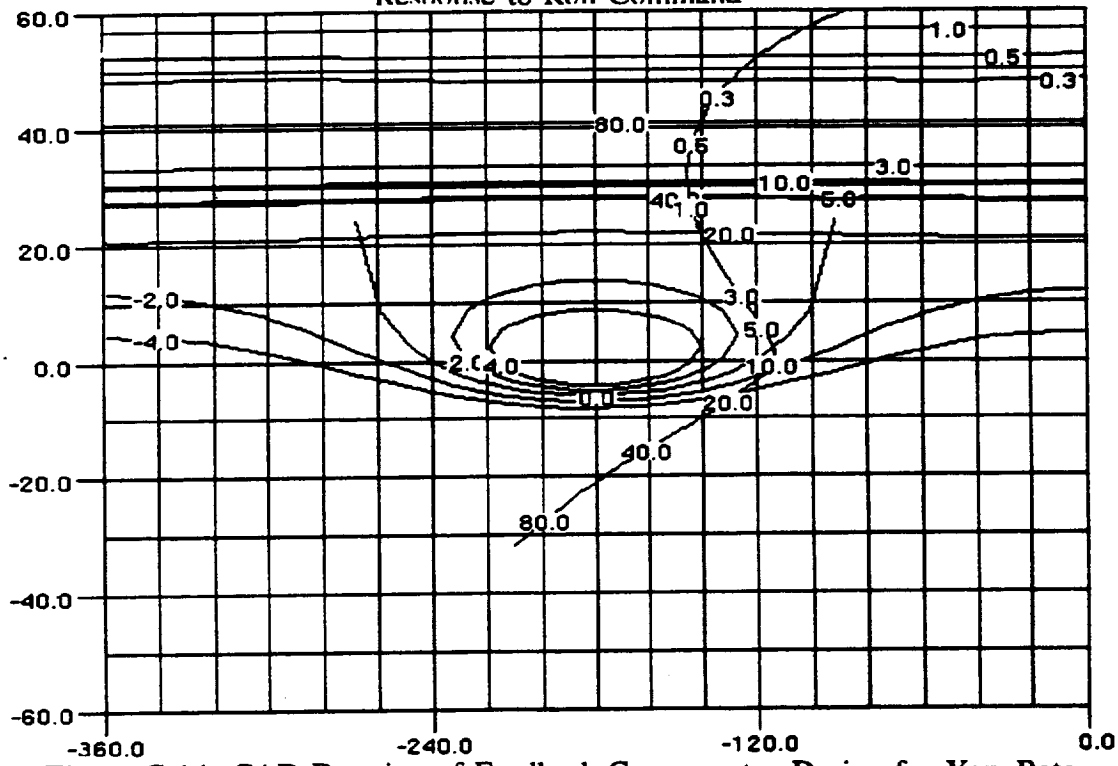

Figure C-14 CAD Drawing of Feedback Compensator Design for Yaw Rate Response to Pitch Command

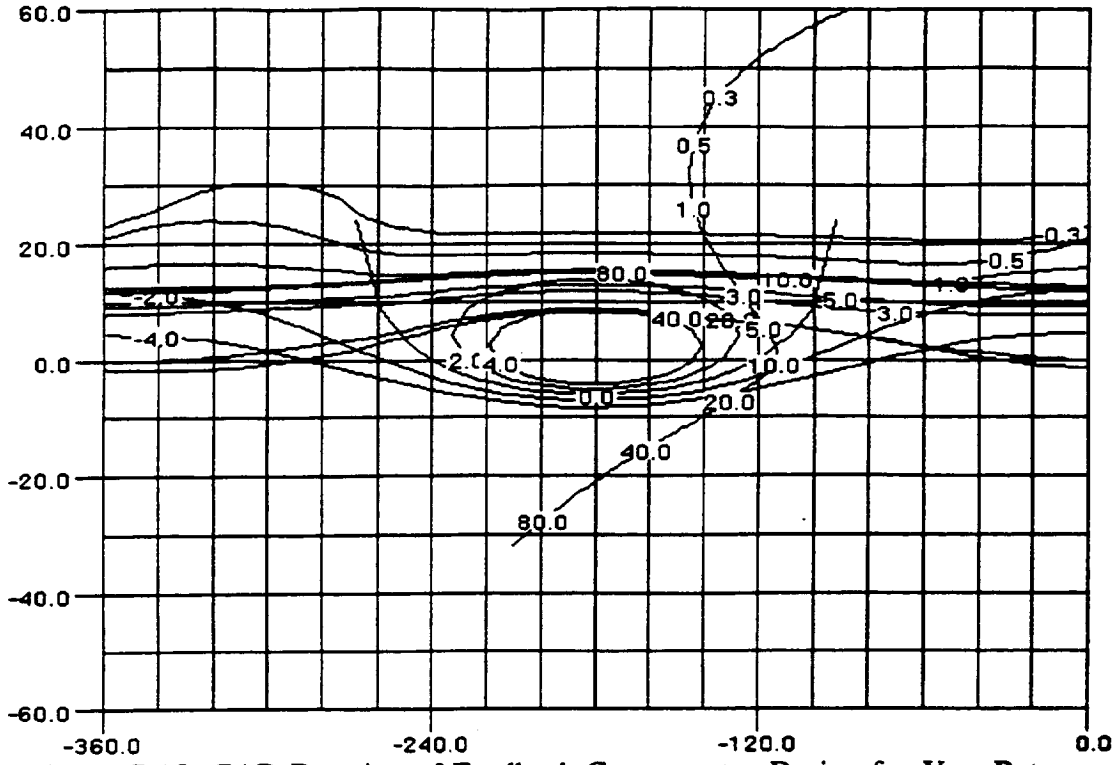

Figure C-15 CAD Drawing of Feedback Compensator Design for Yaw Rate Response to Vertical Velocity Command

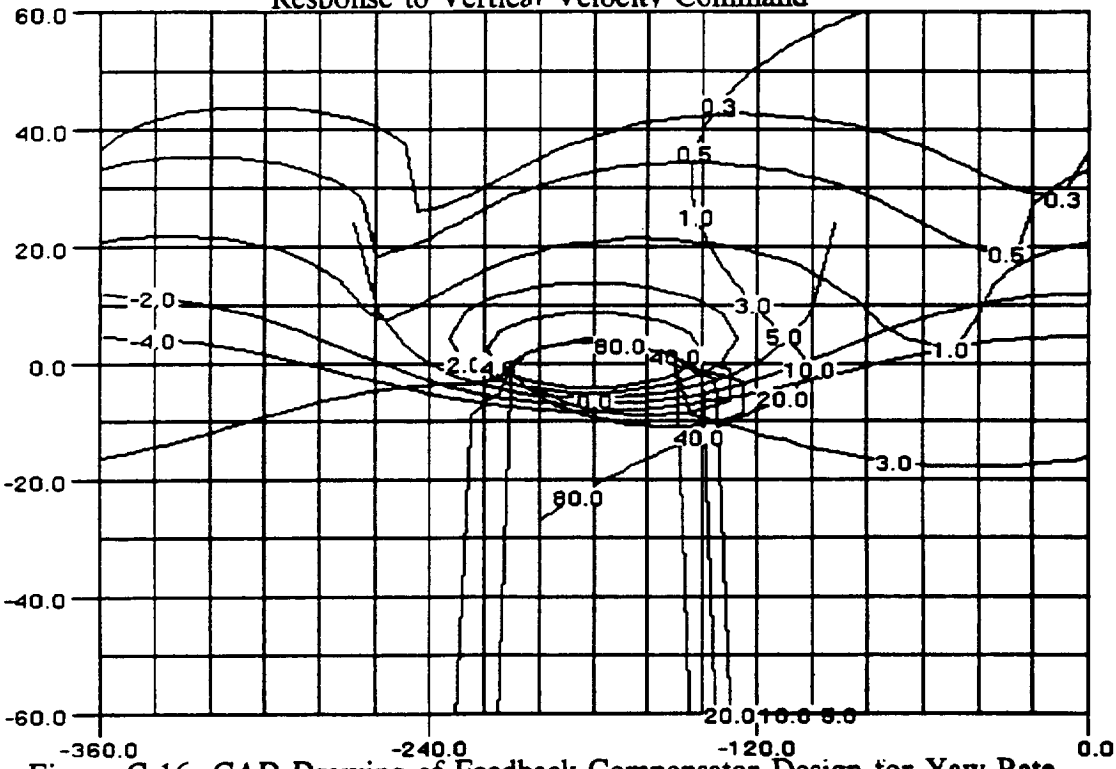

Figure C-16 CAD Drawing of Feedback Compensator Design for Yaw Rate Response to Yaw Rate Command

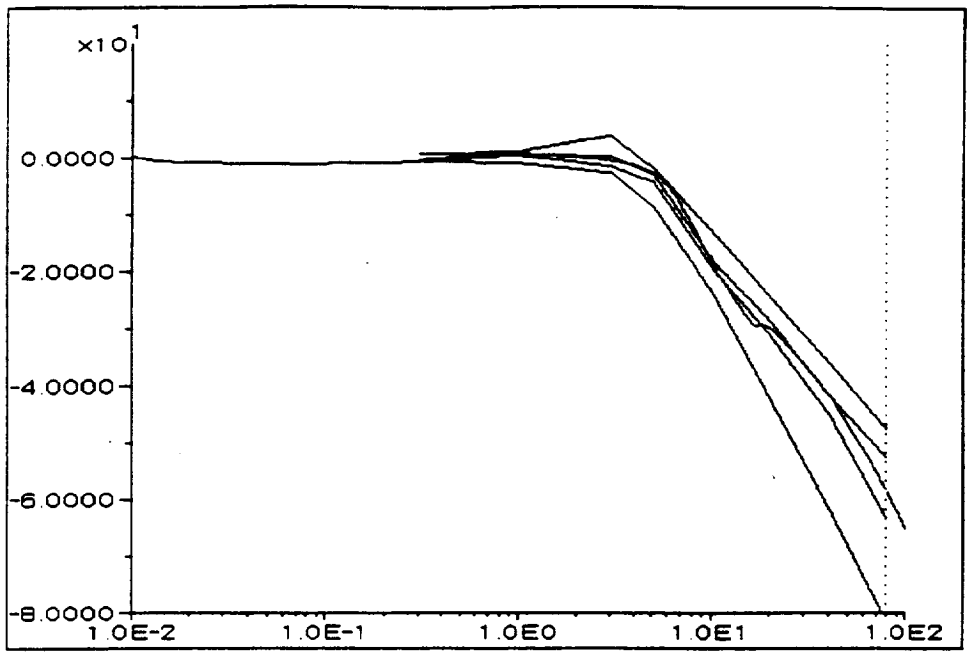

Figure C-17 CAD Drawing of Prefilter Design for Roll Response to Roll Command

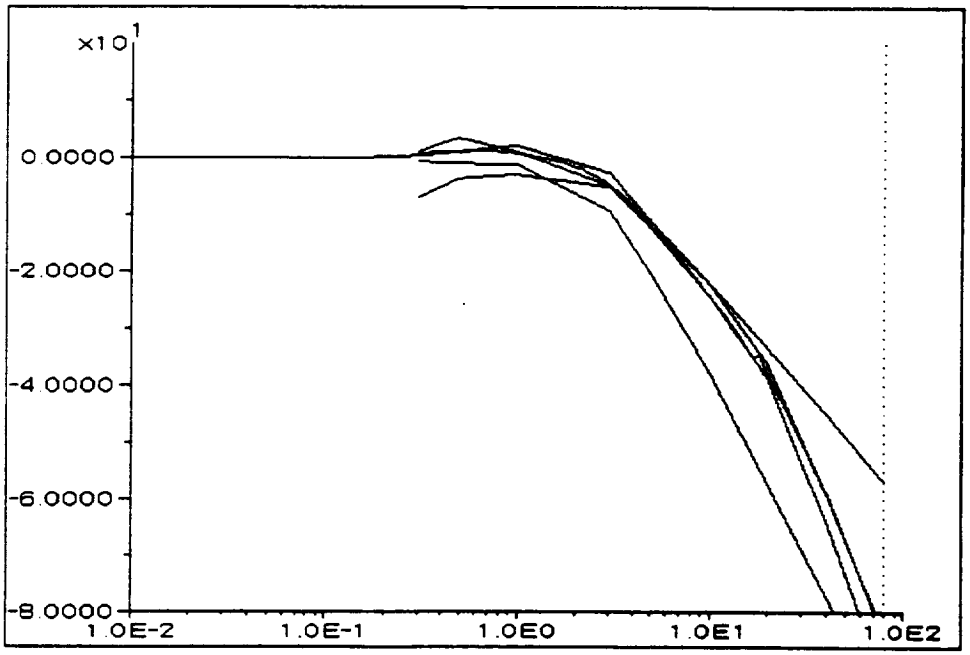

Figure C-18 CAD Drawing of Prefilter Design for Pitch Response to Pitch Command

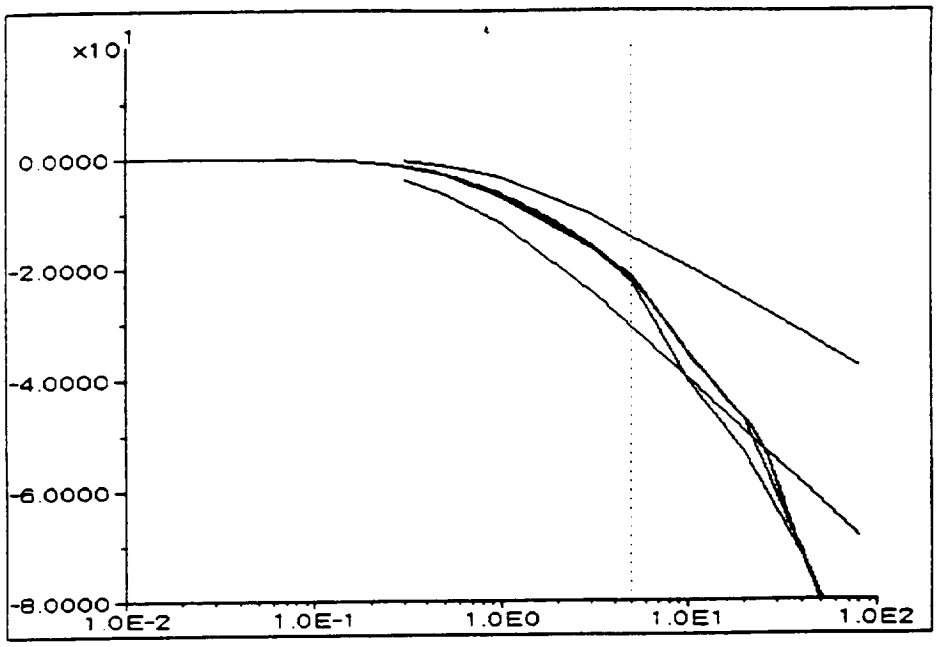

Figure C-19 CAD Drawing of Prefilter Design for Vertical Velocity Response to Vertical Velocity Command

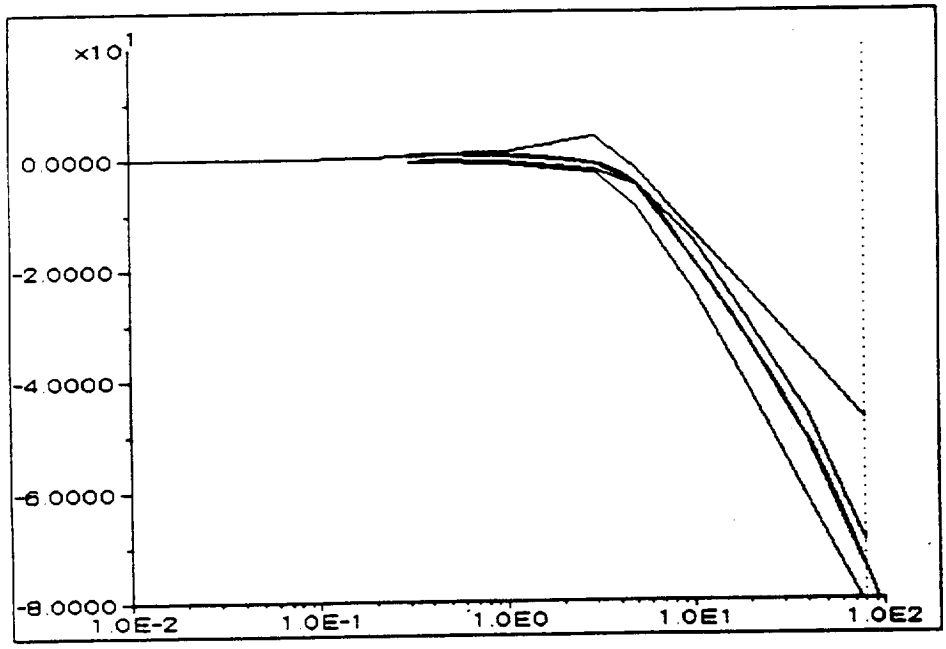

Figure C-20 CAD Drawing of Prefilter Design for Yaw Rate Response to Yaw Rate Command

APPENDIX D

RESULTS - DESIGN 1

Presented in this Appendix are the time histories resulting from the application, as depicted in Fig. 4.15, of the flight control system designed as described in Chapter 4 to each of the six (6) linearized helicopter models which comprised the set of possible plant dynamic models, *P*. Unit step inputs were applied to each of the controller inputs in succession with the following results.

Each solid line represents the response of one of the linearized models to the controller input. In Figs. D-1, D-6, D-11, and D-16, the performance boundary step responses are included as dashed lines.

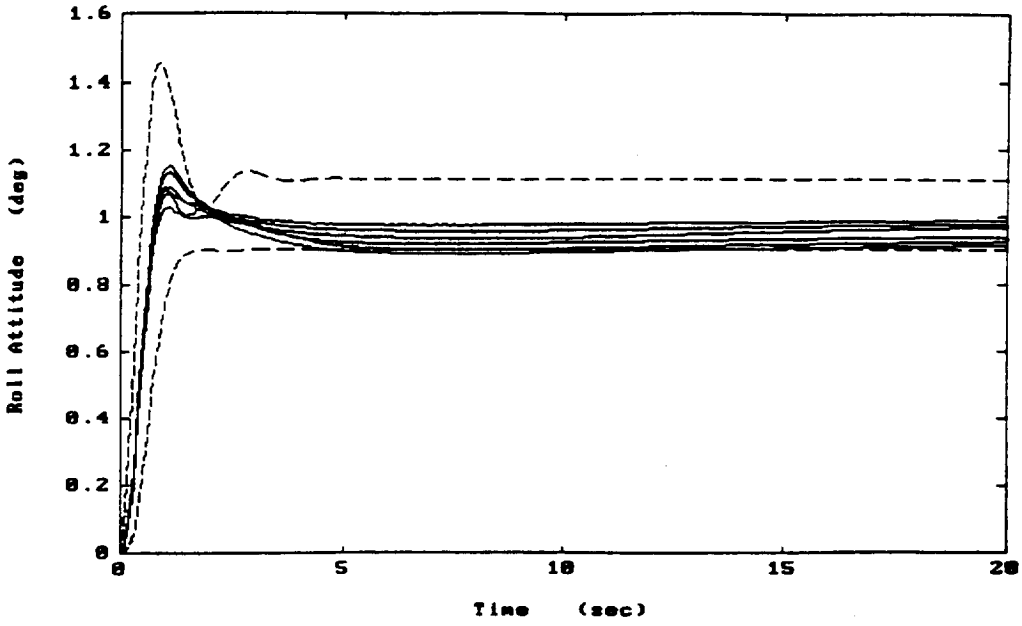

Figure D-1 Roll Attitude Response to a Unit Step to Roll Attitude Command

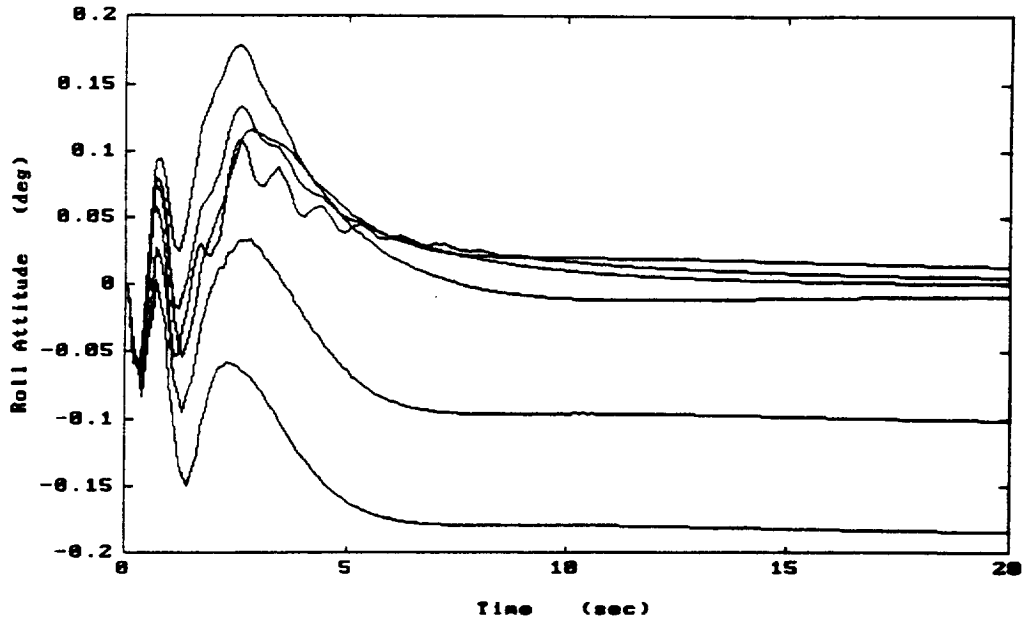

Figure D-2 Roll Attitude Response to a Unit Step to Pitch Attitude Command

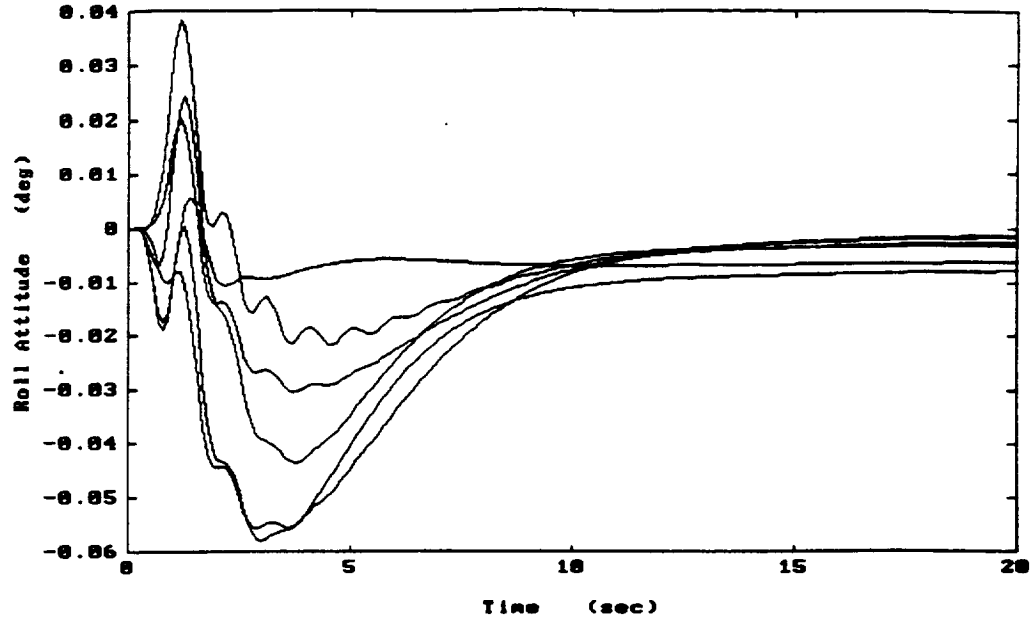

Figure D-3 Roll Attitude Response to a Unit Step to Vertical Velocity Command

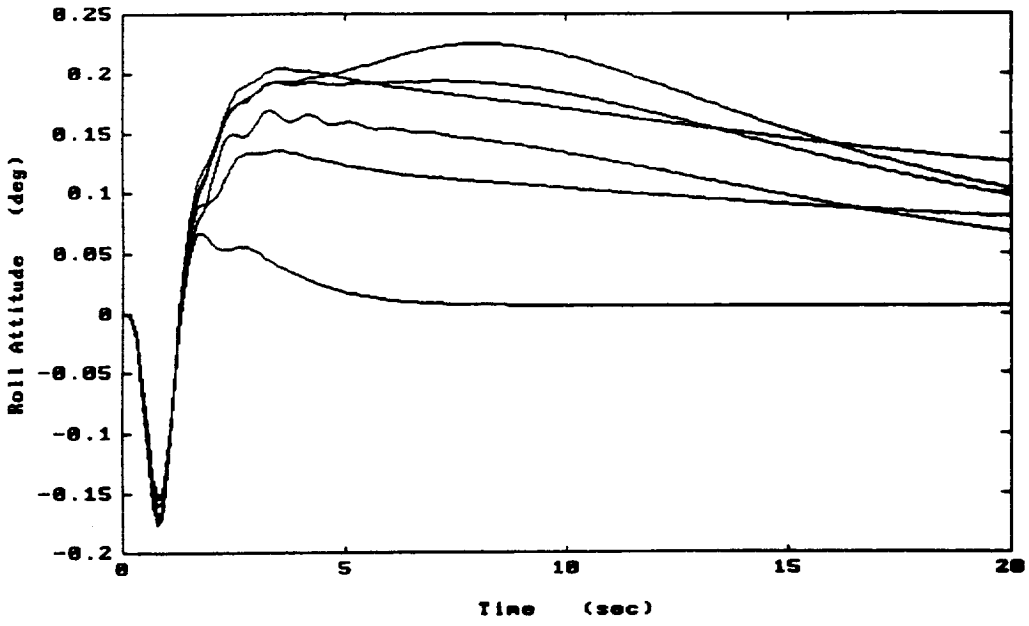

Figure D-4 Roll Attitude Response to a Unit Step to Yaw Rate Command

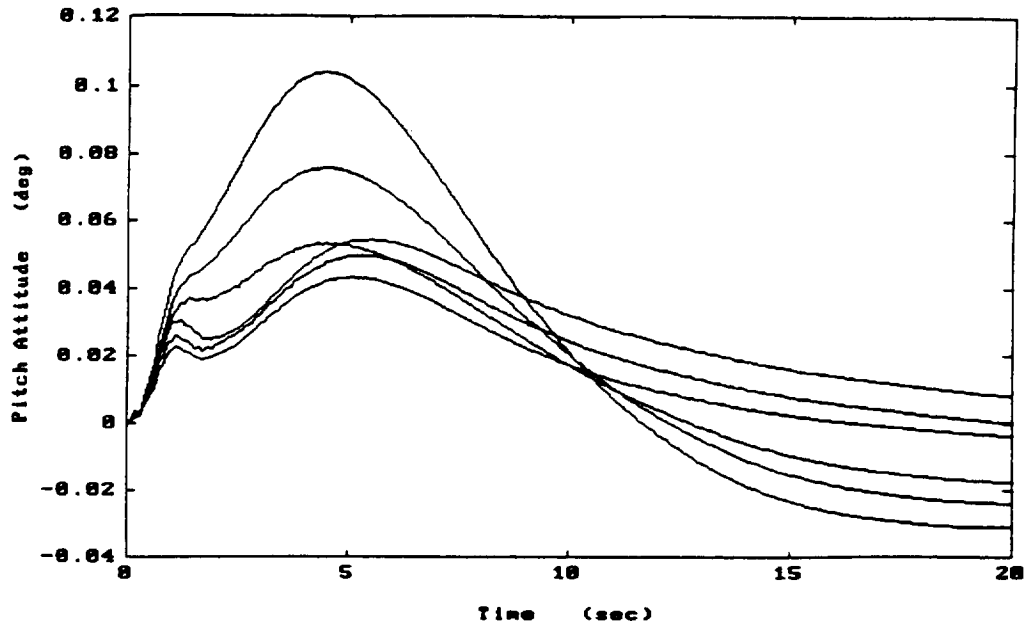

Figure D-5 Pitch Attitude Response to a Unit Step to Roll Attitude Command

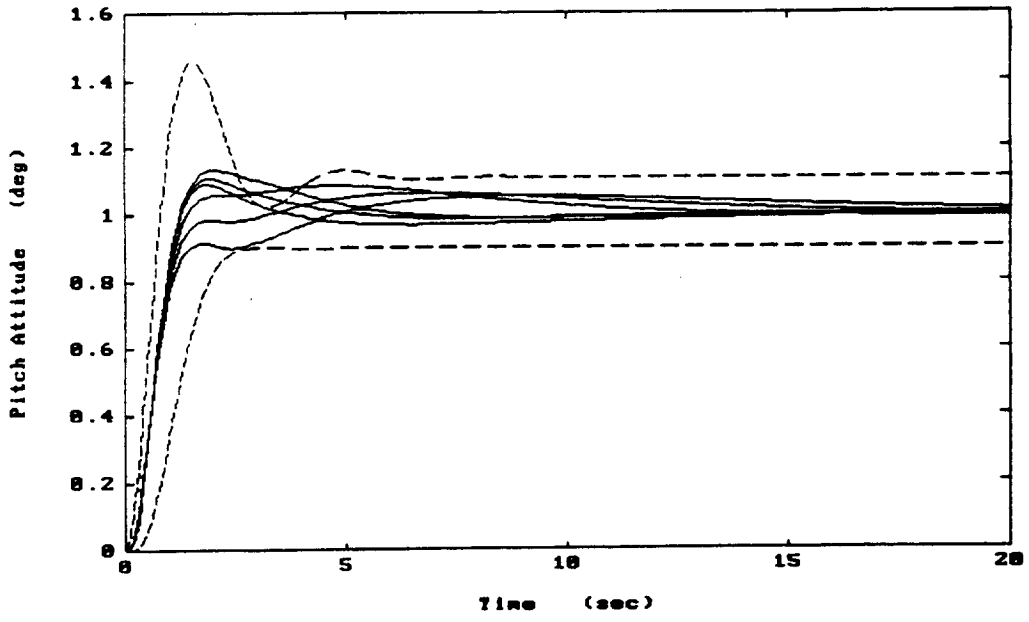

Figure D-6 Pitch Attitude Response to a Unit Step to Pitch Attitude Command

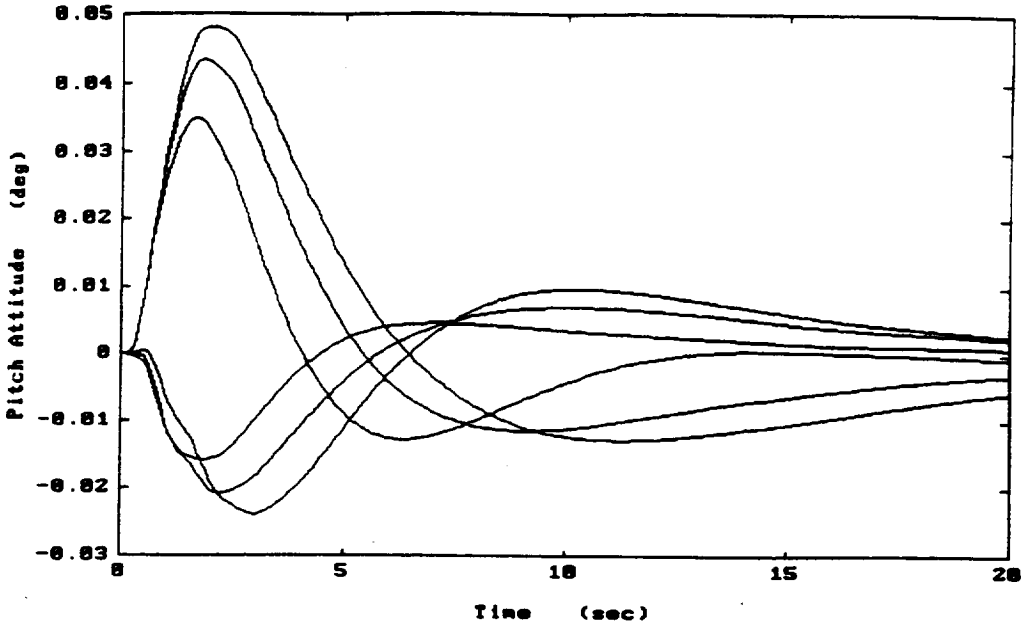

Figure D-7 Pitch Attitude Response to a Unit Step to Vertical Velocity Command

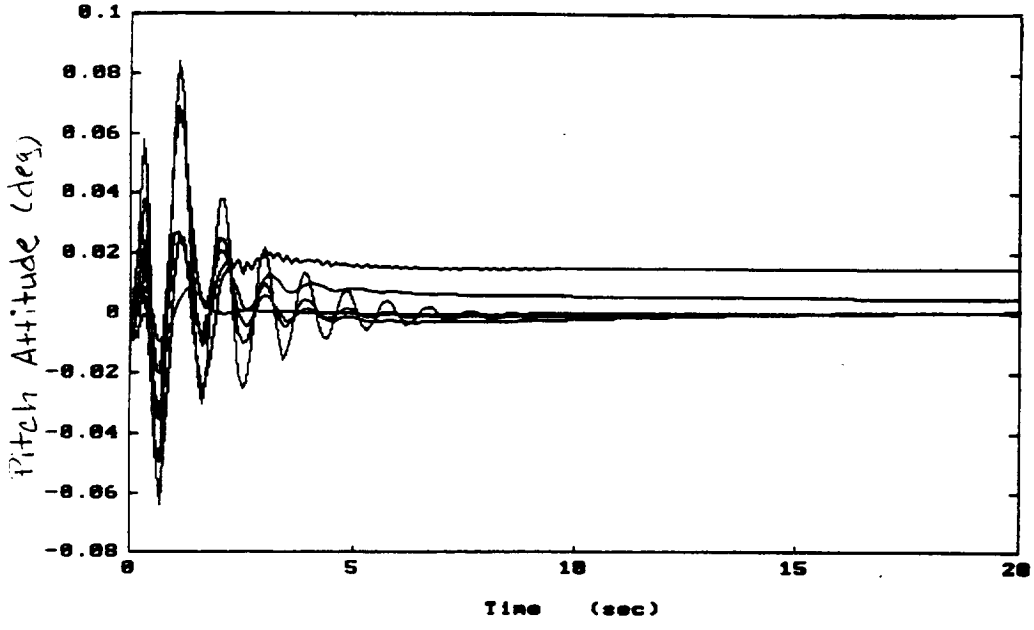

Figure D-8 Pitch Attitude Response to a Unit Step to Yaw Rate Command

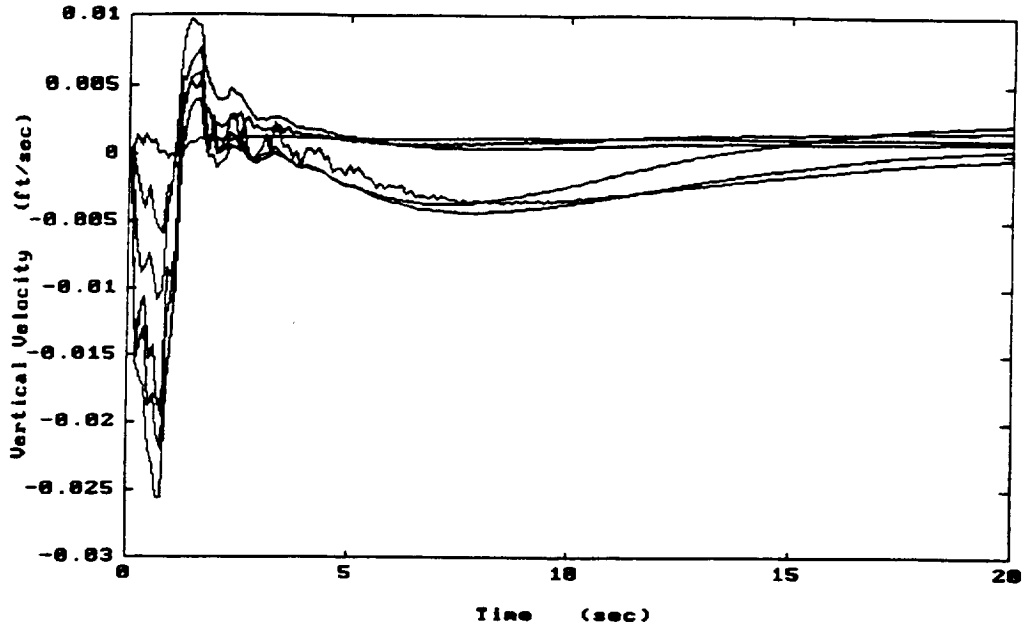

Figure D-9 Vertical Velocity Response to a Unit Step to Roll Attitude Command

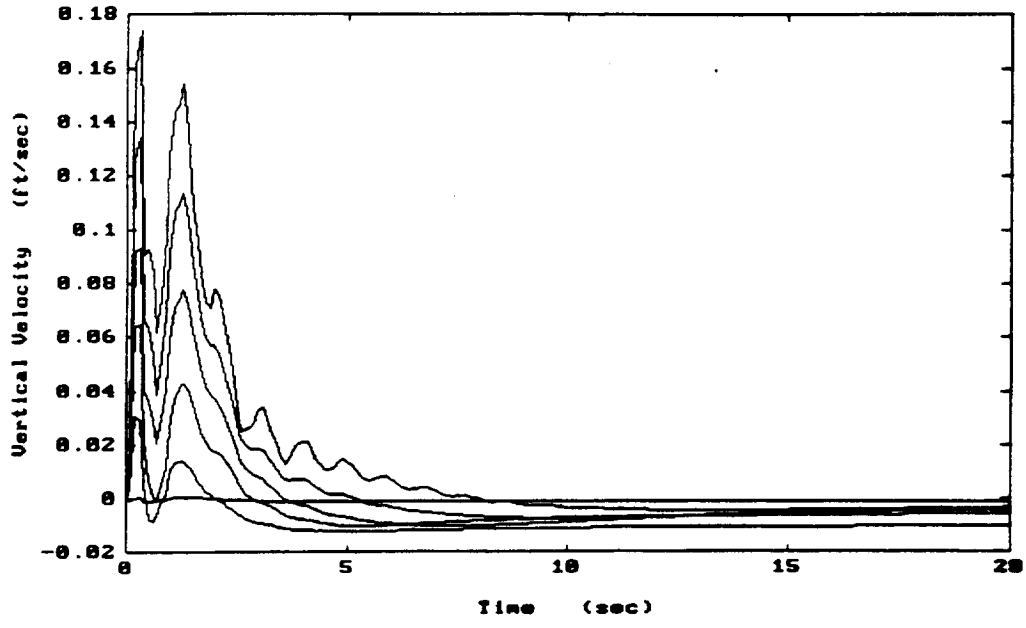

Figure D-10 Vertical Velocity Response to a Unit Step to Pitch Attitude Command

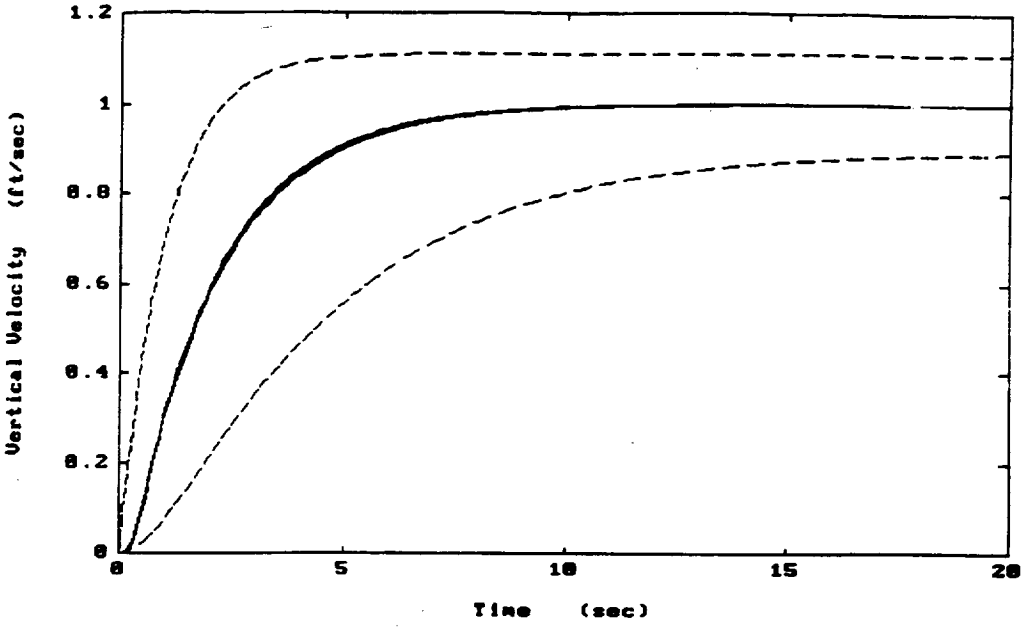

Figure D-11 Vertical Velocity Response to a Unit Step to Vertical Velocity Command

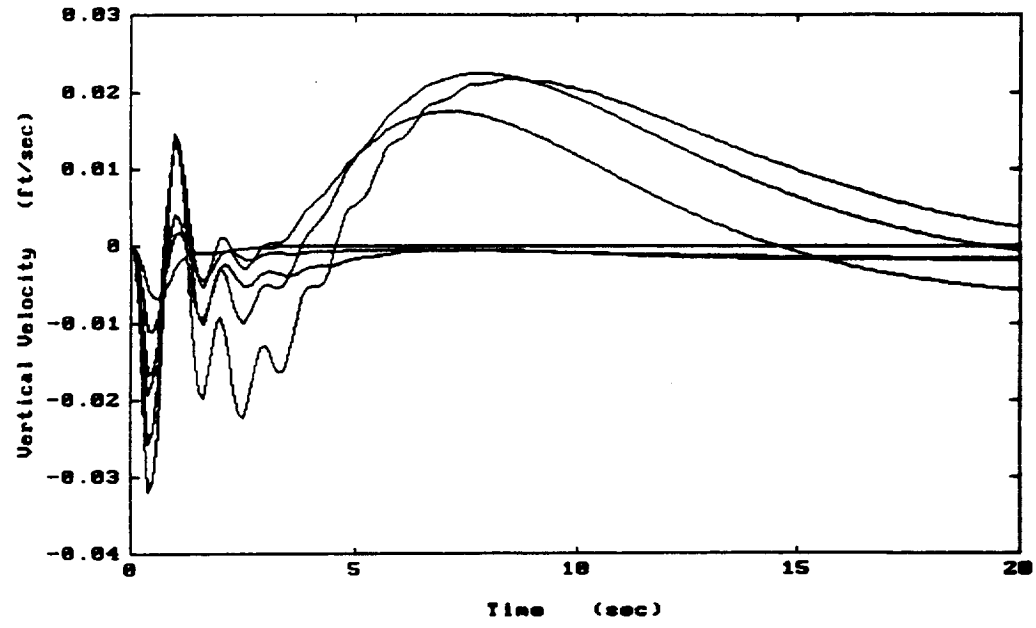

Figure D-12 Vertical Velocity Response to a Unit Step to Yaw Rate Command

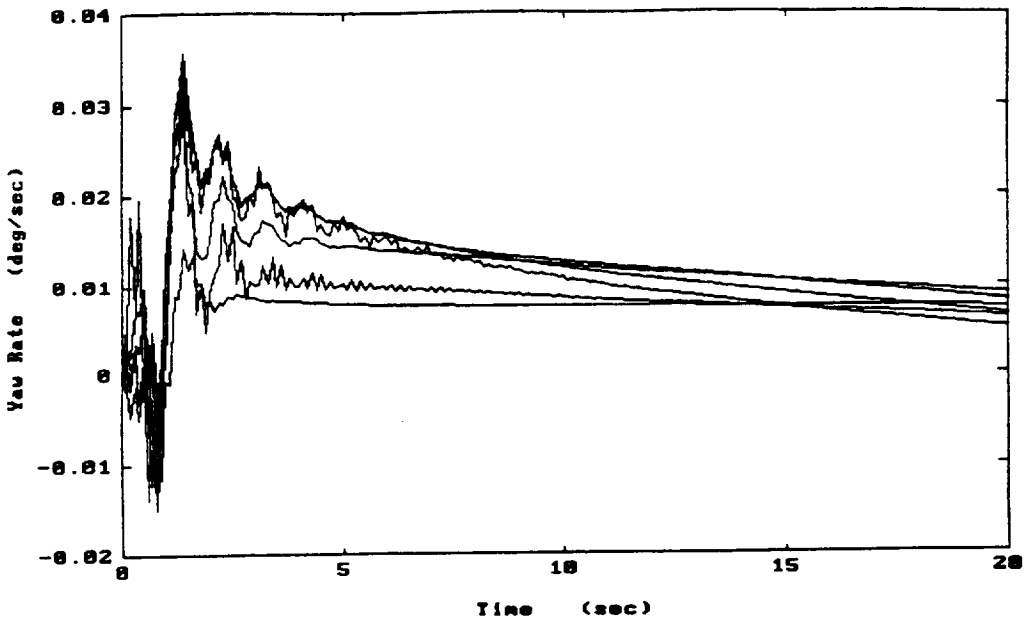

Figure D-13 Yaw Rate Response to a Unit Step to Roll Attitude Command

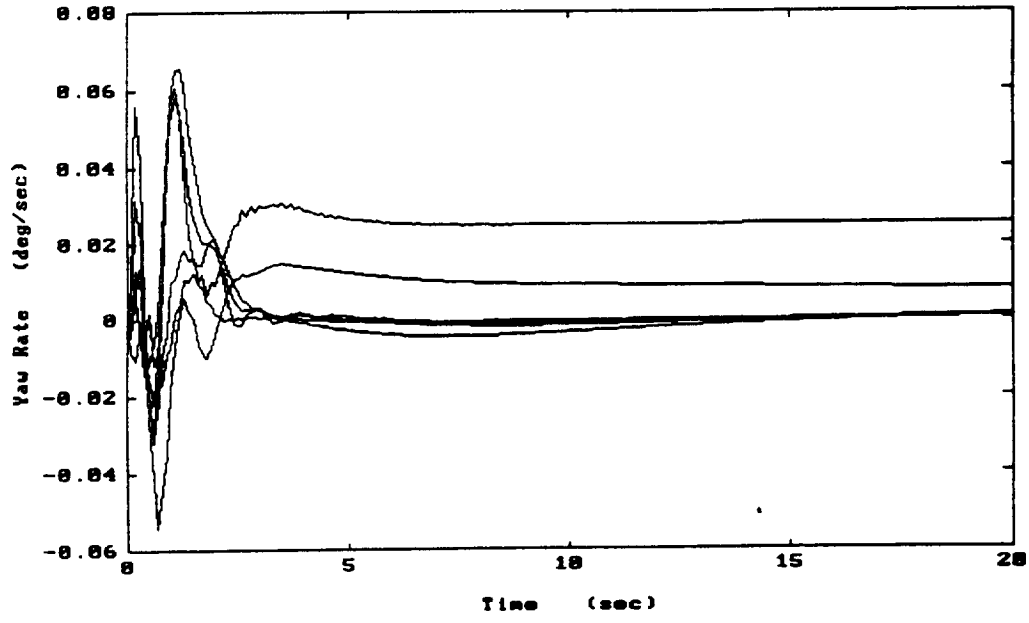

Figure D-14 Yaw Rate Response to a Unit Step to Pitch Attitude Command

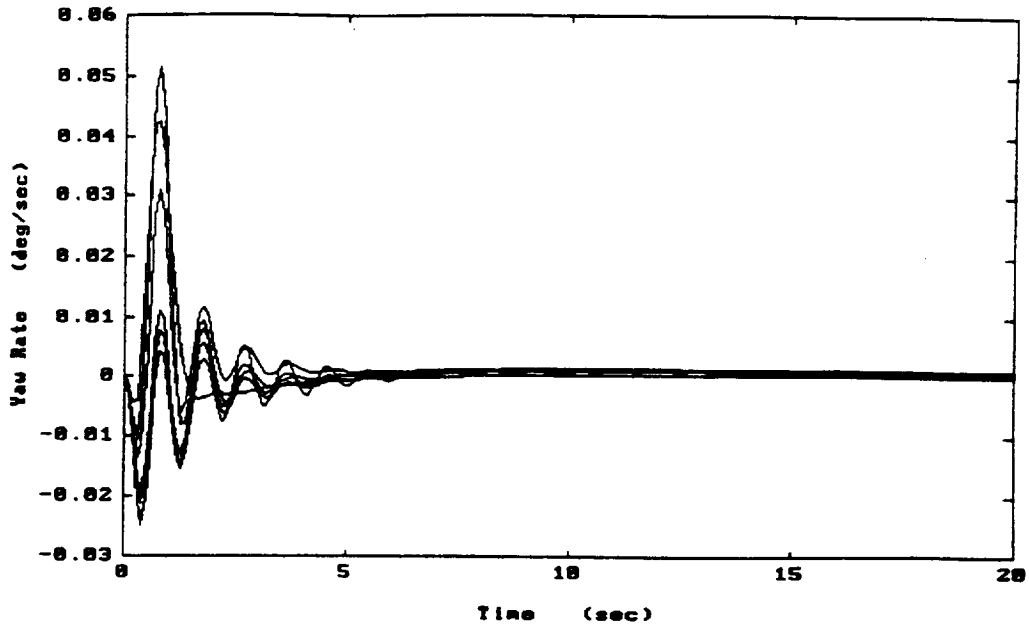

Figure D-15 Yaw Rate Response to a Unit Step to Vertical Velocity Command

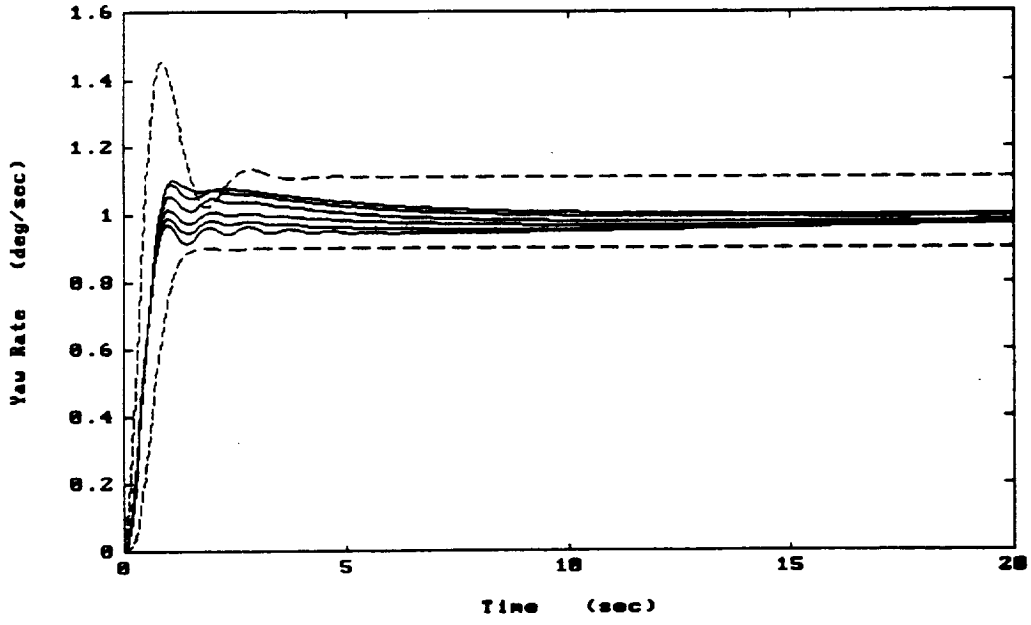

Figure D-16 Yaw Rate Response to a Unit Step to Yaw Rate Command

APPENDIX E

CAD FIGURES FOR SEQUENTIAL LOOP CLOSURE DESIGN

As with Appendix C, these figures are captured screen images from the QFT-CAD software package. As a result, the Nichols chart figures (Figs. E-1 thru E-16) are difficult to decipher. The ordinate on these plots is the open loop magnitude in decibels (db) and the abscissa is open loop phase in degrees. On a color VGA display, the lines denoting the M-circles, the performance and stability boundaries, and the nominal loop transmission are much more easily distinguishable than in these black-and-white figures. Please refer to Appendix C for a description of the features of these figures.

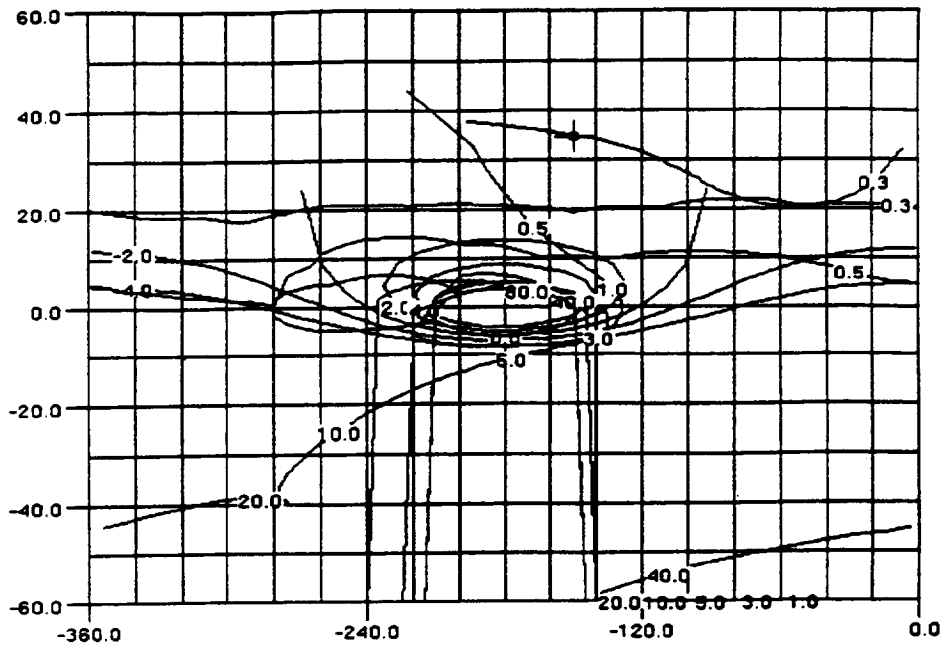

Figure E-1 CAD Drawing of Feedback Compensator Design for Roll Response to Roll Command

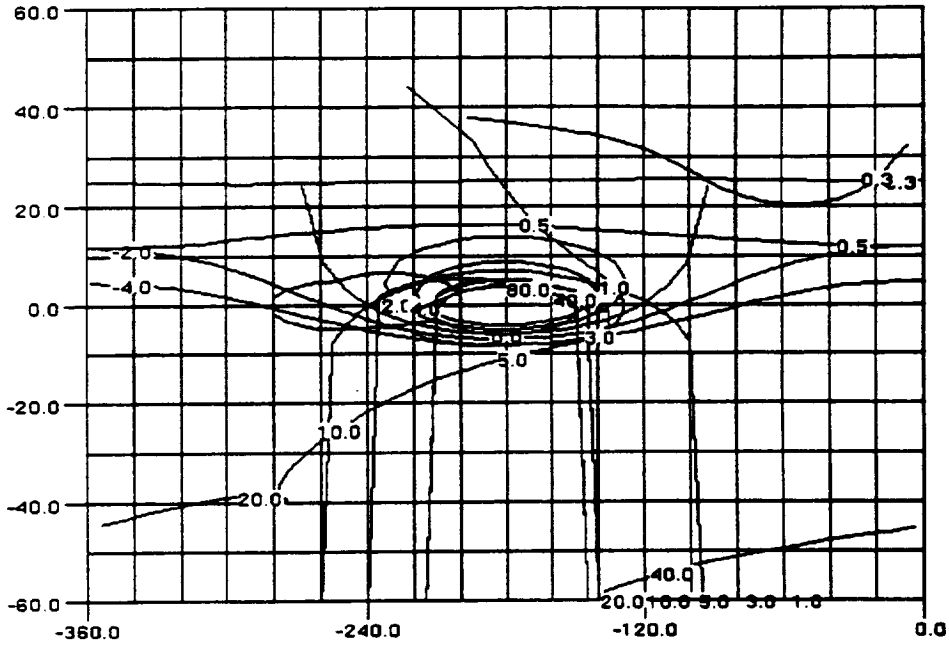

Figure E-2 CAD Drawing of Feedback Compensator Design for Roll Response to Pitch Command

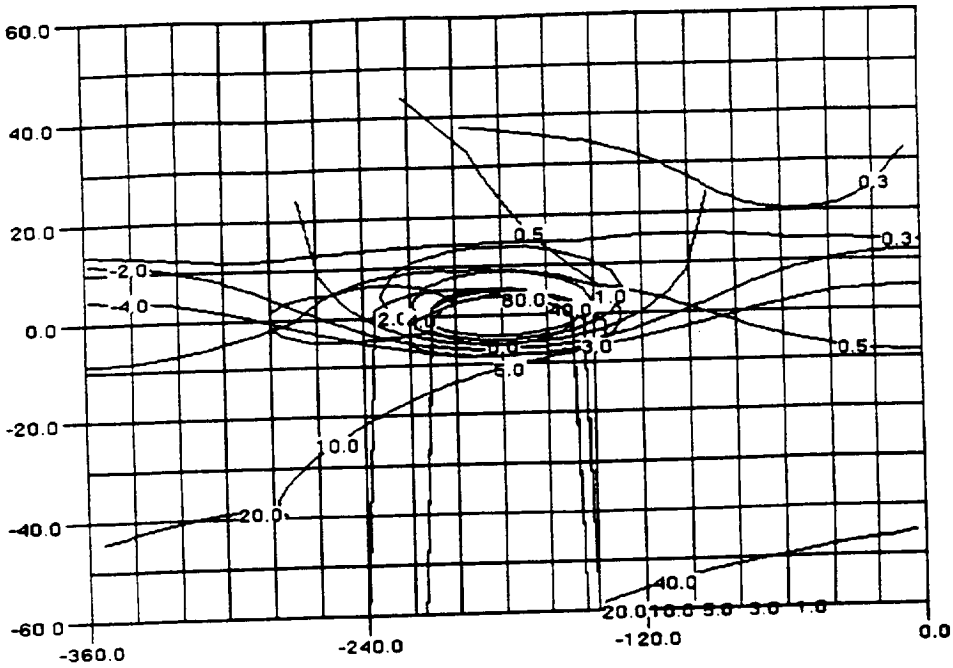

Figure E-3 CAD Drawing of Feedback Compensator Design for Roll Response to Vertical Velocity Command

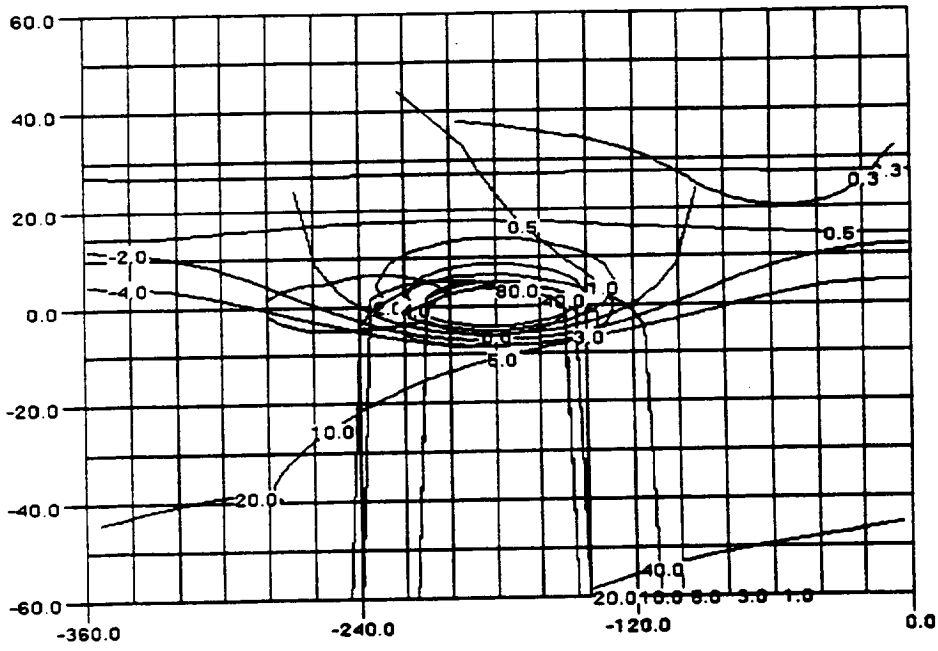

Figure E-4 CAD Drawing of Feedback Compensator Design for Roll Response to Yaw Rate Command

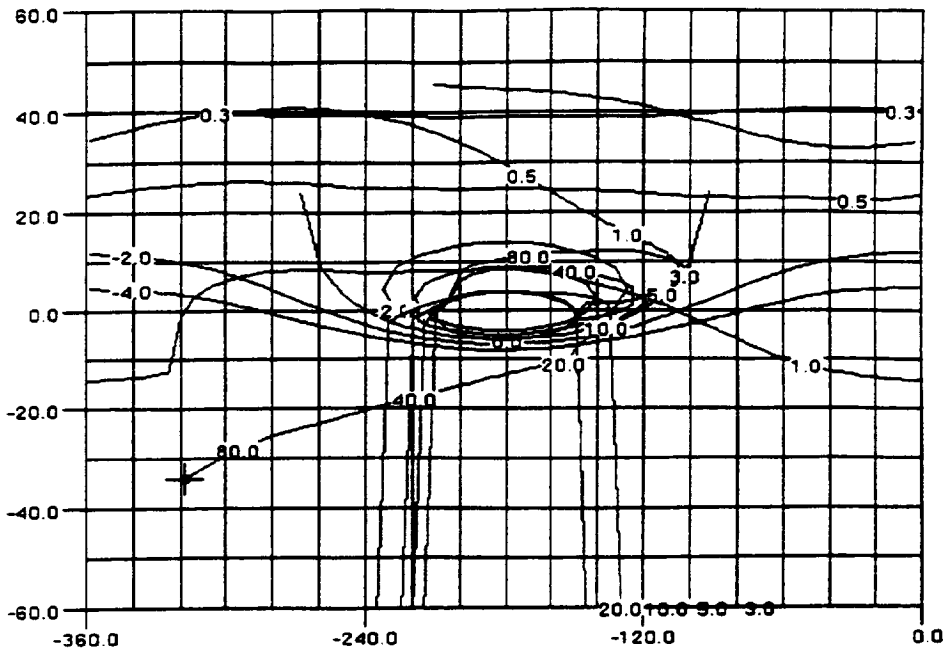

Figure E-5 CAD Drawing of Feedback Compensator Design for Pitch Response to Roll Command

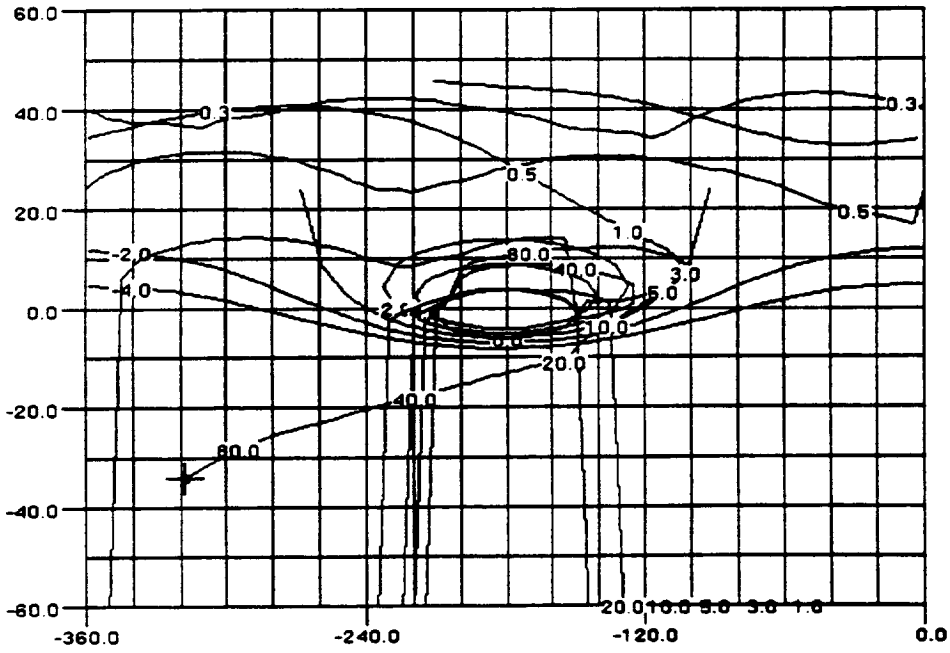

Figure E-6 CAD Drawing of Feedback Compensator Design for Pitch Response to Pitch Command

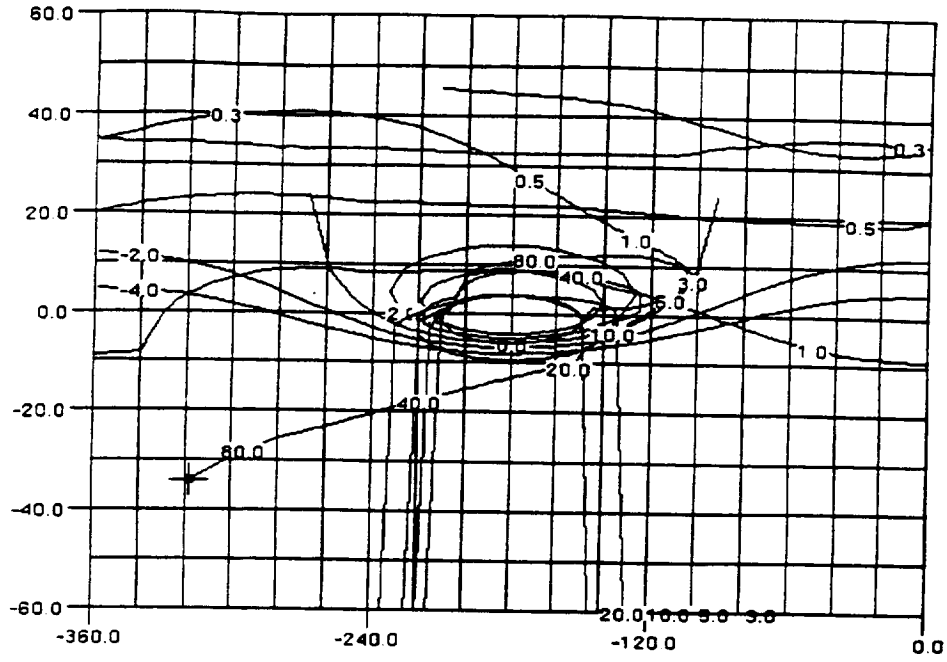

Figure E-7 CAD Drawing of Feedback Compensator Design for Pitch Response to Vertical Velocity Command

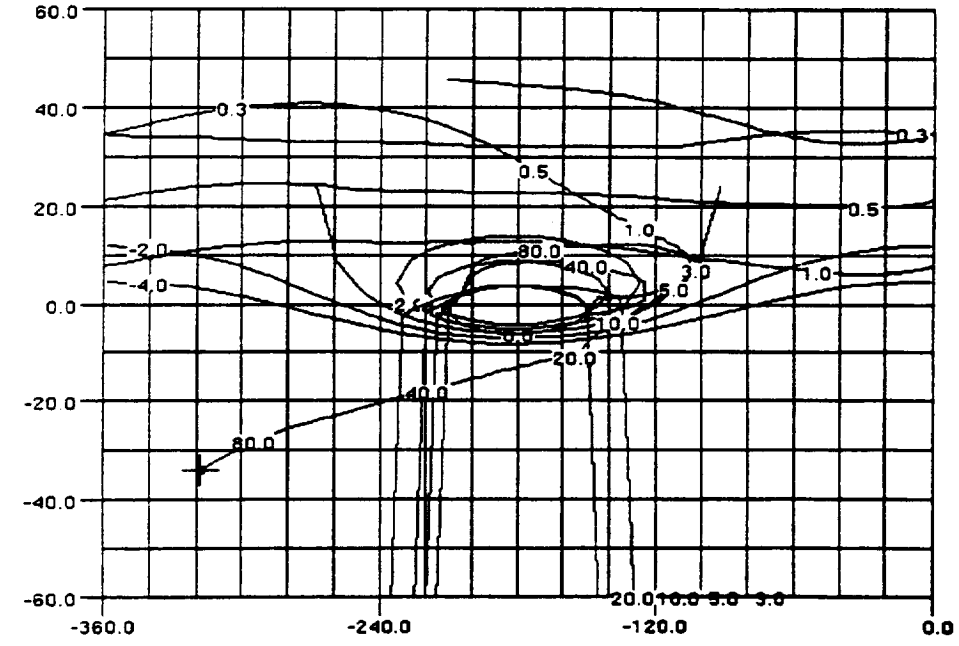

Figure E-8 CAD Drawing of Feedback Compensator Design for Pitch Response to Yaw Rate Command

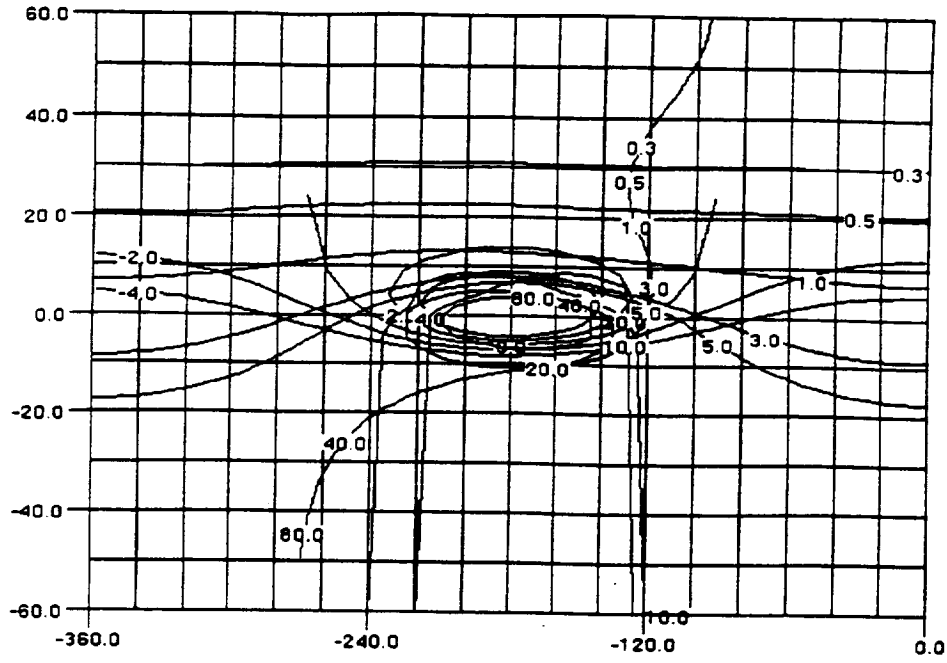

Figure E-9 CAD Drawing of Feedback Compensator Design for Vertical Velocity Response to Roll Command

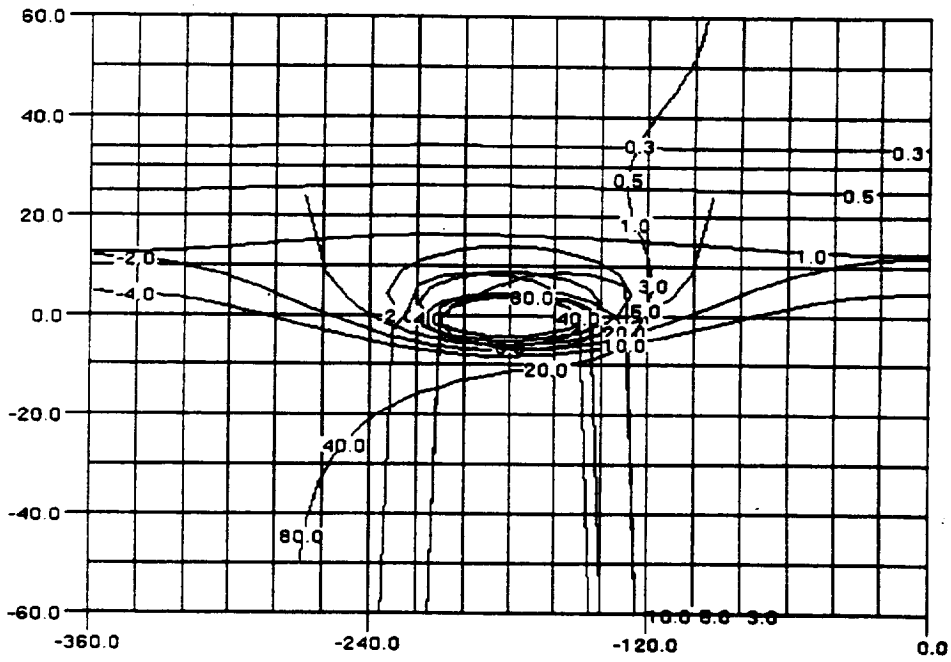

Figure E-10 CAD Drawing of Feedback Compensator Design for Vertical Velocity Response to Pitch Command

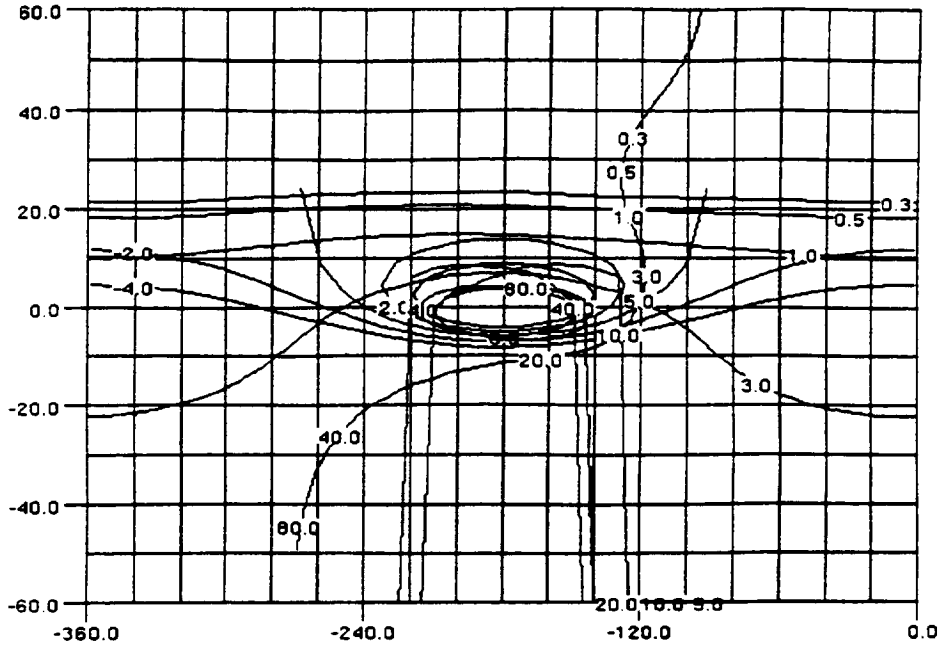

Figure E-11 CAD Drawing of Feedback Compensator Design for Vertical Velocity Response to Vertical Velocity Command

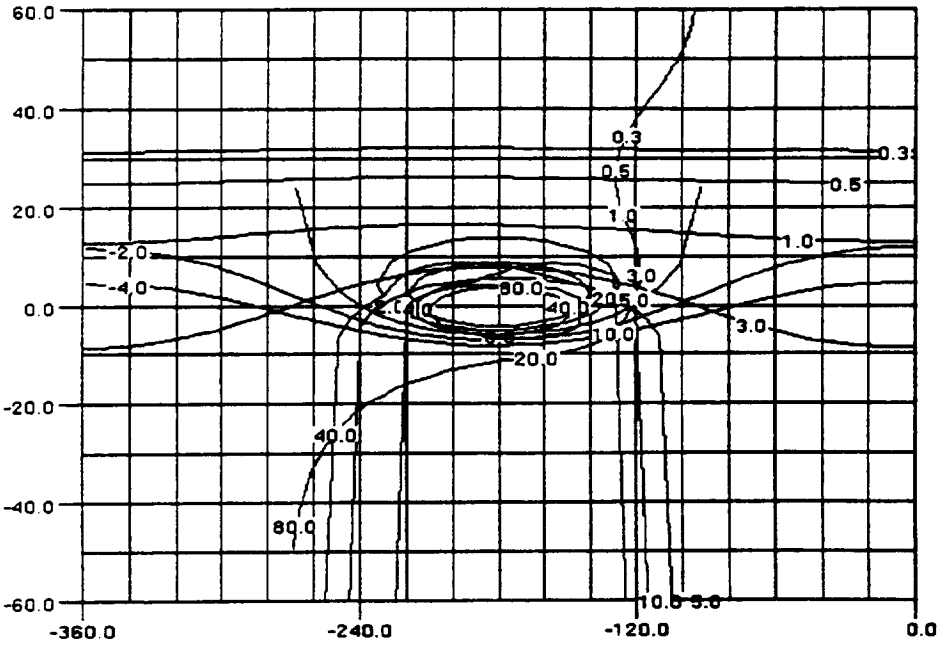

Figure E-12 CAD Drawing of Feedback Compensator Design for Vertical Velocity Response to Yaw Rate Command

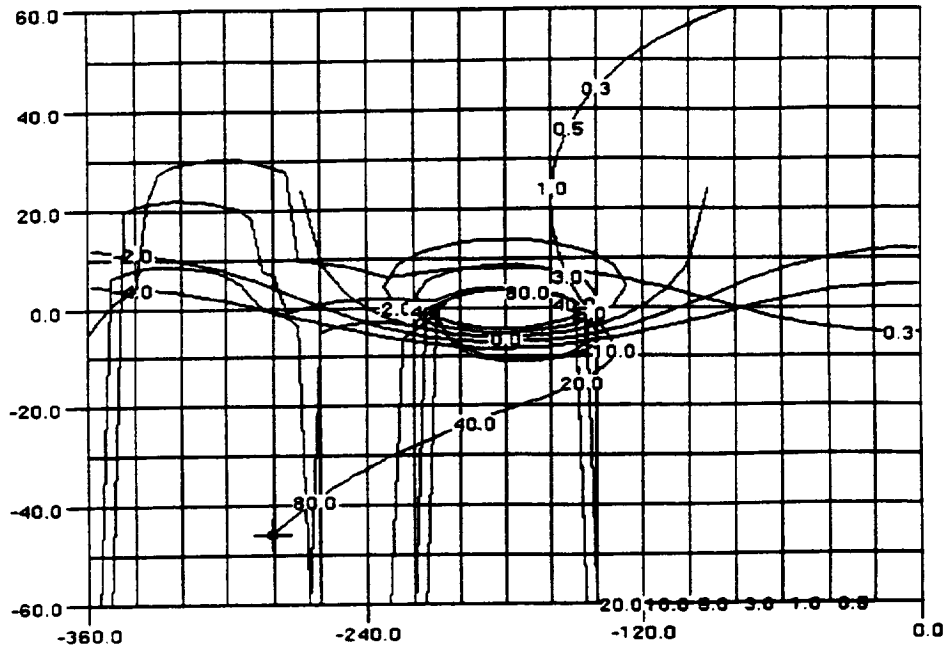

Figure E-13 CAD Drawing of Feedback Compensator Design for Yaw Rate Response to Roll Command

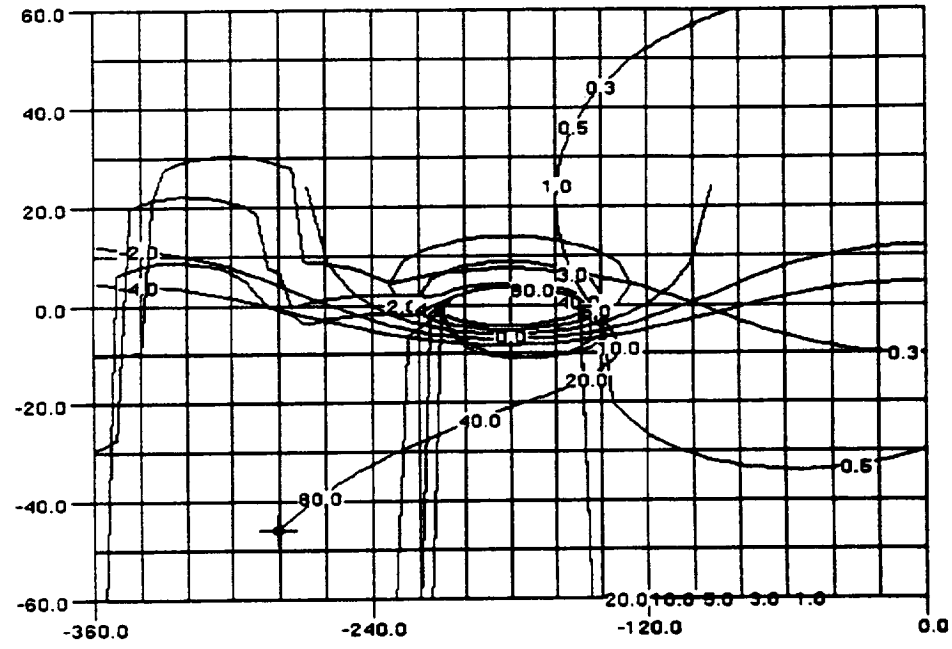

Figure E-14 CAD Drawing of Feedback Compensator Design for Yaw Rate Response to Pitch Command

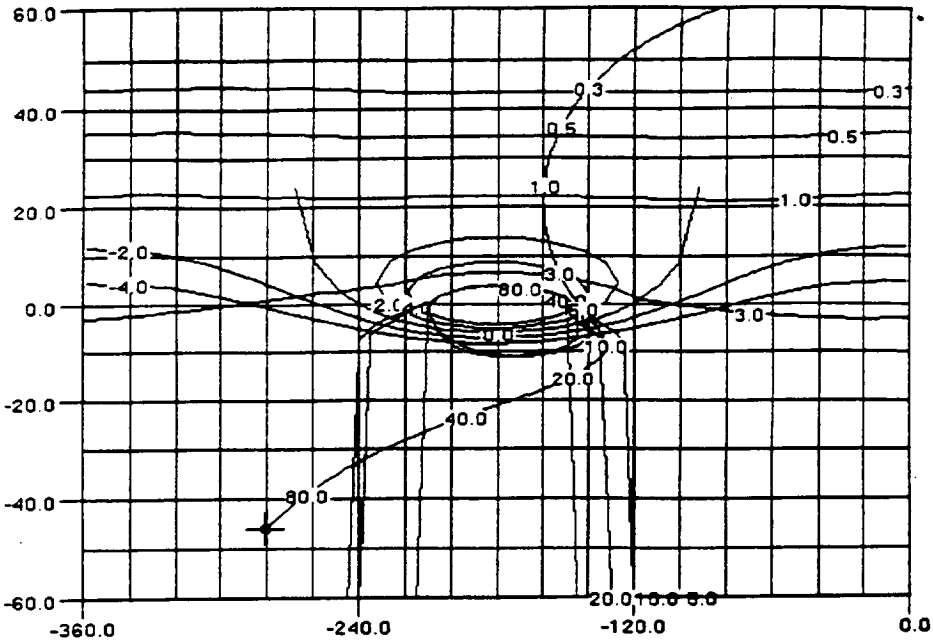

Figure E-15 CAD Drawing of Feedback Compensator Design for Yaw Rate Response to Vertical Velocity Command

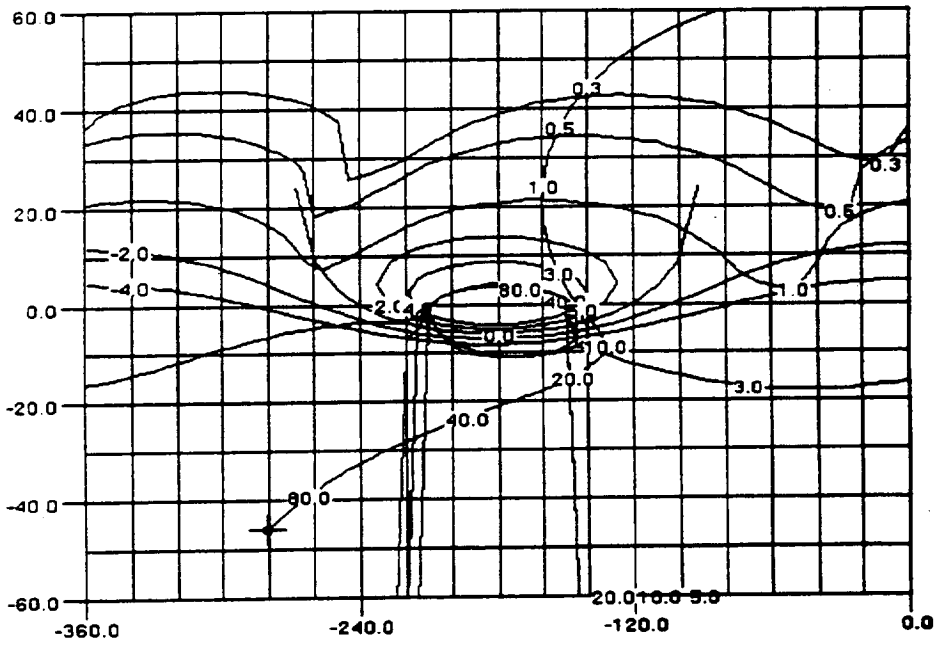

Figure E-16 CAD Drawing of Feedback Compensator Design for Yaw Rate Response to Yaw Rate Command

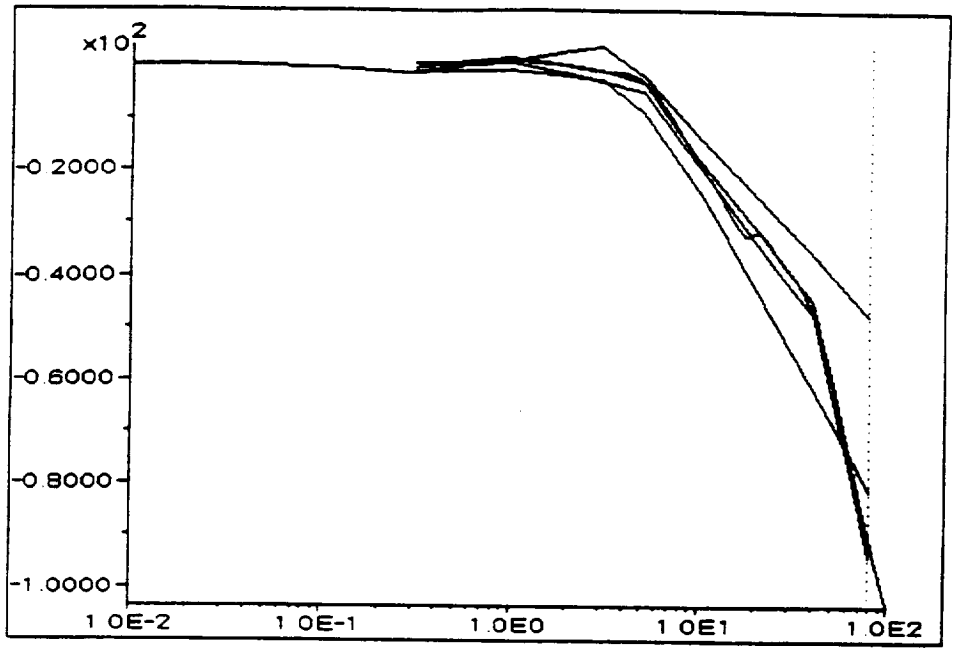

Figure E-17 CAD Drawing of Prefilter Design for Roll Response to Roll Command

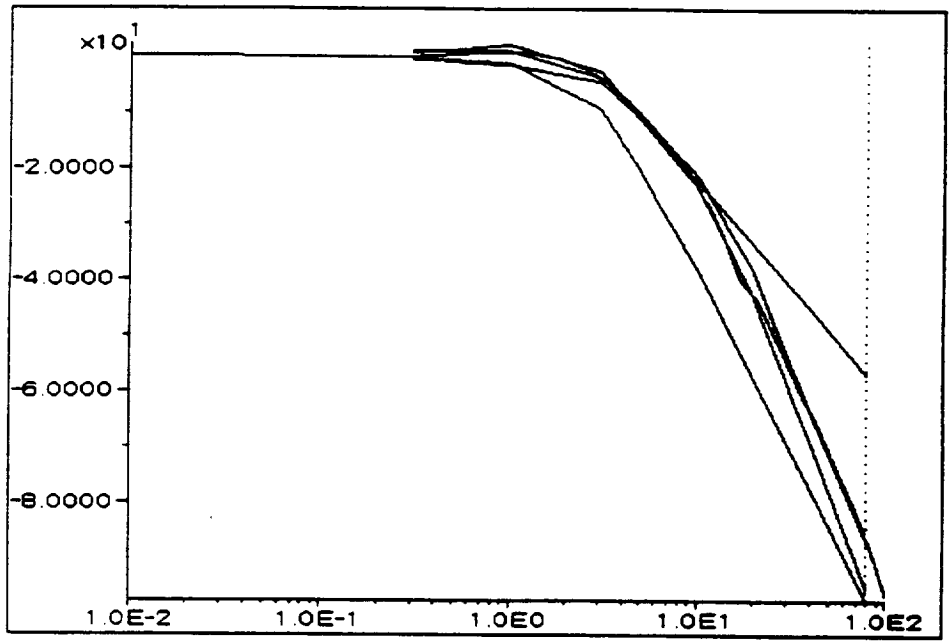

Figure E-18 CAD Drawing of Prefilter Design for Pitch Response to Pitch Command

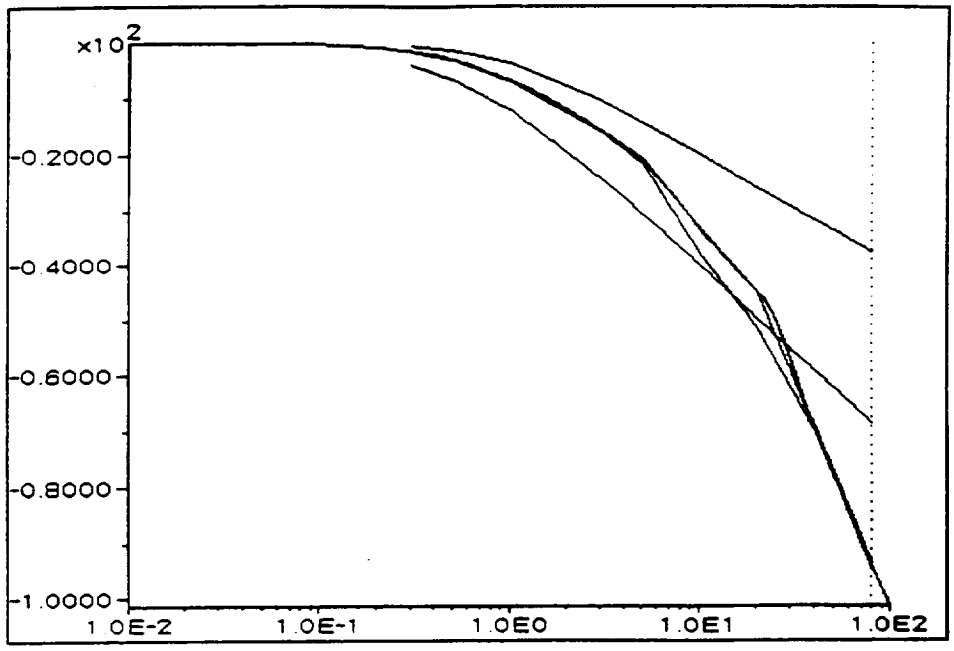

Figure E-19 CAD Drawing of Prefilter Design for Vertical Velocity Response to Vertical Velocity Command

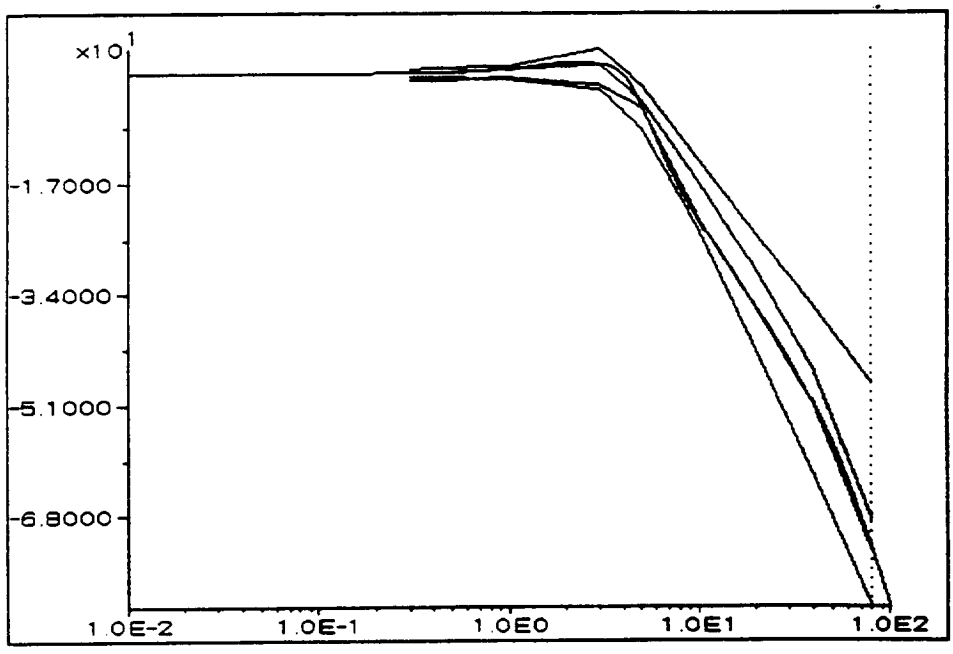

Figure E-20 CAD Drawing of Prefilter Design for Yaw Rate Response to Yaw Rate Command

APPENDIX F

RESULTS - SEQUENTIAL LOOP CLOSURE DESIGN

Presented in this Appendix are the time histories resulting from the application, as depicted in Fig. 4.15, of the flight control system designed the sequential loop closure technique described in Chapter 5 to each of the six (6) linearized helicopter models which comprised the set of possible plant dynamic models, P. Unit step inputs were applied to each of the controller inputs in succession with the following results.

Each solid line represents the response of one of the linearized models to the controller input. In Figs. F-1, F-6, F-11, and F-16, the performance boundary step responses are included as dashed lines.

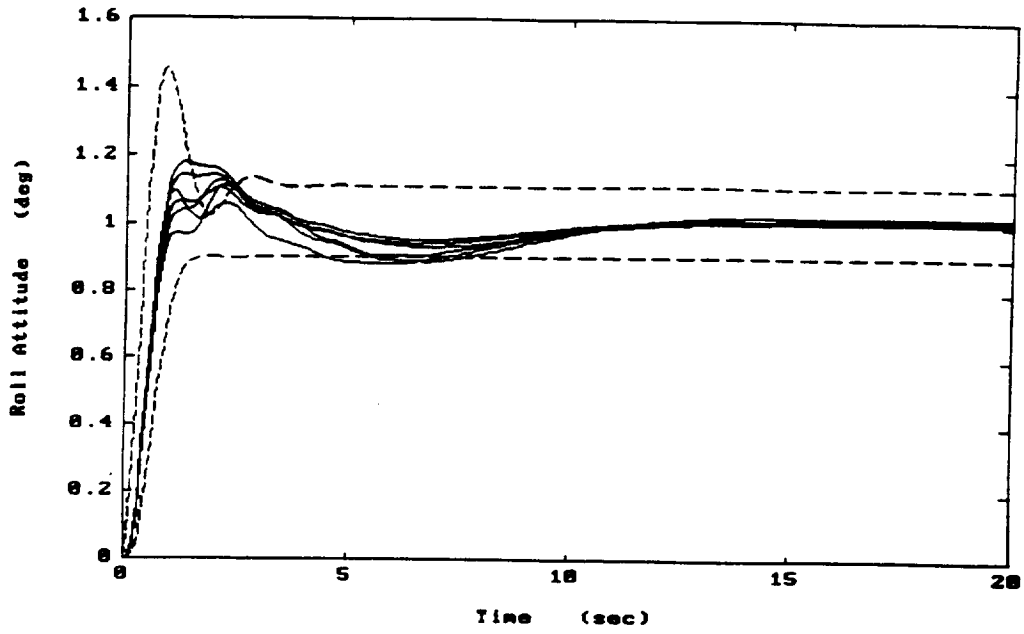

Figure F-1 Roll Attitude Response to a Unit Step to Roll Attitude Command

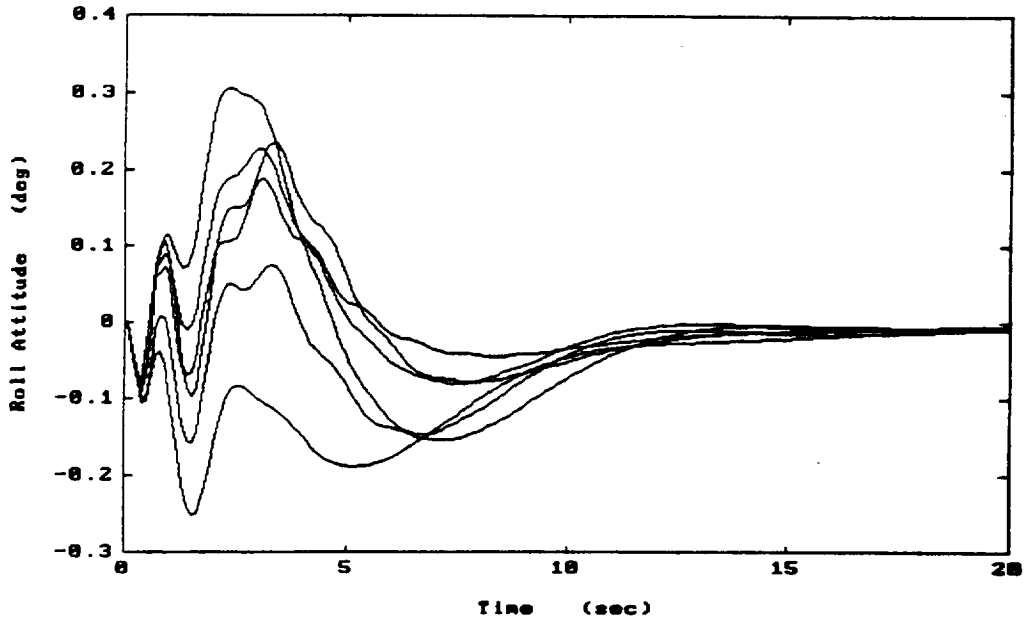

Figure F-2 Roll Attitude Response to a Unit Step to Pitch Attitude Command

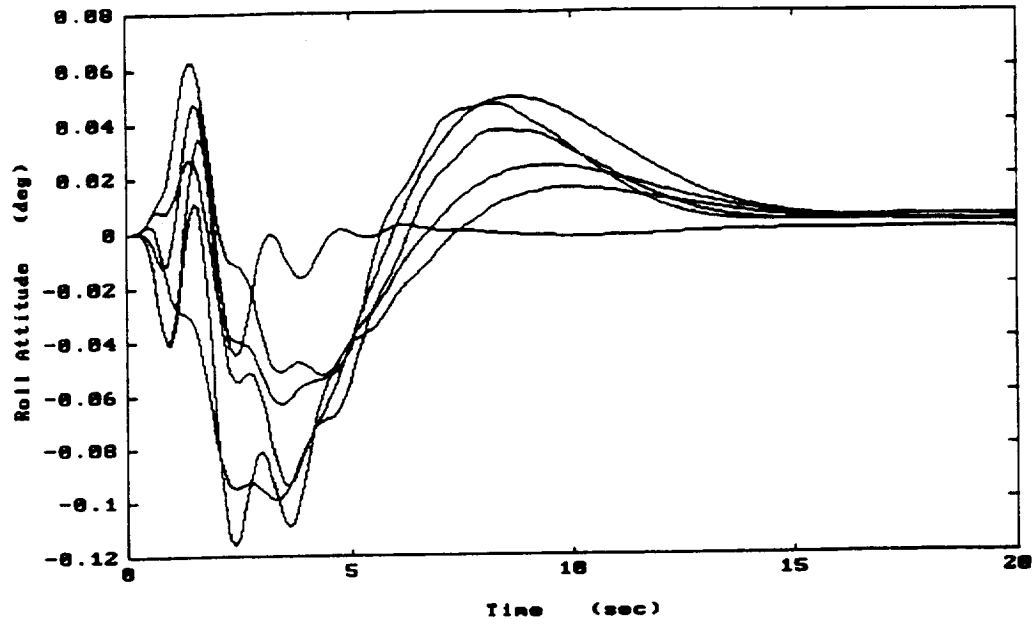

Figure F-3 Roll Attitude Response to a Unit Step to Vertical Velocity Command

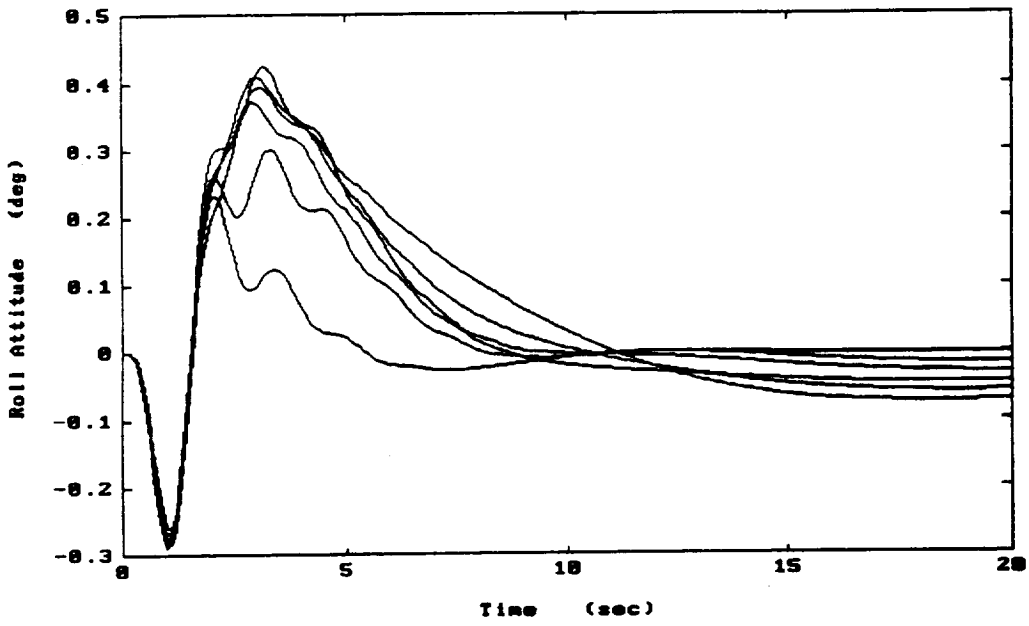

Figure F-4 Roll Attitude Response to a Unit Step to Yaw Rate Command

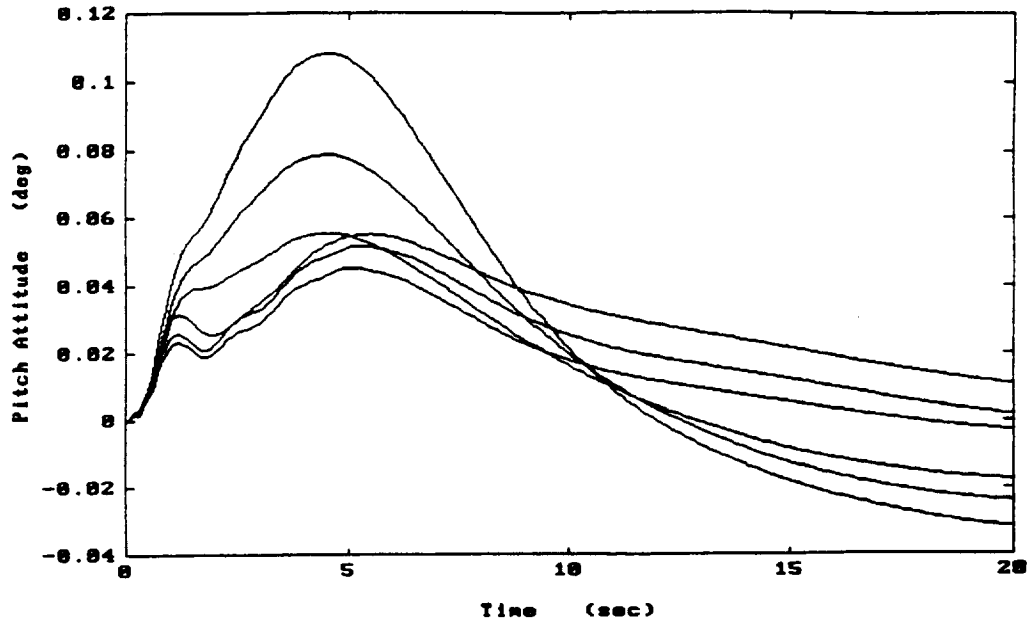

Figure F-5 Pitch Attitude Response to a Unit Step to Roll Attitude Command

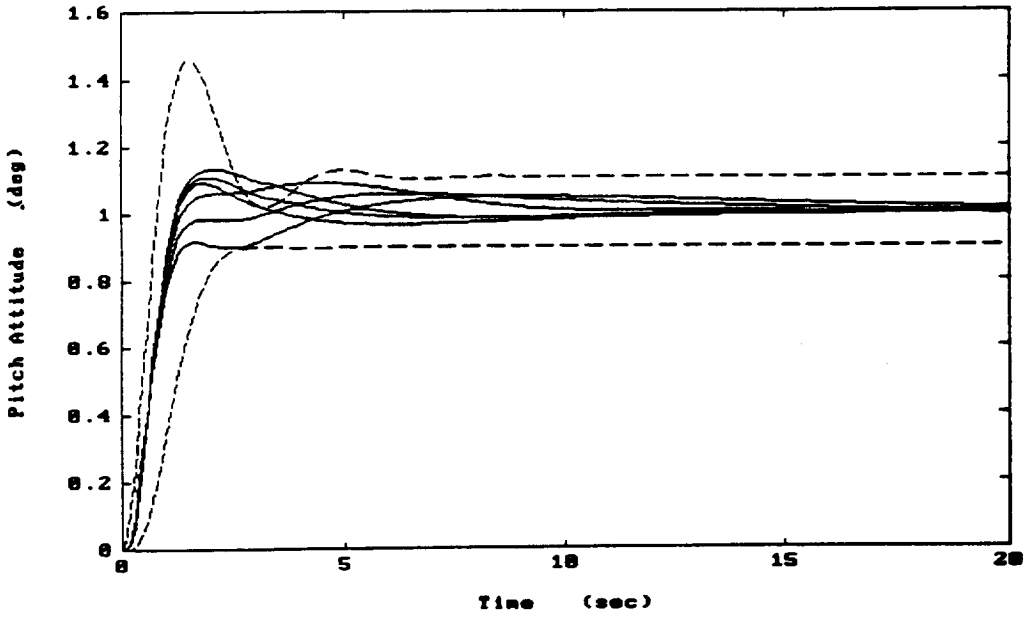

Figure F-6 Pitch Attitude Response to a Unit Step to Pitch Attitude Command

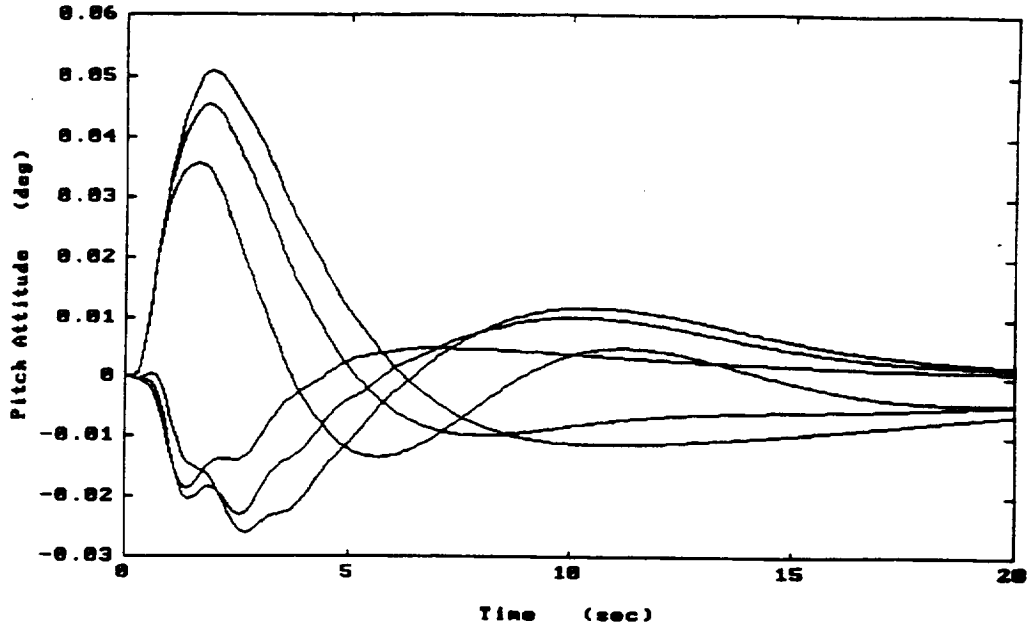

Figure F-7 Pitch Attitude Response to a Unit Step to Vertical Velocity Command

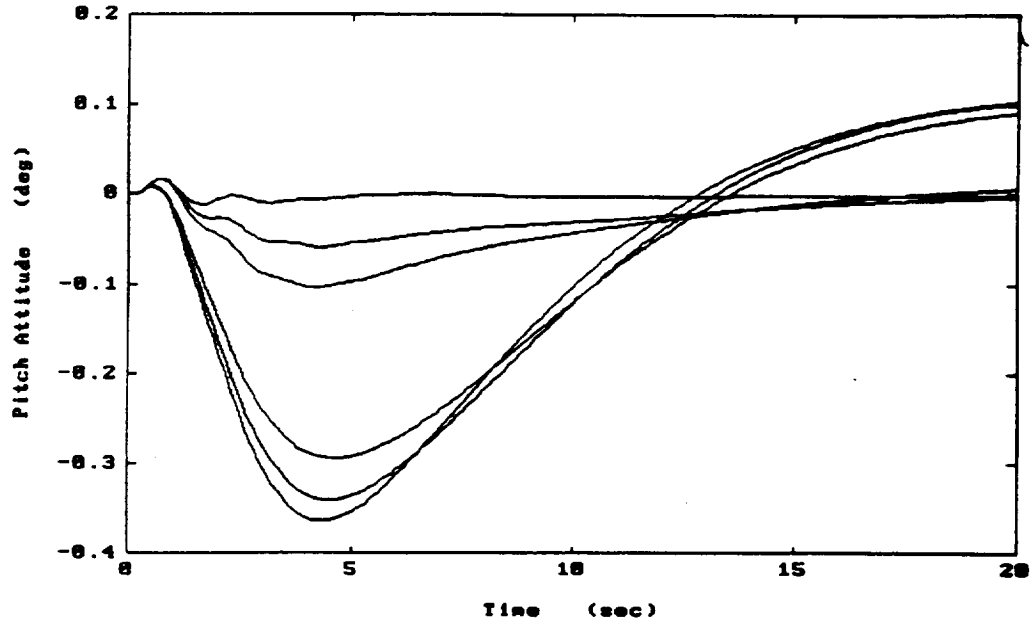

Figure F-8 Pitch Attitude Response to a Unit Step to Yaw Rate Command

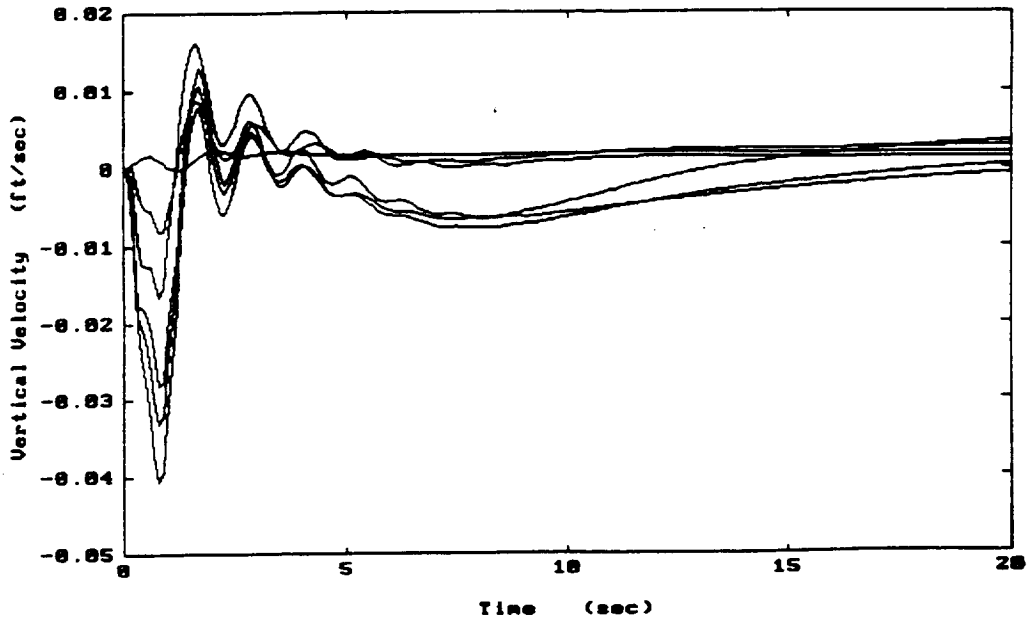

Figure F-9 Vertical Velocity Response to a Unit Step to Roll Attitude Command

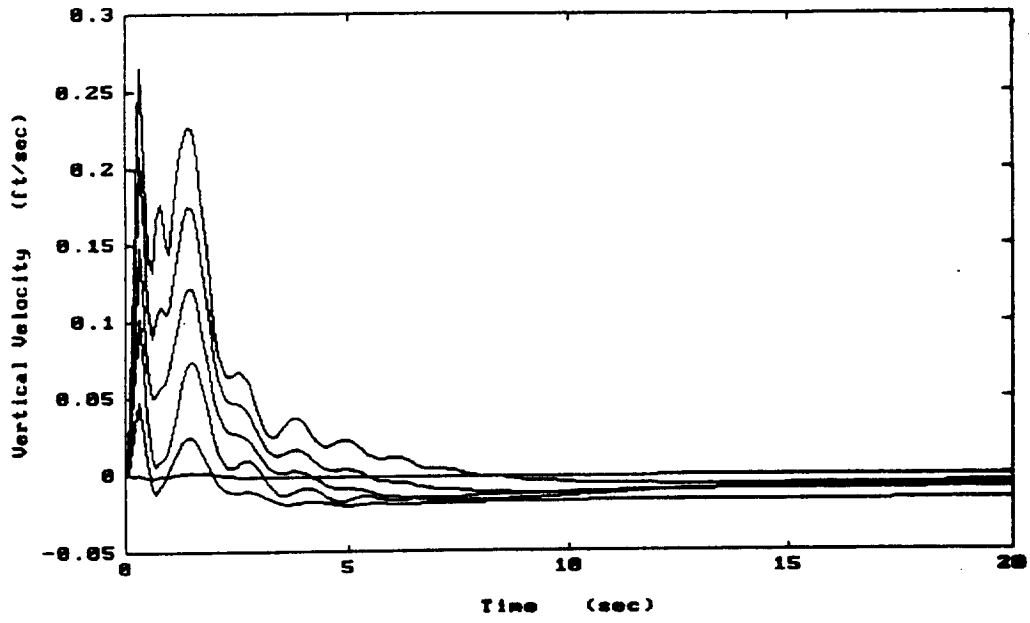

Figure F-10 Vertical Velocity Response to a Unit Step to Pitch Attitude Command

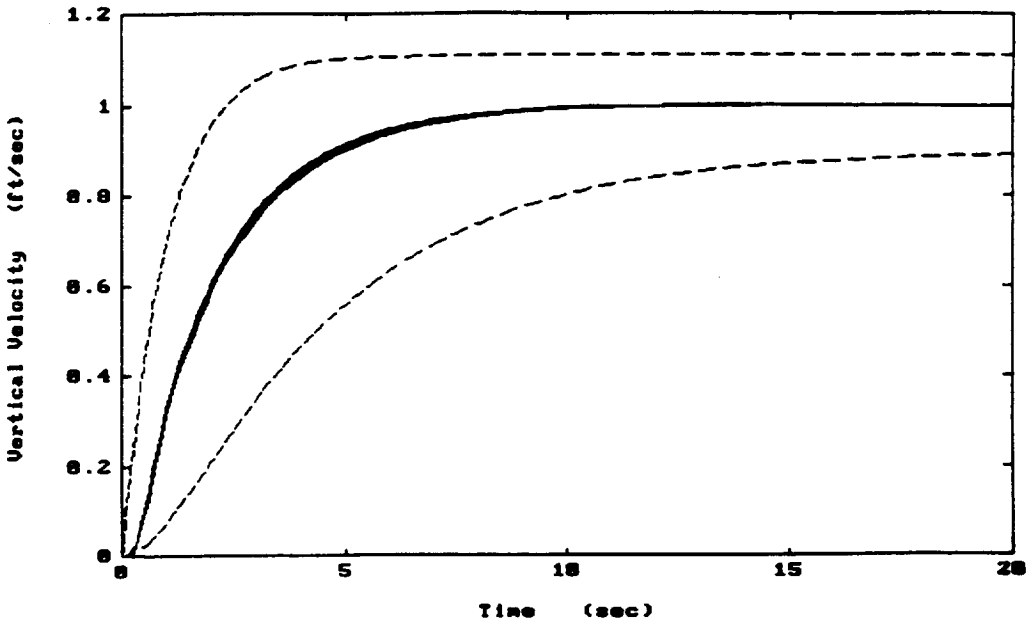

Figure F-11 Vertical Velocity Response to a Unit Step to Vertical Velocity Command

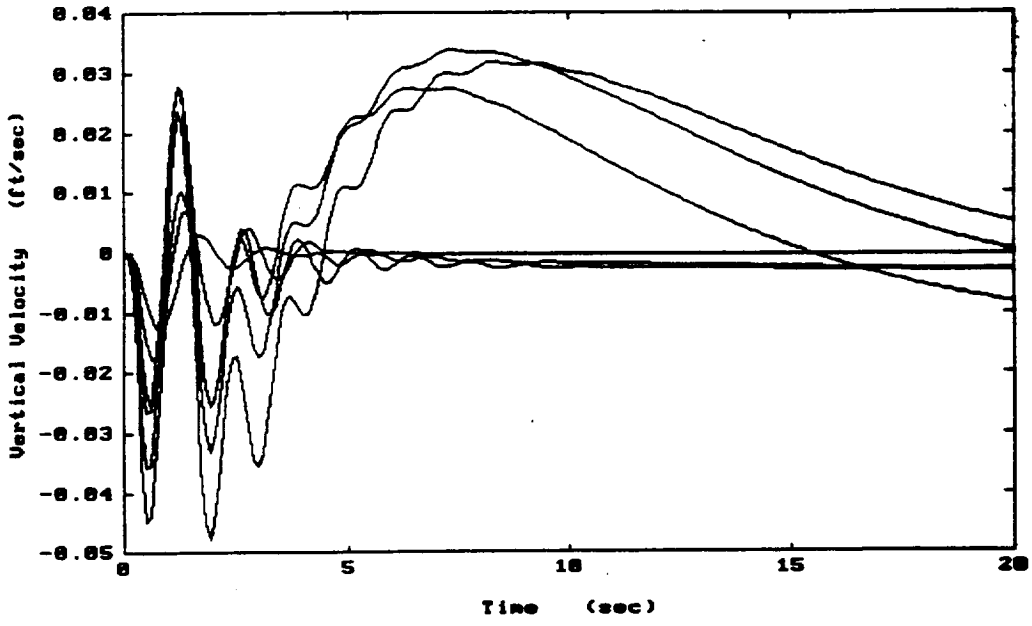

Figure F-12 Vertical Velocity Response to a Unit Step to Yaw Rate Command

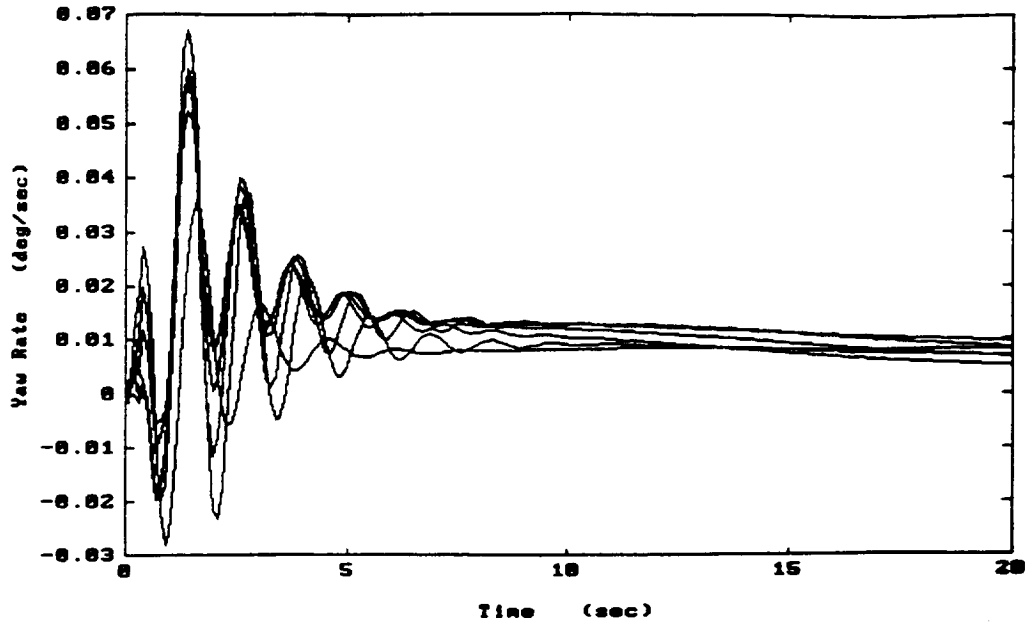

Figure F-13 Yaw Rate Response to a Unit Step to Roll Attitude Command

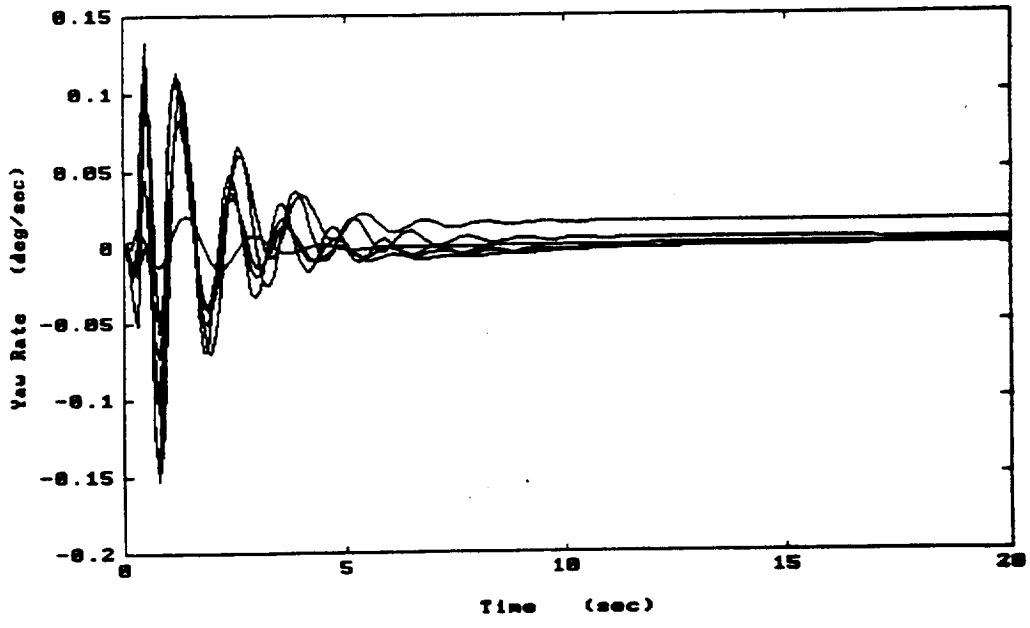

Figure F-14 Yaw Rate Response to a Unit Step to Pitch Attitude Command

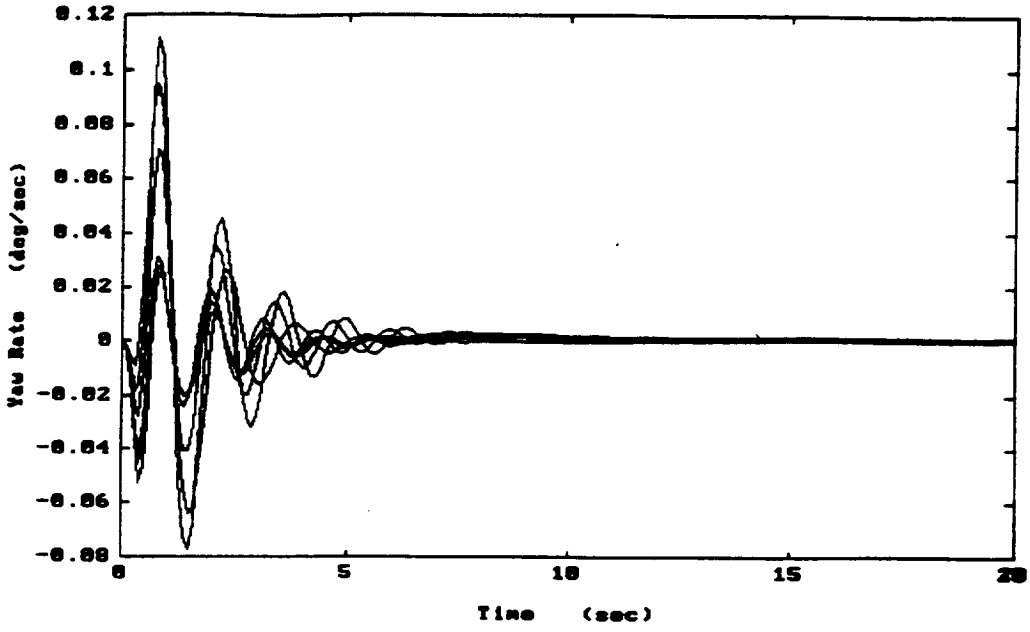

Figure F-15 Yaw Rate Response to a Unit Step to Vertical Velocity Command

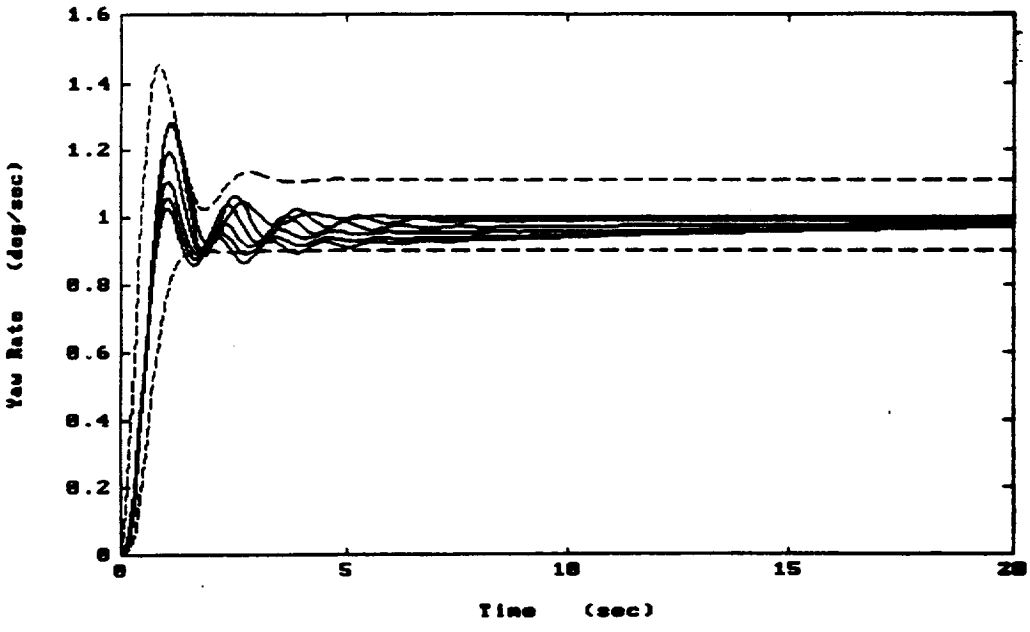

Figure F-16 Yaw Rate Response to a Unit Step to Yaw Rate Command